UNIVERSITÄT PADERBORN
Die Universität der Informationsgesellschaft

FAKULTÄT FÜR
ELEKTROTECHNIK,
INFORMATIK UND
MATHEMATIK

Resource-Efficient Multi-Antenna Designs for Mobile Ad Hoc Networks

— Focus on PHY, MAC and Cross-Layer

Zur Erlangung des akademischen Grades

DOKTORINGENIEUR (Dr.-Ing.)

der Fakultät für Elektrotechnik, Informatik und Mathematik
der Universität Paderborn
vorgelegte Dissertation
von

M. Sc. Feng Xu
aus Jiangsu Provinz, China

Referent: Prof. Dr.-Ing. Ulrich Rückert
Korreferent: Prof. Dr.-Ing. Paul Walter Baier

Tag der mündlichen Prüfung: 19. Mai 2008
Paderborn, den 06. Juni 2008

Diss. EIM-E/239

Acknowledgements

Firstly, I would like to express my deep appreciation to my advisor Prof. Dr.-Ing. Ulrich Rückert for offering me the chance to work in his research group, for his invaluable guidance, motivation, and encouragement on my doctoral work. The group led by him has provided a very good research environment, atmosphere, and infrastructure, which made me concentrate on my work during the past five years.

Moreover, I am very grateful to Prof. Dr.-Ing. Paul Walter Baier, who has also been my Master thesis advisor, for his time and effort spent on reviewing my doctoral thesis. His helpful comments and corrections have helped significantly improve the quality of the thesis.

My sincere gratitude also goes to my former colleague, Dr.-Ing Matthias Grünewald, with whom I closely cooperated and provided me much help on my work. His assistance and help play an important role in the completion of this work. I would like to extend my gratitude to all the colleagues of the System and Circuit Technology, Heinz Nixdorf Institute, especially to Dipl.-Wirt. Ing. Ralf Peveling, M. Sc. Tim Kaulmann, Dipl.-Ing. Boris Kettelhoit, and Dr.-Ing. Markus Köster for their nice help during the past years.

Finally, I would like to thank Dr. Wolfgang Schulz for providing me the chance and assisting me to use the antenna laboratory, and also Dr.-Ing. David Sandel, who assisted me to use the network analyzer.

Feng Xu
June 6, 2008

Abstract

In contrast to centralized wireless networks, mobile ad hoc networks (MANETs) do not rely on any pre-built infrastructure and central control function. The network topology may change rapidly and unpredictably due to mobility, joining and leaving of mobile nodes. In addition to numerous advantages, this distributed operation also causes a series of challenges across all layers of a network. This work focuses on the physical layer, the medium access control (MAC) layer, and the cross-layer optimization to find resource-efficient designs for mobile portable devices.

A number of benefits can be achieved by multi-antenna techniques, including higher data rate, more reliable links (lower bit error rate), and higher spectral efficiency. However, studies show that such techniques usually impose very high requirements on hardware complexity and power consumption, which on the other side may make devices less energy- and cost-efficient. Moreover, to achieve the best possible network performance, the MAC protocol must be adapted accordingly to match the new features due to multi-antenna techniques. Such a process is often called the cross-layer optimization.

In this thesis, a complete PHY & MAC solution for a low complexity six-antenna technique called simplified switched beam (SSB) is studied, which can achieve a proper balance between network performance and resource requirements. SSB can be applied on both TX and RX sides, and only a slight increase on hardware complexity and power consumption is required, compared to a single antenna system. Therefore, it is suitable for mobile portable applications. Its superior network performance is verified using the network simulation tool SAHNE (Simulation Environment for Mobile Ad Hoc Networks). To evaluate the point-to-point link performance of SSB, a test-bed has been implemented applying the FPGA prototyping system RAPTOR2000. Intensive measurements performed in an indoor short range mobile scenario (with and without interference) show that the SSB receiver can help to suppress fading and interference, increase the received signal power, and provide better performances than the single antenna receiver in terms of the reduced bit error rate. The measured signal to noise power ratio (SNR) gain and amount of fading (AoF) closely approach the theoretical predictions.

Contents

Chapter 1

Introduction

1.1 Mobile ad hoc networks (MANETs)

Wireless communication service is increasingly gaining attention due to its ease of use compared to wire-based communications. Traditional wireless networks usually consist of base stations (BSs) that serve a number of mobile stations (MSs), e.g., mobile phones, PDAs, and notebooks. Base stations are interconnected via wireless or wired media to the central unit, and they form the network infrastructure. A communication link between two mobile stations must be established through the infrastructure of the network, and a direct connection between them is not possible though they are in the coverage of each other. Therefore, such wireless networks are called *centralized networks*. Fig. 1.1 illustrates the structure of a local area network (LAN), which is a typical centralized network. In this case, access points (APs), wireless-enabled PCs, and the file server act as BSs, MSs, and the central unit, respectively. Each AP is responsible for one wireless LAN (WLAN). Within one WLAN, a PC must first access the local AP to connect to other PCs. If an inter-WLAN connection is required, multiple APs and the file server must be involved in the operation. Other typical centralized networks are mobile telecommunication networks, e.g., GSM (Global System for Mobile Communications).

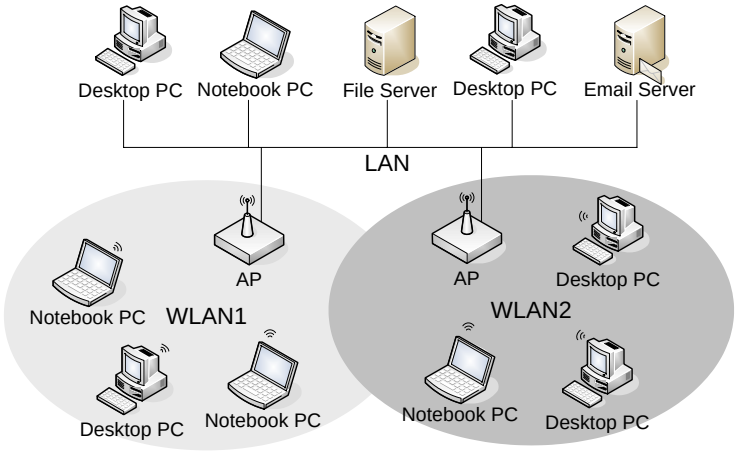

Figure 1.1: Local area network as an example of traditional centralized networks.

Although the centralized control structure may ease some operations like routing, it also leads to many disadvantages. For example, installing and maintaining the infrastructure increases the total cost of ownership, the collapse of the central unit may result in the collapse of the entire network, and the service is only available in the coverage of the base stations.

In the next generation of wireless communication networks, there will be a need for the rapid deployment of independent mobile users. Typical examples include establishing dynamic, survivable, and efficient communication for disaster relief efforts, emergency/rescue operations, and military networks. Such network applications cannot rely on any pre-built infrastructure that provides centralized and organized connectivity, and therefore can be conceived as applications of *Mobile Ad Hoc Networks (MANETs)*. A mobile node in a MANET may act as a router and a host simultaneously, and data packets may be transferred via multi-hops to reach the destination. Due to the mobility, joining and leaving of mobile nodes, the network topology may change rapidly and unpredictably. Moreover, a MANET may operate in a standalone fashion, or can be connected to existent homo-/heterogeneous networks as their extension or intermediate relay.

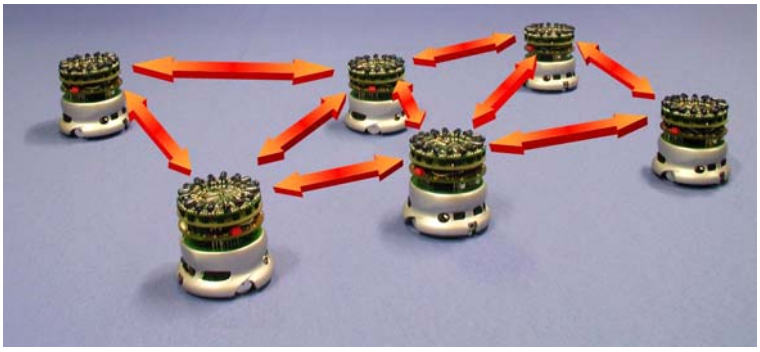

Figure 1.2: Robot communication network as an example of mobile ad hoc networks (MANETs).

The robot communication network illustrated in Fig. 1.2 (a test system developed by the group of System and Circuit Technology, University of Paderborn) is a typical example of MANETs. Its basic property is that a direct link between two nodes can be established if they are located in the coverage of each other. To transmit data to the destination out of the sender's coverage, the multi-hop routing method is used. Each robot is continuously moving. Therefore, it must update its neighboring information frequently enough.

1.2 Resources in wireless communications

Resources in wireless communications mainly consist of *spectrum*, *energy*, and *time*. With the rapid development of wireless communications, spectrum is quickly becoming a scarce resource. For each specific application the allocated frequency band is fixed. For example, UMTS (W-CDMA) can only use the frequency band 1.920-1.980 GHz for the uplink and 2.110-2.170 GHz for the downlink. In the context of fixed spectrum assignment, investigations on increasing the spectrum efficiency are becoming crucial. In MANETs, mobile nodes are mostly powered by batteries with limited energy capacity before recharging. Therefore, low power designs are also research hotspots. Lastly, time can also be regarded as a kind of resource since the nodes operating on the same frequency channel must interlace their activities to avoid collisions. A good time allocation scheme can significantly increase the network throughput.

There are a lot of traditional schemes that can increase the efficiency of the aforementioned basic resources and/or the network capacity based on the reuse principle, e.g., FDMA (frequency division multiple access), TDMA (time division multiple access), CDMA (code division multiple access), and SDMA (space division multiple access). These four schemes are mainly applied in the *point-to-multipoint* communication scenario (one base station with multiple mobile stations, each link is bidirectional) although they are multiple access methods. Recently, two new techniques have come into use that can achieve a higher spectral efficiency on the *point-to-point* link. They are OFDM (orthogonal frequency division multiplexing) and MIMO (multiple-input multiple-out). However, in MANETs we mainly consider the scenario of *multipoint-to-multipoint* without hierarchy. Therefore, all nodes hold an identical rank, and it is possible for each node to communicate with multiple other nodes (unlike in centralized networks, where each mobile station can only communicate with its local base station).

From the real system implementation perspective, *hardware complexity* (including computing capability), *cost*, and *size* must be taken into account as practical aspects. Those aspects should also be treated as resources, especially for mobile portable devices that are strictly constrained by them.

1.3 Definitions on resource-efficiency

We observe the resource-efficiency for MANETs from the perspective of multipoint-to-multipoint networking applications, which is different from other studies based on the point-to-point or point-to-multipoint applications. Two measures on resource-efficiency can be explicitly defined as follows:

Spectrum-efficiency is defined as the total number of active point-to-point links multiplied by the data rate on each link and then divided by the total bandwidth used in the network. It can be expressed as the ratio between the network throughput and the total bandwidth used:

$$\eta_{\mathrm{B}} = \frac{number\ of\ links \cdot datarate\ (\mathrm{bit/s})}{total\ bandwidth\ (\mathrm{Hz})} = \frac{throughput\ (\mathrm{bit/s})}{total\ bandwidth\ (\mathrm{Hz})} \tag{1.1}$$

It should be noted that η_{B} is different from the spectral efficiency used for evaluating different modulation or MIMO techniques although they apply the same unit of bit/s/Hz, since spectral efficiency is based on the point-to-point link [64, 81, 43]. In this thesis, we always assume that all nodes in a MANET operate on the same frequency channel, that is, the total bandwidth used is fixed for each node and for the entire network.

Energy-efficiency is defined as the ratio of the total amount of user data delivered to the total energy consumed. It can be expressed as the ratio between the network throughput and the average power consumption:

$$\eta_{\mathrm{E}} = \frac{total\ amount\ of\ data\ delivered\ (\mathrm{bit})}{total\ energy\ consumed\ (\mathrm{W \cdot s})} = \frac{throughput\ (\mathrm{bit/s})}{average\ power\ (\mathrm{W})} \tag{1.2}$$

It should be noted that the average power here refers to neither baseband signal power nor radiated RF signal power [64], but the power consumption of all active nodes in the network. Therefore, η_{E} depends on the implementation technologies, e.g., to realize the same circuits more advanced silicon technologies can result in less power consumption and die area. In this thesis, we investigate the energy efficiency of different schemes based on the same (state-of-the-art) silicon technology.

The efficiency on other resources like hardware complexity is difficult to explicitly quantify. However, their absolute quantities can be compared for different schemes.

1.4 The objective of this work

Fig. 1.3 shows the Open System Interconnection (OSI) reference model for computer networking as defined by the International Organization for Standardization (ISO) [70]. Each of the seven layers performs a specific set of functions, and in turn provides a distinct set of services to the layer above it. For MANETs, the seven-layer model can be simplified to the four-layer model composed by physical (PHY), medium access control (MAC), network, and user layers. A rough correspondence between them is

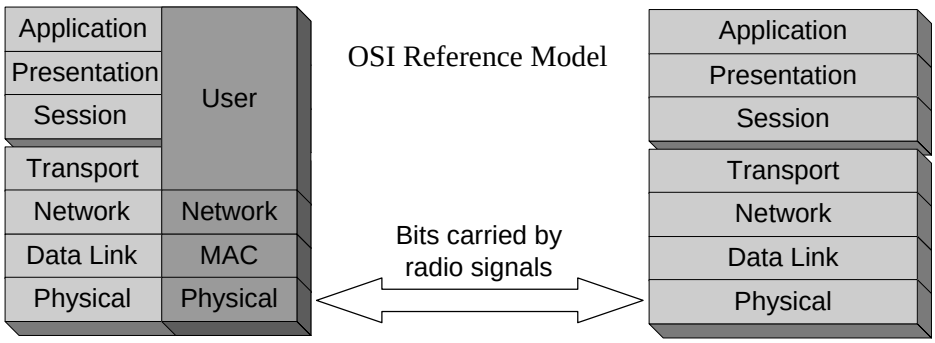

Figure 1.3: MANETs functional-layered model.

also illustrated in Fig. 1.3. The functions performed by each layer protocol are as follows:

- The **physical layer** delivers "raw" bits across the wireless medium. A physical layer protocol defines the electrical characteristics of the medium, the bit rate, the voltages, etc.
- The main functions of the **MAC layer** protocol are to fairly allocate the shared wireless medium to all nodes belonging to the network, and to define methods to ensure the reliability of data delivery.
- The **network layer** protocol defines how nodes discover each other and how packets are routed to their final destinations, that is, to find a proper route between source and destination. Therefore, it is also called routing protocol.
- The functions of the **user layer** depend on the applications. Usually they define how and in which format the data are transferred.

Due to the new properties of MANETs described in the first section, a series of challenges across all layers result. Furthermore, each layer protocol is theoretically independent of the protocols in the layers above and below it. This design allows for new technologies to be incorporated into a protocol layer without affecting the other layers. While this is only the theory, many new designs, especially the ones initiated from the physical layer, require the corresponding adaptations on the upper layers to match their new properties and to achieve the best possible performance. Such matching processes can be called cross-layer optimization. This thesis only concerns the designs on the PHY & MAC layers and cross-layer optimization for MANETs.

MIMO[1] is regarded a promising physical layer technique to the next generation wireless communication networks. The work in this thesis is based on two types of MIMO:

[1] Note that here it refers to the wide-sense MIMO, see Section 2.4.

Beamforming and space diversity. A lot of benefits can be achieved by MIMO, including higher data rate, more reliable links (lower bit error rate), and higher spectral efficiency. However, further studies show that MIMO imposes high requirements on hardware complexity and power consumption, which, on the other side, may decrease the energy efficiency and spectral efficiency (due to the long guard time for signal processing if the computing speed is not high enough), and makes the product less cost-efficient (too expensive). Furthermore, the limited resources (in terms of battery capacity, system size and computing capability) on mobile portable devices reduce its feasibility with state-of-the-art silicon technologies. Therefore, a low complexity scheme that can properly balance the tradeoff between performance and hardware complexity is desirable. Of course, compared to the traditional single antenna design, higher spectrum and energy efficiencies and better performance are still required. The work of this thesis has been carried out under this motivation.

In the past decade, many MAC layer designs have been proposed for MANETs due to various multi-antenna techniques coming into use on the physical layer. Nearly all of those MAC layer designs are verified and evaluated by network simulators. A common feature of them is that the design focus has been laid on the MAC layer and the used physical layer model is very ideal. Furthermore, the impact of the physical layer on the MAC layer has been emphasized, but the reverse impact has been less concerned. Such theoretical investigations can provide valuable design outlines for future networks. However, to apply those outlines for designing a real network, significant efforts have to be paid on aspects like more precise physical layer models, the impact of MAC layer on the physical layer, and the practical limitation due to hardware implementation, etc. This is another motivation of this work.

In summary, in this thesis, the resource-efficiency from the entire network perspective, the feasibility for mobile portable devices under state-of-the-art silicon technologies, and the practicability regarding each detail for implementation are emphasized on the PHY & MAC designs and their corss-layer optimization for MANETs.

1.5 The outline of this thesis

In Chapter 2 an overview on various multi-antenna communication techniques on the physical layer is given, with the focus on introducing their principles and analyzing their requirements on hardware complexity, computational load and power consumption imposed on real system implementations.

In Chapter 3 the traditional MAC layer designs for MANETs based on omni-directional communications are first stated. Then, two new designs, BF-MAC and SD-MAC, are presented, which are based on the beamforming (BF) and space diversity (SD)

gains provided by the physical layer, respectively. Hence, they can be considered as cross-layer designs. An overview on the previous investigations in literature is given, focusing on their novelties and limitations. Based on the previous investigations, a multi-directional-antenna (MDA) based MAC (MDA-MAC) is proposed, together with radiation power control (PC) and transceiver power management (PM). We use a network simulation tool to evaluate the above cross-layer designs.

Motivated by the above studies, the low complexity six-antenna scheme called simplified switched beam (SSB) together with its adapted MAC design SSB-MAC are presented in Chapter 4. Again, we use network simulations to evaluate the above designs.

To evaluate the real system performance, we have implemented a test-bed for SSB. The implementation process is presented in Chapter 5 in detail, and the measurements performed in an indoor environment and the analysis on the results are described afterwards.

Finally, some concluding remarks and suggestions for future research are given in Chapter 6.

Chapter 2

PHY Layer Designs: Multi-Antenna Techniques

In this chapter various multi-antenna communication techniques will be reviewed, which can be roughly classified into smart antennas (SA), space diversity (SD), and multiple-input multiple-output (MIMO) techniques. Those three types of techniques may exhibit different advantageous features since they exploit different properties of wireless channels, e.g., SA systems mainly offer *array gain* and *interference suppression gain* (together called beamforming gain), SD systems result in *diversity gain* that helps to increase the link reliability, while MIMO systems can generate *multiplexing gain* and/or *diversity gain*. As some properties of wireless channels cannot occur simultaneously, or even conflict, SA, SD, and MIMO are appropriate for different environments. However, there are similarities among them, especially between SA and SD, and between SD and MIMO.

In the following, a traditional single antenna communication system will be described first, with a focus on antenna and radio frequency (RF) front-end functions. After that, SA, SD, and MIMO techniques will be introduced, and the similarities and differences between them will also be given. Finally, a cost analysis based on the hardware complexity and power consumption due to the use of those multi-antenna techniques will be presented.

2.1 Traditional single antenna digital communication system

Fig. 2.1 illustrates the block diagram of a single antenna digital communication system, which is composed of the antenna, RF front-end, baseband processor, MAC controller, and host computer. The system must realize all functions throughout all layers shown in Fig. 1.3 if it acts as a communication network node. Simple networking applications may reduce requirements on the components responsible for the MAC- and routing-layer functions. As the main component of the RF front-end, a heterodyne

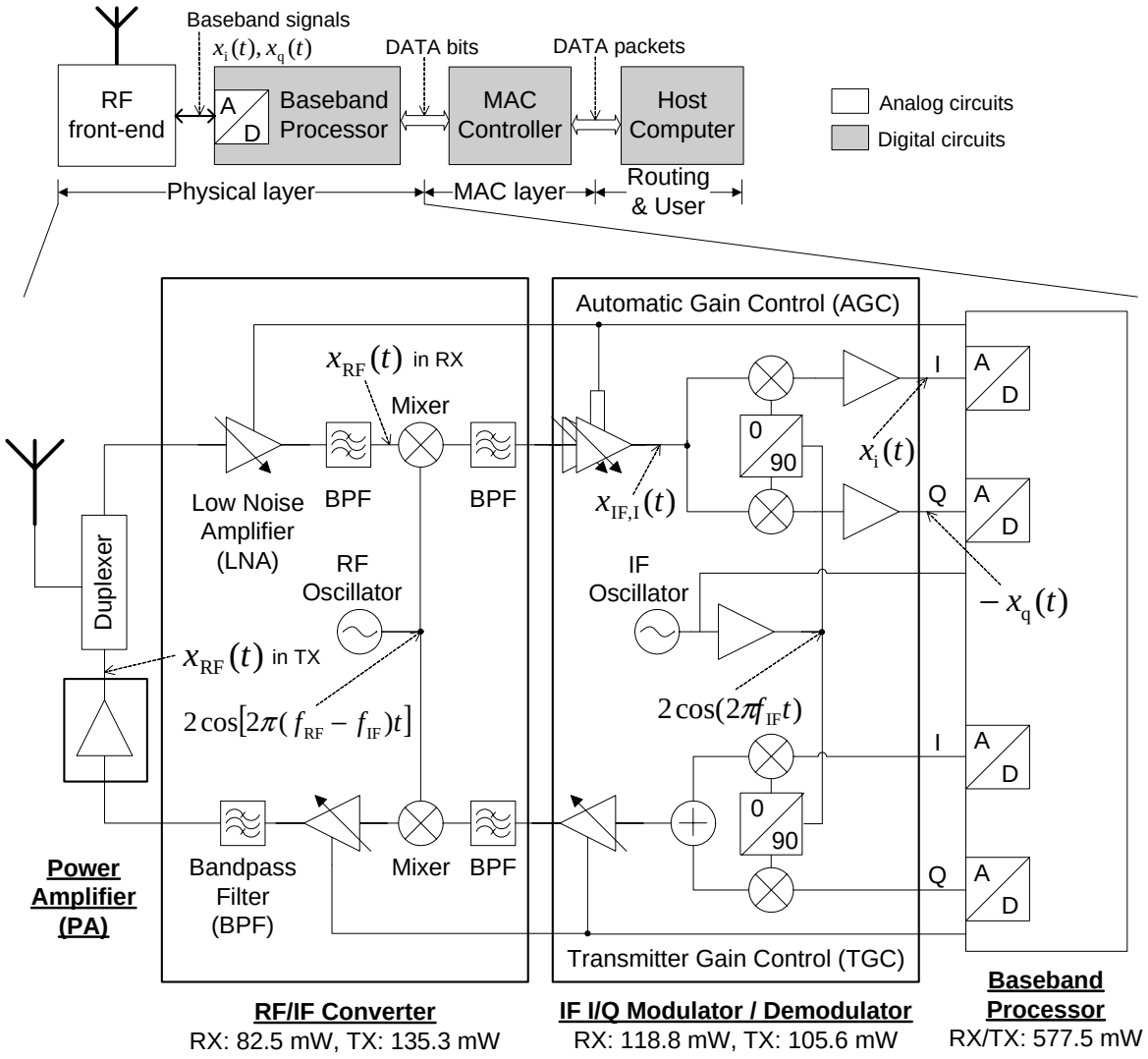

Figure 2.1: The block diagram of a single antenna digital communication unit, and an exemplary heterodyne RF transceiver [15] is further illustrated.

RF transceiver is further illustrated in Fig. 2.1. It is composed of two sub-components, a RF/IF converter and an intermediate frequency in-phase/quadrature (IF I/Q) modem. The antenna detects electromagnetic waves and converts them to RF signals and vice versa. The RF front-end acts as an interface between RF signals and baseband signals, which is indispensable because baseband signals are unsuitable for long range transmission via wireless channels. Main functions of the baseband processor consist of digital modulation/demodulation, coding/decoding, multiplexing/demultiplexing, and so on. It delivers digital DATA bits to the MAC controller in RX, and vice versa in TX. Other data processing functions are performed by the MAC controller and the host computer. In the following, we will introduce the fundamentals on antenna and RF front-end signal processing, as they are useful for understanding multi-antenna techniques, especially for understanding beamforming techniques.

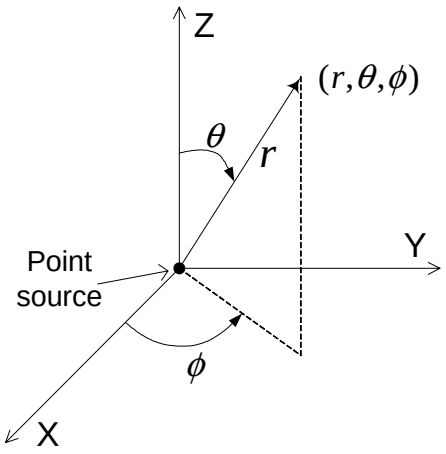

Figure 2.2: Spherical coordinates for a point source of radiation in free space.

2.1.1 Fundamentals on antenna

The contents of this subsection are mainly from [42]. First, we apply the far field assumption, that is, each antenna can be regarded as a point source. Spherical coordinates illustrated in Fig. 2.2 are applied throughout the whole thesis if not additionally specified. Second, any antenna is considered to be strictly reciprocal for signal radiation and detection, that is, any property of signal radiation can be directly used for signal detection. Considering the signal radiation case, the radiated energy streams from the source in radial lines. For one point (r,θ,ϕ) in the free space, the radiated energy flow per unit area and per unit time (W/m^2) is called *power density* $p(r,\theta,\phi)$. Therefore, the total signal power radiated can be calculated as

$$P = \int_0^{2\pi} \int_0^{\pi} p(r,\theta,\phi) r^2 \sin\theta d\theta d\phi. \tag{2.1}$$

If we define $U = p(r,\theta,\phi)r^2$ and substitute it into Eq. (2.1), then we obtain

$$P = \int_0^{2\pi} \int_0^{\pi} U \sin\theta d\theta d\phi. \tag{2.2}$$

From Eq. (2.2) we can find that U is independent of the radius r, that is $U = U(\theta,\phi)$. Furthermore, we can find that $U(\theta,\phi)$ denotes the radiated power per unit solid angle, which is called *radiation intensity*. Thus, the average radiation intensity can be defined as

$$U_0 = \frac{\int_0^{2\pi} \int_0^{\pi} U(\theta,\phi) \sin\theta d\theta d\phi}{4\pi}. \tag{2.3}$$

If an antenna is able to radiate the signal with an equal radiation intensity in any direction, that is $U(\theta,\phi) = U_0$, it is called as an *isotropic* source. However, there is no

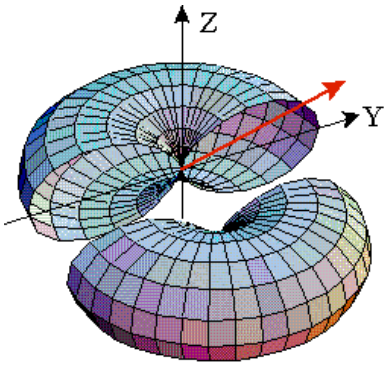

Figure 2.3: The normalized radiation intensity pattern of a half wavelength dipole antenna.

strictly isotropic antenna in reality. Therefore, the *directivity* D of an antenna is defined as

$$D = \frac{U_{\max}}{U_0}, \tag{2.4}$$

where $U_{\max}$ denotes the maximum radiation intensity. The widely-applied parameter, *antenna gain* G, is defined as

$$G = D \cdot \eta, \tag{2.5}$$

where η is called *radiation efficiency*. It is the ratio of the total radiated signal power to the signal power transferred to the antenna. As for the *antenna pattern*, it usually refers to one of the following two parameters: normalized radiation intensity $U(\theta,\phi)/U_{\max}$ or normalized electric field $E(\theta,\phi) = \sqrt{U(\theta,\phi)/U_{\max}}$, depending on the context if not specified. As a typical example, the normalized radiation intensity of the half wavelength dipole antenna is [42]

$$U_{\text{dipole}}(\theta,\phi) = [\frac{\cos(\pi/2 \cdot \cos\theta)}{\sin\theta}]^2, \tag{2.6}$$

whose 3-D pattern is illustrated in Fig. 2.3. From the figure we can see that this type of antenna is omni-directional in the horizontal X-Y plane (that is, its pattern is independent of the azimuth angle ϕ), but is directional in any vertical plane. According to Eqs. (2.3) and (2.4), we can calculate its directivity to be 1.64 (or 2.14 dB). It should be noted that an antenna like a half wavelength dipole is called to be omni-directional although it holds a directivity larger than 0 dB (since it is omni-directional in the horizontal plane). Other types of antennas that exhibit a high directivity in the horizontal plane or over the whole solid angle are called *directional antennas*. A typical directional antenna is the axial mode helical antenna (AMHA) described in Subsection 3.2.2.1. We should also distinguish the above directivity from the beamforming directivity described in Subsection 2.2.1, as the former is caused by the physical characteristic of the antenna itself while the latter results from the array signal processing.

2.1.2 RF front-end signal processing

In the following we apply the deterministic signal processing to reveal the signal conversion from RF signals to baseband signals. This is useful for understanding the beamforming realization described in Subsection 2.2.1. The conversion from baseband signals to RF signals is just a reverse process.

In wireless communications, the transferred information is carried by the (relative) amplitudes and phases of RF signals, that is

$$x_{\mathrm{RF}}(t) = v(t)\cos[2\pi f_{\mathrm{RF}}t + \varphi(t) + \varphi_0], \tag{2.7}$$

in which $x_{\mathrm{RF}}(t)$ is the RF signal, f_{RF} is the carrier frequency, $v(t)$ is the information-carrying amplitude, $\varphi(t)$ is the information-carrying phase, and φ_0 is the initial phase. Assume that the initial phase can be detected and compensated by the receiver circuits (that is, zero mismatch is realized), the RF signal can be expressed as

$$x_{\mathrm{RF}}(t) = \underbrace{v(t)\cos[\varphi(t)]}_{x_{\mathrm{i}}(t)}\cos(2\pi f_{\mathrm{RF}}t) - \underbrace{v(t)\sin[\varphi(t)]}_{x_{\mathrm{q}}(t)}\sin(2\pi f_{\mathrm{RF}}t), \tag{2.8}$$

in which $x_{\mathrm{i}}(t)$ and $x_{\mathrm{q}}(t)$ are baseband signals of the in-phase (I) and quadrature (Q) channels, respectively. For the heterodyne RF transceiver illustrated in Fig. 2.1, the RF signal will be first down-converted to the intermediate frequency (IF) signal $x_{\mathrm{IF,I}}(t)$ by multiplication with the RF oscillator signal $2\cos[2\pi(f_{\mathrm{RF}} - f_{\mathrm{IF}})t]$, and then bandpass filtered, that is

$$x_{\mathrm{IF,I}}(t) = x_{\mathrm{i}}(t)\cos(2\pi f_{\mathrm{IF}}t) - x_{\mathrm{q}}(t)\sin(2\pi f_{\mathrm{IF}}t). \tag{2.9}$$

Note that we use the subscript "IF,I" to denote that this is an I-channel IF signal. If the above RF oscillator signal is replaced by its 90^{o} shifted replica [64] $-2\sin[2\pi(f_{\mathrm{RF}} - f_{\mathrm{IF}})t]$, the Q-channel IF signal can be derived as

$$x_{\mathrm{IF,Q}}(t) = -x_{\mathrm{i}}(t)\sin(2\pi f_{\mathrm{IF}}t) - x_{\mathrm{q}}(t)\cos(2\pi f_{\mathrm{IF}}t). \tag{2.10}$$

It can be seen that $x_{\mathrm{IF,Q}}(t)$ is only a $\pi/2$ delayed replica of $x_{\mathrm{IF,I}}(t)$. Therefore, they are redundant signals that carry the same information and contain both $x_{\mathrm{i}}(t)$ and $x_{\mathrm{q}}(t)$. That is why $x_{\mathrm{IF,Q}}(t)$ is not generated by the heterodyne RF transceiver illustrated in Fig. 2.1. In the I/Q demodulator, $x_{\mathrm{IF,I}}(t)$ is further down-converted and separated as $x_{\mathrm{i}}(t)$ and $-x_{\mathrm{q}}(t)$ that enter into the baseband processor. Recently, many wireless communication systems apply the so called homodyne RF transceiver structure that skips the RF/IF converter and directly converts RF signals into baseband signals. The comparison between those two structures is given in [64] in detail.

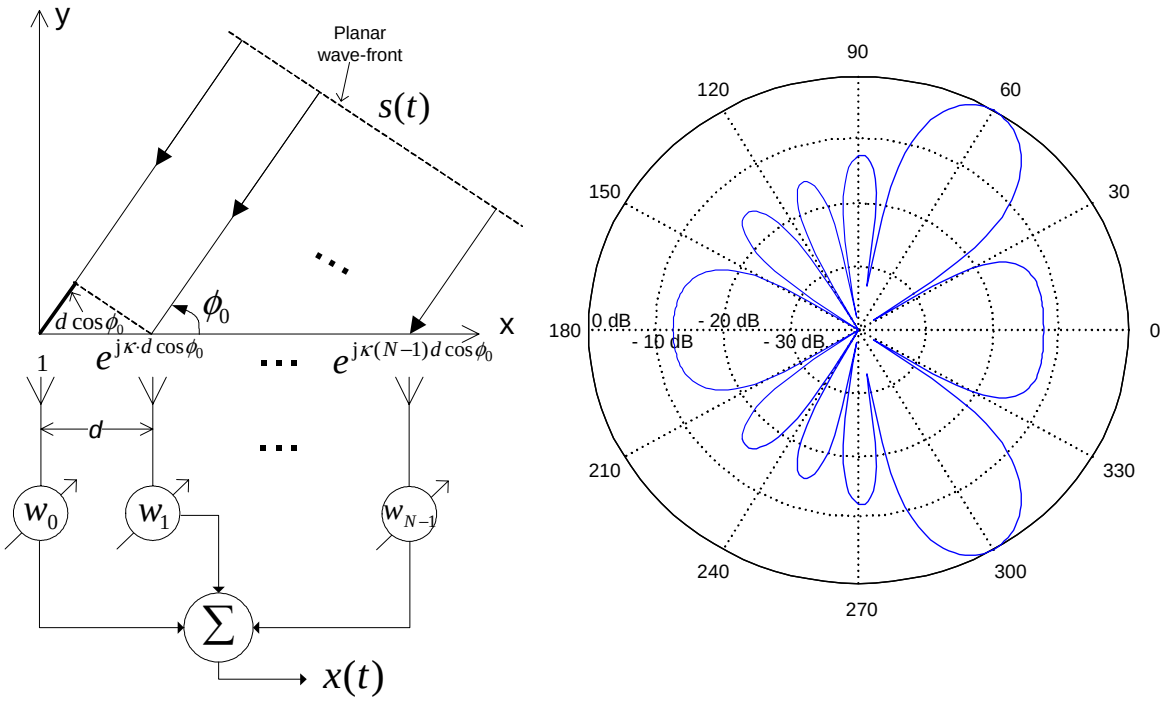

Figure 2.4: Principle of an N-element smart antennas system with a uniform linear array (ULA) configuration and an exemplary radiation intensity pattern (on the horizontal plane) for the incident signal from the direction of 60°, when N equals 6 and d equals the half wavelength.

2.2 Smart antennas (beamforming)

2.2.1 Basic principle

A smart antennas system places emphasis on the array radiation intensity pattern. The capability that makes the system "smart" is to direct the main beam to the desired user and/or put nulls to the interferences without mechanically changing the orientation of the system. This requires to use an antenna array (instead of one antenna) and an array signal processing unit. In the following, we apply a simple example to explain the basic principle of smart antennas. It is worthwhile to note that although receive beamforming is mainly considered in this chapter, transmit beamforming is just its reciprocal process (in case that the direction-relevant information is known in advance). Therefore, they share the basic properties described below.

Fig. 2.4 illustrates an N-element smart antennas system with a uniform linear array (ULA) configuration. The distance between adjacent antennas is d, the carrier wavelength is λ, and the wavenumber is $\kappa = 2\pi/\lambda$. For simplicity, we only consider the horizontal plane and assume that the signal $s(t)$ impinges with the elevation angle

90° and the azimuth angle ϕ_0. If $s(t)$ impinges on the antenna array with a planar wave-front, then the n-th antenna signal experiences a phase shift $+\kappa(n-1)d \cdot \cos\phi_0$ on its carrier compared to the first antenna signal, because its propagation range is $(n-1)d \cdot \cos\phi_0$ shorter. As the size of the antenna array is greatly less than the signal propagation range, the slight variance on amplitude due to $(n-1)d \cdot \cos\phi_0$ is negligible. Therefore, the *array response vector* is

$$\mathbf{a}(\phi_0) = \begin{pmatrix} 1 & e^{\mathrm{j}\kappa d\cdot\cos\phi_0} & \dots & e^{\mathrm{j}\kappa(N-1)d\cdot\cos\phi_0} \end{pmatrix}^{\mathrm{T}}, \tag{2.11}$$

in which $(\cdot)^{\mathrm{T}}$ represents the transpose of a vector. The array response vector is relevant to the antenna array configuration and the signal incident angle ϕ_0. The received signals $s(t)\mathbf{a}(\phi_0)$ of the array are first weighted with a weighting coefficients vector $\mathbf{w}$ and then combined to generate the output signal

$$x(t) = \mathbf{w}^{\mathrm{T}} s(t)\mathbf{a}(\phi_0) + n(t), \tag{2.12}$$

where $n(t)$ denotes the output noise signal. We can find that if the weighting vector $\mathbf{w}$ is chosen to be the complex conjugate of the array response vector $\mathbf{a}(\phi_0)$ of the incident angle ϕ_0, that is

$$\mathbf{w}(\phi) \mid_{\phi=\phi_0} = \mathbf{a}^*(\phi_0), \tag{2.13}$$

then the signals impinging from the direction ϕ_0 on all antennas will be cophased and combined constructively. The way to calculate the weighting vector $\mathbf{w}$ (e.g., Eq. 2.13) is referred to as a *beamforming* algorithm. As a consequence, the radiation intensity pattern with its main beam pointing to ϕ_0 can result. Fig. 2.4 illustrates the radiation intensity pattern of a six-element ULA if the weighting vector of Eq. (2.13) is used and ϕ_0 equals 60°. From it we can see that the signals from directions other than 60° and 300° will be suppressed at least by 12 dB. The figure also reveals one drawback of ULAs, the front-back symmetry, which can be alleviated by using individual directional elements with suitable front-back ratios [49] (but this measure reduces the covered angle range to half), or be eliminated by applying other types of array configurations, e.g., the circular array [3] or some others as in [47]. If the consideration on the elevation angle is required, a more sophisticated 3-D analysis model must be used. The analysis on the 3-D radiation intensity pattern for the N-element circular array has been made in [3]. It is worthwhile to mention the concept array factor (AF) that is emphasized in [3]. AF represents the influence caused by the array processing on the final array pattern, which can be written as

$$\mathrm{AF}(\phi,\phi_0) = \frac{\mid \mathbf{w}^{\mathrm{T}}(\phi_0)\mathbf{a}(\phi) \mid}{\mid \mathbf{w}^{\mathrm{T}}(\phi_0)\mathbf{a}(\phi_0) \mid}, \tag{2.14}$$

in which ϕ_0 denotes the beam peak direction. Given an array of identical antenna elements, the total array (electric field) pattern is

$$E_{\text{total}} = E_{\text{single}} \cdot \text{AF}(\phi,\phi_0), \tag{2.15}$$

in which E_{single} is the electric field pattern of the individual antenna element. Under the assumption that each antenna is an isotropic element, that is $E_{\text{single}} = 1$, the final array radiation intensity pattern is

$$U_{\text{total}} = 20\log(\text{AF}(\phi,\phi_0))/\text{dB}. \tag{2.16}$$

An example is illustrated in Fig. 2.4. Two premises for smart antennas may also be inferred by Fig. 2.4:

1. Far field assumption. This states that the array signal processing is designed for waveforms coming from the far-field ($>$ many wavelengths) as opposed to the near field. This allows the designer to treat any propagating waveform impinging on the antenna array as a planar wave-front, thus implying that the signal propagating difference between two antenna elements can be characterized as a pure delay (phase change). The signal is assumed to have an equal intensity at any point on the planar wave-front.

2. Narrowband assumption. The structure of the smart antennas system given in Fig. 2.4 is only appropriate for narrowband signals. Imagine if a wideband signal impinges on the array, then the array response vector $\mathbf{a}(\phi_0)$ of Eq. (2.11) may cause significant offsets for the frequency components on the upper and low sides of the spectrum (because the wavelength λ of the middle of the spectrum is used usually). This assumption can be analytically examined based on the observation time-bandwidth product (TBWP) of the antenna array aperture. The observation time interval is defined as the time required for a plane waveform to travel completely across the antenna array aperture. This is a function of the signal angle-of-arrival (AOA). TBWP is the product of the observation interval and the signal bandwidth. For a signal to be considered as narrowband for the array, TBWP should be much less than one for all AOAs [79].

The above conditions also imply that the received spatial signals must be sufficiently correlated from one end of the array to the other. This distinguishes the smart antennas techniques from the space diversity techniques. A wideband beamforming scheme is also given in [79]. The basic idea is to first decompose the impinging wideband signals into a number of narrowband components and then perform (traditional narrowband) beamforming on each component independently, and finally compose them

together. This decomposition structure can be realized in either frequency or time domain.

Recall the analysis made in Subsection 2.1.2 and compare it with the above analysis, we may find that the above signal $s(t)$ exactly corresponds to the RF signal $x_{\mathrm{RF}}(t)$. It seems that calculating the coefficients and weighting and combining the array signals can only be carried out at the RF stage, and the output signal $x(t)$ is still an RF signal. However, it is not true in reality. The array response vector $\mathbf{a}(\phi_0)$ of Eq. (2.11) implies that the received signal on the n-th antenna element has experienced a time delay τ_n, which results in a phase shift φ_n on its carrier (note: τ_n is negative for the special case of Fig. 2.4). That is,

$$\varphi_n = -2\pi f_{\mathrm{RF}}\tau_n = \kappa(n-1)d\cos\phi_0. \tag{2.17}$$

In general, corresponding to the delayed RF signal $x_{\mathrm{RF}}(t-\tau_n)$ with a time delay τ_n, its down-converted IF signal can be derived as (refer to Appendix B)

$$x_{\mathrm{IF,I}}(t-\tau_n) = x_{\mathrm{i}}(t-\tau_n)\cos[2\pi(f_{\mathrm{IF}}t - f_{\mathrm{RF}}\tau_n)] - x_{\mathrm{q}}(t-\tau_n)\sin[2\pi(f_{\mathrm{IF}}t - f_{\mathrm{RF}}\tau_n)], \tag{2.18}$$

which reveals that the time delay τ_n remains on the baseband components and the phase shift $\varphi_n = -2\pi f_{\mathrm{RF}}\tau_n$ remains on the IF carrier signal. Therefore, we can conclude that at the IF stage the array response vector (Eq. 2.11) still holds and the exemplary beamforming algorithm (Eq. 2.13) is still valid. Furthermore, the weighting and combining process (Eq. 2.12) can also be performed at the IF stage. As for the baseband beamforming, this process is easier to understand by applying the analytic signal representation. The n-th antenna's analytic baseband signal is (refer to Appendix B)

$$x_{\mathrm{BB}}(t-\tau_n) = [x_{\mathrm{i}}(t-\tau_n) + \mathrm{j}x_{\mathrm{q}}(t-\tau_n)]e^{\mathrm{j}\varphi_n}, \tag{2.19}$$

from which we can see that the phase shift φ_n on the RF or IF carrier signal is still kept by the delayed analytical baseband signal.

Based on the above analysis we may infer that from the signal processing point of view there is no difference when beamforming is performed at the RF, IF, or baseband stage. However, it is significantly different in practice. It is desirable that beamforming is performed directly at the RF stage, since in this case all RF propagation characteristics are fully kept and the calibration requirement on receiver branches is low. But digital RF signal processing still faces severe difficulties due to high requirements on sampling rate and impedance matching. That is why analog beamforming is usually applied at the RF stage, which however limits the system complexity and performance. Digital beamforming is easier to realize at the baseband stage, but this scheme imposes a high calibration requirement on receiver branches. Furthermore, many RF characteristics may be lost in the course of conversion from RF to baseband, and noises are also

inserted in this course. In literature, analog or digital beamforming performed at the IF stage is generally applied. It seems that IF beamforming can benefit from a good tradeoff between RF and baseband beamforming.

It is worthwhile to note that the time delay τ_n on the baseband components is usually ignored because it is too small compared to their period (as the bandwidth is much smaller than the carrier frequency). That is, $x_{\mathrm{i}}(t-\tau_n)$ and $x_{\mathrm{q}}(t-\tau_n)$ are usually treated as $x_{\mathrm{i}}(t)$ and $x_{\mathrm{q}}(t)$, respectively. This technical approximation is permitted by the aforementioned narrowband assumption. Imaging that if τ_n becomes significant, usually occurring for wideband signals, the array signals combination can result in distortion because their baseband components are differently delayed. However, this distortion can be removed by a simple equalization scheme since those delays (τ_n, $n = 0...N-1$) are related with phase shifts φ_n, $n = 0...N-1$ and therefore are known beforehand.

In summary, the design of a smart antennas system may boil down to the following three aspects:

- The beamforming algorithm to calculate the weighting vector $\mathbf{w}$;
- The way to weight and combine the array signals (analog or digital beamformer);
- At which stage the above two operations are carried out: RF, IF or baseband.

In the following, two functionally classified categories of smart antennas, switched beam and steered beam, will be introduced in terms of the above three aspects.

2.2.2 Switched beam (fixed beamforming)

The distinguishing characteristic of a switched beam system is that its directional beams are pre-defined. This imposes less requirements on system complexity at the cost of inferior performance compared to a steered beam system. The basic principle is as follows: K weighting vectors $\mathbf{w}_k$, $k = 0, \ldots, K-1$ are designed in advance, each of which corresponds to a directional pattern with the main beam pointing to the specific direction. Usually K multiple beams cover a desired (plane or solid) angular domain, e.g., 360° around the system. During reception, a "sniffer" is used to go through all beams and determine the one that exhibits the best signal quality, with the assistance of a switch. The best beam is then switched on to receive the data. Whether the system can be used for transmission depends on whether the beamformer is bi-directional. Usually the beamformer is realized at the RF stage for switched beam systems, which makes the use of multiple RF front-ends unnecessary. A key aspect of switched beam systems is which kind of criterion is used to compare the signal

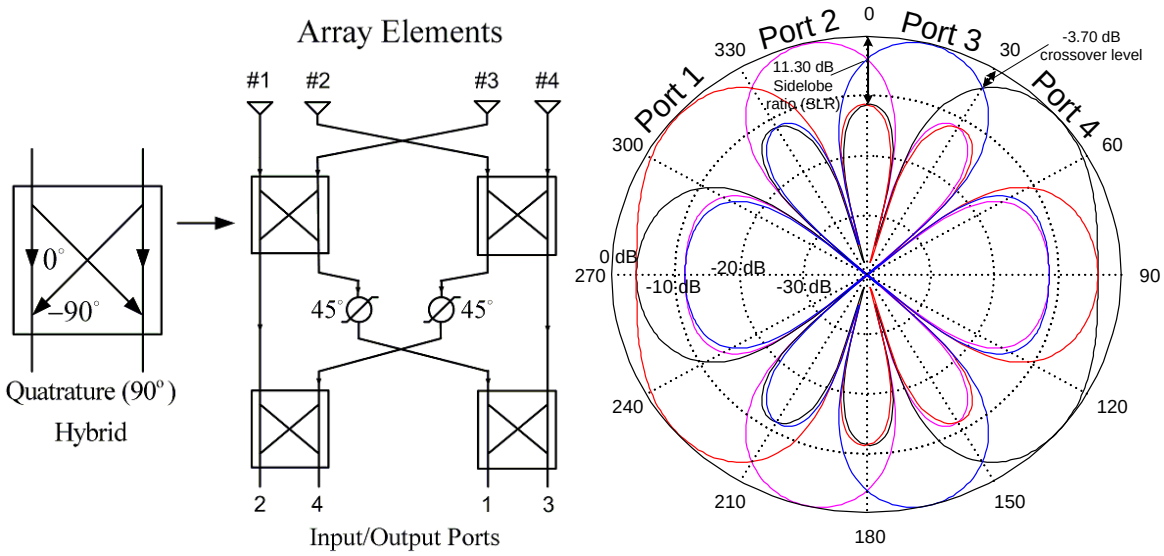

Figure 2.5: A four-element Butler matrix fixed beamforming system and its radiation intensity pattern (with the half wavelength antenna space) [49].

	#1	#2	#3	#4	equivalent weighting vector
Port 1	$-45°$	$-180°$	$45°$	$-90°$	$\mathbf{w}_1 = (\ e^{-\mathrm{j}\pi/4} \quad e^{-\mathrm{j}\pi} \quad e^{\mathrm{j}\pi/4} \quad e^{-\mathrm{j}\pi/2}\ )^{\mathrm{T}}$
Port 2	$0°$	$-45°$	$-90°$	$-135°$	$\mathbf{w}_2 = (\ 1 \quad e^{-\mathrm{j}\pi/4} \quad e^{-\mathrm{j}\pi/2} \quad e^{-\mathrm{j}3\pi/4}\ )^{\mathrm{T}}$
Port 3	$-135°$	$-90°$	$-45°$	$0°$	$\mathbf{w}_3 = (\ e^{-\mathrm{j}3\pi/4} \quad e^{-\mathrm{j}\pi/2} \quad e^{-\mathrm{j}\pi/4} \quad 1\ )^{\mathrm{T}}$
Port 4	$-90°$	$45°$	$-180°$	$-45°$	$\mathbf{w}_4 = (\ e^{-\mathrm{j}\pi/2} \quad e^{\mathrm{j}\pi/4} \quad e^{-\mathrm{j}\pi} \quad e^{-\mathrm{j}\pi/4}\ )^{\mathrm{T}}$

Table 2.1: The phase shift on each route between the four antenna elements and the four ports of the beamforming system in Fig. 2.5 [49].

qualities of the K beams, and a further expectation is the ability to distinguish the desired user signal from the co-channel interference (CCI). This will be elaborated in Subsection 4.3.5.

It is necessary to distinguish the switched beam system from the multi-directional-antenna system described in Subsection 3.2.2.1. The former directional beam is generated by beamforming (array signal processing) while the latter results from the physical characteristic of individual antenna elements.

2.2.2.1 Butler matrix

Proposed by Butler in 1961, the Butler matrix is a typical switched beam system. The essential idea is to apply the Woodward-Lawson synthesis method to generate a set of weighting vectors, and the corresponding beamformers can be realized at the RF stage by applying the usual RF components like Hybrid coupler and phase shifter. For the

details of Woodward-Lawson synthesis and Butler matrix designs, refer to [54, 23, 49] and the references therein.

Fig. 2.5 illustrates a four-element Butler matrix switched beam system and its RF beamformer components, including four 90° hybrid couplers and two 45° phase shifters. Tab. 2.1 lists the phase shift on each route between the four antenna elements and the four RX/TX ports, and the equivalent four weighting vectors. It can be easily shown that those four weighting vectors are mutually orthogonal, that is

$$\mathbf{w}_i^{\mathrm{H}}\mathbf{w}_j = 0, \quad \text{for} \quad i \neq j, \quad i,j = 1,\ldots,4 \ , \tag{2.20}$$

where $(\cdot)^{\mathrm{H}}$ represents the Hermitian transpose. This property is also exhibited by the array radiation intensity pattern illustrated in Fig. 2.5. We can see that the peak of each beam always corresponds to the nulls of other three beams. The above array radiation intensity pattern is obtained under the assumption that a ULA with the half wavelength space d is used and each antenna element is omni-directional. Again, we can find the drawback of front-back symmetry, which can be alleviated by using the directional elements like patch antennas [54, 7]. This array gives a 11.30 dB sidelobe ratio (SLR) and -3.70 dB crossover level [23]. Woodward-Lawson type beams generate a relatively small SLR, which can be improved by combining two beams [54]. It is worth mentioning that the Butler matrix beamforming is bi-directional, which means that each port corresponding to a particular receive beam pattern can also be used for transmitting using the same beam pattern.

2.2.3 Steered beam (adaptive beamforming)

Compared to switched beam, steered beam has the advantage of directing the main beam to the user located in any direction and/or putting nulls in the directions of interferences, hence called adaptive beamforming. In the following, we first focus on describing three types of beamforming algorithms (that calculate the weighting vectors), and then use some examples to describe the other two aspects: beamformer realization and the operating stage (RF, IF or baseband). It should be noted that in most of the literature discussing beamforming, the weighting vector is defined as

$$\mathbf{w} = (\ w_0 \quad \ldots \quad w_{N-1}\ )^{\mathrm{H}} \tag{2.21}$$

instead of $\mathbf{w} = (\ w_0 \quad \ldots \quad w_{N-1}\ )^{\mathrm{T}}$ used above (Subsections 2.2.1 and 2.2.2.1) for the convenience of matrix and vector calculation. From now on, we will use the traditional definition of Eq. (2.21). Therefore, the array factor of Eq. (2.14) should be rewritten as

$$\mathrm{AF}(\phi,\phi_0) = \frac{|\ \mathbf{w}^{\mathrm{H}}(\phi_0)\mathbf{a}(\phi)\ |}{|\ \mathbf{w}^{\mathrm{H}}(\phi_0)\mathbf{a}(\phi_0)\ |}. \tag{2.22}$$

2.2.3.1 DOA-based beamforming

If the signal $s_1(t)$ impinges on an antenna array from the line-of-sight (LOS) direction ϕ_1 and $N_\mathrm{m}-1$ multipath directions ϕ_l, $l = 2,...,N_\mathrm{m}$, then the total received signal vector can be written as

$$\mathbf{x}(t) = \underbrace{\alpha_1 \mathbf{a}(\phi_1) s_1(t)}_{\text{direct path}} + \underbrace{\sum_{l=2}^{N_\mathrm{m}} \alpha_l \mathbf{a}(\phi_l) s_1(t)}_{\text{multipath}} = \mathbf{a}_1 s_1(t), \tag{2.23}$$

in which the complex α_l denotes the phase and amplitude difference between the l-th multipath and the direct path (while α_1 equals 1), $\mathbf{a}(\phi_l)$ denotes the array response vector for the signal from ϕ_l, and $\mathbf{a}_1 = \sum_{l=1}^{N_\mathrm{m}} \alpha_l \mathbf{a}(\phi_l)$ is referred to as the spatial signature (SS) associated with the signal $s_1(t)$ [32]. The essential of DOA-based beamforming is to generate a weighting vector $\mathbf{w}$ such that the combined LOS signal $\mathbf{w}^\mathrm{H}\mathbf{a}(\phi_1)\alpha_1 s_1(t)$ is strengthened, and/or other multipath and interference signals are suppressed. This requires $\mathbf{w}$ to be parallel with $\mathbf{a}(\phi_1)$ and/or orthogonal with $\mathbf{a}(\phi_l)$, $l = 2,...,N_\mathrm{m}$.

The first task of DOA-based beamforming is DOA (direction of arrival) estimation. The early methods are based on the concept of measuring the signal power received from each direction, and the direction with the maximum signal power is determined as the DOA (such a method is applied by the MAC protocol described in Subsection 3.2.1.2). These methods are inherently simple, but suffer from low resolution. The superior algorithms apply the eigen-decomposition of the array covariance matrix of the received data to extract DOA. The most popular methods that fall under this class are MUSIC (multiple signal classification) and ESPRIT (estimation of signal parameters via rotational invariance techniques), see [19] and references therein. They can achieve high-resolution DOA estimation at the cost of much heavier computational load. Further description on this topic is beyond the scope of this thesis. A comprehensive survey has been given in [19]. Other than the intensive computation, they also require a sufficient observation time for the accurate estimation [6]. It should be noted that the number of signals whose directions can be resolved, N_DOA, is restricted for an N-element antenna array. For most algorithms $N_\mathrm{DOA} < N$ holds (e.g., [33, 72]), however in [48] the opposite relation holds due to the processing gain. In practice, the number of directions an array may resolve depends not only on N but also on the array geometry, the available number of snapshots and the spatial distribution of the sources (for details refer to [19] and references therein).

Assume that the DOA of the signal-of-interest (SOI, direct path of the user signal) and/or the DOAs of the signal-not-of-interest (SNOI, including the user multipath signals and co-channel interference) are known at the receiver, mainly there are three types of DOA-based beamforming algorithms:

- The dominant DOA approach [32]. This algorithm only requires the DOA of SOI ϕ_1. Hence, its array response vector $\mathbf{a}(\phi_1)$ can be derived according to the array configuration. The weighting vector $\mathbf{w}$ is just chosen to be $\mathbf{a}(\phi_1)$ to maximize $|\mathbf{w}^{\mathrm{H}}\mathbf{a}(\phi_1)|$. This algorithm only intends to strengthen the desired signal. The same way is used in Eq. (2.13) and an exemplary radiation intensity pattern is illustrated in Fig. 2.4.

- The pseudoinverse DOA approach [32]. In contrast to the first algorithm, this approach requires all DOAs of SNOI (e.g., ϕ_2 and ϕ_3), and their array response vectors ($\mathbf{a}(\phi_2)$ and $\mathbf{a}(\phi_3)$) are derived afterwards. The pseudoinverse of those array response vectors can be applied to obtain the final weighting vector $\mathbf{w}$ such that $\mathbf{w}\perp\mathbf{a}(\phi_2)$ and $\mathbf{w}\perp\mathbf{a}(\phi_3)$. This algorithm intends to suppress the SNOI.

- Minimum variance distortionless response (MVDR) beamforming [19, 6]. This approach only requires the DOA of SOI ϕ_1. It minimizes the beamformer average output power $\mathcal{E}[|\mathbf{w}^{\mathrm{H}}\mathbf{x}(t)|^2]$ $(=\mathbf{w}^{\mathrm{H}}\mathbf{R}_{xx}\mathbf{w})$, subject to maximize $|\mathbf{w}^{\mathrm{H}}\mathbf{a}(\phi_1)|$ (that is, to reach its normalized value 1). The solution is given as $\mathbf{w} = (\mathbf{R}_{xx}^{-1}\mathbf{a}(\phi_1))/(\mathbf{a}^{\mathrm{H}}(\phi_1)\mathbf{R}_{xx}^{-1}\mathbf{a}(\phi_1))$, in which $\mathbf{R}_{xx}$ is the spatial correlation matrix $\mathcal{E}[\mathbf{x}(t)\mathbf{x}^{\mathrm{H}}(t)]$ [6]. This algorithm outperforms the first one at the cost of more complex computation. Its essential is to minimize the power of SNOI by minimizing the entire power while still keeping the power of SOI.

Compared to the above algorithms, two spatial signature (SS) based algorithms proposed in [32] are inferior but much less complex, since not DOAs but SSs of the desired signal ($\mathbf{a}_1$ of Eq. 2.23) and/or interference signals (e.g., $\mathbf{a}_2$ and $\mathbf{a}_3$) are required. SS can be easily obtained via a singular value decomposition (SVD) of the data matrix $\mathbf{X} = (\mathbf{x}_1,...,\mathbf{x}_N)$ or an eigenvalue decomposition of the sample covariance matrix $\mathbf{R}_x = \frac{1}{N}\mathbf{X}\mathbf{X}^{\mathrm{H}}$ [33]. The first SS-based algorithm applies the complex conjugate of the SS as the weighting vector, that is $\mathbf{w} = \mathbf{a}_1^*$, to maximize the desired signal power. And the second one calculates the weighting vector by applying the pseudoinverse of all spatial signatures.

2.2.3.2 Temporal-reference-based beamforming

Different from the DOA-based algorithms, temporal-reference-based beamforming methods apply a known training sequence to adjust the weighting vector $\mathbf{w}$ such that the combined signal keeps the fidelity of SOI and rejects SNOI as much as possible. The advantage of this kind of beamforming algorithm is that no distinct DOAs are required and thus the angular spread of the signal is of less influence. There are two basic types:

- DMI (direct matrix inversion) [49, 65]. This algorithm treats the received array signal vectors $\mathbf{x}(t_q)$, $q = 1,...,Q$ within the training sequence length Q as

an observation block. First the correlation matrix of the received array vector $\mathbf{R} = \mathcal{E}[\mathbf{x}(t_q)\mathbf{x}^{\mathrm{H}}(t_q)]$ and the corss-correlation vector between the received vector and the corresponding training sequence $\mathbf{p} = \mathcal{E}[d^*(t_q)\mathbf{x}(t_q)]$ are calculated. The minimum mean square error (MMSE) criteria is used to minimize the cost function $\mathcal{E}[|\mathbf{w}^{\mathrm{H}}\mathbf{x}(t_q) - d(t_q)|^2]$, which outputs the solution $\mathbf{w} = \mathbf{R}^{-1}\mathbf{p}$.

- LMS (least mean square) [6, 19] is a kind of iterative algorithm that gradually adapts the weighting vector to approach the optimal solution so that the power of the error signal $\varepsilon(t_q) = d(t_{q+1}) - \mathbf{w}^{\mathrm{H}}(t_q)\mathbf{x}(t_{q+1})$ is minimized. The updating solution is $\mathbf{w}(t_{q+1}) = \mathbf{w}(t_q) - 2\mu\mathbf{x}(t_{q+1})\varepsilon^*(t_q)$, $q = 0,...,Q-1$. μ is the convergence factor (or called gradient step) that should be selected very carefully. An intensive discussion on it is given in [19].

Many modified algorithms based on the above two types have been presented in [19, 65]. LMS imposes the least computation complexity of $\mathcal{O}(Q)$, while the complexity of DMI $\mathcal{O}(Q^3)$ is significantly higher [65].

2.2.3.3 Blind beamforming

There are a broad class of blind beamforming algorithms allowing the operation without training sequence, which use underlying characteristics of the signal structure, such as constant modulus or spectral self-coherence to update the weighting vector $\mathbf{w}$. A wide discussion on this topic has been made in [49]. In general, the comparative computation complexity of such algorithms is more than $\mathcal{O}(Q^2)$, stands between LMS and DMI [65]. It should be noted that although the known training sequence is not required, blind beamforming still needs a dedicated duration for converging to the optimal weighting vector, and the convergence rate is usually slower than LMS [37].

2.2.3.4 Some test-bed trials on steered beam

After the above discussions on various beamforming algorithms, other two aspects of steered beam systems, beamformer realization and operating stage, will be discussed in this subsection using some examples from literature.

Most of the steered beam systems realize the beamformer at the IF or baseband stage except one type, phased array antennas that usually do it at the RF stage. The Butler matrix described in Subsection 2.2.2.1 can be regarded as a wide-sense phased array antennas system, while its beamforming is fixed (switched beam). In general, phased array antennas apply digitally controlled phase shifters and RF power combiner/divider to realize beamformer at the RF stage, and the control signals for phase shifters are supplied by the beamforming unit. A wide discussion regarding

phased array antennas has been given in [23]. The recent efforts in this domain focus on the miniaturization of such systems by integrating all components on a single silicon substrate when an extremely high carrier frequency (e.g., 43.763 GHz) is applied [24]. However, such designs may suffer from the low radiation efficiency.

A broad-band (20 Mbit/s data rate applying BPSK with about 90 MHz bandwidth in total) smart antennas test-bed operating on 5.8 GHz has been demonstrated in [34]. An eight-element half wavelength space ULA is used and each antenna is equipped with an individual I/Q RF-IF down-converter. Only the In-phase (I) IF signals are digitalized and used for DOA estimation and beamforming, since the corresponding quadrature (Q) IF signals can be recovered by Hilbert transform. This way reduces the I/O load, but increases the processing overhead. MUSIC and ESPRIT are selected as the DOA estimation algorithms and the pseudoinverse DOA approach is selected as the beamforming algorithm (see Subsection 2.2.3.1). The calculated weighting coefficients for both I/Q IF signals are converted by D/A converters to control the analog beamformer at the IF stage. The use of both I/Q IF signals solves the problem of adjusting both amplitude and phase of each branch signal by the analog beamformer. Compared to the full digital beamforming system, this solution has the disadvantage that when multiple outputs in different beams are needed, the analog beamformer has to be replicated for each output. A PC instead of the real-time DSP is used to execute the DOA estimation and beamforming algorithms offline. Therefore, the test-bed is not yet a real-time communication system.

A digital beamforming smart antennas test-bed operating on 900 MHz has been demonstrated in [33, 32]. An eight-element patch antenna half wavelength space ULA is used, and each antenna is equipped with a RF-to-baseband converter. In the RX mode, eight digitalized baseband signals are processed for DOA estimation and beamforming, and the beamformer is realized digitally afterwards. The corresponding components for TX beamforming are also available. ESPRIT is applied as the DOA estimation algorithm, and the DOA-based algorithms described in Subsection 2.2.3.1 (except MVDR) are applied for beamforming. However, only some characteristics of the combined baseband signal, e.g., spatial signature, gain and SIR, are investigated and data are not extracted. Therefore, the test-bed is not yet a digital communication system, and its bandwidth is not given in the paper. One important conclusion drawn is that the spatial signature (SS) changes significantly with the carrier frequency, which implies that the SS-based beamforming is not suitable for a FDD (frequency division duplex) system. This also bears out that beamforming is very sensitive to the carrier frequency. A Sparc 10 workstation is used for the array signal processing.

A particular smart antennas system called electronically steerable parasitic array radiator (ESPAR) has been presented in [71]. Unlike most smart antennas systems that try best to compensate the mutual coupling effects between antenna elements [34, 11, 82],

this system makes use of the strong coupling among the active center antenna and six varactor loaded parasitic antenna elements. The beamformer (array signals weighting and combining) is inherently carried out at the RF stage by the coupling effect, and the sole RF port is used for data TX/RX. The weighting coefficients can be controlled by changing the load reactance of each parasitic antenna. This scheme exhibits the great advantage of eliminating the necessity of multiple RF front-ends that all other digital beamforming systems require. The MUSIC algorithm can be successfully realized on this scheme, however it is still not efficient enough for real time implementation. Therefore, a temporal-reference-based beamforming algorithm called SPSA is applied on the test-bed, whose essential is similar to the LMS algorithm, however applied with a stochastic processing fashion. That is, a sample block for SPSA instead of a single sample value for LMS is used for each iteration to calculate the mean square error. The test-bed shows that a training sequence with the 5000-bit length (for 50 iterations) can achieve a good convergence. The training sequence with 500 Kbit/s data rate is used, and the TMS320C6701 DSP chip is applied for executing beamforming algorithms at baseband. For each iteration, 100 bits training sequence are used, which consume 0.2 ms to acquire. However, another 32.564 ms must be waited as the guard time to let the DSP execute the beamforming algorithm and change the load reactance of six parasitic antennas accordingly. Therefore, each beamforming process requires 1638.2 ms in total for the present test-bed, which can be reduced to 10 ms regardless of the guard time (assume the future DSP is so fast that the guard time can be ignored). This duration is however still significant even for the current mobile communication standards (e.g., in GSM the slot duration is 0.577 ms and the symbol period is 3.7 μs; and in IS-54 the slot duration is 6.66 ms and the symbol period is 41.6 μs [59]).

2.3 Space diversity techniques

2.3.1 Basic principle

We have mentioned that smart antennas systems emphasize the generated radiation intensity pattern, which directs the peak to the direction of SOI (signal-of-interest) and nulls to the directions of SNOI (signal-not-of-interest). Hence, array gain and interference suppression gain (together called beamforming gain) can be obtained. However, imagining that if a signal arrives with a broad range of directions around the receiver (e.g., 360°) in the horizontal plane and the incident power is uniformly distributed over those directions (the Clarke's scenario [13, 31]), then a smart antennas (beamforming) system cannot work effectively since there are no appropriate directions for pattern peak and nulls. The above condition occurs widely in indoor or urban scenarios that suffer from the rich scattering effect [58], which can be described by the

Rayleigh fading model if no LOS (line of sight) exists [59]. In such scenarios, another category of multi-antenna techniques, space diversity techniques, can be applied to increase the link robustness in terms of the reduced BER (bit error rate), hence lead to diversity gain. A space diversity system redundantly transmits the message by multiple antennas, and signals at the receiver are combined with a dedicated method so that the best signal quality is ensured. In general, two criteria can be used to determine whether a scenario is suitable to beamforming or space diversity:

- *Angle spread* refers to the spread of angles of arrival of the multipaths at a receiver, and the spread of departure angles of the multipaths at a transmitter [59]. For mobile telecommunications systems, the typical values of angle spread in the indoor and mall scenarios reach 360° and 120°, respectively [58]. The experimental studies in [33] show that the RMS (root mean square) angle spread measured in the stationary indoor environment and the outdoor environment without LOS reach 10.03° and 24.88°, respectively. And the authors concluded that the DOA-based beamforming techniques may not be very effective in those two environments. However, there is no explicit threshold on angle spread found in literature, and the angle spread may strongly vary with time in a mobile scenario. Anyhow, angle spread can be used for a rough judgement.

- *Antenna correlation* refers to the signal envelope correlation between two antennas spaced with d. The essential idea behind space diversity is as follows: if several replicas of the same information-carrying signal are received by multiple antennas with a comparable mean power but exhibiting independent fading, then there is a high probability that one or more antennas will not experience deep fading at any given moment. This requires a high decorrelation between multiple antennas. On the contrary, beamforming requires a high correlation between multiple elements of the array, as described in Subsection 2.2.1. Fig. 2.6 illustrates the envelope correlation $J_0^2(2\pi d/\lambda)$ between two antennas with the relative distance d/λ (where J_0 is the first kind zero order Bessel function and λ denotes the carrier wavelength). It should be noted that this result is only valid in the Clarke's scenario mentioned above (can be approximately regarded as a Rayleigh fading scenario). From Fig. 2.6 we can see that a $\lambda/2$ space array can achieve a very small correlation (about 0.1). A further investigation on space correlation has been given in [36]. In non-ideal practical situations, the branch correlation and unequal mean branch power will result in a loss of diversity gain. A correlation of 0.7 is considered acceptable [58]. Furthermore, a dedicated decorrelation measure can be used to compensate this loss [51].

Comparing with beamforming smart antennas systems, space diversity exhibits the superiority on wideband applications because it is not so sensitive to the carrier frequency

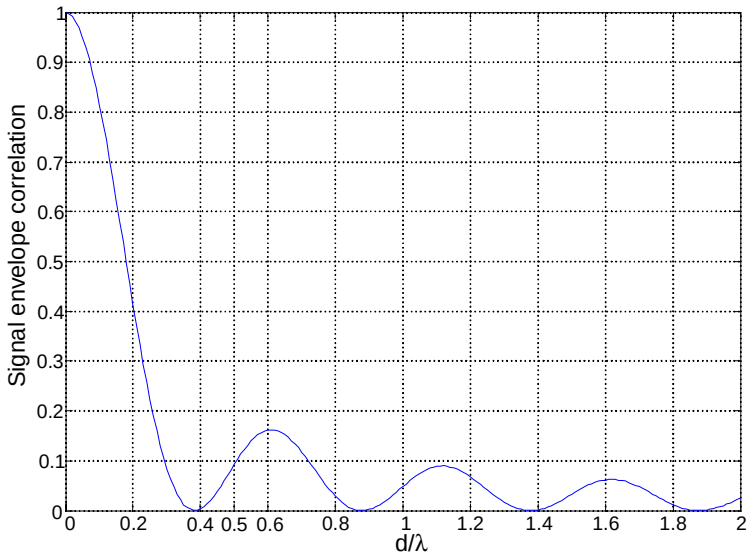

Figure 2.6: Envelope correlation versus spacing in the Clarke's scenario [13, 31].

as beamforming. Moreover, beamforming is strictly dependent on the antenna array configuration, while space diversity only requires a low correlation between antennas. In [81] it is revealed that for a rate-oriented MIMO system that only applies spatial multiplexing, its performance is nearly independent of small details of the array geometry. This also holds for a space diversity system. Roughly speaking, beamforming is proper for narrowband applications in a weak fading scenario, while space diversity is proper for narrow-/wideband applications in a deep fading scenario. However, beamforming and space diversity combining are sometimes used interchangeably in literature (e.g., [65]), because the resulting algorithms are similar [4]. In fact, beamforming can be regarded as a wide-sense space diversity technique because they hold the same property of transmitting or receiving the same information over multiple antennas. In [7], the performance of the LMS beamforming algorithm in a Rayleigh fading scenario is investigated since LMS is a temporal-reference-based algorithm that doesn't rely on DOAs, as described in Subsection 2.2.3.2. In another case, beamforming and space diversity are jointly applied on base stations of the mobile communications networks. Multiple antenna arrays are used on each base station, the beamforming gain is obtained by each individual array, and the diversity gain is achieved by processing signal output from multiple arrays [60, 49] (can be called angle diversity in this case).

Besides space diversity, it is possible to apply diversity on frequency, time and polarization [31]. In this thesis we only focus on the space diversity. Furthermore, it is widely known that the roles of receive and transmit antennas can be interchanged, resulting in transmit diversity. In the following, a brief introduction on receive diversity and transmit diversity will be given.

2.3.2 Receive diversity

Various space diversity techniques for reception have been well-analyzed in the classic book [31] published in 1974. In the following, we consider a scenario with a single antenna transmitter and an N-antenna receiver, which results in a SIMO (single-input multiple-output) channel. And "branch" is used to designate each independent signal path. γ_n denotes the local mean SNR on the n-th branch, and $\Gamma = \overline{\gamma_n}$ is the global mean SNR. In all cases, independent branch fading and equal mean branch power are assumed. That is, $\gamma_1 = \ldots = \gamma_N = \Gamma$. All detailed derivations can be found in [31] if not specially stated.

Selection Diversity (SD) This is the simplest scheme of all types. It selects one from N branches that has the highest SNR and connects it to the subsequent processing unit. The output SNR is given by

$$\gamma_{\mathrm{SD}} = \sum_{n=1}^{N} \frac{\gamma_n}{n} = \Gamma \sum_{n=1}^{N} \frac{1}{n}. \tag{2.24}$$

In practice, the branch with the largest signal plus noise power is usually used, since it is difficult to measure SNR [31].

Maximal Ratio Combining (MRC) This scheme is the most complicated one, however gives the best performance. N received signals must be cophased and weighted (amplified) proportionately to their signal amplitudes and then summed. The essential of this scheme is to strengthen the strong paths whereas weaken the weak paths. The resulting SNR is

$$\gamma_{\mathrm{MRC}} = \sum_{n=1}^{N} \gamma_n = N\Gamma. \tag{2.25}$$

It should be noted that the above cophasing and weighting operation is equivalent to the following process on each branch: first make channel estimation to get the channel state information (CSI) $h_n = \alpha_n e^{\mathrm{j}\phi_n}$ and then carry out a complex weighting with the coefficient h_n^* [1]. If the transmitted signal s_0 is received by a two-element receiver, then the output signal of MRC is

$$r_0 = (\alpha_0^2 + \alpha_1^2)s_0 + h_0^* n_0 + h_1^* n_1, \tag{2.26}$$

where n_0 and n_1 represent the noise signal on antenna 0 and antenna 1, respectively.

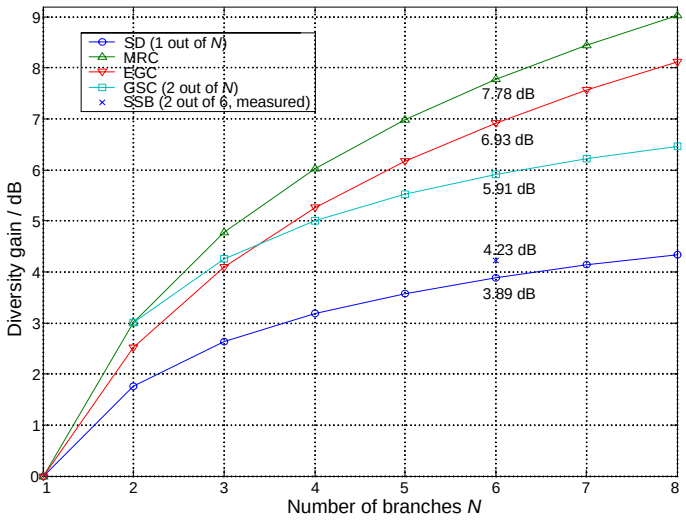

Figure 2.7: Diversity gains of different methods (for SSB refer to Subsection 5.4.4.2).

Equal Gain Combining (EGC) Compared to MRC, this scheme has a reduced complexity by skipping the weighting on amplitude. It combines the N cophased signals directly. Its output SNR is derived as

$$\gamma_{\mathrm{EGC}} = \Gamma[1 + (N-1)\frac{\pi}{4}]. \tag{2.27}$$

Fig. 2.7 gives the diversity gain on SNR ($10\log(\gamma_{\mathrm{output}}/\Gamma)/\mathrm{dB}$) with respect to the SNR of the single antenna receiver. We can observe that EGC only has a slight degradation compared to MRC (up to 1 dB with a finite number of N), however the gain of SD is significantly degraded when N becomes large. MRC and EGC impose higher requirements on hardware complexity since they require N identical RF front-ends. SD only needs one RF front-end, however its performance is not satisfactory. Hence, a proper tradeoff between hardware complexity and performance is favorable. This motivates the recently designed scheme called generalized diversity selection combining (GSC) in [39] or hybrid selection/maximal ratio combing (H-S/MRC) in [80]. They are identical, and we adopt "GSC" to designate it in this thesis.

Generalized Diversity Selection Combining (GSC) The basic idea is to select L branches with largest SNR out of total N diversity branches and combine them using MRC. Therefore, the number of RF front-ends can be decreased from N to L. The closed expression of the resulting SNR has been derived in [39] and [80] independently. That is

$$\gamma_{\mathrm{GSC}} = \Gamma L(1 + \textstyle\sum_{n=L+1}^{N} \frac{1}{n}), \quad N \geqslant L, \quad L \geqslant 2. \tag{2.28}$$

As indicated in [68], the corresponding closed expression if the selected L signals are combined using EGC is not yet clear. The SNR diversity gain of GSC (for $L = 2$) is also given in Fig. 2.7.

2.3.3 Transmit diversity & Space-time coding (STC)

As opposed to the receive diversity SIMO channel, a transmit diversity MISO (multiple-input single-output) channel can result if the transmission occurs between an N-element transmitter and a single antenna receiver. Recall the aforementioned MRC scheme and imagine that if the CSI h_n of each path is known at the transmitter and each signal is weighted according to h_n^* before transmission, then the same diversity gain can be achieved at the receiver as MRC [27]. One disadvantage of this scheme is that a closed-loop solution must be available to let the receiver feed the estimated CSI of N paths back to the transmitter.

Alamouti has proposed a simple transmit diversity that doesn't require any CSI at the transmitter [1]. Consider a 2×1 MISO channel, if the transmitter sends two signals s_0 and s_1 in the following way (refer to Tab. 2.2): in the first symbol period s_0 and s_1 are sent, and in the next symbol period $-s_1^*$ and s_0^* are sent, by two antennas, respectively. Then the received signals are

$$\begin{pmatrix} r_0 \\ r_1 \end{pmatrix} = \underbrace{\begin{pmatrix} s_0 & s_1 \\ -s_1^* & s_0^* \end{pmatrix}}_{(\,\mathbf{s}_0 \quad \mathbf{s}_1\,)} \begin{pmatrix} h_0 \\ h_1 \end{pmatrix} + \begin{pmatrix} n_0 \\ n_1 \end{pmatrix}. \tag{2.29}$$

Assume that the perfect CSI h_0 and h_1 are available at the receiver, then the sent signal can be recovered as

$$\begin{pmatrix} \widehat{s}_0 \\ \widehat{s}_1 \end{pmatrix} = \underbrace{\begin{pmatrix} h_0^* & h_1 \\ h_1^* & -h_0 \end{pmatrix}}_{(\,\mathbf{d}_0 \quad \mathbf{d}_1\,)} \begin{pmatrix} r_0 \\ r_1^* \end{pmatrix} = \mathbf{D} \begin{pmatrix} r_0 \\ r_1^* \end{pmatrix}, \tag{2.30}$$

in which $\mathbf{D}$ denotes the decoding matrix. From Eq. (2.30) we can obtain

$$\begin{aligned} \widehat{s}_0 &= (\alpha_0^2 + \alpha_1^2)s_0 + h_0^* n_0 + h_1 n_1^* \\ \widehat{s}_1 &= (\alpha_0^2 + \alpha_1^2)s_1 - h_0 n_1^* + h_1^* n_0. \end{aligned} \tag{2.31}$$

The decomposed signals in Eq. (2.31) are equivalent to that obtained from the two-branch MRC in Eq. (2.26), which implies that the same diversity gain can be achieved. To estimate two channels h_0 and h_1, pilots must be sent alternatively by two transmit antennas, or orthogonal pilot symbols are sent by them simultaneously. Furthermore, the channel fading must be slow enough so that the CSI is valid over two consecutive symbols. We can note that two transmission codes $\mathbf{s}_0$ and $\mathbf{s}_1$ of Eq. (2.29) are orthogonal ($\mathbf{s}_0^{\mathrm{H}}\mathbf{s}_1 = 0$), and two decoding vectors $\mathbf{d}_0$ and $\mathbf{d}_1$ of Eq. (2.30) are orthogonal, too. The Alamouti scheme was shortly generalized to an arbitrary number of transmit

Table 2.2: Alamouti transmit diversity scheme [1].

	antenna 0	antenna 1
symbol period 0	s_0	s_1
symbol period 1	$-s_1^*$	s_0^*

antennas scheme that is able to achieve the full diversity, called the orthogonal space-time block coding (STBC) by Tarokh et al. [76, 75]. Little earlier, Tarokh et al. have also presented another coding structure called the space-time trellis coding (STTC) in [77]. The common advantage of the above two STCs is that CSI is not required at the transmitter and the full diversity can be achieved.

STBC The Alamouti scheme can be regarded as the simplest STBC application. A general method to design STBC for any (real or complex) signal constellation to achieve the full diversity has been presented in [75], based on the orthogonal design. For modern communication systems, the complex signal constellation (e.g., QPSK, 8PSK, 16QAM, ...) is usually applied to achieve high data rate and spectral efficiency. However, it is shown that a rate 1 STBC cannot be constructed, in general, for any complex signal constellation with more than two transmit antennas [76]. That is, the Alamouti scheme gives the unique complex STBC without redundancy (full rate) up to now.

STTC was presented a bit earlier than the Alamouti scheme in [77], and the previously proposed delay diversity is the special case of STTC. As an example, we consider the four-state QPSK STTC for two transmit antennas. Its STTC has a very simple description (refer to Fig. 2.8):

$b_k a_k$ denotes the source binary sequence that constructs one symbol x_k at the k-th symbol period. $x_{k,\mathrm{TX1}}$ and $x_{k,\mathrm{TX2}}$ denote the encoded symbols to be transmitted by antenna 1 and 2, respectively, which can be described as:

$$\begin{pmatrix} x_{k,\mathrm{TX1}} & x_{k,\mathrm{TX2}} \end{pmatrix} = \begin{pmatrix} b_k & a_k & b_{k-1} & a_{k-1} \end{pmatrix} \begin{pmatrix} 2 & 0 \\ 1 & 0 \\ 0 & 2 \\ 0 & 1 \end{pmatrix} = \begin{pmatrix} 2b_k + a_k & 2b_{k-1} + a_{k-1} \end{pmatrix}, \tag{2.32}$$

in which $b_{k-1}a_{k-1}$ represents the previous symbol. Then, from Fig. 2.8 we can see that the four symbols (2 1 0 3) of one block are sequently transmitted by each antenna, and there is one symbol period delay between two antennas. Furthermore, we can see that an additional symbol period is required for transmitting each block, which slightly reduces the transmission rate. This rate loss will become negligible if the block length is very large.

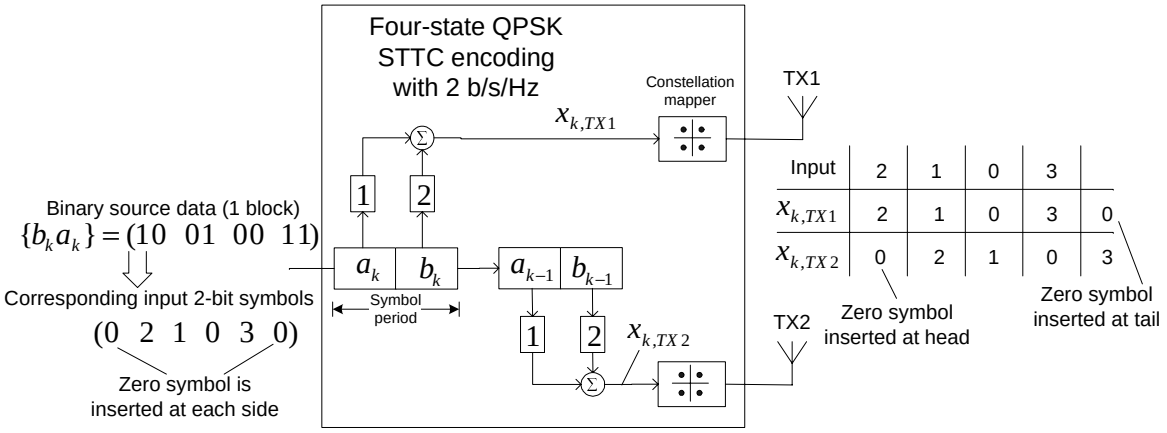

Figure 2.8: Equivalent encoder structure for the four-state QPSK space-time trellis code with two transmit antennas.

Obviously, the above STTC example is exactly a delay diversity scheme, hence the code can be called the repetition code. Several other full-rate full-diversity STTCs for different signal constellations and different numbers of antennas were presented in [77]. However, for a fixed number of transmit antennas, the decoding complexity of STTCs increases exponentially with the transmission rate (that applies the unit bit/s/Hz) [77]. Comparatively, STBC imposes less decoding complexity at the cost of no coding gain [76].

2.4 Multiple-Input Multiple-Output (MIMO)

Any kind of system that applies multiple antennas at both sides of TX and RX can be regarded as a MIMO system, regardless the principle used for the multi-antenna signal processing. However, only the space-time processing techniques that exploit both spatial and temporal signatures of signals are referred to as the strict-sense MIMO techniques, which mainly include the BLAST-family (bell laboratories layered space-time) techniques that can achieve the multiplexing gain or both multiplexing and diversity gains, the above space-time coding techniques that achieve the diversity gain, as well as other improved space-time techniques.

To explicitly state the definition of the multiplexing gain, it is necessary to first explain the channel capacity, also known as spectral efficiency. The well-known Shannon formula gives the upper bound of a SISO channel capacity as $\log_2(1+\mathrm{SNR})$ with the unit bit/s/Hz. It should be noted that this capacity is only for the point-to-point link, which is different from the network capacity (measured by the number of users or throughput). The MIMO channel capacity has been investigated in [78] and [17].

It is shown that under the assumption of $M_{\mathrm{T}} * M_{\mathrm{R}}$ independent fading channels, the capacity grows at least linearly with the number of transmit antennas M_{T} as long as the number of receive antennas M_{R} is greater than or equal to M_{T}. From this perspective, the *multiplexing gain* equals to M_{T}. As opposed to the diversity gain where the same messages are redundantly transferred over multiple paths (due to the use of multiple receive and/or transmit antennas), the multiplexing gain is attributed to the fact that M_{T} independent data streams are simultaneously transmitted by M_{T} transmit antennas while the specified constraint on link quality can still be met. Strict derivations and definitions of multiplexing gain and diversity gain are given in [85]. From the theoretical point of view, the maximum multiplexing gain that is achievable reaches $\min\{M_{\mathrm{T}},M_{\mathrm{R}}\}$. Most of the strict-sense MIMO techniques can be classified into these three categories:

Rate-oriented MIMO: V-BLAST This type of MIMO attempts to achieve the maximum multiplexing gain M_{T} (while $M_{\mathrm{T}} \leq M_{\mathrm{R}}$), however, exhibits no diversity gain. The typical example is the vertical-BLAST [81] system presented by Bell Labs. In this system, each transmit antenna sends an independent data stream (also called layer) simultaneously, and all M_{T} transmit antennas operate on the same frequency channel. At the receiver, the strongest layer is first extracted by nulling out all other weak layers (using zero forcing or minimum mean square error criteria), and then is sliced to the data bits. Those data are remodulated with CSI to estimate the vector signal contribution of the strongest layer, which is subtracted afterwards. And then, the second strongest layer is treated in the same manner, until all layers are decoded.

Diversity-oriented MIMO: space-time coding STTC and STBC only attempt to achieve the full diversity gain without considering the multiplexing gain. As a matter of fact, to achieve the full diversity, many space-time codes presented in [77] and [75] cannot obtain rate 1 (e.g., the Alamouti scheme gives the unique complex STBC that achieves rate 1). Recently, some new space-time codes are proposed that sacrifice some diversity gain to achieve a higher code rate (see [74] and the references therein).

Rate-diversity-oriented MIMO To keep the diagonal coding structure, D-BLAST [16] sacrifices some multiplexing gain, however, obtains the benefit of some diversity gain. In fact, multiplexing gain and diversity gain are often mutually conflicting. It is revealed in [77] that to achieve the full diversity gain $M_{\mathrm{T}}M_{\mathrm{R}}$, the maximum spectral efficiency (or capacity) is determined by the used modulation constellation (e.g., QPSK, 8-PSK and 16-QAM offer 2, 3 and 4 bit/s/Hz, respectively). In that case, there is no multiplexing gain. Authors in [85] have derived a tradeoff curve between them, which shows that the full multiplexing

gain ($\min\{M_{\mathrm{T}},M_{\mathrm{R}}\}$) and the full diversity gain ($M_{\mathrm{T}}M_{\mathrm{R}}$) cannot be achieved simultaneously. A selection criteria has been derived in [25] to determine whether diversity or multiplexing is better suited to the present channel condition. By feeding the decision back to the transmitter via a low-rate channel, a performance improvement on bit error rate over either diversity or multiplexing individually results. Some new space-time techniques have been proposed that pay attention to both diversity and multiplexing gains recently. For details refer to [74] and the references therein.

2.5 A cost analysis on multi-antenna techniques based on hardware complexity and power consumption

In mobile ad hoc networks, mobile portable terminals powered by batteries play the important role. Multi-antenna techniques are desirable for such terminals because of the numerous advantages described in this chapter. However, due to the limited resources available on such devices, in terms of hardware complexity, battery capacity and size, a careful analysis on the tradeoff between performance and resources is very necessary to achieve the aim of resource-efficiency. In this section, we make a rough analysis on the power and hardware complexity imposed by different multi-antenna techniques, based on the open-published test-bed trials. We only consider the real-time test-beds that apply DSPs or FPGAs to carry out the array signal processing since they are closer to real systems.

The first V-BLAST system was presented by Bell Labs in [81]. The 8×12 test-bed (8-antenna transmitter and 12-antenna receiver) operates on the 1.9 GHz frequency band with 30 KHz bandwidth. The uncoded data stream with the 16-QAM modulation is applied, in which 20% is used as a training sequence for the channel estimation. The 25.9 bit/s/Hz spectral efficiency is achieved if only payload is considered, and the actual spectral efficiency is reduced to 20.7 bit/s/Hz due to the training sequence. That is, the test-bed achieves the actual data rate of 621 Kbit/s with the 30 KHz bandwidth, which is a significant improvement over its single antenna competitors. However, no details on hardware complexity and power consumption are given in [81]. Especially, the guard time for real-time signal precessing is not mentioned. I guess it is not a small amount. A recent test-bed on V-BLAST is reported in [43] with more implementation details. The 4×4 test-bed operates on the 1810 MHz frequency band with the 200 KHz bandwidth. The uncoded BPSK data stream with the unit of frame is applied. Each frame is 6.55 ms long, contains a 0.93 ms training sequence, a 1.69 ms data payload (1024 bits in total) and a 3.93 ms guard time (for array signal processing and baseband processing). The achieved spectral efficiency is 3.03 bit/s/Hz

if only data payload is considered, is 1.95 bit/s/Hz if payload with training sequence are considered, and is 0.78 bit/s/Hz if the whole frame is taken into account. That is, the test-bed achieves the actual data rate of 156.3 Kbit/s on the 200 KHz bandwidth, which may not be superior to a single antenna system. The DSP chip ADSP-BF535 from Analog Devices is used for the array signal processing and baseband processing, which offers the computing capability of 600 MMACs (million multiply-accumulates per second). This chip consumes around 1 W power in the high activity.

A real-time steered beam smart antennas test-bed is reported in [71], which has been briefly introduced in Subsection 2.2.3.4. The TI DSP chip TMS320C6701 is used for executing the beamforming algorithm, which provides a 334 MMACs computing capability with around 2 W power consumption in the high activity. However, the present test-bed requires 1638.2 ms for each beamforming process, which is only acceptable in a static scenario. A base station smart antennas test-bed was implemented and tested by Ericsson and Mannesmann Mobilfunk, which was briefly described in [54]. To reach the strict real-time constraint, a cluster of 21 TI C40 floating point DSPs are used in parallel for baseband beamforming.

For the above examples we only take the additional processing overhead imposed by the specific multi-antenna technique into account. They imply that significant improvements over single antenna system can be achieved only at the cost of extremely high computing overhead (e.g., operated by a cluster of DSPs in parallel). Otherwise, the long guard time due to the slow computing speed of a general DSP [that provides up to 1 GMACs (giga multiply-accumulates per second) computing capability] counteracts the benefits of multi-antenna techniques. As a matter of fact, even the most advanced DSP that is commercially available at present (e.g., ADSP-TS201 that provides 4.8 GMACs computing capability with more than 4 W power consumption in the typical activity) cannot solely meet the signal processing requirement. It is indicated in [41] that the computing requirement of a 8×8 MIMO system only for the dynamic channel estimation may exceed 10 GMACs. Other than the burdensome signal processing overhead, multiple RF front-ends and the strict calibration among them are required for most digital beamforming systems (except the special case of [71] and [18]) and all strict-sense MIMO systems. Considering that most mobile devices limit their power consumption for wireless communication up to 500 mW, the power required by even a general DSP is not sustainable, to say nothing of the power consumed by multiple RF front-ends.

Based on the above analysis, we may conclude that digital beamforming and strict-sense MIMO techniques are not achievable on mobile portable devices with the state-of-the-art techniques, due to their extremely high requirements on hardware complexity, computing capability and power consumption. Therefore, we may only consider the

switched beam and space diversity techniques with a small number of antenna elements that impose less requirements on hardware and power for mobile portable devices.

Chapter 3

MAC and Cross-Layer Designs

This chapter presents the designs on the MAC layer and the cross-layer between MAC and PHY for MANETs. The traditional MAC protocol CSMA/CA used by IEEE 802.11 will be introduced first, and a proposal to solve the exposed node problem will be given. CSMA/CA is designed in the context of single antenna omni-directional communications. As described in Chapter 2, a variety of multi-antenna techniques have emerged on the physical layer in the past decades, which can noticeably increase the communication performance on various aspects. To effectively exploit those PHY layer techniques so that more benefits can be obtained for the entire network, adaptations on the MAC protocol are inevitable, hence called cross-layer optimization. Corresponding to different multi-antenna techniques, different adapted MAC protocols, BF-MAC (including Dir-MAC and NULL-MAC) and SD-MAC, are introduced (based on the previous investigations in literature). After that, the proposed MDA scheme will be described in detail, along with its adapted MAC protocol MDA-MAC. As extensions to MDA-MAC, radiation power control (PC) and transceiver power management (PM) that can help to reduce the power consumption will be presented. Network simulations with various configurations have been made by us, whose results prove that MDA-MAC with PM can significantly increase the network performance while the power consumption is kept almost the same, compared to the traditional single antenna system. Finally, a resource-efficiency comparison will be given among MANETs applying the traditional CSMA/CA, Dir-MAC and MDA-MAC (with PM).

3.1 Traditional MAC designs for MANETs

Three basic functions are performed on the medium access control (MAC) layer [55]. **The first function** is to provide a reliable data delivery service to each node of the network. Applying the acknowledgement (ACK) packets and a series of retransmission measures, the reliability of data delivery over wireless media can be significantly improved. **The second function** is to fairly assign the shared wireless medium to all nodes of the network. Since it is assumed that all nodes are operating on the same frequency channel with an omni-directional antenna pattern, the medium access con-

trol only means to assign the operating time slots to all nodes properly. The nodes within the coverage of each other should not access the medium simultaneously to avoid collisions. And **the last function** on the MAC layer is to protect the privacy of the data that it delivers. The designs on the former two functions will be discussed in detail, while the last function is skipped since it is beyond the scope of this thesis.

3.1.1 The CSMA/CA used by IEEE 802.11 MAC

There are two different access mechanisms for the second function mentioned above: the distributed coordination function (DCF) and the point coordination function (PCF). In mobile ad hoc networks (MANETs), DCF is applied as the basic access mechanism since it conforms to the distributed control characteristic of MANETs, while PCF is a kind of centrally controlled mechanism. DCF along with the measures that ensure a high link reliability (the first function mentioned above) are adopted by the IEEE 802.11 MAC protocol for its ad hoc operating mode, which is called CSMA/CA (carrier sense multiple access with collision avoidance).

The basic principle of CSMA/CA is "listen before talk", that is, a node will listen to the medium before beginning a transmission. If the medium is busy with a communication link, then this node must defer its transmission until the end of the ongoing link to avoid collision. It is necessary to clarify the time unit used in CSMA/CA before further description. The basic time unit is "slot", which is defined at the physical layer. Other than slot, SIFS (short interframe space) and DIFS (DCF interframe space) are also used. SIFS is shorter than one slot, and DIFS is equal to SIFS plus two slot times [55]. The details of CSMA/CA are elaborated in [46] and can be outlined as follows:

- The reliable data delivery service is ensured by the use of the acknowledgement (ACK) packet and the retransmission procedure. In CSMA/CA, every uni-cast packet is acknowledged by an ACK packet. A packet is retransmitted if no ACK is received (time-out occurs) until a retry limit is reached. In this case, this packet will be discarded. The channel access of the retransmitting packet is allotted less priority compared to the first-try packet to ensure fairness, as will be depicted later.

- The carrier sense (CS) mechanism is the main measure for collision avoidance. CS is further divided into physical and virtual carrier sensing types. Physical carrier sensing (PCS) is done by the receiver on the physical layer. If the detected signal power is above a sensing threshold P_s, the medium is reported to be busy. For virtual carrier sensing (VCS), over-heard packets are analyzed. The MAC header of each packet contains a duration field that records the remaining transmission time of the ongoing link. If a node over-hears a packet that is not

addressed to it, it sets its network allocation vector (NAV) for the duration of the transmission to indicate that the medium is busy. NAV can be regarded as a countdown, and a non-zero NAV indicates a busy medium.

- The DCF operation for medium access is designed as follows. When a node has a packet to transmit, a check is made for both PCS and VCS. If both mechanisms indicate that the medium is not in use for a duration of DIFS without any interruption, then the node can immediately access the medium and begin to transmit the packet. If either PCS or VCS indicates the busy medium within a DIFS, the node enters into the contention phase, during which the binary exponential backoff procedure is performed.

- To ensure fairness, the binary exponential backoff mechanism is used for the medium access contention if multiple nodes attempt to access at the same time. If a node cannot access the medium via the DCF operation mentioned above, it enters into the contention phase to perform the backoff procedure. It first selects a random backoff duration, which is equally distributed between 0 and the present contention window (CW). Then, both PCS and VCS are checked with the time unit slot. The backoff procedure shall decrease its backoff time once (one countdown) if the medium is determined to be idle for one slot duration. The backoff procedure is suspended by the busy medium. The node shall access the medium immediately after its timer reaches zero, that is, if the accumulated idle time reaches the randomly selected backoff duration. The length of CW will be doubled in case of retransmission (no ACK is received) until its maximum value is reached. This measure allots the retransmitting packet less priority in the contention for accessing the medium.

- The 4-way handshaking procedure is applied to alleviate the hidden node problem. Before a DATA packet is transmitted, the source node first sends a Request-To-Send (RTS) packet to inform the surrounding nodes of the transfer. The reached nodes set their NAVs and remain silent for the duration of the transmission. The destination node answers with a Clear-To-Send (CTS) packet. Hence, all nodes that are in the coverage of the destination node remain silent, too. As the medium has been reserved, the source node then sends the DATA packet and the destination node finishes the entire procedure with an ACK packet. If the source node does not receive the CTS or ACK packet (time-out occurs), it will retry the transmission after performing a backoff procedure.

It is necessary to note that except the 4-way handshaking procedure, the 2-way handshaking procedure (see Fig. 3.3) is also used in the IEEE 802.11 MAC, and two retry counters are associated. The threshold p_{RTS} is used to determine which handshaking procedure and retry counter shall be used for the DATA packet. If the length of

DATA exceeds p_{RTS}, then the 4-way handshaking and the long retry counter should be used. Otherwise, the 2-way handshaking and the short retry counter are used. In the following, we only discuss the long DATA condition if not specified.

3.1.2 Examples for further explanations on CSMA/CA

Figs. 3.1 and 3.2 illustrate how the source node A and the destination node B accomplish a data delivery. If A has successfully accessed the medium through the PCF operation or further through the backoff procedure, then it transmits a RTS packet. The neighboring nodes B and D within A's coverage will receive the RTS packet. Since B is the destination node, it shall access the medium to reply with a CTS packet, while D only needs to set its NAV according to RTS. Nodes A, C and H will receive the CTS packet, then A shall transmit the DATA packet after the SIFS interval, while C and H only need to set their NAVs according to CTS. After having correctly received the DATA packet, node B replies with an ACK packet. The DATA delivery process is finished successfully if this ACK packet is correctly received by node A. Otherwise, it will initiate a retransmission procedure. From Fig. 3.1 we can see that nodes C, D and H set their NAVs such that they keep silent until the end of ACK.

Fig. 3.2 can be used to explain the hidden and exposed node problems. We assume that the 2-way handshaking process is used for the DATA delivery between nodes A and B, that is, node A directly transmits DATA to node B. In this duration, node D can keep silent since its PCS indicates a busy medium by detecting the DATA packet. However, node C is not aware of the DATA reception on B because it is beyond the coverage of node A. Therefore, node C is a **hidden node** for node A. If C transmits any packet while B is receiving DATA, a collision occurs. Similarly, node H may cause the same problem as node C. In comparison with the 4-way handshaking procedure, it is clear that RTS and CTS can effectively solve the hidden node problem. However, the exposed node problem results from the use of RTS-CTS exchange. See Fig. 3.2, node D is out of the coverage of node B, which implies that any transmission of D would not interfere the reception on B. However, due to the RTS packet, node D has to refrain any transmission during the course of the DATA packet delivery (A to B). That is, node D becomes an **exposed node** in this particular duration if it has DATA for G or F. As the time for DATA delivery accounts for the majority of the whole 4-way handshaking procedure, this problem causes a noticeable waste on the overall channel utilization.

One further explanation is regarding the SIFS interval in Fig. 3.1. In some literature (e.g., [29]) it is stated that the destination node only requires a SIFS idle medium duration in the DCF process to access the medium. The source node still needs to perform DCF to access the medium (again, a SIFS idle medium duration is required)

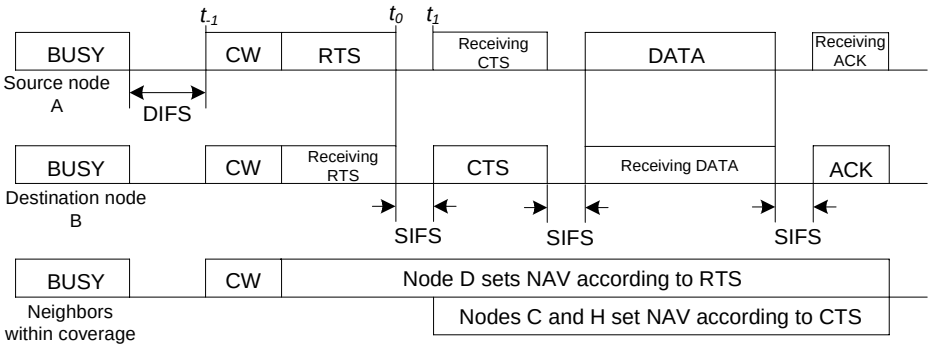

Figure 3.1: An exemplary channel access operation of CSMA/CA.

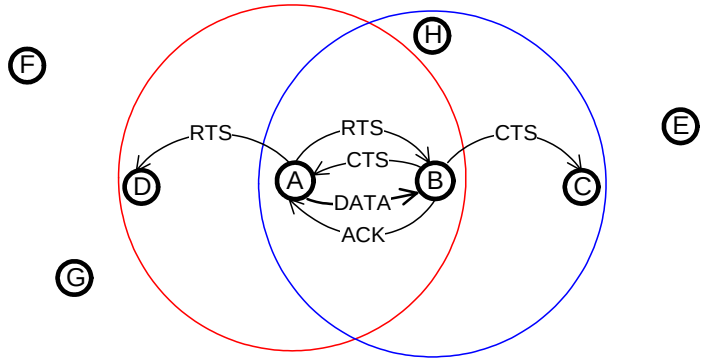

Figure 3.2: An exemplary scenario explaining the hidden and exposed node problems (the red and blue circles represent the coverage of the source and the destination, respectively. The same for Fig. 3.4).

for transmitting the DATA packet, although it has successfully received the CTS packet. However, this can be a misapprehension to CSMA/CA. As indicated by the official document [46] (P76), a node may access the medium only if it determines that the medium is idle for greater than or equal to a DIFS period, regardless of the type of the packet to be sent. At first glance, it seems that the SIFS interval for the destination node B in Fig. 3.1 is disobedient to the above statement. However, as will be explained in the following, it is not the case. The idle medium duration T_{idle} is calculated by

$$T_{\text{idle}} = t_1 - t_{-1}, \tag{3.1}$$

in which t_1 denotes the time instant when a node accesses the medium, and t_{-1} denotes the time instant when this node begins to sense the medium to be idle for both PCS and VCS (e.g., node B in Fig. 3.1). The basic condition to access the medium is $T_{\text{idle}} \geq$ DIFS. The time instant t_0 when the node has a packet to transmit can stand between t_{-1} and t_1. For the destination node B in Fig. 3.1, $t_1 - t_0$ equals SIFS for the CTS transmission, and the condition $T_{\text{idle}} \geq$ DIFS can still be met (as the time for receiving RTS is not regarded as the busy medium duration for node B). Moreover,

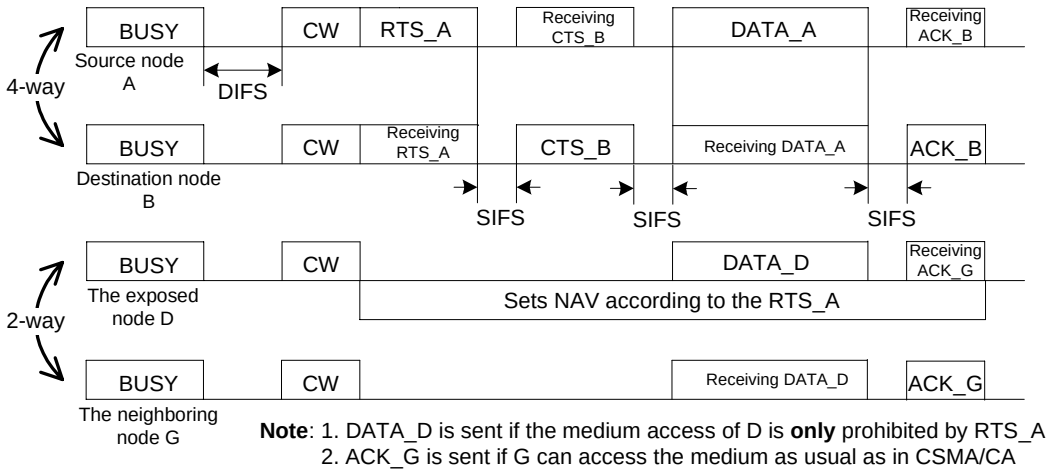

Figure 3.3: A solution to solve the exposed node problem.

as the channel has been reserved by the RTS-CTS exchange, both the source and destination nodes do not need to perform the DCF process again to access the medium for sending DATA and ACK afterwards. Three SIFS intervals illustrated in Fig. 3.1 are mainly used for the purpose of RX/TX switching.

3.1.3 My proposal to the exposed node problem

As indicated above, the exposed node problem may cause a noticeable waste on the channel utilization. An effective solution to solve this problem can be, particularly for the scenario of Fig. 3.2, node D initializing a 2-way handshaking procedure to deliver DATA to node G while node B is receiving the DATA packet from node A, in case that the medium access of D is only prohibited by the RTS packet from A, that is, the CTS of the same 4-way procedure is absent, see Fig. 3.3. This 2-way procedure finishes successfully if ACK from G is correctly received by D. There are two crucial premises for this solution. First, the DATA packets sent by A and D must have the same length and be transmitted simultaneously. Second, node G will reply with an ACK packet only if it can access the medium as usual as in CSMA/CA. That is, node G would not send ACK if it heard RTS from A, because in this case two ACK packets sent by G and B respectively collide at A, which results in a failing 4-way handshaking procedure between A and B. The above solution is not limited to the special case of the exposed node D in Fig. 3.2, but can be generalized to any node that is exposed. This solution is motivated by the Intelligent Collision Avoidance (ICA) scheme proposed in [69], however they are not identical since ICA prevents the exposed node to receive any packet.

3.2 BF-MAC

As indicated in Chapter 2, many advantages result from the use of multi-antenna techniques on the physical layer. Two of them are array gain and interference suppression gain due to beamforming. Therefore, they can be called beamforming (BF) gain. When beamforming is used in the point-to-multipoint scenario (e.g., in a cell of the mobile communication network one base station with multiple mobile stations exist), it brings a kind of SDMA (space division multiple access) effect that can increase the system capacity (the number of mobile stations). This is attributed to the directed radiation pattern that can be used to spatially separate the users of different locations although they are operating on the same frequency channel simultaneously. Imagine that if beamforming is used in a multipoint-to-multipoint scenario like MANETs (where it is possible for each node to communicate with multiple neighboring nodes), then a similar effect like in the cellular mobile communication network can result, as will be explained later. Due to this new property on the physical layer, corresponding modifications on the MAC layer must be made to obtain the maximum benefits, which can be regarded as a cross-layer design process. In this section, we focus on MAC designs making use of beamforming, which are therefore generally called BF-MAC.

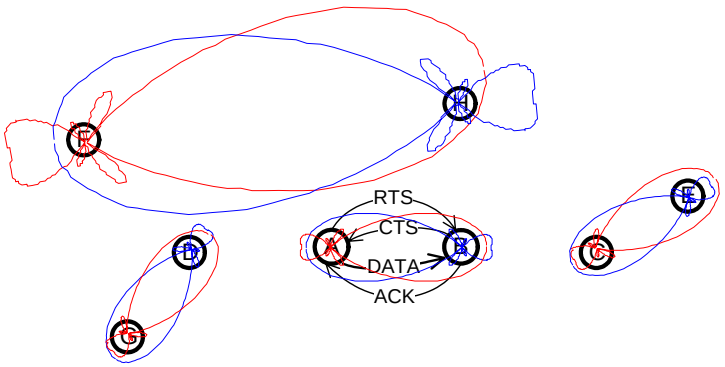

Figure 3.4: Space reuse factor can be increased by using directed radiation pattern in CSMA/CA.

Fig. 3.2 shows a scenario in which no other communication links can be active during the 4-way handshaking process between nodes A and B. This is caused by the omni-directional signal radiation property. However, if the radiation pattern on each node can be directed to its intended destination node, then four communication links can be concurrently active in the same scenario since less space is consumed by each link, as shown in Fig. 3.4. Furthermore, with the same radiation signal power, the higher gain of the directed radiation pattern on either TX side or RX side, or both sides, can result in a wider coverage than the traditional omni-directional case. This helps to decrease the hop count of a multi-hop delivery between source and destination nodes (e.g., F–H

in Fig. 3.4 instead of F–D–A–B–H in Fig. 3.2) in MANETs. Therefore, a series of modifications on the MAC protocol and even routing protocol are required to match the above beamforming property offered by the physical layer. The modifications on the routing protocol are beyond the scope of this thesis. In the following, an overview of previous investigations on adjusting the CSMA/CA will be first given, then a multi-directional-antenna (MDA) based MAC protocol proposed by us will be presented.

3.2.1 An overview of previous investigations

Recently, a variety of BF-MAC designs have been proposed in academia for MANETs, and most of them are based on the CSMA/CA that is designed for omni-directional communications. The principal contents of CSMA/CA, including the DCF procedure to access the medium, the backoff procedure for channel contention, the retransmission procedure and the 4-way handshaking procedure, are usually kept unchanged. Modifications are mainly focused on the operations for packet transmission/reception (TX/RX), physical carrier sense (PCS), and virtual carrier sense (VCS, or network allocation vector (NAV)). I will introduce them on the following eight items: 1. The assumed directional technique on the physical layer; 2. The location (direction) acquisition means; 3. RTS TX/RX; 4. CTS TX/RX; 5. DATA TX/RX; 6. ACK TX/RX; 7. PCS; 8. VCS or NAV.

3.2.1.1 Ko et al.'s work

Ko et al. have proposed the so called directional MAC (D-MAC) in [38] on March 2000. The main principles are listed as follows:

- The assumed directional technique on the physical layer is a multiple directional antennas system, which is, however, not explained explicitly in the paper. It can be regarded as a system similar to the multi-directional-antenna scheme (MDA, see Subsection 3.2.2) proposed by us, but only one directional antenna can be active for reception or transmission at one moment. The omni-directional transmission is also used in the paper, which requires the use of all directional antennas. The above two statements are not contradictory only if the omni-directional transmission is realized by the sequential transmission over all directional antennas. However, this operation causes additional overhead.

- It is assumed that each node knows its own location by using an additional global positioning system (GPS) device, and all of its neighbors' locations are known in advance. In a mobile scenario, the location information is updated via RTS-CTS exchange or using periodic beacons.

- RTS TX/RX. Case 1: if none of the source node's directional antennas is blocked, the RTS packet is transmitted omni-directionally (ORTS). Case 2: if any directional antenna is blocked, then a directional RTS (DRTS) will be sent, provided that the directional antenna pointing to the destination is not blocked. Otherwise, the source node has to defer its transmission until the corresponding directional antenna is unblocked. The prerequisite of sending DRTS is that the destination's location is pre-known at the source node, which is one of the assumptions used in this work. The reception of RTS is not stated, but must be directional.
- CTS TX/RX. CTS is always transmitted omni-directionally. The reception of CTS is not stated, but must be directional.
- DATA TX/RX. TX is directional. RX is not stated, but must be directional.
- ACK TX/RX. TX is directional. RX is not stated, but must be directional.
- PCS is performed on a per-antenna basis.
- VCS or NAV is not clearly stated, implied to be performed on a per-antenna basis.

This is an early work on the BF-MAC designs. The major limitations are on the following aspects: the assumed directional scheme on the physical layer is not stated clearly, as a consequence the reception means is not stated as well; the overhead caused by the omni-directional transmission through all directional antennas sequentially is not considered; the location acquisition solution is very ideal (the precision of GPS is limited, and it is not available indoors); the omni-directional transmission of RTS/CTS limits the space reuse factor. As will be described later, the location acquisition and the directional reception may cause a significant overhead on the network. Since the omni-directional antenna is not used, there is no asymmetric range problem [10, 40] (which will be discussed in Subsection 3.2.2.3). The network simulator NS-2 is applied to evaluate their proposals. Mobility is not considered in the simulations.

3.2.1.2 Nasipuri et al.'s work

Nasipuri et al. have proposed another BF-MAC in [53] on September 2000. The main principles are listed as follows:

- The assumed directional technique on the physical layer is similar to the one used in [38]. A slight difference is that the parallel transmission over all directional antennas is allowed. That is, unlike in [38], the omni-directional transmission doesn't cause any time overhead here.

- The neighbor's direction is obtained by selecting the directional antenna that generates the maximum signal strength. As the parallel reception is not allowed, this operation must be done sequentially through all directional antennas and thus causes an additional time overhead.
- RTS TX/RX. Since the direction of the destination is not known in advance, the source node transmits RTS omni-directionally. RTS is received directionally on the destination node.
- CTS TX/RX. The destination node transmits CTS omni-directionally, although it detects the direction of the source node. CTS is received directionally on the source node.
- DATA TX/RX. DATA is always transmitted and received directionally, because the directions of both source and destination are known after the exchange of RTS-CTS.
- The way for ACK TX/RX is not stated in the paper.
- PCS is not explicitly stated. Implied by the assumed directional scheme, PCS should be performed per-antenna sequentially.
- VCS or NAV is not stated, a similar concept off-the-air (OTH) period is used.

This is also an early work on the BF-MAC designs. Compared to the work of [38], it goes one step ahead by achieving the direction of the neighbor without relying on the GPS service. The major limitations are on the following aspects: Again, the assumed directional scheme on the physical layer is not stated explicitly; the overhead of the direction acquisition process is not considered (this is also the overhead of the directional reception); the omni-directional transmission of RTS/CTS limits the space reuse factor. As the omni-directional antenna is not used, there is no asymmetric range problem. An event driven network simulator is applied to evaluate their proposals, however its name is not given. The mobility up to 10 m/s is considered in the simulations.

3.2.1.3 Bellofiore et al.'s work

Bellofiore et al. have proposed a BF-MAC in [7] on May 2002. As this work is accomplished by a group of physical layer researchers, more details regarding the directional scheme are elucidated. The main principles are listed as follows:

- The assumed directional technique on the physical layer is a type of smart antennas technique, steered beam (or called adaptive beamforming). The least mean

square (LMS) algorithm is primarily used for beamforming. Furthermore, the overhead caused by the training sequence for LMS is taken into account, which makes the designed MAC protocol more realistic. Although not explicitly stated, it is implied that the parallel transmission and/or reception on one node is not allowed.

- The neighbor's direction is obtained by using some direction of arrival (DOA) estimation algorithm, e.g., ESPRIT [19]. In fact, the DOA information is not necessary for the LMS beamforming and the MAC operations. It can be used to accelerate the convergence of the LMS algorithm (by selecting a proper initial value), and therefore shorten the training sequence. However, this effect is not stated in the paper, and the DOA estimation itself also causes an additional overhead. More descriptions regarding the LMS beamforming and the DOA estimation can be found in Subsection 2.2.3.

- RTS TX/RX. RTS is transmitted and received omni-directionally.

- CTS TX/RX. CTS is transmitted and received omni-directionally.

- DATA TX/RX. DATA is transmitted and received directionally. It must be noted that two extra packets, RXTRN and TXTRN, are transmitted before sending DATA (see Fig. 3.5). They are used as the dedicated training sequence to let the destination node and the source node calculate their weighting coefficients using the LMS algorithm, respectively. Both RXTRN and TXTRN are transmitted with the omni-mode. After those two packets, the directional radiation patterns on both source and destination nodes are generated.

- ACK is transmitted and received directionally.

- PCS is not stated explicitly, but implied to be the same as in CSMA/CA, that is, omni-directional.

- VCS or NAV is modified. As shown in Fig. 3.5, the NAV is recorded until the end of TXTRN, and the delivery of DATA and ACK is not included in NAV. The possible reason for such a design is that the probability for DATA and ACK to cause collisions is low due to the use of the directional transmission and the PCS function.

The importance of this work is for the first time analyzing the impact of the training sequence on the network performance. The paper concludes that a training period greater than 20% of the entire link length reduces the network throughput considerably. The major limitations are on the following aspects: The way to realize the omni-directional transmission and reception is not stated, hence the asymmetric range

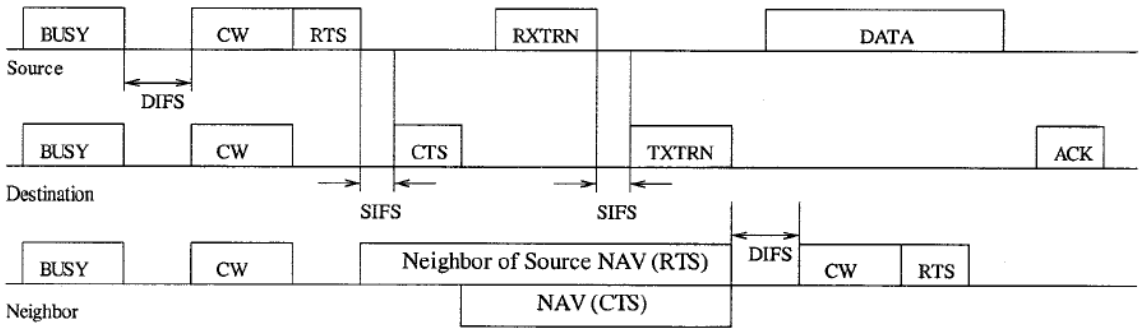

Figure 3.5: The proposed MAC protocol in [7].

problem is not analyzed as well; the omni-directional exchange of RTS-CTS limits the space reuse factor (however, the main measure used in the paper is to decrease the length of NAV). OPNET is used as the network simulator, and mobility is not considered in the simulations.

3.2.1.4 Takai et al.'s work

Takai et al. have proposed a BF-MAC protocol that uses the directional exchange of RTS-CTS [73] at June 2002. The main principles are listed as follows:

- The assumed directional technique on the physical layer is a type of smart antennas technique called steered beam. However, it applies the simplest DOA-based beamforming algorithm that only directs the main beam to the intended node and has no interference nulling capability. The directional reception is emphasized in the paper. Both the omni-directional and directional modes are used, however, a power control scheme is used to roughly generate the same transmission range. This alleviates the asymmetric range problem. The way to realize the omni-directional TX/RX is not stated. It is implied that a dedicated omni-directional antenna is used for this intention.

- The neighbor's direction is obtained by using some angle of arrival (AOA) estimation means. In this paper, the term AOA instead of DOA is used, however their essentials are the same. The overhead caused by the AOA estimation is not taken into account. It is assumed in the paper that an AOA updating occurs for every reception so that the directional pattern is adjusted (for the present RX operation and the next TX operation) accordingly.

- RTS TX/RX. If the AOA of the destination node is known by the source node beforehand, RTS is transmitted directionally; otherwise, it is transmitted omni-directionally. RTS is received directionally by the destination node.

- CTS TX/RX. CTS is transmitted and received directionally.
- DATA TX/RX. DATA is transmitted and received directionally.
- ACK TX/RX. ACK is transmitted and received directionally.
- PCS is not stated in the paper. It is implied to be directionally performed.
- VCS and VAV. DVCS (directional VCS) and DNAV (directional NAV) are the main contributions of this paper. Each DNAV is associated with a direction and a beam width (which result in an angular domain), and multiple DNAVs can be set on one node. The node is not allowed to transmit any packet in the direction covered by the angular domain of a DNAV until this DNAV expires. Interoperability between the DNAV and the usual NAV is adequately considered since the latter can be regarded as a DNAV with the 360° beam width. It is also stated in the paper that DNAV is independently proposed in the early version (as a technical report) of [10].

The main limitation of this work is that the overhead caused by the AOA estimation is neglected, in spite of another overhead caused by the beamforming calculation. Those overheads may cause a significant impact on the network performance, as indicated by [7] (although different beamforming and MAC operations are used in [7]). Their selected network simulator is QualNet, and the random way point with 10 m/s is used as the mobility model.

3.2.1.5 Some other works

Lal et al. have proposed a BF-MAC protocol based on the assumption of the parallel directional transmission/reception capability on each node [44, 45]. They claimed that the parallel directional reception on a node requires the prospective transmitters to synchronize their transmissions. Therefore, an additional Ready-to-Receive (RTR) packet is used to reach this aim. The destination node first sends a RTR packet omni-directionally, then multiple source nodes can synchronize and start the 4-way handshaking procedures with the same destination node in parallel, all are performed directionally. Choudhury et al. have proposed to use the multi-hop RTS scheme to exploit higher gains of directional TX/RX operations [10]. In that paper, DNAV has been independently proposed, and new problems caused by using directional communications, asymmetric range and deafness, have also been analyzed. Ramanathan has made a comprehensive discussion on the use of directional communications in ad hoc networks [62] on Oct. 2001, which is also an early work in this area. One novelty of this paper is the analysis on the directional neighbor discovery and the link power control,

which have been scarcely investigated on the MAC layer before. One important conclusion drawn in [62] is that for ad hoc networks, when just spatial reuse is considered, switched beams are nearly as good as steered beams (and a lot less expensive). The circular directional RTS scheme has been proposed by Korakis et al. in [40] so that the location of the destination is not required in advance, and this scheme also alleviates the asymmetric range problem. However, the overhead caused by sending a circular RTS and the directional reception (called selection diversity, identical to the one used in [53]) are not considered. In [29], the author has assumed an ideal smart antennas system on the physical layer. Each receiver applies the buffer & post-processing means to perform the DOA estimation and/or beamforming so that the training period is not required for receiving or sensing any packet directionally, and the packet itself (e.g., RTS) is used as "pilot signals". Therefore, no additional overhead is imposed like in [7]. Since no omni-directional operations are applied, the proposed protocol doesn't suffer from the asymmetric range problem. Furthermore, it is also assumed that each node is capable of generating multiple directional beams simultaneously. As a result, the protocol doesn't encounter the deafness problem. Such a system is theoretically feasible, however, may not be sustainable even for a base station due to its extremely high complexity, to say nothing of a mobile portable device. One novelty of [29] is the use of another type of DNAV. Unlike in [73] the blocking beam width of DNAV is fixed, an adaptive way is used in [29]. The DOA θ_k and the received signal power $P_{\text{in},ki}$ of the overheard packet from node k are additionally recorded in the DNAV of node i. When node i attempts to transmit a packet in the direction θ_j (to node j) with the radiation pattern $G_{ij}(\theta)$, then the interference that can be experienced by node k is estimated as $P_{\text{in},ik} = P_{\text{in},ki} \cdot G_{ij}(\theta_k)/G_{ij}(\theta_j)$ (provided that for all nodes the radiation power and the maximum beam gain to any direction are constant). If $P_{\text{in},ik}$ reaches the sensing threshold, then this transmission will be blocked, otherwise it will be performed like in the condition that no NAV is set.

Recent works on BF-MAC designs begin to move the effort from directing the main beam to the intended partner to deeply nulling the interference, e.g., [52, 57, 56]. The authors claimed that the previous investigations based on directional radiation patterns require near-ideal free space propagation conditions with line of sight (LOS), hence are not applicable in a rich scattering multi-path propagation environment, like indoor or urban outdoor environment. Thus, the investigation on BF-MAC designs has divided into two branches: Dir-MAC that is based on the directional radiation pattern to the intended partner (e.g., [38, 53, 62, 7, 73, 10, 44, 45, 40, 29]), and NULL-MAC that is based on deeply nulling the interference partner (e.g., [52, 57, 56]). However, both directional radiation pattern and interference nulling are properties of the beamforming (smart antennas) technique, whose performance would anyway degrade in a rich scatting multi-path environment. Relevant discussions will be further given in Sections 3.3 and 3.4.

3.2.2 Multi-directional-antenna (MDA) based BF-MAC (MDA-MAC)

MDA-MAC is a kind of Dir-MAC design (refer to Subsection 3.2.1.5), which is based on the directional radiation pattern pointing to the intended partner. However, it differs from other Dir-MAC designs in the directional scheme assumed on the physical layer. We have elaborated every detail of MDA-MAC such that all additional overheads caused by the directional communication are adequately considered. Therefore, MDA-MAC may be comparatively more realistic than other Dir-MAC designs.

3.2.2.1 The MDA scheme assumed on the physical layer

Until now there are two approaches to realize the directional communication: The beamforming (smart antennas) technique and the multi-directional-antenna scheme. The directional radiation of the former scheme is realized by properly processing the antenna array signals (each antenna element may still be omni-directional), while the latter scheme relies on the physical characteristic of the antenna element itself, i.e., directional antenna. If multiple directional antennas are used on the same node with a proper orientation, then the whole azimuth can be covered and the mechanical turning is not required. This is called the multi-directional-antenna (MDA) scheme. Note, in this thesis MDA is regarded as a special case of beamforming techniques, therefore MDA-MAC is regarded as a type of Dir-MAC. Many previous studies on Dir-MAC designs apply the ideal sectorized or flat-topped directional radiation model [53, 62, 40], which ignores or simplifies the effects of side-lobes and back-lobe in some extent. However, none of these models can be realized by any actual antenna or smart antennas array. To simulate the network performance more precisely, we apply the radiation pattern of a real-world antenna to substitute the above-mentioned ideal radiation models. It should be noticed that the concept of "directional antenna" has been interchangeably applied in literature, which may refer either to a smart antennas array or to a directional antenna element. In this thesis, it refers in particular to a directional antenna element.

Studying existent directional antenna elements, we found that the AMHA (axial mode helical antenna) holds a very high directivity while its structure is quite simple, see Fig. 3.7. It has been theoretically well-analyzed since its invention in the late 1940's [42], and can be practically realized due to its essence of simplicity. Thus, we apply the AMHA as the actual directional antenna model. To simulate the node equipped with 4, 6 and 8 AMHAs, we calculated three configurations of the AMHA model, which approximately hold the HPBW (half power beam width) of 90°, 60° and 45°, respectively. Kraus' formulas listed in [42] to calculate HPBW and directivity are estimation formulas. To avoid large offsets, we first obtain the radiation field pattern

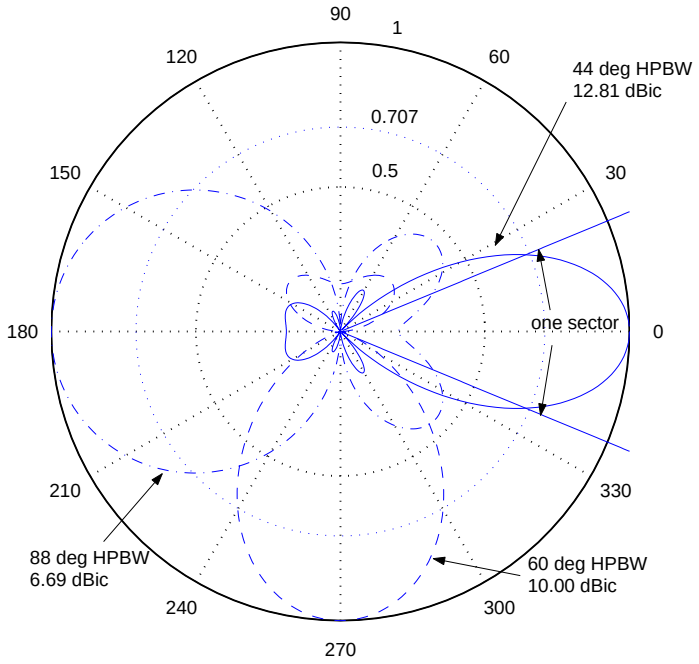

Figure 3.6: Three types of axial mode helical antenna radiation field patterns (normalized).

according to Kraus' formulas, then measure the resulting HPBW and calculate the directivity according to its exact definition [42] (see also Subsection 2.1.1)

$$D = \frac{\text{maximum radiation intensity}}{\text{average radiation intensity}}. \tag{3.2}$$

The field pattern given by Kraus' formulas is normalized (that is, its maximum value is 1), and we further assume a perfect radiation efficiency factor ($\eta = 1$), then the antenna gain can be calculated by

$$G/\text{dBic} = 10\lg\frac{4\pi}{\int_0^{2\pi}\int_0^{\pi} E^2(\theta,\phi)\sin\theta d\theta d\phi} \tag{3.3}$$

since $G = D * \eta$ [42]. The applied unit dBic denotes the antenna gain with reference to an isotropic circular polarization antenna. The physical parameters of the three AMHAs applied are listed in Tab. 3.1. It is necessary to note that the parameters used to design the 88° HPBW AMHA are far beyond the restrictions of Kraus' formulas, see Fig. 3.7. Thus, this type is not physically realizable. Fig. 3.6 illustrates the normalized radiation field patterns of the three AMHAs applied in this thesis.

Our proposed communication system applies K identical AMHAs, each of which is designed so that its HPBW is approximately $360\,°/K$. Furthermore, we suppose that all nodes are located in the horizontal plane, and the antenna elements on each node are oriented so that their main beam directions distribute equally (circularly) around

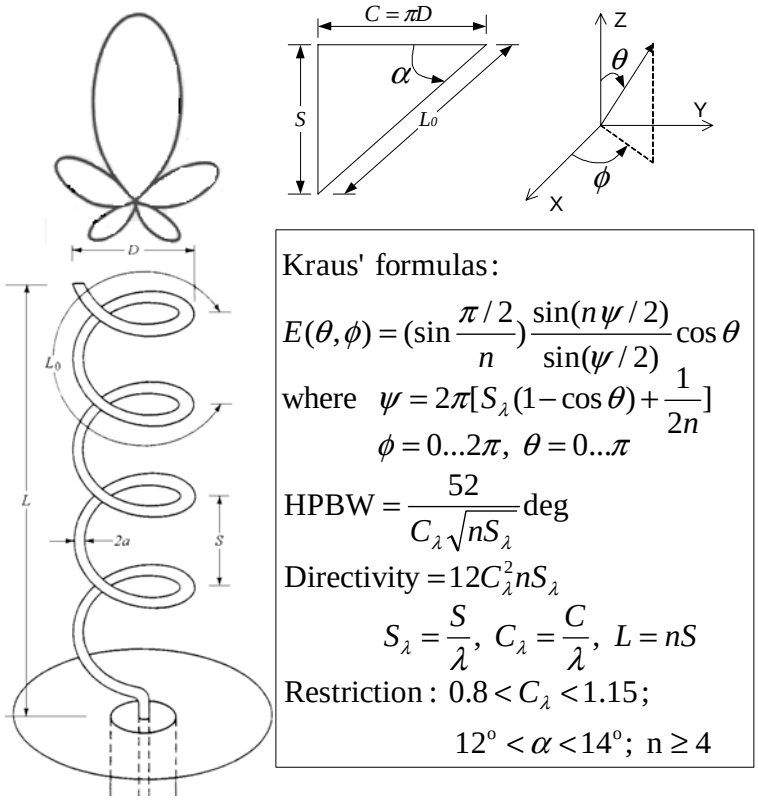

Figure 3.7: Axial mode helical antenna (AMHA) [42].

Number of sectors K	Circle number n	α	C_λ	HPBW	Gain/dBic
8	7	12°	1.07	44°	12.81
6	4	12.6°	0.76	60°	10
4	1.06	10°	1.3	88°	6.69

Table 3.1: The physical parameters of the three used AMHAs.

it in the horizontal plane. This divides the space around the node in K sectors (see Fig. 3.6). For each directional antenna, an own independent transceiver (refers to RF transceiver + Baseband unit) is used in the system. Since an increased amount of computing power is necessary to process the medium access control (MAC) protocol, the transceivers are connected to a multiprocessor (see Fig. 3.8). The multiprocessor can perform the medium access control for all transceivers in parallel. In [20], a suitable design method has been developed to implement network protocols for such a system and to map them on the multiprocessor such that its parallel processing capabilities can be exploited.

Finally, the functions of the assumed MDA scheme on the physical layer can be summarized as follows: A node is capable of parallel transmission, parallel reception, and parallel transmission and reception in its K sectors. No omni-directional antenna is used on the node.

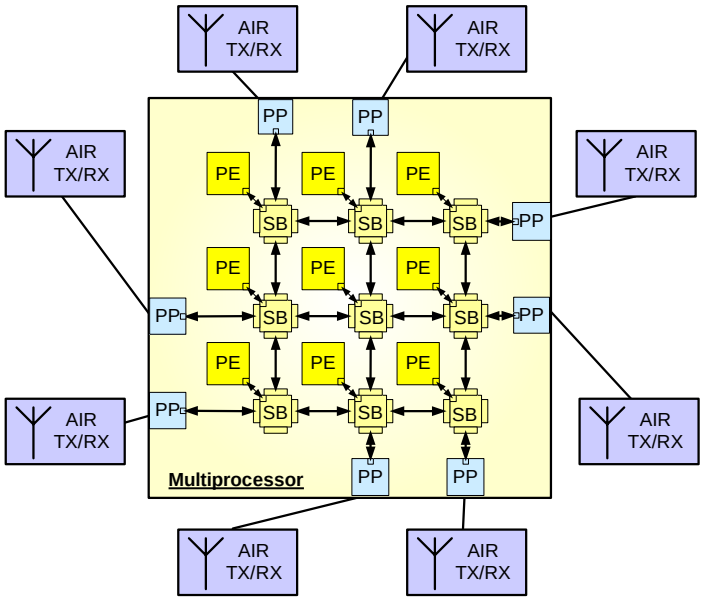

Figure 3.8: The proposed eight-sector communication system structure. The multiprocessor has a number of *processing engines* (PEs) that exchange messages via *switch boxes* (SBs). *Physical ports* (PPs) connect the air transceivers.

3.2.2.2 Main operations of MDA-MAC

Similar to the previous works described in Subsection 3.2.1, MDA-MAC is also based on the original CSMA/CA protocol. The main contents of CSMA/CA, including the DCF, backoff, retransmission and 4-way handshaking procedures are kept without changing. Furthermore, those procedures are performed in each sector independently. Modifications are focused on the operations for packet TX/RX, PCS and VCS (or NAV). I will describe them according to the 8-item fashion used in Subsection 3.2.1 except the first item, since it is already described in Subsection 3.2.2.1.

- The neighbor's direction is obtained by using the optimal reception sector selection (ORSS) operation. When a signal impinges on a node, it can be detected by multiple adjacent sectors on the node simultaneously due to the parallel reception capability. The sector that detects the highest reception power is determined as the optimal reception sector (ORS), and only the packet received by the ORS is further processed as the received packet and transferred to the upper layer if it is a DATA packet. The replicas of this packet received by other sectors will be tagged (to indicate that they are not received by the ORS) and be handled like overheard packets for PCS and/or VCS (NAV updating). Furthermore, this ORSS operation nearly causes no additional time overhead because multiple receptions on the node can occur simultaneously.

- RTS TX/RX. RTS is transmitted directionally in the selected sector. The sector to transmit RTS is determined by the neighborhood discovery described in Subsection 3.2.2.5. RTS is received directionally by the ORS of the destination node.
- CTS TX/RX. CTS is transmitted directionally by the ORS that received RTS. CTS is received directionally by the sector that transmitted RTS on the source node (provided that this sector is the present ORS: premise 1).
- DATA TX/RX. DATA is transmitted directionally by the sector that transmitted RTS and received CTS on the source node, and is received directionally by the sector that received RTS and transmitted CTS on the destination node (provided that this sector is the present ORS: premise 2).
- ACK TX/RX. ACK is transmitted directionally by the ORS that received RTS and DATA on the destination node, and is received directionally by the sector that transmitted RTS and DATA on the source node (provided that this sector is the present ORS: premise 3).
- PCS is performed by each sector individually.
- VCS or NAV is performed by each sector individually, that is, each sector is associated with its own NAV.

It should be noted that the above three premises must be fulfilled for a successful 4-way handshaking procedure, in which the first one is the most important. If the first one is not fulfilled, then time-out occurs in the sector that transmitted RTS because CTS is only transferred to the present ORS. In other sectors, CTS is only treated like an overheard packet. We don't use the sector updating to resolve this problem because the long DATA packet sent by the updated sector may cause collisions with a high probability (because the channel has not been reserved for this sector). Those three premises may not be fulfilled in the scenario with mobility. Therefore, mobility causes a performance degradation for MDA-MAC. The effect of mobility has been reported in [83] in detail.

3.2.2.3 Asymmetric range problem

As indicated in [10], the asymmetric range between omni- and directional mode operations may cause a new hidden node problem. The main reason for this problem is the use of omni-mode sensing for both PCS and VCS. A node may not be aware of a directional communication link in vicinity since the directionally transmitted RTS or CTS is not sensed by it (in the omni-mode). Hence, when it attempts to initialize a

new link by sending a directional RTS (with a higher coverage), it may collide with the directional link that is still in progress. The circular RTS scheme proposed in [40] may alleviate this problem to some extent, however, cannot completely resolve it. Because in that design CTS is not circularly transmitted, and thus the node near to the destination may still cause this problem. Furthermore, this solution also causes an additional time overhead on the network. To solve the asymmetric range problem thoroughly, an effective solution is to dispense with any kind of omni-directional operation. If only directional operations are applied, there exists no range asymmetry. The proposed MDA-MAC doesn't use any omni-directional operation, therefor it doesn't suffer from the asymmetric range problem.

3.2.2.4 Deafness

Deafness is another problem appearing in the Dir-MAC designs, as indicated in [10]. If a node is not capable of generating multiple directional beams concurrently, then it becomes deaf on all directions other than the direction of the beam that is in communication progress. Therefore, a new hidden node problem may be caused by deafness. To solve this problem, multiple directional beams must be generated simultaneously on a node. This aim can be met by the smart antennas system at the cost of significantly higher complexity. Since the proposed MDA scheme is capable of parallel directional transmission and/or reception, it can alleviate the deafness problem.

3.2.2.5 Neighborhood discovery (ND)

At the starting phase of an ad hoc network, no neighbor information is available for any node. The nodes must perform neighborhood discovery to find the reachable neighbors. Furthermore, a node should be able to track its neighbors when they move from one sector to another, and delete the neighbors from the list when they move out of the radial range. In the following, we first propose three neighborhood discovery algorithms, and the simulation results regarding their performance against mobility will be given afterwards.

- ND1. Since for the MDA scheme each node only uses its optimal sector to communicate with the reachable neighbors, the neighborhood discovery is performed independently in each sector, and each sector maintains an independent neighbor list. Each sector of the node sends a broadcast HELLO packet periodically. The HELLO packet only includes its own MAC address. It is generated by a global time-driven event of the node, which uses the following equation to calculate the generating time for the HELLO packet:

$$t = t_{\text{current}} + T_{\text{ND}} + [\text{rand}(0,\Delta t_{\text{ND}}) - \Delta t_{\text{ND}}/2], \tag{3.4}$$

where t_{current}, T_{ND} and Δt_{ND} denote the current time, the discovery period and a small jitter, respectively. The jitter is used to ensure that the HELLO events of K sectors on a node don't execute simultaneously but with a random time pause. It also avoids the collision of HELLO packets sent by the neighboring nodes if they join the network and initiate the neighborhood discovery at the same time. When the HELLO packet is generated in one sector, it will be sent as soon as possible. Before transmitting, the node must perform the carrier sense in this sector to access the medium as usual as in CSMA/CA, and all neighboring nodes that can overhear the HELLO packet will update their neighbor lists in ORSs. The entry of each neighbor recorded in the neighbor list is associated with a time-out T_{n} and an update time. If no new packets have been received from the neighbor for T_{n} seconds since the update time, which means the neighbor has moved out of the angular and/or radial range of this sector, its entry will be removed from the neighbor list of this sector. Not only the HELLO packet, but also all other kinds of overheard or intended packets can update the neighbor list of the ORS. It is possible that one node's adjacent sectors have recorded the same neighbor, in this case only the sector with the latest update time is used when this node needs to transmit packets to that neighbor.

- The basic operation of ND2 keeps the same as ND1. The only difference is that a time-driven HELLO_ACK event is immediately initiated for the ORS that receives the HELLO packet. A broadcast HELLO_ACK packet is generated rand(0,Δt_{ND}/2) seconds later by this event and then it is transmitted by this sector as soon as possible, so that the initiating node can update its neighbor list instantly. Note, the broadcast packet and uni-cast packet differ in the fact that the former doesn't need to be acknowledged while the latter does. Similarly, before transmitting HELLO_ACK the sector must also perform carrier sense to access the medium as usual as in CSMA/CA. By this measure, ND2 is expected to be able to track the neighbor more effectively in the mobile scenario, because the moving neighbor can let the initiating node update its neighbor list faster.

- Based on ND1 and ND2, ND3 further adds the current neighbor list into the HELLO packet as its payload. The receiving node doesn't reply if it finds its address in the HELLO packet, otherwise it replies a broadcast HELLO_ACK with the same manner as in ND2. ND3 is expected to overcome the disadvantage of ND2 that one HELLO may result in numerous HELLO_ACKs from all reachable neighbors, which increase the overhead of neighborhood discovery, while the advantage of faster response to the neighbor movement remains.

We have performed intensive simulations to evaluate the above three ND algorithms in both static and mobile scenarios, see [83]. Simulation results showed that in all

scenarios ND1 and ND3 have achieved the similar performance (ND1 is slightly better), while ND2 is always inferior. ND2 applies instant HELLO_ACK packets to more quickly update the neighbor list of the initiating nodes. However, when the node density is high, one HELLO packet may result in numerous HELLO_ACK replies because all its reachable neighbors need to answer within the short duration of the jitter $\Delta t_{\mathrm{ND}}/2$. Those HELLO_ACK packets add a considerable overhead on the network and may cause serious interferences on data communications. ND3 is originally designed to hold the advantages of both ND1 and ND2 so that even a higher performance can be achieved, but this aim is not reached, too. The possible reason is that the length of the HELLO packet becomes long if the current neighbor list is included into its payload. This increased overhead may counteract its advantage of less HELLO_ACK replies.

Another conclusion drawn in [83] is that in mobile scenarios, the network throughput doesn't always increase when more directional antennas are used on one node (while it does in static scenarios). Simulations showed that the six-sector MDA system has achieved a higher throughput than the eight-sector MDA system in the same mobile scenario, and the 10 m/s mobility causes apparent throughput degradations for all systems except the six-sector MDA system.

3.3 Space diversity MAC (SD-MAC)

As described in Section 2.3, one advantage resulting from multi-antenna techniques is the so called space diversity, which is applied to increase the link robustness in terms of a reduced BER. A space diversity system (including a transmitter and a receiver) redundantly transfers the message by a number of antennas, and signals at the receiver are combined with a dedicated method so that the best signal quality is ensured. A more complex way employing space diversity is the scheme space-time coding, which further contains two types: Space-time trellis codes (STTC) and space-time block codes (STBC). Space-time coding techniques don't require the channel state information (CSI) at the TX side, however, the CSI must be extracted first at the RX side before performing space-time decoding.

Similar to the BF-MAC designs, CSMA/CA should also be properly adapted to match the space diversity property on the physical layer, hence called space diversity MAC (SD-MAC). SD-MAC has been barely investigated before, only in [29]. One significant difference between SD-MAC and BF-MAC is, each operation in SD-MAC is treated to be omni-directional. The main functions of CSMA/CA, including the DCF, back-off, retransmission, and 4-way handshaking procedures are kept without changing. Modifications are focused on the operations for packet TX/RX, PCS and VCS (or

NAV). I will describe them in the way similar to the 8-item fashion used in Subsection 3.2.1. However, the second item regarding the way to detect the locations of neighbors doesn't exist for space diversity, and the first item has been depicted in Section 2.3 in detail (of course, here it refers to the diversity technique but not the directional technique). It is assumed that the source node and the destination node use n and m antennas, respectively.

- RTS TX/RX. RTS is transmitted by n antennas using the selected space-time coding scheme, which doesn't require the CSI. RTS is received by m antennas using the corresponding space-time decoding so that the space diversity gain can be exploited to increase the link robustness. RTS must contain pilot signals at its beginning to let the destination node or other overhearing nodes estimate the CSI. The CSI of $n \cdot m$ channels between n transmit antennas and m receive antennas must be known at receivers before performing the space-time decoding.

- CTS is transmitted by m antennas using the selected space-time coding scheme. However, CTS may not contain pilot signals in case that the channel coherence time is long enough (see Subsection 4.3.3) and the $n \cdot m$ CSI estimated while receiving RTS can be transferred back by a dedicated way. Usually, CTS should contain pilot signals to let overhearing nodes perform the VCS.

- DATA TX/RX is similar to RTS TX/RX. One slight difference is, DATA doesn't need to contain pilot signals in case the interval between RTS and DATA is shorter than the channel coherence time. Because in this condition the destination can apply the CSI estimated while receiving RTS for the space-time decoding. However, if this condition is not met, then pilot signals are still required for DATA. Usually, this condition can be met since the length of the control packet (like RTS or CTS) is significantly shorter than the channel coherence time.

- ACK TX/RX is similar to DATA TX/RX. In case that the interval between CTS and ACK is shorter than the channel coherence time, the CSI estimated (or acquired) while receiving CTS can be applied for receiving ACK. Therefore, pilot signals are not necessary for ACK. However, the above condition occurs with a less possibility because the length of DATA is significantly longer than the length of control packets, hence the interval between CTS and ACK may exceed the channel coherence time. In this case, pilot signals are still required for ACK.

- PCS. CSI and space-time decoding are not necessary for PCS, since its function is only to detect whether there is a carrier in the air. If any one of the receiving antennas detects a carrier whose strength reaches or exceeds the sensing threshold, a busy medium is determined; otherwise, an idle medium is determined.

- VCS or NAV. CSI is required to perform the VCS. NAV is treated in the same way as in CSMA/CA, only one NAV is used by each node. In case that DATA and ACK don't contain pilot signals, they cannot be overheard by neighboring nodes. However, this condition doesn't cause any obvious impact on the MAC operations since NAV is most probably set by overhearing RTS and/or CTS.

3.4 BF-MAC vs. SD-MAC

BF-MAC and SD-MAC are two considerably different MAC protocols for MANETs, which are designed to match the beamforming (BF) and space diversity (SD) gains of the physical layer, respectively. BF-MAC can be further divided into two types: Dir-MAC and NULL-MAC, as described in Subsection 3.2.1.5. The former is based on the directional radiation pattern to the intended partner, while the latter is based on deeply nulling the interference partners. BF and SD have different requirements on their application environments. BF requires a high correlation among antenna elements so that the impinging signal exhibits a planar wave-front for the array and the signals on different antennas only differ in their phases. SD requires multiple antenna elements to be sufficiently uncorrelated so that the signal on each antenna has experienced an independent fading. It is obvious that the above two requirements are opposite and cannot be met for the same array in the same environment simultaneously.

Those two abstract requirements can be converted to the concrete requirements on angle spread (AS) [59]. AS at a receiver refers to the spread of angles of arrival of multipaths, and AS at a transmitter refers to the spread of departure angles of multipaths. It can be intuitively conceived that a small AS corresponds to the condition for beamforming, while a large AS corresponds to the condition for SD. It is apparent that if the intended signal impinges on the receiver with a broad range of directions, then the receiver is not able to determine in which direction it should direct the main beam and in which directions it should put nulls. Dir-MAC requires a strictly small AS for its applying environment, while NULL-MAC imposes a somewhat relaxed requirement on AS. Authors of [52, 57, 56] claimed that NULL-MAC is applicable in a rich-scattering multipath propagation environment, like indoor or urban outdoor environment. However, if the degree of scattering exceeds some threshold, NULL-MAC will become less effective. In a rich-scattering environment that exhibits a very large AS, only SD-MAC can function effectively. Therefore, there should exist two thresholds in terms of AS, say θ_1 and θ_2. θ_1 can be used to determine whether a rich-scattering environment is appropriate for SD-MAC or NULL-MAC, and θ_2 is used to determine whether a weak-scattering environment is appropriate for NULL-MAC or Dir-MAC. A way to measure the AS can be found in [33]. However, it remains open how to determine those two thresholds.

3.5 Radiation power control (PC)

As mentioned in Section 3.2, directional radiation patterns can decrease the space occupied by the ongoing link so that the space reuse factor is increased and more links can be established simultaneously in the same area. Referring to Fig. 3.4, it is apparent that in addition to using directional patterns, radiation power control (PC) is applied. In Fig. 3.4, if the signal of A or B is not adapted so that they have the same coverage as those of F or H, then the other two links (D–G and C–E) cannot be established concurrently. Therefore, PC can help to further increase the space reuse factor by reducing the interference to other nodes. However, on the other side PC may cause a negative effect since it weakens the receiver's ability against interference.

In the following, the PC scheme proposed by us will be introduced, which is based on the MDA-MAC protocol (see Subsection 3.2.2), or can be regarded as an extension to MDA-MAC. Then network simulations will be described in Section 3.7 to evaluate the performance of PC. Note that the term radiation power means the radiated signal power, which is different from the power consumed by a node for transmission. As the term transmission power (P_t) is widely used in literature, we also use it in the following. It is identical to the radiation power described above.

The goal of the power control approach is to maintain a given nominal reception power $P_\mathrm{r,nom}$ at the destination node such that a target bit error rate is not exceeded. The reception power P_r depends on the transmission power P_t, the gain G_t and G_r of the transmitter and receiver antennas, respectively, and the path loss L_P between the nodes:

$$P_\mathrm{r} = (P_\mathrm{t} + G_\mathrm{t} + G_\mathrm{r} - L_\mathrm{P})/\mathrm{dBm}. \tag{3.5}$$

The gains G_t, G_r and the path loss L_P depend on the positions and orientations of the two nodes. They are constant as long as the nodes do not move and rotate. With the above assumptions, the nominal path loss of the incoming signal at the receiver can be calculated by

$$L_\mathrm{nom,in} = (P_\mathrm{t,in} - P_\mathrm{r,in})/\mathrm{dB}, \tag{3.6}$$

in which $P_\mathrm{t,in}$ is the transmission power of the sender and $P_\mathrm{r,in}$ is the measured reception power at the receiver. The incoming nominal loss $L_\mathrm{nom,in}$ of the receiver is exactly the outgoing nominal loss $L_\mathrm{nom,out}$ of the sender, which can be used to calculate the optimal transmission power $P_\mathrm{t,opt}$ of the sender for the next packet. That is

$$P_\mathrm{t,opt} = (P_\mathrm{r,nom} + \underbrace{[P_\mathrm{t,in} - P_\mathrm{r,in}]}_{L_\mathrm{nom,out}})/\mathrm{dBm}. \tag{3.7}$$

$P_{\mathrm{t,in}}$	$P_{\mathrm{r,in}}$	sec_{in}	$P_{\mathrm{t,out}}$	sec_{out}

Figure 3.9: Fields that need to be added to the MAC header.

Note that each node only applies $L_{\mathrm{nom,out}}$ (but not $L_{\mathrm{nom,in}}$) to calculate its optimal transmission power. Therefore, the receiver needs to transfer the information regarding $L_{\mathrm{nom,out}}$ (of the sender) back to the sender. To realize such a power control scheme, each node has to maintain a list of known neighbors and record $P_{\mathrm{t,in}}$ used at the sender and $P_{\mathrm{r,in}}$ measured at the receiver for all exchanged packets. For this purpose, a few fields have to be added to the MAC header of the packet that is transmitted next by the initiating node (see Fig. 3.9). They are: the transmission power $P_{\mathrm{t,in}}$, the reception power $P_{\mathrm{r,in}}$, and the transmission sector sec_{in} that have been extracted from the last received packet (transmitted by the partner node), the transmission power $P_{\mathrm{t,out}}$ and the sector sec_{out} that are used to transmit the current packet. $P_{\mathrm{t,in}}$ and $P_{\mathrm{r,in}}$ are intended to let the partner node calculate its optimal transmission power $P_{\mathrm{t,opt}}$ according to Eq. (3.7), in case that the partner's optimal reception sector to receive this packet is the one that sent the last packet (sec_{in}). And $P_{\mathrm{t,out}}$ and sec_{out} are intended to let the partner node feed the corresponding information back in the next packet so that the initiating node can also calculate its optimal transmission power. Note that this approach can also be used if the channel is non-reciprocal, because the nominal loss of the incoming and outgoing connections are measured separately. Therefore, communication systems based on frequency division duplex (FDD) or infrared light are also supported. Infrared systems have a separate transmitter and receiver. The field-of-view of the receiver and the half power beam width of the transmitter may not be equal, hence non-reciprocal channels occur. Additionally, our approach can easily be extended to apply the closed-loop power control if the signal power cannot be measured accurately enough.

Each source node can immediately adapt its transmission power after receiving the replying packet from its destination node. And the destination node can also adapt its transmission power if its outgoing nominal loss $L_{\mathrm{nom,out}}$ is fed back from the source node by the next packet. In the following packet exchanges, $P_{\mathrm{t,opt}}$ of the source or destination is updated continuously. Hence, if the nodes start to move, the transmission power is updated accordingly as long as the nodes communicate frequently enough. Furthermore, the above power control scheme can also be involved into the neighborhood discovery process (refer to Subsection 3.2.2.5 and [21]). And a series of operations are also designed to deal with the accidental conditions that may occur, e.g., the optimal reception sector is not the one that sent the previous packet so that the outgoing nominal loss derived from the received packet cannot be applied to calculate the optimal transmission power. All those details have been elaborated in [21].

3.6 Transceiver power management (PM)

The use of the MDA scheme may result in a higher space reuse factor, as illustrated by Fig. 3.4 and will be further justified by network simulations. However, due to the additionally required hardware for processing the signals from the increased number of antennas, the energy consumption is increased drastically. A good idea to solve this problem is to switch off the transceivers of sectors when it is not necessary for the node to perform communication in their directions. In addition, the transceiver must be restarted in time when it has packets to process, so that the network performance would not be affected too much. This scheme is called transceiver power management (PM). Note that the transceiver here refers to the combination of a RF transceiver and a baseband processing unit, which are basic components of a communication system.

In this section, a detailed energy model that covers sending, receiving, and carrier sensing will be given, and a PM scheme will be proposed on the basis of the previously proposed MDA-MAC. Similar to PC, PM can also be regarded as an extension to MDA-MAC. Moreover, it is possible to apply both PC and PM on the basic MDA-MAC protocol.

3.6.1 Energy model for the transceiver

A black-box energy model for the components of the transceiver will be described in this subsection. Feeney et al. have shown that a linear approximation can be used to model the power consumption of an 802.11b based WLAN network card [14]. They have measured the complete energy consumption (including the MAC protocol processor) for different types of traffic (broadcasting, point-to-point, overhearing, etc). We have developed a model of the energy consumption of the transceiver only, to include it in our simulation environment (see Section 3.7). Hence, different operations (receiving, sending, discarding packets and sensing the medium state) can be differentiated by collecting the required information in each simulated node. This has also the advantage that the (reception) energy consumed for unsuccessful attempts to acquire the channel (i.e., messages lost due to collisions) can be considered.

For the transceiver, we assume three modes of operation: *sending* (TX) and *receiving* (RX) packets as well as *sensing* (SX) the state of the medium. The energy consumed if one packet is received is estimated by

$$E_{\mathrm{RX}}(p) = P_{\mathrm{RX}} \cdot p/B, \tag{3.8}$$

where p is the size of the packet in bits, B is the data rate at which the packet is received, and P_{RX} is the power consumption of the transceiver in the RX mode. In the

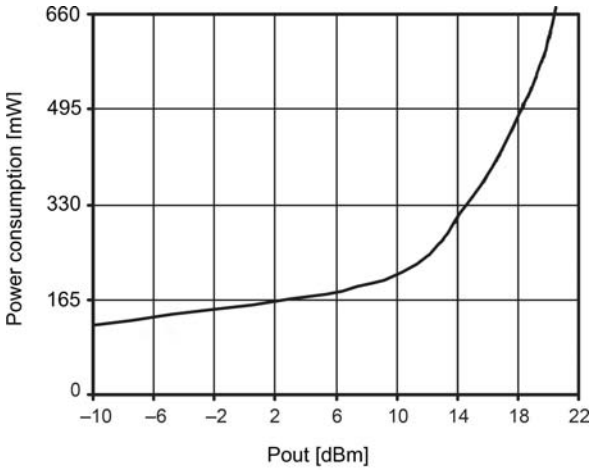

Figure 3.10: Power consumption of the power amplifier in dependence of the output radiation power [61] .

SX mode, the transceiver constantly listens if any signal power can be detected that is above the sensing threshold P_{s}. If a signal is detected, the transceiver switches to the RX mode. In modern digital communication systems, the power consumption in the SX mode is nearly as high as in the RX mode, since the baseband processing is also required for sensing the medium. This effect has also been experimentally verified by Feeney et al. They have measured that the power consumption in the sensing mode is only 12-18 % lower than in the receiving mode [14]. The following equation is used to estimate the sensing energy:

$$E_{\mathrm{SX}}(\Delta t) = P_{\mathrm{SX}} \cdot \Delta t, \tag{3.9}$$

where Δt is the duration that the transceiver is in the sensing mode and P_{SX} is the power consumption of the sensing mode. As for the transmission energy, the effect of radiation power control (PC, see Section 3.5) on the energy consumption is also taken into account, hence the power consumption of the power amplifier must be included. The following equation is used to calculate the energy consumed to send one packet:

$$E_{\mathrm{TX}}(p) = (P_{\mathrm{TX}} + P_{\mathrm{PA}}(P_{\mathrm{t}})) \cdot p/B, \tag{3.10}$$

where P_{TX} is the static power consumption (for RF transceiver and baseband processor), and the function $P_{\mathrm{PA}}(P_{\mathrm{t}})$ describes the dynamic power consumption of the power amplifier in dependence of the output power (which is treated as the transmission power P_{t} here). For the simulations, we have sampled the power curve that can be found in the data sheet of the Philip's 2.4 GHz SA2411 power amplifier [61] at 2 dBm steps and used a linear interpolation to obtain P_{PA} (see Fig. 3.10). It can be seen that the power efficiency of the amplifier is relatively low if the output power is below

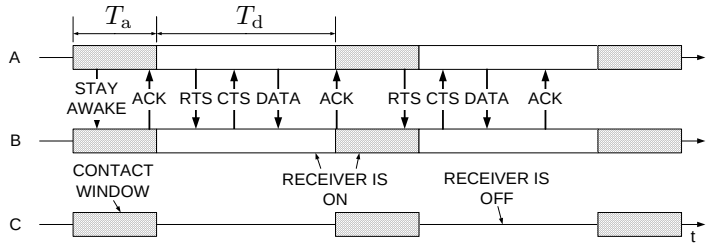

Figure 3.11: An example that shows how control and data packets are exchanged if power management is applied.

10 dBm. Hence, within this power domain, PC would not have a big impact on the total energy consumption of the node, which will also be proved by the simulation results in Section 3.7. Compared to the RM- and HCB-energy models in [66, 26] that assume that the power consumption of the amplifier and its generated radiation power have a linear relation, our TX energy model more accurately reflects the real energy consumption at the source node.

As for the static power consumption P_{TX}, P_{RX} and P_{SX}, the values provided in the data sheets of the Intersil's PRISM 11 Mbps 802.11b reference chip set [30] are used and listed in Tab. 3.3 (also see Fig. 2.1). Note that we assume a 15 % reduction of P_{RX} to obtain P_{SX} (in accordance with the results by Feeney et al.) since the data sheet of the PRISM chip set does not differentiate between the sensing and receiving modes.

3.6.2 Power management mechanism

If the MDA with K AMHAs is used, the sensing energy becomes K times large because K receivers are sensing the channels compared to one in the omni-directional case. For transmitting data from one node to another, only one sending sector and one receiving sector are required. Hence, all receivers except the one in the ORS of the destination node can be switched off during reception. However, there must exist time periods in which all receivers are switched on in order to start new transfers in other directions.

A simple power management strategy comparable to the one found in the IEEE 802.11 specification [46] is proposed. It uses periodically occurring contact windows in which all receivers are powered on. Outside the contact windows, only the receivers that are required for the current communication tasks remain powered on, the other ones are switched off. During the contact windows, the nodes that have buffered data packets use STAY AWAKE control packets to request the destination node to keep the receiver that is responsible for the ORS powered on. In order to implement this power management scheme, the clocks in the nodes have to be synchronized. This can be established by using the distributed clock synchronization (e.g., IEEE 802.11

manages to synchronize the clocks of all nodes with an offset of a few microseconds). The contact windows have a width of T_a seconds and a distance of T_d seconds (see Fig. 3.11). The following function decides whether the contact window is active:

$$cwin(t) = \begin{cases} 1 \quad \text{if} & t \geq \#cwin(t) \cdot (T_\mathrm{a} + T_\mathrm{d}) \wedge \\ & t \leq \#cwin(t) \cdot (T_\mathrm{a} + T_\mathrm{d}) + T_\mathrm{a} \\ 0 \quad \text{else} & \end{cases} \tag{3.11}$$

with $\#cwin(t) = \lfloor t/(T_\mathrm{a} + T_\mathrm{d}) \rfloor$. Each instance of a MAC layer has an *awake neighbors list* (ANL) that contains all neighbors that are known to be awake outside the contact window. Each entry contains the address adr of the neighbor and the time point $t_\mathrm{s}(adr)$ when it falls back to sleep.

If a packet needs to be sent, a check is performed first to see whether the destination is awake. The destination is awake if $cwin(t)$ is one or the ANL contains an entry for the destination for which $t < t_\mathrm{s}(adr)$ is fulfilled. The transmission of the packet is deferred until the start of the next contact window if the destination is not awake. The transmission of broadcast packets is always deferred if the contact window is not active. This is due to the fact that broadcast requires that all neighbors have turned on their receivers.

To keep a neighbor awake outside the contact window, a STAY AWAKE packet is transmitted before the data packet if no valid entry is found in the ANL. The packet is treated like a data packet whose size is below the RTS threshold p_RTS. Hence, the usual medium access and 2-way handshaking procedures are applied, which must occur in a contact window. The MAC layer of the ORS in which the control packet is received will set an internal sleep time-point t_s that points to the end time of the upcoming $\#awake$ number of contact windows:

$$t_\mathrm{s} = (\#cwin(t) + \#awake) \cdot (T_\mathrm{a} + T_\mathrm{d}) + T_\mathrm{a}. \tag{3.12}$$

Outside the contact window, if the sleep time is not reached ($t < t_\mathrm{s}$), the MAC layer keeps its receiver on. The sleep time is constantly updated when the MAC layer receives data packets. With this mechanism, the destination node will leave its receiver on as long as data packets are received. Hence, only one STAY AWAKE control packet needs to be transmitted for a burst of data packets. The optimal announcement traffic indication message (ATIM) approach in 802.11 requires that each node sends an ATIM in every ATIM window if it has more data to sent. Therefore, our dynamic update of the sleep time reduces the overhead. If the initiating node receives the acknowledgment for the STAY AWAKE or data packet, it will update the corresponding entry for the destination in its ANL. The time point $t_\mathrm{s}(adr)$ is updated according to Eq. (3.12).

Fig. 3.11 shows an example how the PM works. The number of awake periods is set to $\#awake = 1$. Node C and B lie in one of A's sectors. Node A has buffered data for node B. Hence, it sends a STAY AWAKE request to node B during the next contact window. B acknowledges the request and keeps its receiver on in the sector that has received the request. Then two 4-way handshaking procedures are performed between the active sectors of A and B. In this duration, all other sectors of A and B enter into the sleep and active modes periodically as usual. Since node A doesn't have further data packets to transmit in the third contact window, node A and B turn off all their receivers at the end of the third contact window. Node C is not involved in the communication, therefore it always switches off all its receivers outside the contact windows.

The use of contact windows will introduce an extra delay before the transmission of a burst of data packets starts. In the worst case, the initiating node has to wait T_d seconds until the next contact window starts to send the STAY AWAKE packet. Then it has to wait for the ACK from the receiver. If T_a is not large enough, this procedure may take several contact windows (in case the time-out event doesn't occur yet). Values for T_a, T_d and $\#awake$ should be carefully selected. The duration of the contact window T_a should be large enough such that every node can get an acknowledgment for its STAY AWAKE requests, therefore a duration of 50 ms is used in simulations. To obtain approximately the same sensing energy compared to a single transceiver system, we set the distance T_d between contact windows to $T_\mathrm{d} = (K-1) \cdot T_\mathrm{a}$. However, the above setting is only a try, the optimal values can be selected after numerous simulations.

3.7 Network simulation

We have implemented the CSMA/CA protocol, along with its extensions of MDA-MAC, radiation power control (PC) and transceiver power management (PM) in our packet processing library (PPL). The PPL allows a rapid implementation of network protocols. It has a hardware abstraction layer that allows to reuse the same implementation in different target environments, e.g., network simulators and real communication systems [20]. We have used the network simulator SAHNE (Simulation of an Ad Hoc Networking Environment) to verify the correct functionality of the implementation [67]. In addition to the omni-directional antenna, the MDA scheme described in Subsection 3.2.2.1 is modeled in SAHNE. The propagation model is based on the free space model. Time is slotted in SAHNE, and packets are transferred over several time slots, depending on their size. Collisions are simulated by using a signal-to-interference ratio threshold SIR_min. The highest packet power is regarded as the signal power, and the summed power of all other packets is regarded as the interference power. With

Table 3.2: Used performance measures.

Throughput S	Accumulated number of bits received by all destinations divided by the time point when the latest packet has been received.
End-to-end delay D_{E2E}	The time the data packets have been in delivery.
Radiation energy E_{RF}	Accumulated radiation energy required for sending packets of any type (a fraction of E_{TX}).
E_{TX}	Accumulated energy consumption for transmitting all packets.
E_{RX}	Accumulated energy consumption for receiving all packets.
E_{SX}	Accumulated energy consumption for sensing the medium.
E_{DX}	Accumulated energy consumption for unsuccessful receptions (discarding packets).
Total energy E	$E = E_{\mathrm{TX}} + E_{\mathrm{RX}} + E_{\mathrm{SX}} + E_{\mathrm{DX}}$
Packet delivery ratio PDR	The ratio of number of received packets at all destinations to the number of sent packets at all sources.

the help of the statistic functions inside the PPL, we have collected information about the network performance (see Tab. 3.2).

3.7.1 Simulation configurations

The simulation parameters are summarized in Tab. 3.3. Each simulated node is equipped with K 2.4 GHz 11 Mbps transceivers. The parameters for the transmitter and the medium access layer were adjusted according to the IEEE 802.11b specification [46]. For the MDA scheme, its half power beam width for each sector is set to $360\,°/K$. The maximum transmission power $P_{\mathrm{t,max}}$ was set such that each node can reach each other in the considered area, independent of their orientation.

The simulation scenario is a $w \times h$ area in which N nodes were randomly placed. G nodes were randomly selected as traffic generators, each of which sends $\#p$ packets with the fixed size p_{data} to other G randomly selected nodes as fast as possible. The simulation stops if all packets generated are delivered. Traffic sources cannot act as traffic destinations. All nodes perform the third neighborhood discovery algorithm (ND3, see Subsection 3.2.2.5). Therefore, even if a node is not a traffic generator it generates additional loads. No control packets are exchanged for route discovery, the routes are obtained by using the global network knowledge from SAHNE and the neighbor lists recorded on each node, based on the hop-minimal criteria. All possible combinations of N, G and K listed in Tab. 3.3 are iterated, with and without PC, with and without PM. Power control was first applied to DATA and ACK packets only (denoted by PC) and afterwards to all types of packets (denoted by PC+(CP)), see [21] for detail. Each scenario was simulated W times, with different seed values for the random number generators. A log file is generated after each simulation run

Table 3.3: Parameter settings.

Number of nodes	$N = \{20, 35, 50\}$	Time slot duration	$t_{\text{slot}} = 20\,\mu\text{s}$
Number of traffic generators	$G = \{1, 5, 10\}$	Sent packets per generator	$\#p = 750$
Air interfaces per node	$K = \{1, 4, 6, 8\}$	Simulations per scenario	$W = 5$
Data packet size	$p_{\text{data}} = 578\,\text{bytes}$	Area width and height	$w = h = 443\,\text{m}$
Max. transmission range	$d = 627.61\,\text{m}$	Sensing/reception threshold	$P_{\text{s}} = P_{\text{r}} = -76\,\text{dBm}$
Nominal reception power	$P_{\text{e,nom}} = -75.9\,\text{dBm}$	Signal-to-interference ratio	$SIR_{\text{min}} = 10\,\text{dB}$
Radio frequency	$f = 2.4\,\text{GHz}$	Reception power	$P_{\text{RX}} = 0.78\,\text{W}$
Sensing power	$P_{\text{SX}} = 0.66\,\text{W}$	Static transmission power	$P_{\text{TX}} = 0.82\,\text{W}$
Neighborhood discovery period	$T_{\text{ND}} = 0.5\,\text{s}$	Neighborhood discover jitter	$\Delta t_{\text{ND}} = \pm 0.05\,\text{s}$
RTS/CTS threshold	$p_{\text{RTS}} = 64\,\text{bytes}$	Min. contention window	$CWS_{\text{min}} = 32\,\text{slots}$
Max. contention window	$CWS_{\text{max}} = 1024\,\text{slots}$	Max. short and long retries	$RC_{\text{s}} = 4$, $RC_{\text{l}} = 7$
Awake periods	$\#awake = 1$	Awake time	$T_{\text{a}} = 50\,\text{ms}$
Max. TX power	$P_{\text{t,max}} = \{20, 12.6, 6, 0.4\}\,\text{dBm}$	Interframe spacing	$t_{\text{IFS}} = 40\,\mu\text{s}$
Antenna gain	$G_{\{t,r\}} = \{0, 6.7, 10, 12.8\}\,\text{dBic}$		

is finished, and the relevant values to calculate the performance measures (see Tab. 3.2) are extracted from this log file by using Matlab. The performance measures were first computed per node, then accumulated over all nodes and finally averaged over all performed simulation runs W per scenario. Mobility is not considered in these simulations. In summary, the considered scenario can be regarded as a worst case situation because a very high channel contention occurs (all traffic generators can reach their destinations with one hop and start to transmit data at the same time).

3.7.2 Results

First, in all performed simulations, the packet delivery ratio (PDR) is always above 99.5 %. This proves that the MDA-MAC implementation along with its extensions function well and provide a reliable access to the medium.

Fig. 3.12 contains exemplary diagrams showing the average throughput, delay and radiation energy for $N = 35$ nodes and $G = 10$ traffic generators. It can be seen that compared to the omni-directional case, the eight-sector MDA scheme increases the throughput up to a factor of 3 while deceasing the time required for the communication task by over 40 %, and a reduction up to 73% on the end-to-end delay is also obtained. However, it can be observed that power control (PC) doesn't cause obvious impacts on the performance of throughput and end-to-end delay in all cases. This result can be explained by the analysis made in Section 3.5 that the positive and negative effects of PC counteract each other. From the right figure of Fig. 3.12 we can see that an apparent reduction on the radiation energy E_{RF} is obtained if PC is applied on DATA and ACK packets, for both omni-directional and eight-sector MDA schemes. A further 4% reduction can be obtained if PC is applied on all types of packet. However, the reduction on E_{RF} only has a slight effect because later we can find that E_{RF} only accounts for a very small proportion of the total energy consumption E.

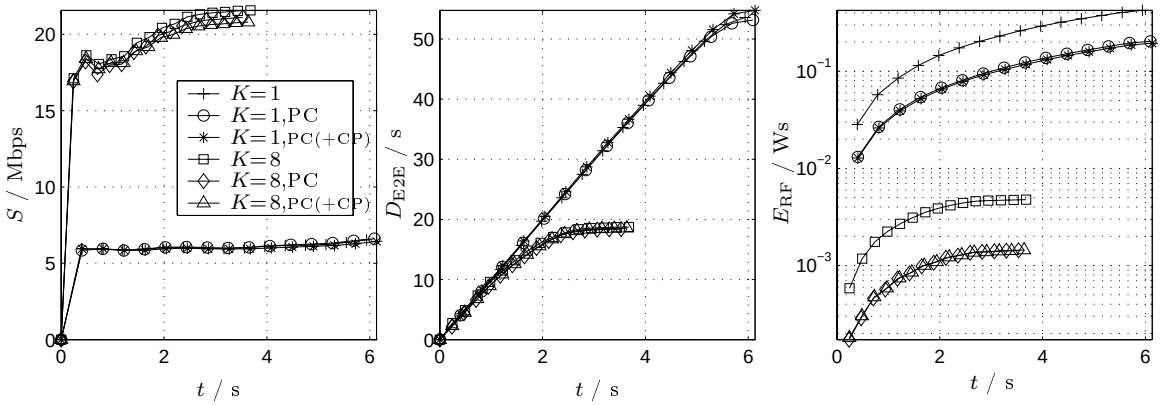

Figure 3.12: Exemplary throughput, end-to-end delay and total radiated energy ($N = 35$, $G = 10$) versus simulation time.

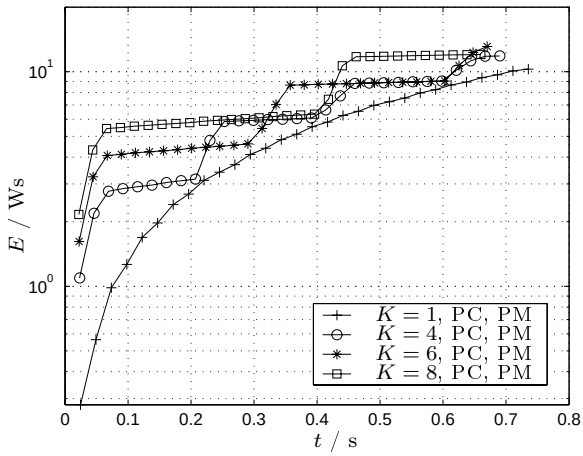

Figure 3.13: Exemplary total energy consumption ($N = 20$, $G = 1$) versus simulation time.

The effect of the power management can be seen in Fig. 3.13. It shows that the energy consumption in the contact window increases faster because all receivers are powered on. Outside the contact windows, only the senders and receivers that are responsible for communication are powered on. Hence, the energy consumption increases slower compared to the single transceiver system, due to the higher gain of directional antennas. However, because of the periodically occurring contact windows, the energy consumption for multiple transceivers always stays above the energy of the single transceiver system.

Fig. 3.14 illustrates an exemplary energy distribution when the same amount of tasks are assigned to different schemes. It can be observed that for the cases without using PM, PC helps to reduce the energy for receiving packets E_{RX} (less overhearing occurs) and discarding packets E_{DX} (less collisions occur) because of less radiation power. But the effect on the total energy is very small since the saving on E_{DX} and E_{RX} is nearly

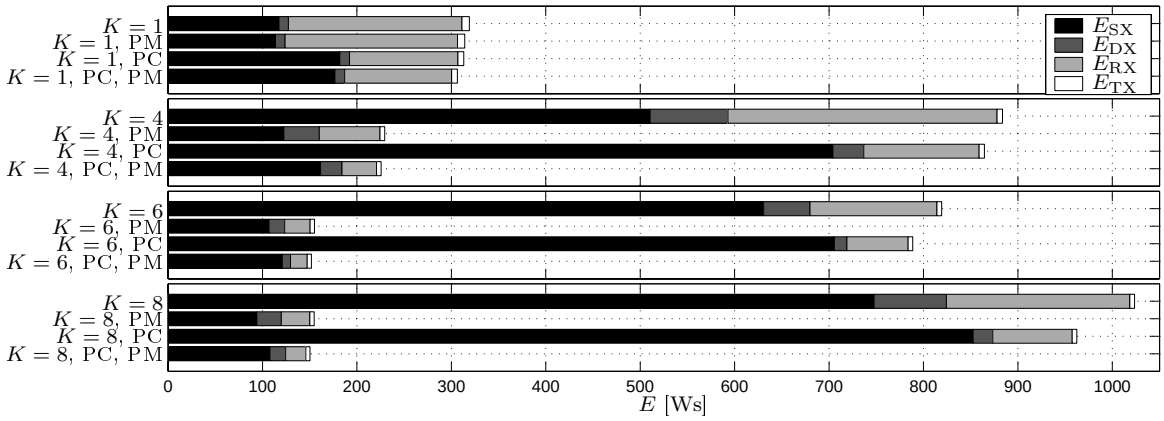

Figure 3.14: Exemplary energy distribution ($N = 35$, $G = 10$).

compensated by the increase on the sensing energy E_{SX}. The energy for transmitting packets E_{TX} is reduced if directional transmission is used. However, E_{TX} only accounts for less than 3 % of the total energy consumption E. As indicated by Fig. 3.12, PC can result in some reduction on E_{RF}, while E_{RF} is a part of E_{TX}. Hence, power control and the higher gain of directional antennas don't have a significant impact on the total battery energy consumption. On the other hand, it can be seen that the total energy consumption is drastically decreased (down to 1/8) if PM is used for MDA systems. From Fig. 3.14 we can see that the resulting energy consumption for the six- or eight-sector MDA system with PM only reaches around half of the energy consumed by the single antenna system. Therefore, the proposed power management plays the main role on extending the battery operation time.

3.8 Resource-efficiency comparison

In Tab. 3.4, a comparison among different combinational designs on the physical and MAC layers is given. For the first case (traditional designs), the network throughput is S_{omni} and the average power consumption is P_{omni}. The corresponding energy-efficiency and spectrum-efficiency are $\eta_{\mathrm{omni,E}}$ and $\eta_{\mathrm{omni,B}}$, respectively, according to their definitions given in Section 1.3. For the third case, the network throughput can be increased up to $3S_{\mathrm{omni}}$ (refer to [22], also implied by Fig. 3.12). To finish the same amount of tasks, the energy consumption of the six-sector MDA network with PM is reduced to around half of the energy consumed by the traditional network (see Fig. 3.14), and the used time is also reduced (but is longer than half of the time used by the traditional network, implied by Fig. 3.12). Therefore, the average power consumption of the six-sector MDA network with PM is less than the traditional network. It is estimated as around P_{omni} conservatively in Tab. 3.4. The above estimation results in

Table 3.4: Resource-efficiency comparison.

PHY+MAC designs	Network throughput	Average power consumption	Resource-efficiency	Hardware complexity
Single antenna omni-directional system + CSMA/CA	S_{omni}	P_{omni}	$\eta_{\text{omni, E}}$ $\eta_{\text{omni, B}}$	• 1RF transceiver • 1 baseband unit • 1MAC controller
six-antenna DBF smart antennas system + Dir-MAC	$< 3S_{\text{omni}}$	$>> P_{\text{omni}}$	$<< \eta_{\text{omni, E}}$ $< 3\eta_{\text{omni, B}}$	• 6 RF transceivers • 1 array signal pross. unit • 1 baseband unit • 1 MAC controller
six-sector MDA system + MDA-MAC, PM	$3S_{\text{omni}}$	$\sim P_{\text{omni}}$	$\sim 3\eta_{\text{omni, E}}$ $3\eta_{\text{omni, B}}$	• 6 RF transceivers • 6 baseband units • 1 multi-processor MAC controller

the increase of both efficiencies of energy and spectrum to about $3\eta_{\text{omni,E}}$ and $3\eta_{\text{omni,B}}$, respectively. As for the second case, the average power consumption is significantly higher than P_{omni} since a significantly higher power is consumed by each node (refer to the analysis in Section 2.5). Moreover, the PM scheme described above cannot be applied on the smart antennas (SA) system because SA requires all antenna branches to operate in parallel to generate the directional radiation pattern. Its network throughput is estimated to be less than $3S_{\text{omni}}$ since it is not able to perform communications in multiple sectors in parallel (as MDA systems). The above estimation results in an energy-efficiency that is significantly smaller than $\eta_{\text{omni,E}}$, and a spectrum-efficiency that is smaller than $3\eta_{\text{omni,B}}$.

From Tab. 3.4 we can see that the six-sector MDA scheme outperforms the other two schemes in both energy and spectrum efficiencies. However, the hardware complexity required by it is very high, along with the consequent higher cost and larger size, a reduced degree of feasibility on mobile portable devices results. This motivates to find a low complexity scheme though less performance improvement can be obtained. That is, to achieve a proper tradeoff between performance and hardware requirements.

Chapter 4

Simplified Switched Beam (SSB): PHY + MAC Design and Simulation

In this chapter, a six-antenna low complexity communication scheme called simplified switched beam (SSB) will be presented. Its motivation, design details on the physical layer, and the adapted MAC protocol SSB-MAC will be given first. Then its MAC layer performance will be evaluated by network simulations. Finally, a resource-efficiency comparison will be made among MANETs applying the single antenna scheme, the SSB scheme, and the six-sector MDA scheme. We will see that SSB can achieve a good tradeoff between performance and hardware requirements.

4.1 Motivation

In Chapter 2 we have described the principles of different multi-antenna techniques and analyzed the additional requirements on hardware complexity and power consumption imposed by them, compared to the traditional single antenna system. Many existent test-bed trials reported in literature imply that significant performance improvements can be achieved only at the cost of extremely high computing overhead and power consumption, which are not sustainable for mobile portable devices with the state-of-the-art technologies. Considering the limited resources available on mobile portable devices, in terms of battery capacity, computing capability, and size, the present focus shall be laid on the switched beam and space diversity schemes that require relatively low hardware complexity and power.

4.2 Antenna array selection

In [54] an eight-element Butler matrix switched beam system has been presented. As described in Subsection 2.2.2.1, the beamforming of a Butler matrix system is operated at the RF stage by general RF components like couplers and phase shifters, hence complex signal processing and multiple RF front-ends are not required. This

exhibits great advantages compared to the digital beamforming (DBF) steered beam systems. However, three shortcomings may prevent it from being applied on mobile portable devices. First, although the system operates on the 2.4 GHz ISM (industrial-scientific-medical) frequency band, the size of the eight-element uniform linear array (ULA) with the half wavelength space still reaches 44 cm, which is too large for portable devices. This can be solved by increasing the carrier frequency, which however results in complete new designs on the antenna and other RF components. Second, the eight beams only cover a 114° angular range in the horizontal plane, which is not sufficient for mobile devices since they usually require an omni-directional coverage. Finally, the sequential selection process through eight beams causes a lot of capacity loss.

In [5] a Bluetooth system applying antenna diversity has been presented. Two schemes can be used optionally, both of which apply the two-antenna half wavelength space array. The first scheme is the selection diversity, see Subsection 2.3.2, which selects the antenna with the higher signal power for data reception. The second one is the so called angle diversity scheme, which switches between the broadside pattern and the end-fire pattern [42], also based on the signal power. Broadside and end-fire patterns require the in-phase (0° phase shift) and counter-phase (180° phase shift) antenna feeds, respectively. Fig. 4.1 illustrates two array factors, from which we can observe that they are orthogonal (the peak of one pattern always corresponds to the null of the other pattern). The experimental measurements of [5] justifies that the angle diversity scheme outperforms the selection diversity scheme with respect to the link robustness. However, the design of [5] leaves two potentials for improvements. First, two patterns divide the whole azimuth too roughly. From Fig. 4.1 we can see that the half-power angular coverage of the end-fire pattern ($2 \times 120°$) is two times the size of the broadside pattern ($2 \times 60°$). Second, the system applies two Bluetooth transceivers so that the signal powers of two antennas or two patterns can be measured simultaneously, however only one transceiver is used for data reception. This parallel selection process may achieve the benefit of less capacity loss, but causes a significant hardware waste because the Bluetooth transceiver is the key and most expensive component of the system. Comparing the broadside pattern with the end-fire pattern, the former appears to be advantageous on the following two aspects:

- Its half power beam width (HPBW) is narrower (in the horizontal plane);
- It requires an in-phase antenna feed, which means that phase shifters are not required at the RF stage for signal combination and division. This avoids the additional loss caused by the phase shifting error, decreases the hardware complexity, and therefore is easy to implement.

To thoroughly compare the performance of the broadside and end-fire patterns, it is necessary to investigate their 3-D radiation intensity patterns. According to [3] (also

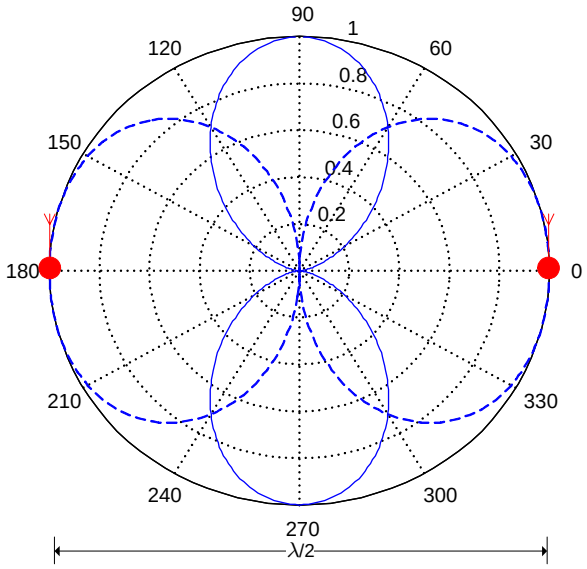

Figure 4.1: Two-antenna half wavelength space AFs in the horizontal plane: broadside case (solid line), end-fire case (dashed) [42].

refer to Eq. 2.14), the array factors of the broadside case and the end-fire case can be described by

$$\begin{aligned} \mathrm{AF}_{\mathrm{broadside}} &= |\cos[\tfrac{\pi}{2} \cdot \sin\theta \cdot \cos\phi]| \\ \mathrm{AF}_{\mathrm{endfire}} &= |\sin[\tfrac{\pi}{2} \cdot \sin\theta \cdot \cos\phi]|, \end{aligned} \tag{4.1}$$

in which θ and ϕ denote the elevation angle (0° to 180°) and the azimuth angle (0° to 360°), respectively. If we assume that each antenna is an isotropic element, then the radiation intensity of the array equals AF^2 (refer to Subsection 2.2.1). According to Eqs. (2.3) and (2.4), the directivity of the array can be derived as

$$D = \frac{4\pi}{\int_0^{2\pi}\int_0^{\pi} \mathrm{AF}^2(\theta,\phi)\sin\theta d\theta d\phi}. \tag{4.2}$$

Substituting Eq. (4.1) into Eq. (4.2) we can obtain

$$D_{\mathrm{broadside}} = D_{\mathrm{endfire}} = 2 = 3 \text{ dB}, \tag{4.3}$$

which shows that the directivities of both patterns are the same. However, from Fig. 4.1 we can find that the beam width of the end-fire case is much wider than that of the broadside case. To explain this contradiction, the observation should not be limited in the horizontal plane, but be made in the three-dimensional space. Fig. 4.2 shows the 3-D array factors of both cases according to Eq. (4.1). We can observe that the array factor of the broadside case is omnidirectional in the Y-Z plane (vertical plane), while the end-fire case array factor is directional in any vertical plane. Fig. 4.1 shows their

array factors in the X-Y plane (horizontal plane). However, the directivity is defined as the ratio of the maximal radiation intensity to the averaged radiation intensity over all solid angles, not just over the azimuth angles.

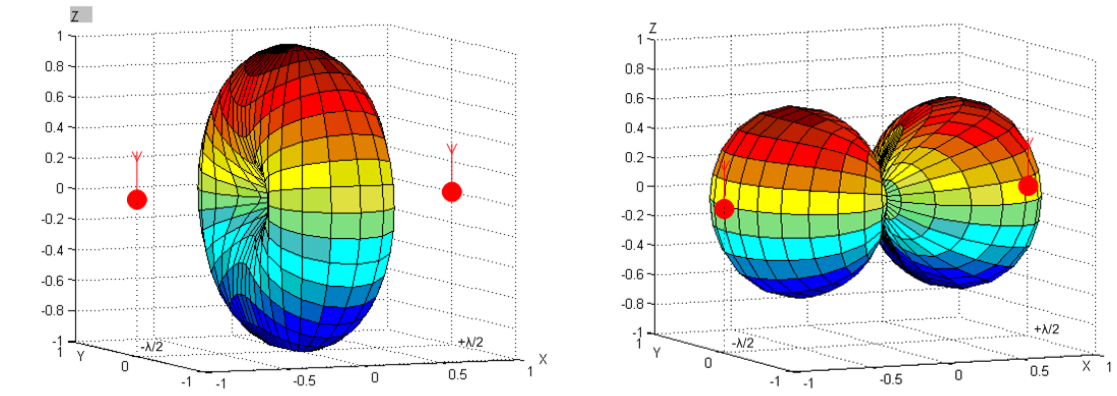

Figure 4.2: 3-D AFs of the two-antenna half wavelength space array: broadside case (left) and end-fire case (right).

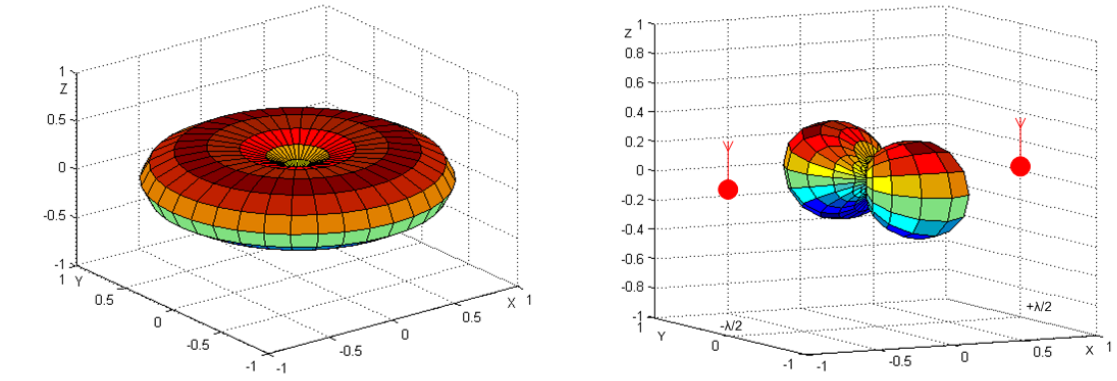

Figure 4.3: 3-D normalized radiation pattern of the half wavelength dipole (left), and the overall radiation intensity pattern of the broadside case array when dipole is used as its antenna element (right).

In general, when we call an antenna omnidirectional, this means it holds the same radiation intensity over all azimuth angles (in the horizontal plane). When an antenna is called isotropic, then it holds the same radiation intensity over the whole solid angles. Isotropic antenna doesn't exist in reality, but there are many omnidirectional antennas, e.g., half wavelength dipole, normal mode helical antenna (NMHA) [42]. In most cases, nodes in mobile ad hoc networks communicate with each other in the horizontal plane, thus the broadside case pattern has the disadvantage that the radiation power in the

vertical direction is wasted. However, this disadvantage can be compensated by the directivity of the antenna element. Many antennas, e.g., the half wavelength dipole radiates no power in the vertical direction. The normalized radiation intensity pattern of the half wavelength dipole is [42]

$$U_{\text{dipole}}(\theta,\phi) = [\frac{\cos(\pi/2 \cdot \cos\theta)}{\sin\theta}]^2, \tag{4.4}$$

in which θ denotes the elevation angle. It reveals that the pattern is irrelevant to the azimuth angle ϕ, which is also illustrated three-dimensionally by Fig. 4.3. Applying Eqs. (2.15), (4.1) and (4.4) we obtain the radiation intensity pattern of the two-element broadside case half wavelength dipole antenna array

$$U_{\text{broadside}}(\theta,\phi) = [\frac{\cos(\pi/2 \cdot \cos\theta)\cos(\pi/2 \cdot \sin\theta \cdot \cos\phi)}{\sin\theta}]^2, \tag{4.5}$$

which is shown in Fig. 4.3 three-dimensionally. We can see that this pattern exhibits good directivity in both horizontal and vertical planes. Together with its low complexity requirement on implementation, this array design is suitable for mobile portable devices.

4.3 The design of SSB

4.3.1 Basic principle

According to the analysis in Section 4.2, the two-element broadside case half wavelength dipole antenna array is suitable for mobile portable devices due to its low complexity requirement on implementation and good directional property. However, one broadside pattern cannot achieve the whole azimuth coverage because it only generates a bi-directional beam with about 60° half power beam width on each side, see Fig. 4.1. A good solution is to use three such arrays on the same node with a proper orientation. Hence, we consider the circular array configuration illustrated in Fig. 4.4. We can see that the resulting radiation intensity pattern gives a 13.6 dB sidelobe ratio and a -3 dB crossover level, which are comparable to the four-antenna Butler matrix pattern, see Fig. 2.5. Of course, in this case three beams are not orthogonal to each other.

The block diagram of the proposed simplified switched beam (SSB) is illustrated by Fig. 4.5. The resulting three bi-directional beams are able to cover the whole azimuth around the node. Electrical switching is used to realize communication in any intended beam, which will be called sector in this thesis. With the assistance of an in-phase RF combiner & divider, the antenna pair on the diagonal can generate a broadside

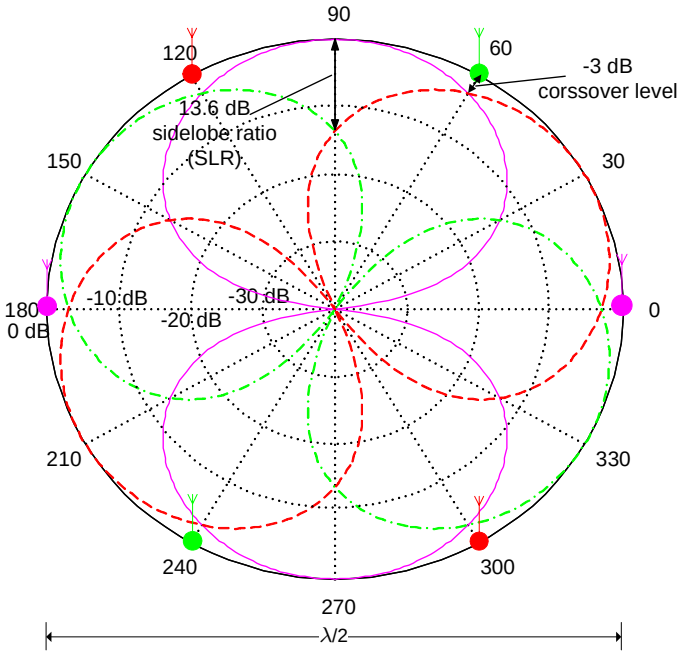

Figure 4.4: The intensity radiation pattern of the simplified switched beam (SSB) scheme in the horizontal plane (with dB scale).

pattern. For example, in Fig. 4.5 the antenna pair with the orientations of 120° and 300° can generate the bi-directional beam pointing to the directions of 30° and 210° (S1). At one moment, only one antenna pair is switched on for data reception or transmission. It should be noted that the same sector can be used for either reception or transmission, because each RF component of SSB can operate in both directions.

To keep the hardware complexity and power overhead low, only one signal processing branch (composed of one RF transceiver and one baseband processor) is used for SSB. However, the saving of hardware would cost an additional time overhead, as will be explained later. Two high speed RF switches are applied to select the intended antenna pair. The decision which pair should be switched on is based on the received signal strength. Before receiving data, the system needs to perform an optimal reception sector selection (ORSS) process, during which three antenna pairs are switched on sequentially. In each turn, the RF transceiver's received signal strength indicator (RSSI) is digitalized and cached in the judging unit. When three values are obtained, the judging unit makes the decision and sends a command to switch on the antenna pair that generated the largest RSSI for reception. Immediately after that, it informs the baseband unit via a READY signal that the RF front-end is ready for reception. The following data transmission uses the same antenna pair due to the reciprocal property of the radio channel. On the transmitter side, a training duration needs to be reserved before transmitting valid data, during which pilot signals are sent. Due to the use of a single signal processing branch (unlike the case in [5]), the ORSS process

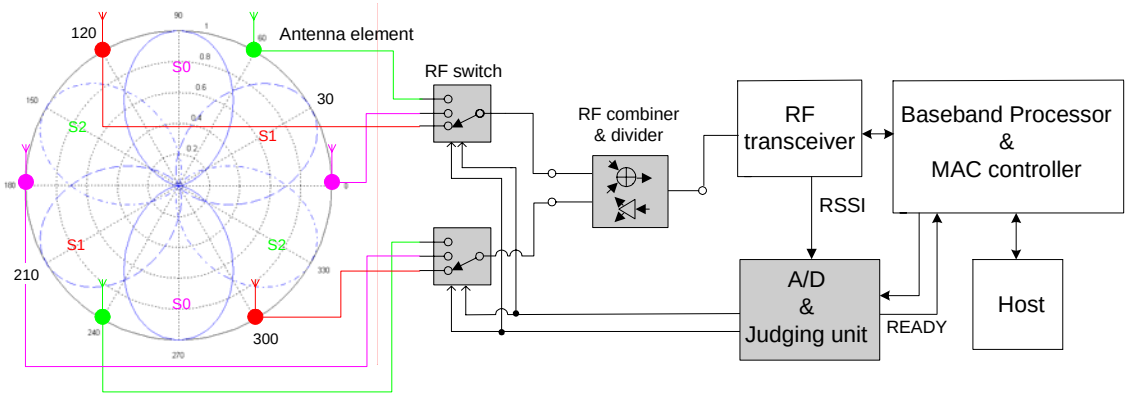

Figure 4.5: Simplified Switched Beam (SSB) Scheme

consumes more time, which causes an additional overhead to the system. In the idle state, the node turns off the A/D unit to save power. Three antenna pairs are switched on sequentially with a proper interval (which will be discussed in Subsection 4.3.2). When the RF transceiver detects any power exceeding the sensing threshold P_s, it will immediately activate the A/D chip and start up the ORSS process.

Comparing this scheme with the six-antenna digital beamforming (DBF) system, SSB decreases the number of RF transceivers from six to one, thus hardware cost and power consumption are saved considerably. The computing requirement is also reduced dramatically. The DBF system needs to calculate six coefficients, weight and combine six digital IF or baseband signals while SSB only needs to make a simple comparison. Of course, it can be intuitively concluded that its performance improvement is less than that of the DBF system, since its array pattern can be regarded as a 60° HPBW main beam but accompanying with a very large back-lobe (identical to the main-lobe).

In Fig. 4.5, the gray-marked components are additional ones compared to the single antenna system. Thanks to the progress on chip technologies, they would not occupy much board area. If 2.4 GHz (ISM band) is applied as the carrier frequency, the diameter of the antenna array is 6.25 cm, which is appropriate for most portable devices. It can be further decreased with a higher carrier frequency. And more important, those additional components would not cause much power dissipation, too. The in-phase RF combiner & divider is a passive component. A modern RF switch chip consumes less than 1 mW power, which is nearly negligible for the whole system. Although the A/D & judging unit may consume considerable power under the continuous operating mode (some hundreds of milliwatt), they can be powered on only in the short training duration. Looking over the available ICs for wireless LAN, we found that the average power consumption of a transceiver & baseband & MAC unit is never less than 500 mW. Say the A/D & judging unit also consumes 500 mW and is powered on for 10% of the total communication time (note that these two values are estimated conservatively for real

systems), then these additional components cause a 10% power overhead. Nowadays many transceiver & baseband chips are able to directly output the digital RSSI value since the digital baseband processing requires a high speed A/D module anyway. In this case, SSB nearly causes no extra power overhead and its hardware complexity can be further decreased. With the cost of those sustainable resources on mobile portable devices, higher performances can be achieved, as will be shown in Section 4.4.

4.3.2 Analysis on the length of the training period

In [7], the training period places an upper limit on the convergence speed of the direction of arrival (DOA) estimation and beamforming algorithms. For those algorithms, the longer the training period, the more sufficient convergence they can achieve, and thus a more accurate radiation pattern can be generated. This conclusion doesn't hold for the SSB system. For SSB, the length of the training period only depends on the reaction speed of the hardware. Enlarging the length of the training period would not help to increase the precision of the ORSS process. On the contrary, it will cause more overheads to the network. The length of the training period T_{TR} can be expressed as:

$$T_{\mathrm{TR}} = 3 * (T_{\mathrm{sw}} + T_{\mathrm{RSSI}} + T_{\mathrm{ad}}) + T_{\mathrm{comp}} + \Delta t, \tag{4.6}$$

in which T_{sw} is the response time of the RF switch, T_{RSSI} is the analog RSSI generating time, T_{ad} is the A/D conversion and data acquisition time, T_{comp} is the comparison time of the judging unit, and Δt is an appropriate margin. The interval between two switches is set to $T_{\mathrm{sw}} + T_{\mathrm{RSSI}} + T_{\mathrm{ad}}$. It is indicated that the state-of-the-art RF switch can sustain switching cycles of over 7×10^9 times [15] with the response time on the order of nanosecond, and the 3-value comparison can be easily accomplished in a few nanoseconds, too. Therefore T_{sw} and T_{comp} can be ignored. An up-to-date RF transceiver may output the valid RSSI value as fast as 1 μs (e.g., TEMIC's Bluetooth transceiver & baseband chip T2901), and T_{ad} is less than 2 μs if an A/D chip with the 500 ksps sampling rate is applied (e.g., MAXIM's A/D chip MAX120). With these available components, one training period T_{TR} can be set up to 20 μs. It can be further decreased with the cost of higher power overhead and chip expense. In [54] the duration 8×3.48 μs is reserved for the eight-beam Butler matrix switched beam system, which seems somewhat tight.

4.3.3 SSB-MAC: the associated MAC protocol

As indicated in Section 3.2, when a new technology is applied on the physical layer, the MAC protocol must be adapted accordingly to match the new property. Similarly, SSB also requires the corresponding modifications on CSMA/CA to achieve the best

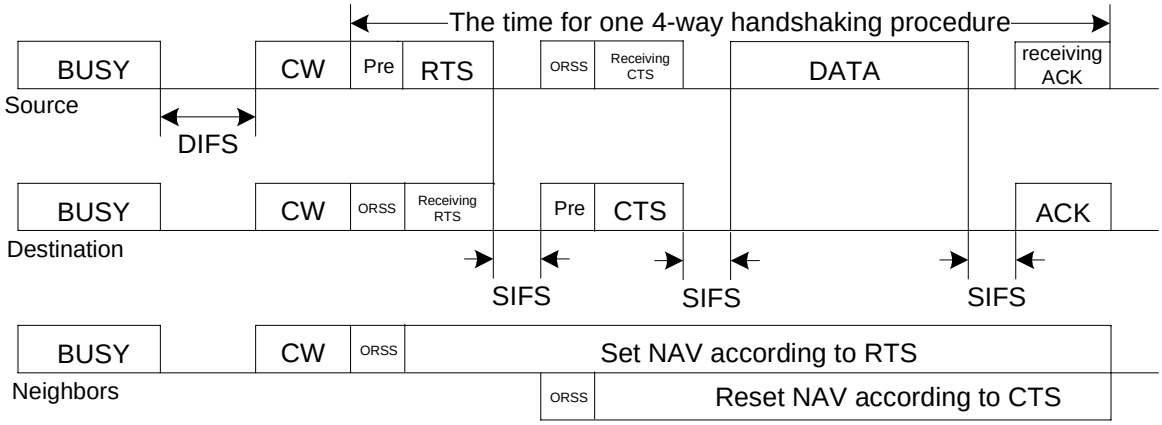

Figure 4.6: The proposed SSB-MAC protocol.

possible performance for MANETs. The adapted CSMA/CA for SSB can be called SSB-MAC. In the following, we elaborate the SSB-MAC according to the 8-item format used in Subsection 3.2.1 (the first item has been addressed above):

- The neighbor's direction is obtained by using the optimal reception sector selection (ORSS) process, as described in Subsection 4.3.1.
- RTS TX/RX. RTS is transmitted directionally in the selected sector. The sector to transmit RTS is determined by the neighborhood discovery, which is elaborated in [84] (similar to the one described in Subsection 3.2.2.5). RTS is received directionally in the determined optimal reception sector (ORS) of the destination node. It should be noted that a preamble (training sequence) must be used at the beginning of RTS to let the destination carry out ORSS, see Fig. 4.6.
- CTS TX/RX. CTS is transmitted directionally by the ORS that received RTS. CTS is received directionally by the ORS of the source node, which is updated and may not be the one that transmitted RTS. Similar to RTS, a preamble (training sequence) is also used at the beginning of CTS to let the source carry out ORSS, see Fig. 4.6. After the successful exchange of RTS and CTS, a directional link has been established between source and destination and their ORSs are fixed until the end of the 4-way handshaking procedure.
- DATA TX/RX. DATA is transmitted directionally by the ORS that received CTS on the source node, and is received directionally by the ORS that received RTS on the destination node.
- ACK TX/RX. ACK is transmitted directionally by the ORS that received DATA (or RTS) on the destination node, and is received directionally by the ORS that received CTS on the source node.

- PCS. When the node is in the idle state (does not send or receive any signal), the RF switch switches on three antenna pairs sequentially with the interval given in Subsection 4.3.2. In each turn, the detected RSSI will be compared with a threshold to determine whether there is carrier in the air. That is, a directional PCS is performed in each sector individually.

- VCS is performed by each sector individually, that is, each sector is associated with its own NAV.

From above description we can see that the ORS is always treated as the optimal transmission sector (OTS) due to the reciprocal property of the radio channel. To ensure the validity of the determined ORS through the whole 4-way handshaking procedure, one constraint required by SSB-MAC is that the time for one 4-way handshaking procedure (see Fig. 4.6) should not exceed the channel coherence time τ_c. A popular rule of thumb for estimating the channel coherence time is [63]

$$\tau_c = \frac{1}{f_d}\sqrt{\frac{9}{16\pi}} = \frac{0.423}{f_d}, \tag{4.7}$$

in which f_d is the maximum Doppler frequency. It can be calculated by

$$f_d = f_0\frac{|\overrightarrow{v}|}{c_0}, \tag{4.8}$$

in which f_0 is the carrier frequency, c_0 is the light speed in vacuum and $\overrightarrow{v}$ denotes the relative speed between transmitter and receiver.

4.3.4 Beamforming vs. Diversity

As indicated in Chapter 2, multi-antenna techniques can result in three types of gains: beamforming gain, diversity gain, and spatial multiplexing gain. The first can increase the user signal power, enlarge the transmission range and suppress the interference. The second can enhance the link robustness in terms of the reduced bit error rate (BER). And the last gain helps to increase the point-to-point link capacity (or spectral efficiency). Furthermore, as indicated in Chapter 3, a higher space reuse factor in the multipoints-to-multipoints scenario can be achieved when beamforming is used together with the associated BF-MAC protocol. SSB was motivated by beamforming, and its original intension is to increase the network capacity by the beamforming gain, since the link between two SSB systems consumes less space than two omni-directional single antenna systems, and thus more links can be established simultaneously in the same area. However, by further investigations we find that SSB is also a special case of

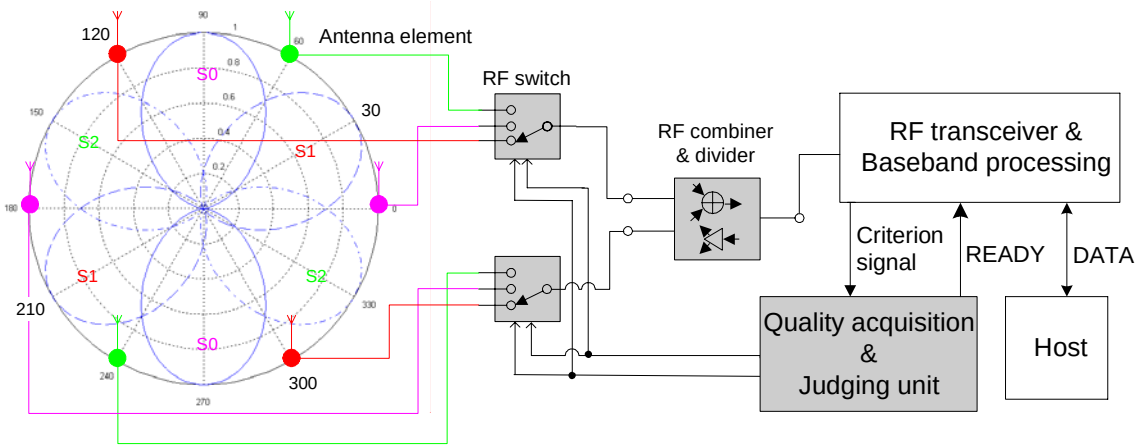

Figure 4.7: The general structure of the SSB Scheme.

the antenna diversity scheme, which is called generalized diversity selection combining (GSC) in [39] or hybrid selection/maximal-ratio combining (H-S/MRC) in [80].

Besides the discussion in Subsection 2.3.1, it is necessary to highlight again the relationship between beamforming and space diversity techniques. Beamforming is suitable for a weak-fading environment where the impinging signal exhibits a small angle spread, while diversity is suitable for a rich-fading (e.g., Rayleigh fading) environment where the intended signal impinges on the receiver with a broad range of directions and different arriving time due to the multi-path propagation. Beamforming requires a high correlation among antenna elements so that the impinging signal exhibits a planar wave-front for the array and there is only a phase difference between signals on different antennas, while diversity requires them to be sufficiently uncorrelated so that the signal on each antenna has experienced an independent fading. SSB uses the array with the half wavelength space, which can offer a small enough correlation in a rich-fading environment (e.g., an indoor scenario with arbitrary scatters) [36], and is able to generate a broadside directional beam in a weak-fading environment (e.g., an outdoor scenario or the anechoic chamber laboratorial environment) [42]. Therefore, SSB can be regarded as either a beamforming or a diversity scheme, depending on the place where it is applied. In a rich-fading scenario where SSB's space diversity property plays the main role, the transmission of OTS also results in the transmit diversity gain.

4.3.5 Interference suppression (IS) technique

The basic SSB design (see Subsection 4.3.1) uses the **RSSI-based criterion** for beam selection. A serous problem encountered by all switched beam systems is the disturbance caused by the co-channel interference (CCI). During the ORSS process, if the RSSI signal is measured on the CCI but not on the intended signal, then the deter-

mined sector gives the largest power for interference. This would result in even worse performances than the single antenna receiver. Therefore, an interference suppression (IS) technique must be adopted. The key idea is to find a way to distinguish between the interference and the intended signals to ensure that ORSS is only performed on the latter. However, the receiver is not able to make the correct determination by using the RSSI only. Therefore, two other criterion signals are considered.

BER-based criterion On each sector, a fixed number of pre-known data is received and the bit error rate (BER) is calculated. By comparing three BERs, the ORS can be correctly determined since the measured BER for the CCI must exceed a threshold, and the smallest BER most probably corresponds to the sector with the highest SNIR (signal to noise plus interference power ratio). However, this scheme has the following weakness. If the time for BER measurements is reserved short to avoid a large capacity loss, then the measured BER may not be accurate enough for the correct ORS determination. On the other side, if sufficient time is used for accurate BER measurements, then the resulting capacity loss may be too high. A worse consequence in this case is that there is no time left for data transmission before the radio channel changes if the length of the overhead is comparable to the channel coherence time τ_c. In [54], the eight-beam Butler matrix switched beam system applies 48 bits data on each beam to measure BER, which may be too short for accurate BER measurements.

LQI-based criterion The function of LQI (link quality indicator) is indicated by its name. This criterion signal is composed of two parts: RSSI and correlation. The RF transceiver should carry out RSSI measurement and pilot signal correlation simultaneously, and a proper combination of the two outputs generates the LQI. The LQI-based scheme can avoid the wrong determination of the RSSI-based scheme caused by the CCI, since it may generate a high RSSI, but only a small correlation value. The difficulty faced by this scheme is to realize the correlator during the preamble, as this may require an additional processing module (because partial baseband processing functions are required for correlator). At present, some RF chips (e.g., the ZigBee chip CC2420 from Chipcon) perform this operation after the correct detection of the preamble (while receiving data). However, this late-coming correlation value cannot be used by ORSS. It will be shown later (see Subsection 5.3.2.6) that our test-bed applies a quasi-LQI-based scheme to resolve this difficulty using a currently available RF chip.

For the further differentiation between the interference signal and the user signal, or even between different users in a multi-user scenario, the color code can be used for the correct sector selection (e.g., CDVCC used in IS-54 or SAT tone used in AMPS) [59]. Fig. 4.7 illustrates a general block diagram of SSB.

4.4 Network simulation

In this section, we evaluate the performance of the SSB + SSB-MAC cross-layer design for MANETs via network simulations. The measurement is based on the ideal broadside beam shape obtained by the free space model (see Fig. 4.4), which is not realizable in a rich-fading indoor environment. Therefore, the performance measured in this section gives the upper bound for a real network. However, the benefits of the inherent receive diversity and transmit diversity (when SSB is used in an indoor scenario) on the physical layer have not been taken into account.

4.4.1 Simulation configurations

We have implemented the CSMA/CA protocol along with its modifications for the SSB scheme in our packet processing library (PPL). The PPL allows a rapid implementation of network protocols. It has a hardware abstraction layer that allows to reuse the same implementation in different target environments, e.g., network simulators and real communication systems [20]. We have used the network simulator SAHNE [67] to verify the correct functionality of the implementation. Three systems are modeled in SAHNE. The first model is a single antenna system that transmits/receives signals omni-directionally. The proposed SSB system is the second model, whose antenna element is selected as the half wavelength dipole antenna that holds the 2.15 dBi directivity (with reference to an isotropic antenna) [42]. It can transmit/receive signals in one of three sectors exclusively. The third system model uses the six-sector MDA scheme (see Subsection 3.2.2.1). Six axial mode helical antennas (each one holds the 60° HPBW and the 10 dBi directivity) are applied on each node, and they are oriented such that their main beam directions distribute equally (circularly) around the node in the horizontal plane. This divides the space in six sectors. Furthermore, the node is able to communicate in six sectors in parallel. We apply the first and third models as the lower and upper bounds for the proposed SSB system, respectively. Corresponding to these three systems, the usual CSMA/CA, SSB-MAC and MDA-MAC are used. The propagation channel is based on the free space model. Time is slotted in SAHNE, and packets are transferred over several time slots, depending on their size. With the help of the statistic functions inside the PPL, we have collected information about the network throughput, which is defined as the accumulated number of bits received by all destinations in the elapsed time until the reception of the last packet.

All simulation parameters are summarized in Tab. 4.2. The parameters for the transmitter and the medium access layer were adjusted according to the IEEE 802.11b specification [46]. The communication scenario consists of n nodes that are randomly placed in a square area. Among these nodes, g traffic sources are randomly selected

Table 4.1: Simulated scenarios.

high density, extreme busy scenario	N=50, $g = 20$, $w = h = 443$m
high density, average busy scenario	N=50, $g = 10$, $w = h = 443$m
average density, extreme busy scenario	N=50, $g = 20$, $w = h = 1000$m
average density, average busy scenario	N=50, $g = 10$, $w = h = 1000$m

Table 4.2: Parameter settings.

Number of nodes	$N = \{50\}$	Time slot duration	$t_{\text{slot}} = 20\,\mu$s
Number of traffic generators	$G = \{10, 20\}$	Sent packets per generator	$\#p = 260$
Air interfaces per node	$K = \{1, 3, 6\}$	Simulations per scenario	$W = 3$
Antenna (array) gain	$G_{\{t,r\}} = \{0, 5.15, 10\}$dBi	Training period length	$T_{\text{TR}} = \{0, 1\}$slot
Data packet size	$p_{\text{data}} = 578$ bytes	Area width and height	$w = h = \{443, 1000\}$m
Max. transmission range	$d = 627.61$ m	Sensing/reception threshold	$P_{\text{s}} = P_{\text{r}} = -85$ dBm
SIR threshold	$SIR_{\min} = 12$ dB	Radio frequency	$f = 2.4$ GHz
Neighborhood discovery period	$T_{\text{ND}} = 0.5$ s	Neighborhood discover jitter	$\Delta t_{\text{ND}} = \pm 0.05$ s
Neighbor delete time-out	$T_{\text{n}} = 1$ s	Transferred bytes per time slot	$l_{\text{slot}} = 28$ bytes
RTS/CTS threshold	$p_{\text{RTS}} = 64$ bytes	Min. contention window	$CWS_{\min} = 32$ slots
Max. contention window	$CWS_{\max} = 1024$ slots	Max. short and long retries	$RC_{\text{s}} = 4$, $RC_{\text{l}} = 7$
Transmission power	$P_{\text{t}} = \{11, 6.7, -3\}$ dBm	Interframe spacing	$t_{\text{IFS}} = 40\,\mu$s

that send DATA packets to g randomly selected traffic destinations. Traffic sources cannot act as traffic destinations. Every traffic generator sends $\#p$ DATA packets to its destination as fast as possible. Four scenarios are designed for simulations, as described in Tab. 4.1. The transmission power P_{t} of each model is adjusted such that every node can reach every other node independent of their orientations in the high density scenario. The maximum transmission range d of different models in all scenarios is the same, as described in Tab. 4.2. Every setting was simulated W times on different scenarios that use different seed values for the random number generators. The performance measures shown are the average of all performed simulations. The neighborhood discovery algorithm ND3 (described in Subsection 3.2.2.5) has also been implemented. Mobility is not taken into account, thus all nodes stop creating HELLO packets after 0.5 s to avoid the additional overhead.

4.4.2 Results

Fig. 4.8 (left) gives the throughput in the high density scenario, as described in Tab. 4.1. Results show that the SSB system achieves up to two times the throughput of the omni-directional system. This implies that in the directional case more links exist in the same area simultaneously. Furthermore, the throughput enhancement of the extreme busy scenario (g=20) is higher than that of the average busy scenario (g=10). This is reasonable because a higher load may force the network to establish more links concurrently (this holds for the average density scenario, too. See Fig. 4.8 (right)). The six-sector system achieves a higher throughput than the SSB scheme as expected, since its back-lobe is much smaller. However, we can observe that directional schemes

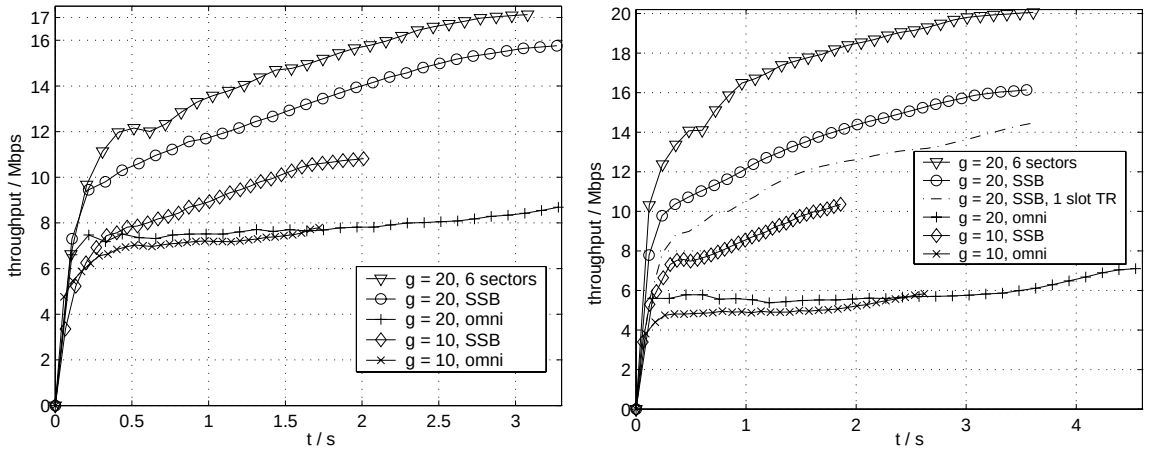

Figure 4.8: Throughput of the high density scenario ($n = 50$, $w = h = 443$m) (left) and the average density scenario ($n = 50$, $W = h = 1000$m) (right), all versus simulation time.

don't always show the advantage on the task finishing time as expected. After a careful analysis on the original data, we found that it is caused by the routing protocol and the data processing way we applied. In simulations, a general shortest hop routing method is applied, and the average throughput of W runs is used in the figure. However, the worst case task finishing time (not the average one) is used in the illustration. Usually, there will be a slight difference on the task finishing time of different simulation runs with the same setting. In case that occasional congestions occur on certain links of one simulation run, its task finishing time will be distinctly longer than other runs and thus the overall average throughput is degraded. This phenomenon suggests that the routing protocol also needs to be investigated to effectively overcome the congestion problem, especially in the case of directional communications.

Fig. 4.8 (right) gives the throughput of the average density scenario. In this scenario, the number of nodes keeps the same, but the area is enlarged. It can be noticed that the throughput enhancement due to the directional link is higher than that of the high density scenario, in either the extreme busy load or the average busy load condition. In the average density scenario, packet deliveries via multiple hops are more likely to occur for both omni- and directional communications since the area is larger and the single-hop communication range d is the same. This condition offers the directional system more potentials to increase the network performance. The throughput difference between the six-sector system and the SSB system is larger than that of the high density scenario. This can also be explained by the area enlargement.

All above results just illustrate the performance upper bound for SSB, since the length of the training period is set to 0 slot. In the last set of simulations, T_{TR} is set to 1 slot (20 μs), and the result is given by the dashed line in Fig. 4.8 (right). Its

performance is below its upper bound as expected, whereas it can still achieve up to two times the throughput of the omni-directional system. Comparing this result with the performance of the six-sector MDA system, nearly one third of the throughput is degraded. However, the hardware complexity required by SSB is significantly lower.

4.5 Resource-efficiency comparison

Similar to Section 3.8, a comparison among different combinational designs on the physical and MAC layers is given in Tab. 4.3. The first and third cases are kept the same as in Tab. 3.4, and the SSB + SSB-MAC is listed as the second case. As indicated in Section 4.4 and Subsection 4.3.1, respectively, its network throughput is increased up to $2S_{\text{omni}}$ and the average power consumption is increased to $1.1P_{\text{omni}}$. Therefore, the corresponding energy-efficiency and spectrum-efficiency can be calculated according to the definitions given in Section 1.3. From Tab. 4.3 we can see that for both energy and spectrum efficiencies the SSB scheme stands between the omni-directional scheme and the six-sector MDA scheme. Compared to the former scheme, it achieves higher performance and resource efficiency at the cost of few additional components; compared to the latter scheme, its performance and resource efficiency are lower, however, significant savings on hardware cost and complexity are obtained. Therefore, a proper tradeoff between performance and hardware requirements is achieved by the SSB scheme.

Table 4.3: Resource-efficiency comparison.

	Network throughput	Average power consumption	Resource efficiency	Hardware complexity
Single antenna omni-directional system + CSMA/CA	S_{omni}	P_{omni}	$\eta_{\text{omni, E}}$ $\eta_{\text{omni, B}}$	• 1 RF transceiver • 1 baseband unit • 1 MAC controller
SSB system + SSB-MAC	$2S_{\text{omni}}$	$1.1P_{\text{omni}}$	$1.82\eta_{\text{omni, E}}$ $2\eta_{\text{omni, B}}$	• 1 RF transceivers • 1 baseband unit • 1 MAC controller • Few additional components
six-sector MDA system + MDA–MAC, PM	$3S_{\text{omni}}$	$\sim P_{\text{omni}}$	$\sim 3\eta_{\text{omni, E}}$ $3\eta_{\text{omni, B}}$	• 6 RF transceivers • 6 baseband units • 1 multi-processor MAC controller

Chapter 5

SSB Test-bed Implementation and Measurements

This chapter mainly describes the details of the SSB test-bed implementation and experiments. The performance of SSB on the physical layer has been evaluated by the experiments performed in the office environment. The analysis on the measured data reveals that in this indoor scenario the SSB test-bed can help to suppress fading and interference, increase the received signal power, and result in a better link quality in terms of the reduced BER. Furthermore, the measured SNR gain and AoF (amount of fading) closely approach the theoretical predictions.

5.1 Carrier frequency band selection

Since the purpose of the test-bed is to evaluate the performance of SSB, but not for a specific application, the degree of freedom for the selection of the carrier frequency band is large. The selection mainly relies on the availability of the RF front-end components, including antenna, RF switch, RF combiner & divider and RF transceiver. In addition, the size, cost and power consumption of those components should also be taken into consideration. The selection is made among the following three ISM (industrial, scientific and medical) bands: 900 MHz, 2.4 GHz and 5 GHz. Finally, we choose the 2.4 GHz frequency band based on the following considerations:

- First of all, 900 MHz is eliminated from the selection list due to the resulting large size of the antenna array. As described in Section 4.3, the diameter of the SSB circular antenna array is half the wavelength, which is 16.67 cm, 6.25 cm and 3 cm for 900 MHz, 2.4 GHz and 5 GHz, respectively. Since SSB is expected to be used on mobile portable devices, the diameter of 16.67 cm is not acceptable.
- 5 GHz is superior to 2.4 GHz with respect to the size requirement and the interference power. At present, there are much less applications on the 5 GHz band than on the 2.4 GHz band. Hence, the former frequency band is not so crowded as the latter. However, due to the same reason (less applications exist)

the RF front-end components operating in the 5 GHz band are more difficult to obtain on the market. Furthermore, many existent applications (e.g., 802.11a) on this band apply the OFDM technique, whose advantage is dispensable for the test-bed, but extra complexity and power consumption are imposed.

- As there are a lot of applications operating in the 2.4 GHz band presently, e.g., WLAN 802.11b/g, Bluetooth and Zigbee, more types of low cost RF front-end components are available on the market. The size of the antenna array operating on 2.4 GHz is acceptable for most mobile portable devices. The interference signal existing in this band can be purposely used to test the interference suppression design of the test-bed.

5.2 Hardware implementation

The SSB test-bed comprises the RF components and circuits. Many lessons have shown that an imperfect RF PCB layout leads to bad performance even for the best system design. A good RF PCB layout includes very careful designs on RF tuning, matching, and phase shifting for all components operating on the radio frequency. To avoid those troublesome issues at the first stage, we decide to build a development table for SSB, which uses the evaluation board for each RF component and RF coaxial cables to connect them. The evaluation board for each RF chip supplied by the respective manufacturer can ensure an accurate input/output impedance matching, and uses SMA (SubMiniature version A) RF connectors for good usability. The use of RF connectors and cables between RF chips can introduce an additional loss compared to the compact board design. However, the absolute radiated or received RF power is not the main concern of the test system, hence the insertion loss does not degrade the overall performance.

Fig. 5.1 illustrates the system block diagram of the SSB test-bed. Each antenna element includes an SMA connector on its own end. To build the designed array, as shown in Fig. 4.5, six RF cables must be applied to reserve enough space for the six-antenna array so that each antenna can be correctly connected to the corresponding port of the RF switch board. The shape of the six-antenna array is illustrated in Fig. 5.6. Via two further RF cables, two RF switch boards are connected to the RF combiner & divider board. Together with the ninth RF cable, all above components compose the RF part of the SSB system, which can substitute the single antenna used in the traditional communication systems.

The RF chip CC2400 [9] is the most important component of the whole SSB test-bed, which includes the complete functions of RF transceiver and baseband processing. We use its development kit for the fast and easy prototyping of its functions. There is a

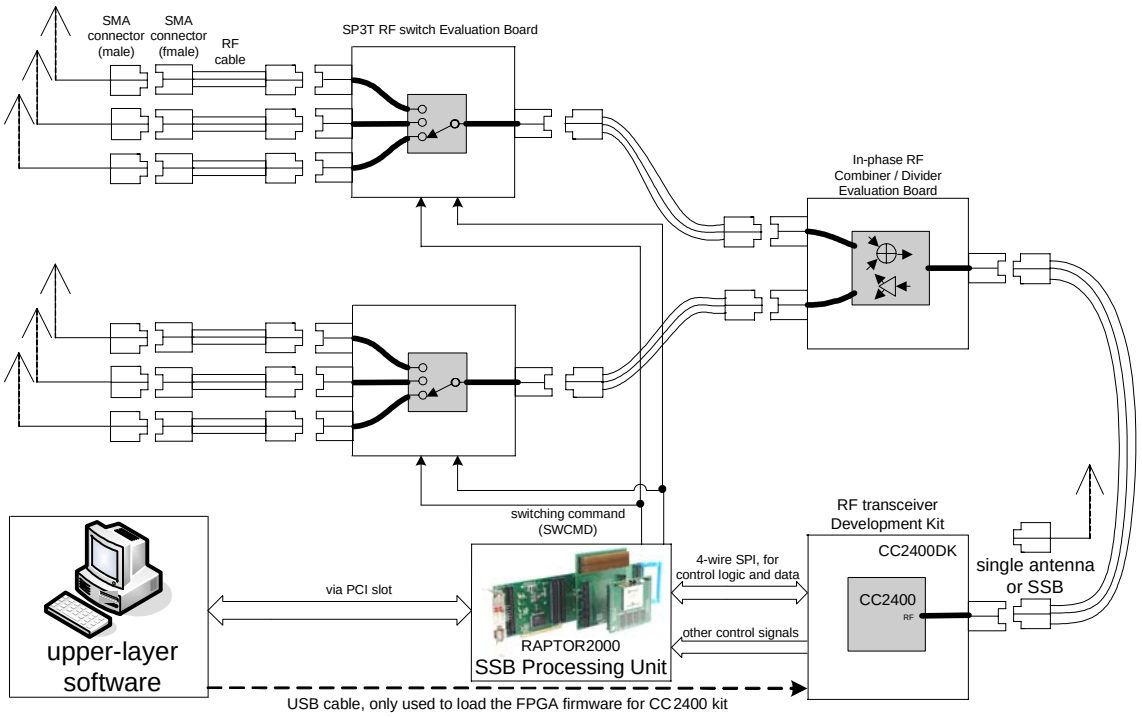

Figure 5.1: The development table for SSB.

test port on the kit. After the kit loads the FPGA bitstream file (firmware) via the USB cable, this test port can fully emulate the SPI (serial peripheral interface) port on the chip. The strobe commands and data can be transferred via this port so that the RF chip can be fully controlled to operate on the TX, RX or IDLE mode.

The RAPTOR2000 board [35] is a fast FPGA prototyping system. Three functions have been implemented on this system. The first function is an interface between the SPI port on the CC2400 (as slave) and the PCI bus, that is to get the data from the computer and convert them into the SPI format or the reverse operation (refer to Section A.1). The second function includes the physical carrier sense (PCS) and optimal reception sector selection (ORSS) processes. They will be described in Subsections 5.3.2.2 and 5.3.2.3, respectively. The last one is the interference suppression (IS) function, which will be described in Subsection 5.3.2.6 in detail.

In this SSB test-bed system, the computer as well as the upper-layer software running on it still play an important role. All of the RX, TX, IDLE states control on CC2400 is carried out by them. For the real portable system, those functions can be executed by the MAC controller chip.

5.2.1 Antenna

The selected antenna is a normal mode helical antenna (NMHA) that operates in the 2.4 GHz band. The radiation intensity pattern of a NMHA is very similar to the

pattern of the widely used half wavelength dipole antenna, which is omni-directional in the horizontal plane and is featured as a "∞" shape in the vertical plane [42] [also refer to Fig. 4.3 (left)]. Its size is smaller than the half wavelength dipole antenna at the cost of a reduced radiation efficiency. The antennas used by the single antenna TX station, the single antenna RX station and the SSB RX station are the same in the experiments (see Section 5.4). As the absolute radiated or received power is not the main concern of the test-bed, the antenna performance would not greatly influence the overall performance of the test-bed.

5.2.2 RF switch

The RF switch plays a key role in controlling the RF signal flow to/from the RF transceiver. Besides its most common application as a RX/TX switch, it is also widely used in switched beam systems (e.g., Butler Matrix [54]) and multi-protocol terminals (e.g., an IEEE 802.11 a/b/g device). For the SSB test-bed, two SP3T (single pole three throw) switches are required for the antenna pair selection, as illustrated in Fig. 5.1.

The most important parameters revealing the performance of an RF switch include insertion loss, isolation, and response time on the specific frequency domain. Low insertion loss, high isolation, and fast response are desired. As indicated by [15], the state-of-the-art RF switch can provide very good performance with high isolation ($>$ 20 dB), low insertion loss ($<$ 0.1 dB) and extremely short response time (in the order of nanosecond) across an ultra-wide bandwidth ($>$ 100 GHz). Although the commercial availability of such devices at a sustainable price still requires time, it anyway ensures the possibility of the best possible performance of SSB in practice.

The selected RF switch for the test-bed is the SP4T FET IC AS204-80 from Skyworks. On the 2.4 GHz frequency band it typically provides an insertion loss of 0.6 dB, an isolation of 32 dB, and a response time less than 200 ns. Its power consumption accounts for a negligible proportion of the whole system power, around 2.5 mW. It is able to deal with an RF power up to 0.8 W. Moreover, it is a bidirectional device, which means that its performance on the RF signal either entering into the pole or leaving the pole keeps the same. All of those properties perfectly meet the requirements of the test-bed. Finally, its evaluation board is also available, as shown in Fig. 5.2, which ensures easy use and fast prototype.

5.2.3 RF combiner & divider

As shown in Fig. 5.1, the RF combiner & divider combines two RF signals into one in the RX process and divides one RF signal into two flows in the TX process, that is, it

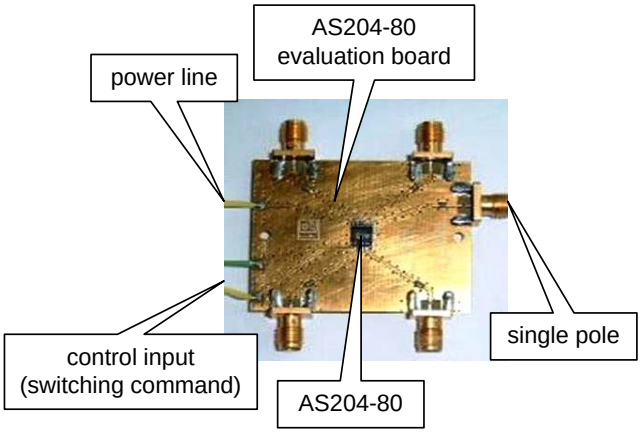

Figure 5.2: The evaluation board of the RF switch AS204-80

is a bidirectional device. Furthermore, this device must operate in-phase as required by SSB. The ideal operation would result in the following two properties: in the RX process, if the two received RF signals have the same phase and amplitude, then the output signal obtains a 3 dB gain, and may experience a phase shift in dependence of the internal circuit design; in the TX process, the signal to be transmitted is divided into two flows, each with a 3 dB loss and the same phase shift. The basic principle of this device is based on the 3 dB Wilkinson power divider, refer to [50] for details.

The 4A1305 2-way Wilkinson surface mount package from Anaren is selected as the RF in-phase combiner & divider in the test-bed. It is a passive component with the performance of 0.4 dB insertion loss and 12 dB isolation on the 2.4 GHz frequency band. It is able to deal with the RF power up to 5 W. The 0.4 dB insertion loss implies that in the RX process the combined signal maximally achieves a 2.6 dB gain (even though they are strictly in-phase and have the equal amplitude), and in the TX process each of the separated signal experiences a 3.2 dB loss (compared to the input signal). The two separated signals in the TX process have strictly the same phase and amplitude, however the two signals to be combined in the RX process may not be in-phase and/or have the same amplitude. In this case 4A1305 can still work, but some signal power will be dissipated on its internal resistor so that an additional insertion loss will be caused. The more different the two signals to be combined are, the more loss they encounter. Fig. 5.3 illustrates the evaluation board used by the test-bed.

5.2.4 RF cables

From Fig. 5.1 we can see that two types of RF cables are used by the development table, one type uses the male SMA connector on both sides, and the other type uses the male and female SMA connector on each side, respectively. The length of all RF cables is kept the same, 12 cm, to ensure an equal phase shift on them. Except for

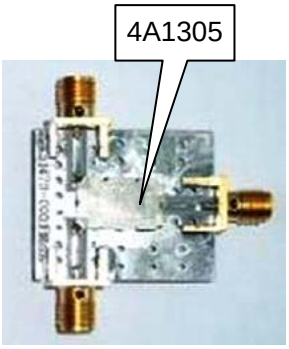

Figure 5.3: The evaluation board of the RF combiner & divider 4A1305

the phase shift, the insertion loss caused by them is another parameter that has an impact on the performance of the test-bed. In the experiments their S-parameters are measured using an RF network analyzer.

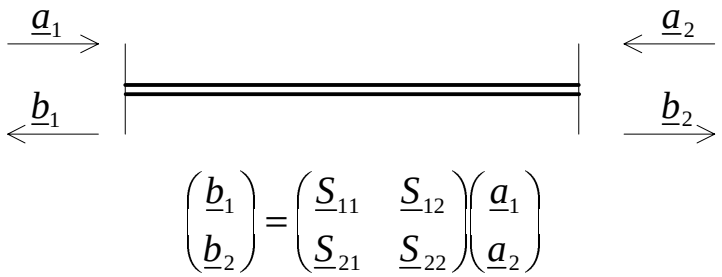

Figure 5.4: S-parameters of an RF cable.

S-parameters are widely used to describe the transmission characteristic of a passive RF component [50]. The definition is given by the equation illustrated in Fig. 5.4. From it we can easily obtain

$$\underline{b}_2 = \underline{S}_{21} \cdot \underline{a}_1 + \underline{S}_{22} \cdot \underline{a}_2, \tag{5.1}$$

and

$$\underline{b}_1 = \underline{S}_{11} \cdot \underline{a}_1 + \underline{S}_{12} \cdot \underline{a}_2. \tag{5.2}$$

For each side $\underline{a}$ denotes the incident signal and $\underline{b}$ denotes the reflected signal. If the intended signal transmission direction is from left to right and assume that the incident signal $\underline{a}_2$ on the right side is zero, then the following relations

$$\underline{b}_2 = \underline{S}_{21} \cdot \underline{a}_1 \tag{5.3}$$

and

$$\underline{b}_1 = \underline{S}_{11} \cdot \underline{a}_1 \tag{5.4}$$

Table 5.1: Measured S-parameters on 2.3924 GHz.

RF cable	$\underline{S}_{11}$/dB	$\underline{S}_{12}$/dB	$\underline{S}_{21}$/dB	$\underline{S}_{22}$/dB
Male-Male 1	-39.619	-0.1825	-0.1407	-37.086
Male-Male 2	-34.426	-0.2033	-0.1513	-34.838
Male-Female 1	-23.187	-0.2434	-0.1980	-24.908
Male-Female 2	-23.393	-0.2057	-0.1622	-23.523

Table 5.2: Measured S-parameters on 2.4423 GHz.

RF cable	$\underline{S}_{11}$/dB	$\underline{S}_{12}$/dB	$\underline{S}_{21}$/dB	$\underline{S}_{22}$/dB
Male-Male 1	-24.598	-0.2001	-0.1684	-22.645
Male-Male 2	-23.479	-0.2180	-0.1850	-22.001
Male-Female 1	-23.783	-0.2327	-0.1996	-29.490
Male-Female 2	-23.457	-0.1902	-0.1639	-26.849

hold. In a real system the strength of the signal $\underline{a}_2$ depends on how much the next component matches the right port of the cable, which is negligible on the network analyzer. Therefore, from Eqs. (5.3) and (5.4) it can be concluded that $|\underline{S}_{21}|$ can be regarded as the (forward) transmission rate (also called coupling), and $|\underline{S}_{11}|$ can be regarded as the (reverse) reflection rate (also called return loss). Therefore, the insertion loss can be derived as

$$L = P_{\text{in}}/\text{dBm} - P_{\text{out}}/\text{dBm} = -20\lg|\underline{S}_{21}| = -\underline{S}_{21}/\text{dB} \tag{5.5}$$

Tabs. 5.1 and 5.2 give the measured S-parameters on the frequencies that closely approach 2400 MHz and 2433 MHz, respectively. For each type, two cables have been measured. Two results can be observed from Tabs. 5.1 and 5.2: First, the insertion loss is very small, always less than 0.2 dB; second, the symmetric shape of the cables can be reflected by the similarity between $\underline{S}_{11}$ and $\underline{S}_{22}$, and between $\underline{S}_{12}$ and $\underline{S}_{21}$. It should be noted that when a S-parameter is expressed in the logarithmic scale (e.g., $\underline{S}_{21}$/dB), its phase is omitted, as $\underline{S}_{21}$ is a complex value.

5.2.5 RF transceiver & Baseband component

The key components of a wireless communication system are the RF transceiver and the baseband processing unit, which are usually separately implemented. Nowadays they are tending to be integrated into a single chip to save power and area. The RF transceiver means the RF front-end blocks for transmitting and receiving RF signals, which mainly consist of the up-conversion block and the power amplifier for TX, the down-conversion block and the low-noise amplifier for RX, and other auxiliary circuits

like filters, see Fig. 2.1. The baseband processing unit mainly realizes the digital modulation and encoding functions in TX, and the digital demodulation and decoding functions in RX. The RF transceiver and the baseband processing unit are interfaced with A/D converters in RX and D/A converters in TX, therefore the former is an analog component while the latter is fully digital. In [64] various structures to design the RF transceiver and the baseband processing unit have been addressed in detail.

In summary, the RF transceiver & Baseband component realizes all the physical layer functions of a wireless communication system. In the TX process, it gets the digital MAC layer packet from the MAC controller, automatically adds a proper physical layer header and/or tail on it, and then converts it to an RF signal radiated into the air. In the RX process, it converts the RF signal detected from the air into an digital packet and removes its physical layer header and/or tail automatically, and then transfers it further to its MAC controller.

In the work of [54], significant time and effort have been spent to implement and construct all blocks of RF transceiver & baseband processing for the switched-beam antenna system. As for a test-bed system, there is usually no special requirement on its RF transceiver & baseband processing unit so that they need not be implemented particularly. Therefore, I guess the reason for such an implementation is that there was no integrated single chip for RF transceiver & baseband processing operating on the intended frequency band available at that time. Thanks to the recent progress on chip integration, many single-chip solutions for RF transceiver & baseband processing are commercially available now. Other than the single-chip solutions, numerous two-chip solutions are also available on the market. For the SSB test-bed, the basic requirements are the following:

1. Operating in the ISM 2.4 GHz frequency band;
2. Covering the complete functions of RF transceiver and baseband processing;
3. Supporting RSSI measurements, and it is more advantageous if the chip can directly output the digital RSSI values;
4. Powerful and flexible development tools should be available, and good technical support from the manufacturer is especially expected.

Concerning the fourth requirement, a further expectation is that a chip evaluation board should be available to avoid additional efforts on designing the external RF circuits around the chip, e.g., the matching circuits for the antenna. Other requirements include a large dynamic range of the RSSI measurement, programmable TX power and programmable length of the preamble, which acts as a part of the physical layer header.

The first candidate chip I selected was MAX2822 from MAXIM. This is a two-chip solution since MAX2822 only covers the RF transceiver functions and requires a compatible baseband processor. This solution is highlighted by the fact that MAX2822 is a 2.4 GHz 802.11b PHY compatible transceiver integrating power amplifier and TX/RX switch, since our investigated MAC layer protocol is based on the IEEE 802.11b specification. However, two disadvantages make it inappropriate. First, it doesn't support the RSSI measurement directly, which causes difficulties on the optimal reception sector selection (ORSS) process, while ORSS is the key operation of SSB (refer to Section 4.3). This can be solved by applying the RX_AGC and RF_GAIN signals, which are the output of its compatible baseband chip and are used by MAX2822 for the automatic gain control (AGC) purpose. The second but more serious disadvantage is that its compatible baseband processing chip, IPN2120 from InProComm or the 802.11b series baseband/MAC chip from Atmel, is not available in small quantity.

The second candidate chip I have found was ATR2406 from Atmel, which meets the requirements 1 to 3, although it only outputs an analog RSSI signal. Similarly, two disadvantages make it inappropriate for the SSB test-bed. First, its analog RSSI output requires to use an additional A/D converter, which increases the complexity and power consumption. This drawback is not critical and could be overcome if ATR2406 is the unique choice. Actually, I have found a proper A/D converting chip MAX1117 from MAXIM for this purpose. However, the more serious problem is that the aforementioned fourth requirement was not met at the time of the development, although the manufacturer claimed the availability of its development kit. Therefore, attention has to be paid to other choices.

The finally selected chip is CC2400 from Chipcon, which offers the single-chip solution that perfectly meets all above four requirements. In addition, CC2400 provides other functions that make it particularly suitable for the SSB test-bed:

- It supports the carrier sense (CS) function. If a carrier is detected in the air, then CC2400 outputs an active PCS_N digital signal until the carrier signal disappears. The CS function is based on the RSSI measurement. If the measured RSSI value is above the threshold register RSSI_CS_THRES[5:0] value, which can be configured in advance, then PCS_N becomes active.

- The length of its preamble is programmable. The preamble is automatically inserted and removed by CC2400, and its length can be configured flexibly from 1 to 32 Bytes. As will be analyzed in Subsection 5.3.2.3, a 32 Bytes preamble is long enough for the ORSS process even in the worst case.

- It supports the synchronization word indicator function. The original purpose of this function is to interrupt the associated microprocessor to read the received

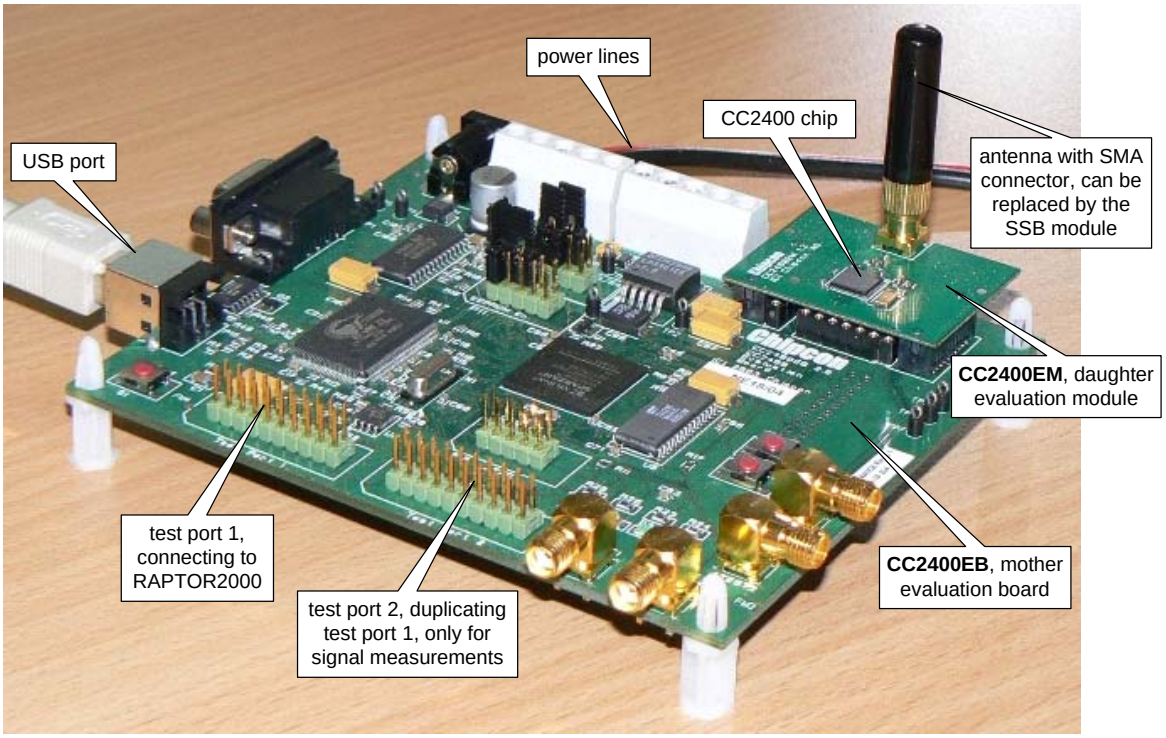

Figure 5.5: The CC2400 development kit, consisting of the CC2400EM daughter board and the CC2400EB mother board.

data from the FIFO of CC2400. However, as will be described in Subsection 5.3.2.6, this function is used by the test-bed to distinguish between the interference signal and the user signal. The resulting interference suppression function of the test-bed works very well, as indicated by the experiments described in Subsection 5.4.4.

- It supports the multi-channel operation. 84 frequency channels are available ranging from 2400 to 2483 MHz, each with the 1 MHz bandwidth. The 2.4 GHz ISM band is shared by many applications. Hence, it is advantageous to apply the frequency hopping spread spectrum (FHSS) or the multi-channel solution to combat co-channel interference. Although the SSB test-bed doesn't apply this function sufficiently, it supplies a good upgrading opportunity to further increase the performance of the test-bed. Anyhow, this function enables the test-bed to operate on different frequency channels with and without interference to test its interference suppression function, as will be described in Subsection 5.4.4.

Another property of CC2400 to be highlighted is its powerful development kit, including hardware and software. Fig. 5.5 illustrates its development kit composed of one mother evaluation board CC2400EB and one daughter evaluation module CC2400EM. All the external RF circuits around the CC2400 chip are integrated on CC2400EM,

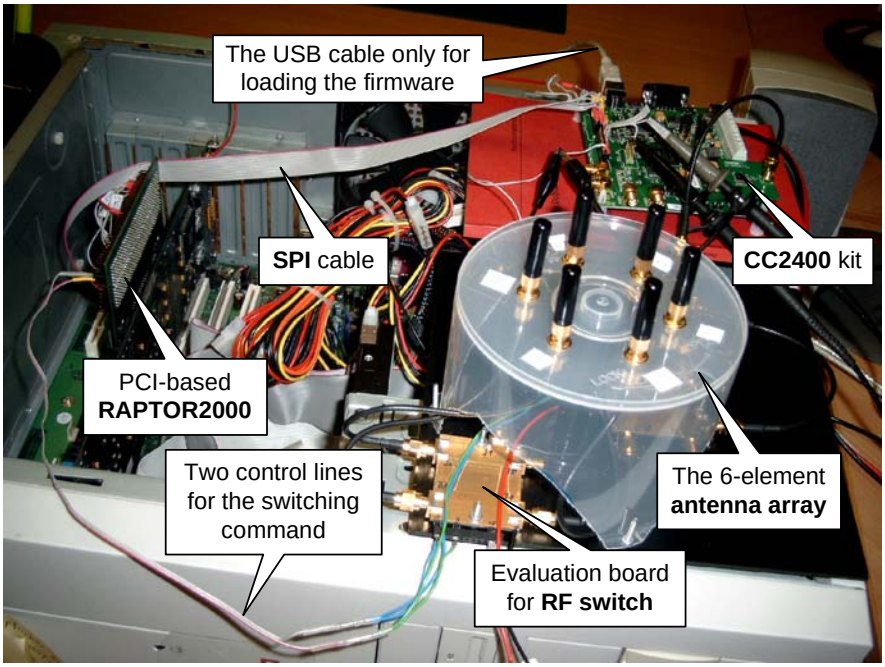

Figure 5.6: The developed SSB test-bed.

and the antenna is installed on the SMA connector so that it can be easily replaced by the SSB antenna array module, as illustrated in Fig. 5.1. The USB port is for the communication between the host computer and CC2400EB so that the latter can be fully controlled by the associated SmartRF software [9]. This condition is marked as the **operating mode 1**. Furthermore, the USB port can be used to load the firmware for the FPGA on CC2400EB so that its test port 1 can emulate all the digital I/O ports of the CC2400 chip. Via the test port 1, CC2400 can be fully controlled by a control unit (e.g., a microprocessor). This condition is marked as the **operating mode 2**. In this case, the USB cable is not necessary any more and can be either disconnected or kept after the firmware is loaded. The operating mode 2 stays until the kit is powered down. The kit must select one operating mode at one time. In the experiments described in Section 5.4, the TX station is operating in mode 1 and the RX station is operating in mode 2. While operating in mode 2, the test port 2 on CC2400EB duplicates all the signals of the test port 1 via the FPGA for measuring purpose, because direct measurements on the test port 1 may interfere its operation. The figures given in Section A.5 are all measured on the test port 2. Fig. 5.6 shows the developed SSB test-bed, in which the RF combiner & divider is hidden by the antenna array. From it we can see that the single antenna and the antenna array can be installed alternatively on the SMA port of CC2400EM. Attention must be paid to the following points (Subsections 5.2.5.1 and 5.2.5.2), which are closely related to the use of CC2400 on the SSB test-bed.

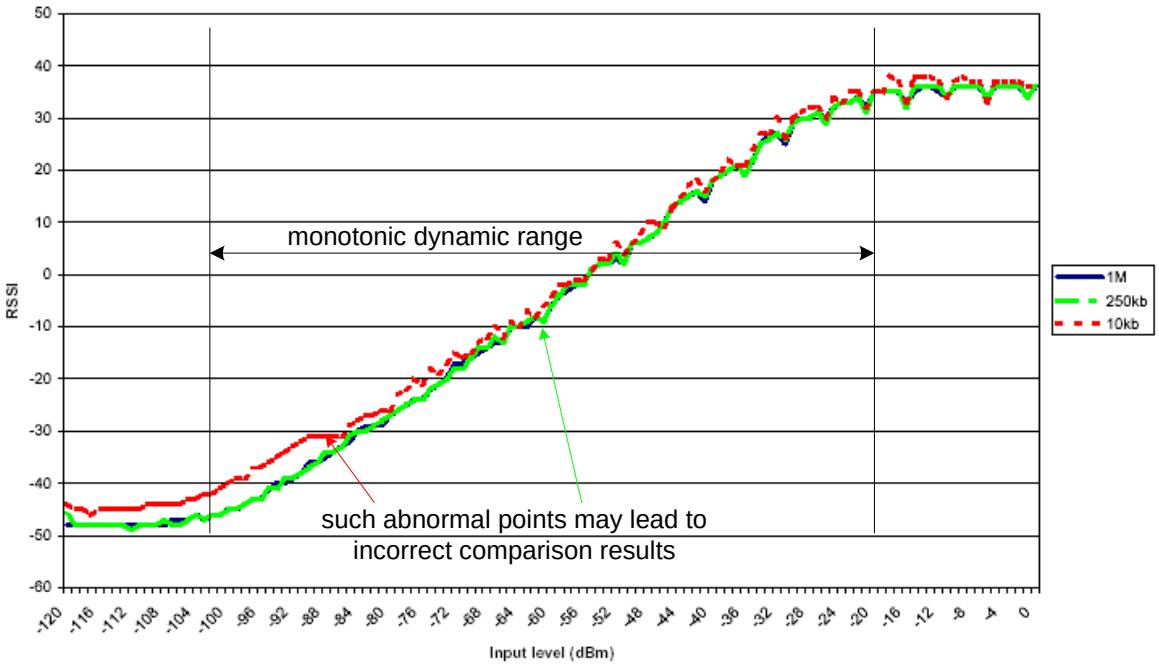

Figure 5.7: Typical RSSI values vs. input power [9].

5.2.5.1 RSSI measuring performance

The RSSI (received signal strength indicator) signal, as indicated by its name, is used to indicate the received RF signal strength. It can be used for the auxiliary functions like link quality monitoring or physical carrier sense. However, the RSSI measurement becomes crucial for the SSB test-bed, because its accuracy and response time directly influence the correct and fast determination of the optimal reception sector, and, therefore, determining the final performance of the SSB system. The RSSI measuring performance depends on the following two parameters:

Monotonic dynamic range is the range from the minimum to the maximum power of the input RF signal, in which the RSSI output increases monotonically. In other words, for any two RF signals within this range, the smaller RSSI value must correspond to the smaller RF signal, while the larger RSSI value must correspond to the larger one. The author of [54] emphasized the importance of the linearity of the dynamic range for their switched beam system. However, I think the monotony is more important than the linearity of the dynamic range since the RSSI measurement is only used for comparing the strengths of the input RF signals relatively. A large dynamic range is always desirable because it indicates the system's capability to deal with signals with a wide range of strength. For the SSB system, different sectors may lead up to a 20 dB difference of the RSSI

value in practice. Therefore, it definitely requires a large dynamic range. Fig. 5.7 illustrates the curves between the measured RSSI values and the input RF signal strengths under different options: 1 Mbit/s, 250 Kbit/s or 10 Kbit/s data rate. It can be seen that with the 1 Mbit/s data rate CC2400 can output the RSSI value with an approximate 80 dB quasi-monotonic dynamic range. The abnormal points marked in the figure may result in incorrect comparison results. However, they would not seriously influence the performance of the entire system since the proportion of such values is very small, especially for the 1 Mbit/s option used by the test-bed. It should be noted that the ± 4 dB RSSI accuracy given in the data sheet of CC2400 is only for its absolute value. This parameter is acceptable since only the relative comparison is required by the SSB test-bed.

RSSI response time is the settling time for the RSSI output, that is the duration from the appearing moment of the RF signal to the moment that a valid RSSI output is generated. This parameter is particularly important to SSB since it determines how much time the ORSS process requires. The shorter the RSSI response time, the less time the ORSS process consumes, and thus the less capacity loss results. It depends on the way to generate the RSSI.

There are two fast ways to generate the RSSI signal:

- Use a Schottky diode RF detector, which is in fact a power-to-voltage converter. The output is an analog signal. The advantages of this solution are simplicity, low cost, and fast response. The response time claimed by such components (e.g., LTC5536 from Linear Technology Corporation) is as short as 20 ns. If a digital RSSI is required, then this signal must be further converted by an A/D converter, which takes another 2 μs if the 500 ksps sampling rate can be achieved (e.g., MAXIM's chip MAX120). However, this solution exhibits the serious disadvantage of a low dynamic range, which is usually less than 50 dB. Furthermore, the common Schottky diode RF detectors cannot deal with low power signals. The typical minimum value they can detect is -30 dBm, which is not acceptable for most up-to-date RF transceivers since they usually claim a sensitivity around -90 dBm (e.g., MAX2822, CC2400, CC2500, ATR2406).

- A quadrature detector is usually employed by the automatic gain control (AGC) component as its input. On the receiver side, the RF signal is down-converted, filtered and finally A/D converted before entering into the baseband processing unit. Due to the strong variation of the received RF signal power (that may be caused by channel fading and distance variation), the A/D converter must provide a large dynamic range. However, this kind of A/D converter is not efficient on power and cost. The goal of AGC is to keep the amplitude of an

incident RF signal relatively constant, so that the requirements on the A/D converter can be relaxed. On the other hand, AGC helps to increase the dynamic range of the entire receiver. More details regarding AGC can be found in [2] and [12]. The principle of the quadrature detector is to first form the instantaneous mean power of the I and Q channels after the down-conversion as

$$P_{\mathrm{RSSI}} = \frac{y_{\mathrm{I}}^2 + y_{\mathrm{Q}}^2}{2} \tag{5.6}$$

and then low pass filter P_{RSSI} to obtain a time average of the received power, as described in [2] in detail. The phase coherence doesn't need to be considered for this solution because $\cos^2\theta + \sin^2\theta = 1$. The above process can be realized by either analog circuits or digital processing, while the former is advantageous with respect to response time. Furthermore, the key parameter that influences the response time is the bandwidth of the low pass filter, which trades off between the speed and noise performance [2]. A very small bandwidth will result in a slow tracking of the received power (long response time), while a large bandwidth will lead to a noisy power estimate (short response time, but worse RSSI accuracy). Moreover, the use of AGC further increases the response time of RSSI since the AGC loop itself needs time to settle down. Therefore, the RSSI response time relies on how an RF transceiver implements the above processes.

CC2400 claims a 20 μs RSSI response time under the default 4 bits RSSI averaging filter length. Considering the settling time of the AGC loop, a 30 μs duration is reserved for each sector in the ORSS process, as described in Subsection 5.3.2.3.

5.2.5.2 AGC vs. VGA

The VGA (variable gain amplifier) is the key component of the AGC loop in CC2400. However, CC2400 can be configured in such a way that its AGC function is disabled, and then the gain of VGA can be manually set. In other words, the RX channel gain in CC2400 anyway relies on VGA, whose gain is given by AGC if AGC is activated, or otherwise is manually set. It should be noted that if the AGC function is enabled, then the gain of VGA has already been taken into account for RSSI generation (that is, the present gain of VGA is subtracted automatically). If AGC is disabled and the manual VGA gain is used, then the present VGA gain must be subtracted from the RSSI output afterwards.

As described in the above Subsection 5.2.5.1, the use of AGC increases the dynamic range of the RSSI measurement, however, decreases its response speed. Therefore, it is necessary to determine whether to use AGC for the RSSI measurement. For this purpose, two experiments have been carried out, see Tabs. 5.3 and 5.4. In both

Table 5.3: Experiment 1 of the RSSI measurement (5 runs, in each run the VGA_GAIN is constant, see Tab. 5.4 left), AGC is disabled.

P_t/dBm	RSSI1/dBm	RSSI2/dBm	RSSI3/dBm	RSSI4/dBm	RSSI5/dBm
0	-44	-37	-45	-36	-60
-5.2	-44	-46	-45	-42	-60
-10	-44	-56	-49	-47	-60
-15	-44	-56	-53	-54	-60
-25	-44	-56	-65	-70	-63

Table 5.4: Left: The VGA_GAIN setting of experiment 1; Right: Experiment 2 of the RSSI measurement, AGC is enabled.

RSSI sequence	VGA_GAIN setting
RSSI1	0x08
RSSI2	0x01
RSSI3	0x91
RSSI4	0x11
RSSI5	0xD1

P_t/dBm	RSSI/dBm	VGA_GAIN
0	-36	0x12
-5.2	-40	0x05
-10	-48	0x91
-15	-53	0x93
-25	-63	0xD2

experiments, CC2400 on either the TX or RX station operates in mode 1 described before. All configurations can be set via the SmartRF studio software and all values of readable registers can be read from it. The distance between the TX and RX stations is kept constant, and the transmission power P_t of the TX station can be manually set in the experiments. In experiment 1 the AGC function of CC2400 on the RX station is disabled, and its VGA gain is set manually, as shown in Tab. 5.4 (left). In experiment 2 the AGC function is enabled and the corresponding VGA gain given by AGC can be read out, as shown in Tab. 5.4 (right). Except for AGC and VGA settings, all other configurations are the same for both experiments. From Tab. 5.3 and Tab. 5.4 (right) we can observe that in case AGC is disabled, the output RSSI value cannot correspond to the transmission power P_t; however, if AGC is enabled, P_t and RSSI values can correspond satisfactorily. This implies that the dynamic range of the RSSI measurement is not acceptable for the SSB test-bed if AGC is disabled. Therefore, **the AGC function must be enabled** although it results in a larger time overhead due to a longer ORSS process.

By the way, although the value of VGA_GAIN[7:0] can be read from the register AGCCTRL of CC2400, its relationship to the actual gain is not given in [9]. After carrying out some experiments, I found that the VGA of CC2400 offers the gain with a 66 dB dynamic range and by the step of 2 dB. The corresponding values of VGA_GAIN[7:0] (from the maximum to minimum gain direction) are: 0x08-0x0D, 0x01-0x07, 0x11-0x17, 0x91-0x97, 0xD1-0xD7.

5.3 Software stack

The software stack of this test-bed consists of two parts, the upper-layer software (ULS) and the SSB processing unit (SPU). The former is coded by C++ and runs on a Linux-based computer, and the latter is programmed by VHDL and is executed on the FPGA prototyping system RAPTOR2000.

As described in Section 1.4, a real networking communication node should cover all the functions from the user layer, network layer (routing), MAC layer to the physical layer. Generally speaking, the application software runs on the host computer, routing and MAC protocols are executed by some dedicated processing unit like a microprocessor, DSP, FPGA or ASIC, and all functions on the physical layer are realized by the RF transceiver & baseband processing unit. Until now, only a part of the aforementioned functions have been realized on the test-bed. A simple user layer function is realized by the ULS. Since the test-bed is only used for point-to-point communication tests, the routing function is not necessary and only a simple MAC function (e.g., to ensure that the receiver is ready before the transmitter sends data) is required, which is accomplished by the cooperation between the ULS and the SPU. All the physical layer functions are realized by the CC2400 chip. The SPU is composed of two subcomponents: an interface between CC2400 and the host computer (called SPI Master) and the SSB controller, see Fig. 5.9.

5.3.1 Upper-layer software (ULS)

As mentioned above, the main intention of the test-bed is to verify the effectiveness of SSB on the physical layer, that is to show the diversity gain with respect to the single antenna system based on the performance measures like BER (bit error rate) and AoF (amount of fading). Therefore, only a simple user layer function is realized by the the ULS. Fig. 5.8 illustrates its flow diagram. When the test-bed needs to receive data that are composed of multiple packets, then it must perform multiple packet receptions, each of which is an independent process. In each process, the computer must first send a RX command to CC2400 via the SPU. CC2400 is ready for reception only after this command is written to its dedicated register. The packet reception is automatically carried out by the cooperation between CC2400 and the SPU. The quasi-idle state FSON (see [9]) of CC2400 indicates that the whole packet reception is finished and the packet is saved in the RX FIFO of the SPU. Furthermore, three RSSI values of three sectors are also saved in the register of the SPU. Then, those values are read and saved on the memory of the host computer. If not all the packets have been received, the host computer must immediately repeat the same packet reception process to avoid the case that the packet is sent and the receiver is not ready (this

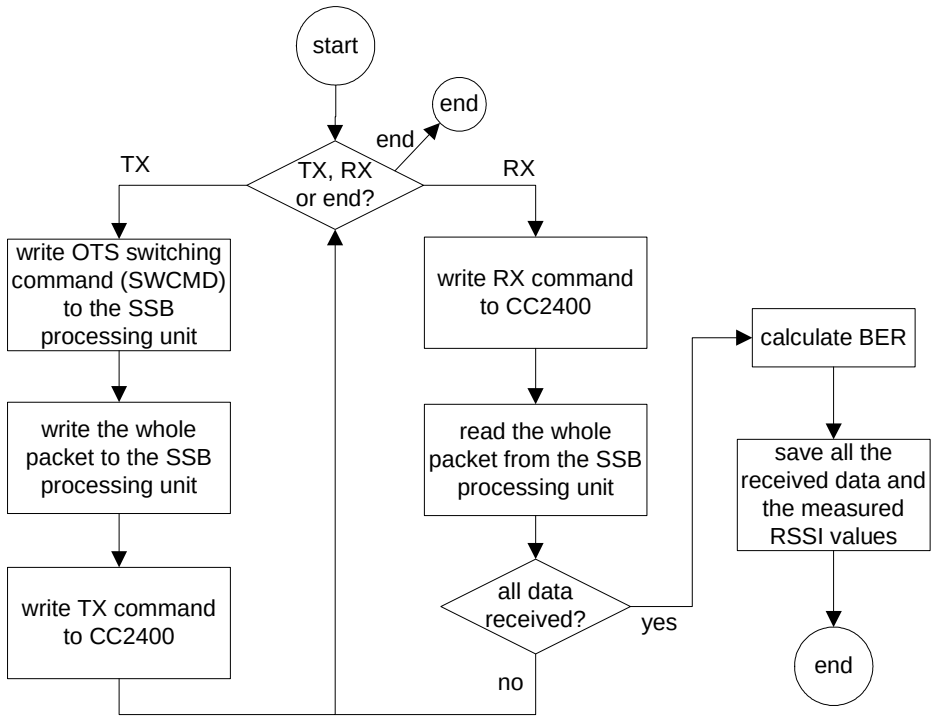

Figure 5.8: The diagram of the upper-layer software (ULS).

causes a packet loss). This is also the reason why the received packets are saved on the memory, but not on the hard disk of the host computer. The latter operation requires more time and may cause packet losses. If the complete data have been received, the ULS will analyze the data and save them on the hard disk.

If the test-bed is used as a transmitter, then additional MAC functions should be applied to obtain the optimal transmission sector (OTS) in advance. A dedicated MAC protocol has been elaborated in Subsection 4.3.3. However, this protocol has not yet been implemented on the test-bed. If the OTS is aware, then its corresponding switching command (SWCMD) should be sent to the SPU to switch on the OTS, after that the whole packet is written to the TX FIFO to be transmitted by CC2400. When the TX command is written to the dedicated register of CC2400, the packet will be transmitted into the air by CC2400 in cooperation with the SPU.

It should be noted that both RX FIFO and TX FIFO have a capacity that can save the whole packet.

5.3.2 SSB processing unit (SPU)

Fig. 5.9 illustrates the block diagram of the SSB processing unit (SPU), which mainly consists of two components. The first component is called **SPI master**, which implements a serial peripheral interface between the internal bus and the SPI port of

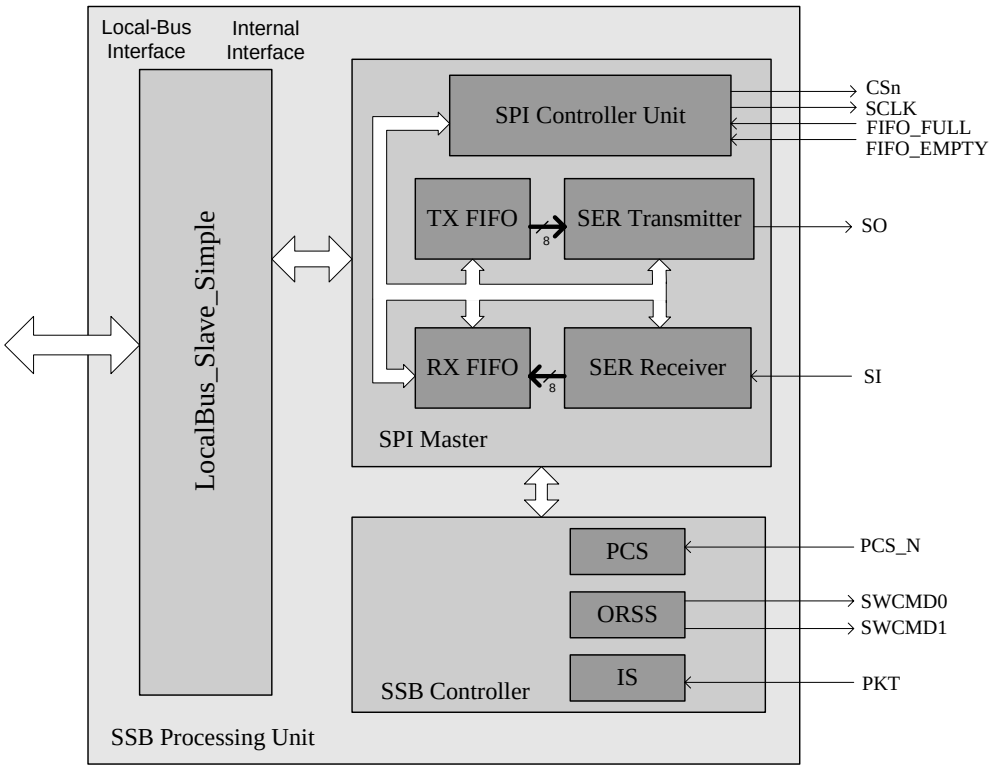

Figure 5.9: SSB processing unit (a VHDL design runs on RAPTOR2000)

CC2400. Master means that the clock signal SCLK and the chip selection signal CSn are generated by this component. The second component is called **SSB controller**, which realizes the functions of PCS (physical carrier sense), ORSS (optimal reception sector selection) and IS (interference suppression). An assistant component called LocalBus_Slave_Simple is also included in the SPU, which is a bus converting logic between the internal bus and the local bus. The RAPTOR2000 mother board applies a PCI bridge chip PLX 9054, which functions as an interface between the local bus and the PCI bus.

Fig. 5.10 illustrates the state transitions of the SPU. Before receiving the RX or TX command from the ULS, the SPU stays in the idle state, during which CC2400 stays on the FSON state, which is a quasi-idle state [9]. If the ULS sends the RX command, then the SPU transits to the PCS state, during which the directional physical carrier sense is carried out. If the PCS module detects any carrier above the sensing threshold in the air, it immediately transits to the ORSS state, in which the optimal reception sector (ORS) is determined. However, a dedicated interference suppression (IS) measure is applied by the ORSS module, which is able to distinguish between the intended signal and the interference signal. If the ORSS module determines that the carrier detected by the PCS module is an interference, then the SPU transits back from the ORSS state to the PCS state. Otherwise, the SPU enters into the RX process. After receiving

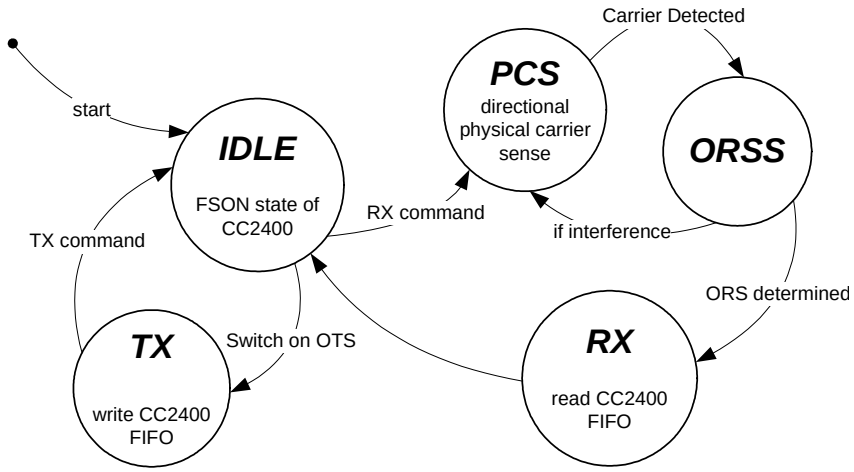

Figure 5.10: The overall state transitions of the SPU.

the whole data, it transits back to the IDLE state. If the test-bed needs to transmit data, the optimal transmission sector (OTS) must be known in advance, as mentioned above. During the IDLE state, if the SPU receives an OTS switching command from the ULS, it immediately outputs the corresponding switching command (SWCMD) and then transits to the TX state, during which the whole data are written to its TX FIFO. After receiving the TX command from the ULS and transferring it further to CC2400, the SPU transits back to the IDLE state. In the following, I will describe the operations performed in each state in detail.

5.3.2.1 IDLE operation

During the IDLE state of the SPU, CC2400 stays in the quasi-idle FSON state, which means that its oscillator and PLL are running, however its baseband processing unit is not running. It should be noted that the PCS_N signal of CC2400 that indicates carrier sensing is not available in this condition. It is only available after CC2400 receives the RX command and transits to the RX state. Therefore, the PCS function is not possible when the SPU is in the idle state. This is caused by the fact that the RSSI signal is generated by the baseband processing unit. Presently, most RF transceiver & baseband chips use this design to save circuits and expense. However, this design results in the fact that the chip consumes nearly the same power for carrier sensing and data reception. A worse condition is that in an ad hoc network the communication nodes carry out PCS for most of their operating time. This observation may motivate a low power design that if a dedicated component with a low power consumption is designed for PCS, then the average power of the RF transceiver & baseband chip can be significantly reduced. This is possible because most functions of data reception (baseband processing) are not required for RSSI signal generating.

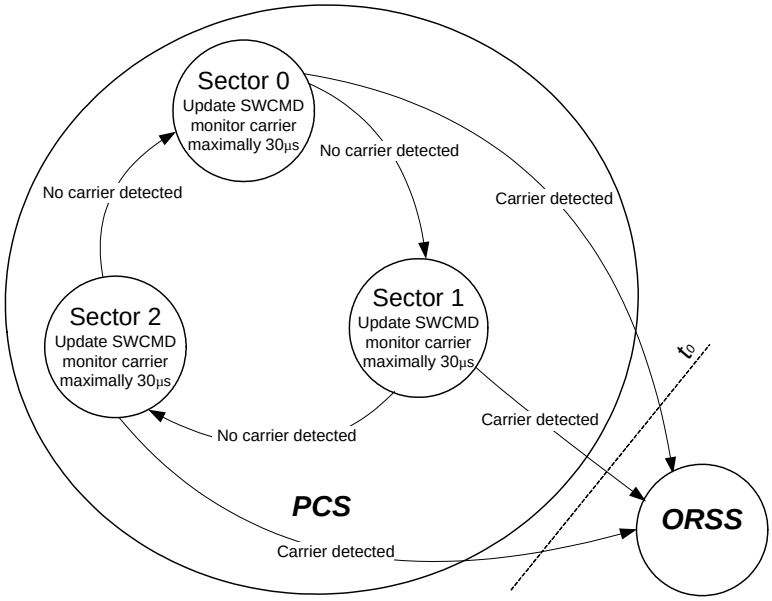

Figure 5.11: The PCS state machine of the SPU

5.3.2.2 PCS operation

Fig. 5.11 illustrates how the SPU performs the directional physical carrier sensing during the PCS state. CC2400 supports the carrier sensing function that is able to output the signal PCS_N to indicate whether a carrier appears in the air (that is, whether the generated RSSI value is above the sensing threshold). Each time after the switching command (SWCMD) is sent, the PCS_N signal is monitored by the PCS module. If a valid PCS_N signal appears within 30 μs, then the SPU transits to the ORSS state immediately. Otherwise, it updates SWCMD and repeats the same operation. The reason for the maximal waiting time to be set to 30 μs is that CC2400 is able to generate the valid RSSI signal 20 μs after the appearance of the carrier signal (for the default setting, however this duration can be modified [9]). PCS_N is generated by the comparison between the RSSI value and the preset sensing threshold. The remaining 10 μs are reserved as a margin. As shown in Fig. 5.11, the time instant for the SPU to transit from the PCS state to the ORSS state is marked as t_0.

5.3.2.3 ORSS operation

Fig. 5.12 shows the packet format received by the SSB test-bed. Each data packet consists of a 32-Byte preamble, a 4-Byte synchronization word and a 225-Byte data. The first 28 Bytes of the preamble are reserved for the ORSS process carried out by the SPU, the remaining 4 Bytes of the preamble are used by CC2400 to perform data slice (bit decision), and the synchronization word is for CC2400 to extract the data

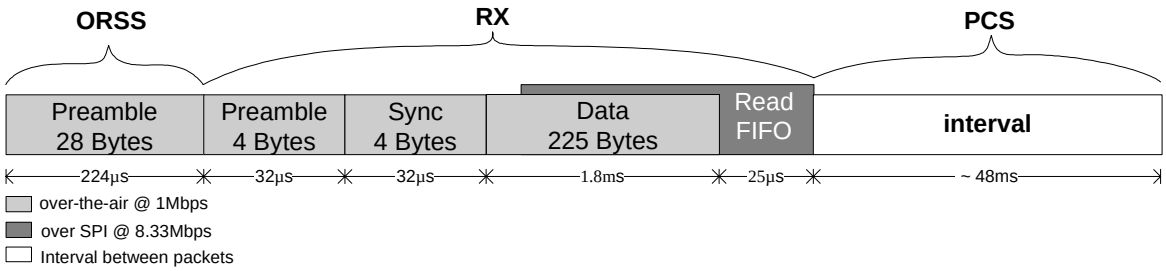

Figure 5.12: Data packet format

rate and perform data decision [9]. Therefore, in this design around 11% of the packet length is added as an additional overhead for ORSS. Fig. 5.12 also gives the interval between packets, which is relatively constant, around 48 ms. This interval is decided by the TX station, which is a CC2400 kit controlled by its SmartRF software studio via the USB cable. On this software, the maximum transmission packet rate is 20 packets/second (refer to Fig. 5.14).

The reserved 28 Bytes preamble has the length of 224 μs at the 1 Mbit/s data rate. Fig. 5.13 illustrates how this preamble is utilized during the ORSS process. Each time before reading RSSI, 30 μs is waited to let CC2400 settle down the RSSI value. Accessing the register of CC2400 that records the RSSI value over SPI and writing it into the SPU only take around 2 μs (2 Bytes @ 8.33 Mbit/s). Each time after the RSSI value is obtained, SWCMD is updated to obtain the RSSI value of the next sector. After obtaining three RSSI values, the ORSS module determines the optimal reception sector (ORS) and sets the corresponding SWCMD. After that, the SPU transits to the RX state. The ORS SWCMD will be always kept during the RX state.

In the best condition, ORSS takes less than $4 * 32$ μs (RSSI settling and accessing). However, this duration may be significantly increased in the worst case. To explain the above conclusion, we need the assistance of Fig. 4.5 in Section 4.3. In the test-bed 224 μs are reserved for the ORSS process, this duration is enough even for the worst case condition.

Best case ORSS At the initial condition there is no carrier signal in the air and the SPU stays in the PCS state, whose operation is shown in Fig. 5.11. Assume that at the time instant t_{-1} the carrier signal impinges on the test-bed from one direction of the sector 0 (S0), and exactly at t_{-1} the SPU updates its SWCMD to switch on the sector 0. In this case, the SPU will detect the carrier maximally 30 μs after t_{-1} and then immediately transit to the ORSS state at the time instant t_0 (see Fig. 5.11). This is a typical example of the best case, in which t_0 is very near to the beginning of the preamble and the duration T_{pre} in Fig. 5.13 (the difference between t_{-1} and t_0) is less than 30 μs.

Worst case ORSS In the worst case, we again assume that at the time instant t_{-1} the carrier signal impinges on the test-bed from one direction of S0. However, in this case the SPU updates its SWCMD to switch on S0 slightly ahead of t_{-1}. As a result, the RSSI signal is not settled down (that is, a valid PCS_N doesn't appear) at the time instant of the next sector switching. This waists nearly 30 μs. After that, the antenna pair for S1 and S2 are switched on sequentially. Since they are not the optimal reception sector, CC2400 may not be able to generate a high enough RSSI value. This waists 60 μs. Finally, S0 is switched on again and then the SPU detects the carrier and transits to the ORSS state (this may also consumes some microseconds, but at most 30 μs). In total, almost four times of 30 μs are wasted in this worst case example. In this case, T_{pre} in Fig. 5.13 is at most 120 μs.

Two conditions will make the SPU transit back from the ORSS state to the PCS state, as shown in Fig. 5.10:

- The SPU transits to the ORSS state at t_0 because it detects a valid PCS_N signal in the PCS state. As shown in Fig. 5.13, after t_0 the ORSS module will first wait for 30 μs to let RSSI be settled down by CC2400. In this duration, the PCS_N signal is continuously monitored. If the valid PCS_N signal disappears, then the SPU immediately transits back to the PCS state. Because the disappearance of the valid PCS_N signal in this condition implies that it was only a glitch.
- The interference suppression (IS) function of the ORSS module determines that the detected carrier is an interference signal, but not the intended signal. Therefore, the resulting ORS is for the interference, which would seriously deteriorate the reception. In this case, the SPU transits back to the PCS state. The IS function will be described in Subsection 5.3.2.6 in detail.

Finally, it should be noted that the PCS & ORSS operation is an extremely time-critical task, and each of its sub-task must be finished within the appointed time so that the whole process doesn't exceed the length of the 28 Bytes preamble. Otherwise, the SPU and CC2400 cannot enter into the RX state in time as expected, which results in a packet loss. This is one of the crucial reasons that PCS & ORSS is not implemented in the upper-layer software (ULS). Actually at the beginning of this implementation task, I have tried to realize PCS & ORSS in the ULS. Two switching command signals are generated by the ULS to control the antenna array, and the SPU outputs one status signal that relays the PCS_N signal output by CC2400, and another status signal to show whether the TX FIFO of the SPU is empty. Status monitoring is realized on the ULS by continuously reading the address that points to the corresponding status signal. The first status signal helps the ULS to receive the PCS_N signal of CC2400, and the

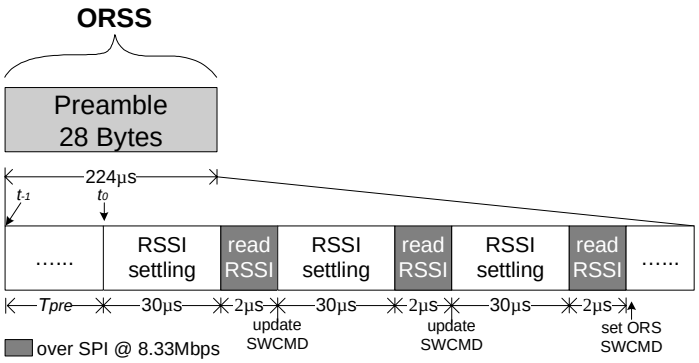

Figure 5.13: Preamble used for ORSS

second status signal helps it to control the interval 30 μs (the details will be described in Subsection A.4.1). After sending the RX command to CC2400 (via the SPU), the ULS always monitors the first status signal and updates SWCMD with an interval of 30 μs if no valid status for PCS_N appears in this duration. If a valid status is read by the ULS, then it immediately begins the ORSS operation. In the ideal condition, PCS & ORSS can be successfully accomplished by the ULS in time. However, this solution caused very frequent packet losses in the experiments. The reason is that the ULS is not capable of the instant response to the transitions of two status signals, since the ULS is programmed by C++ and runs on a Linux-based PC, which is a multi-course system. In the PCS operation, the status signal for PCS_N cannot be instantly detected by the ULS if the PC is just interrupted by other operating tasks. Similarly, if the status signal for the TX FIFO of the SPU is not instantly detected by the ULS, a longer duration than the appointed 30 μs will be spaced. The above two misplays result in the consequence that the ORSS process exceeds the length of the 28 Bytes preamble.

5.3.2.4 RX operation

The RX operation of the SPU is to read the received data from the FIFO of CC2400. To clearly describe this operation, it is necessary to first introduce the FIFO accessing method for CC2400.

CC2400 can be used on either the buffered or un-buffered mode [9]. The buffered mode is advantageous for packet data communications since some packet handling hardware supports are available in this operation mode, e.g., preamble generation & CRC word computation, and their automatic insertions in TX and extractions in RX. Hence, the buffered mode of CC2400 is applied by the SSB test-bed. In the buffered mode an 8-bit wide 32-byte long First-In First-Out (FIFO) block is used for buffering the data to be transmitted in TX or received in RX. The same FIFO is shared by packet transmission and reception.

During the RX operation of CC2400, if the length of the received packet is shorter than 32 Bytes, then the whole packet can be cached in the FIFO of CC2400 and the SPU only needs to read the packet from this FIFO for its RX operation. However, if the length of the packet is longer than 32 Bytes, which is very usual for the up-to-date data communication protocols, and also occurs for the test-bed, then the data must be read out from FIFO by the SPU while CC2400 is receiving data from the air and writing them into FIFO. In this case, the SPU must properly collaborate with CC2400 so that its average reading speed from FIFO is equal to CC2400's writing speed to FIFO. If the SPU reads too fast, then the data read from FIFO are incorrect after it becomes empty. On the contrary, if the SPU reads too slow, then FIFO will become full and result in the abnormal state transition on CC2400 (from the RX state to the FSON state). This terminates the operation of the whole test-bed if a time-out function is not associated.

The SPU accesses the FIFO of CC2400 via SPI, which operates on the speed of 8.33 Mbit/s. However, CC2400 receives the data from the air with the speed of 1 Mbit/s and writes them into FIFO with the same speed. Therefore, particular measures must be adopted by them to ensure the successful data reception. The detailed description about this design is given in Subsection A.3.2. In the RX operation of the test-bed, the SPU automatically reads the whole data packet (even it is longer than 32 Bytes) from CC2400 and saves them into its RX FIFO. The ULS only needs to detect the end of this operation and read the whole packet from the RX FIFO of the SPU afterwards.

5.3.2.5 TX operation

Similar to the RX operation, if the data packet to be transmitted is longer than 32 Bytes, the SPU needs to write data into the FIFO of CC2400 while CC2400 is transmitting data into the air. The SPU must collaborate with CC2400 properly so that its average writing speed is equal to the transmitting speed of CC2400. If the SPU writes too fast, then the FIFO of CC2400 becomes full, which results in the consequence that CC2400 transits from the TX state to the FSON state abnormally. On the contrary, if the SPU writes too slow, then the FIFO becomes empty before all data are written and CC2400 treats it as the end of the packet. In this condition, CC2400 finishes the TX operation and transits to the FSON state. Both the abnormal transitions on CC2400 result in the consequence that only a part of the data packet is transmitted, and this incomplete packet transmission will cause an unsuccessful packet reception.

Similarly, the SPU is able to accomplish the above collaborative operation automatically, and the ULS only needs to write the whole data packet to the TX FIFO of the SPU for data transmission. The only difference from the RX operation is, in the TX

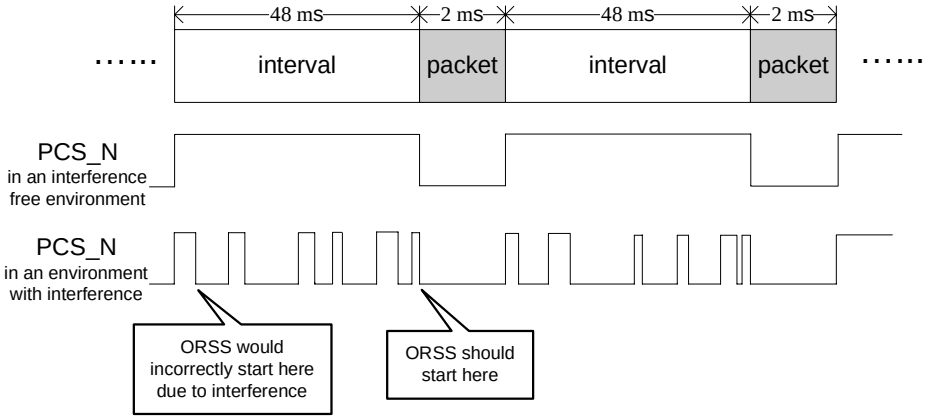

Figure 5.14: PCS_N signal in the environment with and without interference.

operation the SPU needs to first write a part of the packet (less than 32 Bytes) to the FIFO of CC2400, and then sends the TX command. After CC2400 begins to transmit data, the SPU operates according to the usual route described above. This is because immediately after CC2400 gets the TX command it begins to read data from its FIFO and transmit them into the air.

5.3.2.6 Interference suppression (IS) measure applied by the test-bed — a suboptimal solution

As mentioned in Subsection 4.3.5, interference may cause serious disturbance on the correct determination of ORS. If the ORSS process is performed on the interference signal but not the intended user signal, then the determined ORS is incorrect (not for the user signal), which would result in even worse performances than the single antenna system. The main reason for the above consequence is that the physical carrier sensing (PCS) function of CC2400 is based on the RSSI measurement. If the measured RSSI value is above the sensing threshold, no matter caused by the interference signal or the user signal, then CC2400 outputs a low PCS_N signal. As described in the above Subsections 5.3.2.2 and 5.3.2.3, if the signal PCS_N stays low for 30 μs then the SPU determines the appearance of a carrier signal and performs the ORSS process afterwards. However, a 30 μs long interference signal can also cause such an operation. To solve this problem, the optimal solution is to use LQI (link quality indicator) to replace RSSI as the criterion signal (refer to Subsection 4.3.5 for detail). LQI is composed of two parts: RSSI and correlation. However, CC2400 is not able to perform the correlator during the preamble. In this subsection, a suboptimal interference suppression (IS) solution will be introduced. This solution enables CC2400 to distinguish the intended signal from interference.

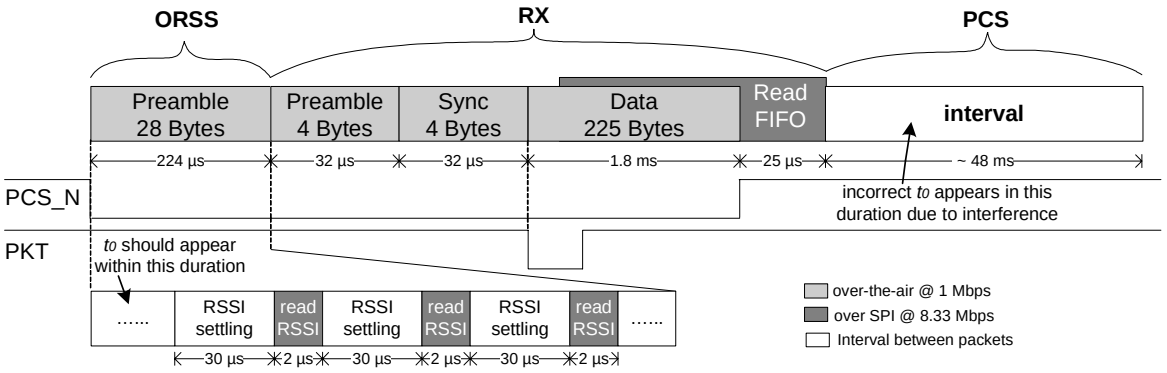

Figure 5.15: Interference suppression measure used in the test-bed.

We have detected strong interference on the 2433 MHz frequency channel since IEEE 802.11b/g WLAN service is available in our building. It is found that this interference signal appears randomly and discontinuously in the air, and its power at the RX site is around -65 dBm when it appears, which is beyond the sensing threshold -72 dBm. Since this power is relatively stable, the interference strength can be described by the proportion of the time when it appears, which is estimated to be more than 50%. An exemplary wave of the PCS_N signal in the environment with and without interference is given in Fig. 5.14. A possible solution to distinguish the interference is to increase the sensing threshold, which is however not always effective since the powers of both the user and interference signals are variable. Hence, a higher sensing threshold decreases the dynamic range of the SSB receiver.

An effective solution is to use the PKT signal generated by CC2400. PKT is a synchronization indicator signal, which appears after the correct detection of the whole synchronization word. It is usually used as an interrupt to let the control unit (e.g., a microprocessor) read the received data. In the test-bed, it is additionally used to distinguish between the interference signal and the intended user signal, because the synchronization word cannot be detected due to interference, and therefore PKT would not appear. The test-bed implements the IS function as follows. After the ORSS process is finished, the ORSS module begins to count the time and monitor the signals PCS_N and PKT. Two conditions will make the SPU transit back to the IDLE state: the signal PCS_N becomes invalid (high state), or a valid PKT doesn't appear and the counting time exceeds 192 μs ($=224+64-32*3$). The former condition implies that the user signal disappears, which cannot occur for the data packet at that moment most probably. The second condition means that no synchronization word is detected, and therefore the ORSS process must be performed on the interference (at least at the beginning). If neither of them occurs, then the SPU transits to the RX state after detecting the PKT signal. Furthermore, the PKT signal is also monitored during the ORSS process. If it appears in this process, then the SPU determines the

Table 5.5: Device utilization summary of FPGA.

Logic Utilization	**Used**	**Available**	**Utilization**
Number of Slice Flip Flops:	177	38,400	1%
Number of 4 input LUTs:	249	38,400	1%
Logic Distribution:			
Number of occupied Slices:	178	19,200	1%
Number of Slices containing only related logic:	178	178	100%
Number of Slices containing unrelated logic:	0	178	0%
Total Number 4 input LUTs:	305	38,400	1%
Number used as logic:	249		
Number used as a route-thru:	56		
Number of bonded IOBs:	83	404	20%
Number of Block RAMs:	2	160	1%
Number of GCLKs:	1	4	25%
Number of GCLKIOBs:	1	4	25%

ORS according to the existent three RSSI values and transits to the RX state at once, otherwise it finishes ORSS and waits for the valid PKT signal as usual. This condition occasionally happens when the former ORSS process is (partially or wholly) operated on interference.

As mentioned above, this solution is not the optimal one but a quasi-LQI-based scheme, since PKT can only appear after the synchronization word. Our measurements show that this suboptimal scheme can effectively mitigate the interference effect so that the test-bed is able to make correct determinations on ORS in the indoor environment with interference, which will be described in Section 5.4 in detail.

5.3.2.7 Device utilization summary of the SPU

The FPGA used by the test-bed to run the SPU functions is a Virtex XCV2000E from Xilinx. After the entire procedure that generates the bitstream file in the Xilinx ISE V7.0 environment, the device utilization summary is reported, as shown in Tab. 5.5. This procedure consists the steps *Synthesize*, *Implement Design*, and *Generate Programming File*, in which the second step is further composed of *Translate*, *Map*, and *Place and Route* processes. From the report we can see that only few resources are consumed by the SPU, which implies that the resource-efficient measures (see Subsection A.3.3.2) used while designing the SPU are effective.

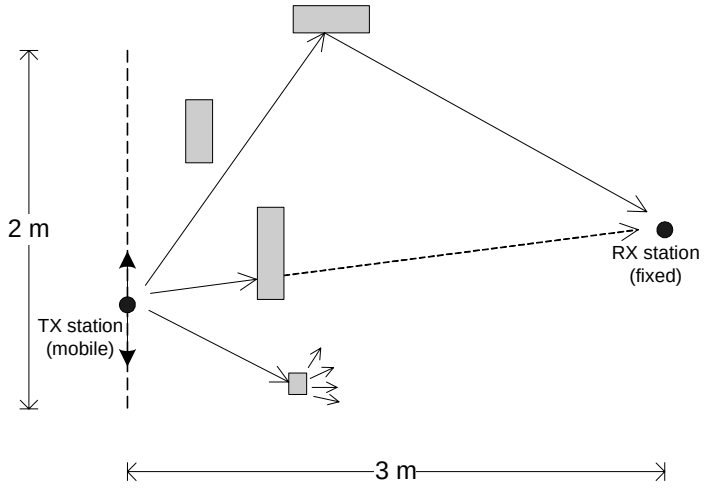

Figure 5.16: Indoor measurement scenario.

5.4 Test-bed measurements and analysis

5.4.1 Scenario

Figure 5.16 illustrates the experiment scenario. The TX station is equipped with an omni-directional antenna and moves on the track (marked as the dashed line) forward and backward with the approximate speed of 0.5 m/s. The RX station is fixed, and can use the SSB system or an omni-directional antenna alternatively. The measurements are performed in an office, which is a typical indoor scenario. The effect of reflection is mainly caused by the wall and the roof, and various objects in the office (e.g., equipments and people) may become scatters and/or obstacles between the TX and RX stations. The multi-path propagation and the mobility of the TX station lead to fast fading of the indoor channel, and the shadowing effect caused by the obstacles is the main reason for slow fading. In this rich-fading environment, the intended signal may impinge on the RX station from diverse directions with a broad angle range, hence the prerequisites for beamforming cannot be fulfilled (refer to Subsection 2.3.1). Therefore, in this case the beamforming effect of the SSB system is not the main contributing factor to the final performance. What really contributes is its space diversity gain. This conclusion can also be revealed by the analysis on the measured results in Subsection 5.4.4.

5.4.2 Selected measures

Wireless communication channels are usually time variant, which means that the channel impulse responses measured on different time instants appear different. Approx-

imately, the impulse response functions obtained in the multiple experiments can be considered as sample functions of a wide sense stationary (WSS), ergodic stochastic process, which means that the autocorrelation function of any two channel impulse responses only depends on the time difference, but not the time instants of measuring. The received signal is the convolution of the transmitted signal and the channel impulse response. Therefore, the received signal power P_r can be approximately regarded as a random variable of a WSS ergodic stochastic process.

The free space propagation model gives the following relationship between the transmission power P_t and the received power P_r [31]:

$$P_\mathrm{r} = P_\mathrm{t} \cdot (\frac{\lambda}{4\pi d})^2 \cdot G_\mathrm{t} \cdot G_\mathrm{r}, \tag{5.7}$$

in which λ, d, G_t and G_r denote the carrier wavelength, transmission distance, antenna gain of the transmitter and antenna gain of the receiver, respectively. The propagation loss can be defined as:

$$\alpha/\mathrm{dB} = 10\lg(P_\mathrm{t}/P_\mathrm{r}). \tag{5.8}$$

From Eqs. (5.7) and (5.8) we can obtain

$$\alpha/\mathrm{dB} = 20\lg(\frac{4\pi d}{\lambda}) - 10\lg(G_\mathrm{t} \cdot G_\mathrm{r}). \tag{5.9}$$

Eq. (5.9) reveals that the basic propagation loss is attributed to the transmission distance d between the TX and RX stations. From Fig. 5.16 we can see that this distance varies slightly from the maximum value of 3.16 m to the minimum value of 3 m due to the movements of the TX station. According to Eq. (5.9), this variance of distance on the carrier frequency 2.4 GHz only causes a slight variance (about 0.46 dB) on the received signal power.

During each run of measurements, the TX station continuously sends 1000 known data packets with the constant (maximum) transmission power of 0 dBm and the approximate speed of 20 packets/sec at the data rate of 1 Mbit/s. Each packet includes 32 Bytes preamble, 4 Bytes synchronization word and 225 Bytes user data. The RX station records the RSSI value for each packet and calculates the bit error rate (BER) after receiving all 1000 packets. That is, in each experiment run 1.8 Mbits data are used for the BER measurement. If the SSB system is used by the RX station, then for each packet three RSSI values are recorded for three sectors, respectively. Apparently, **BER is the first measure** to compare the performance between the single antenna receiver and the SSB receiver.

As we have explained before, the received signal power P_r is a random variable of an ergodic stochastic process, and the effect of attenuation variance caused by the slight distance change during the measurement can be ignored (compared to the variance

caused by fading). Therefore, the average value of the 1000 RSSI values recorded in each measurement run:

$$P_{\text{ave}}/\text{dBm} = \mathcal{E}\{P_{\text{r}}\} = 10\lg(\frac{1}{1000}\sum_{i=1}^{1000} P_{\text{r},i}/\text{mW}) \tag{5.10}$$

is the second measure. This measure can be used to compare the gain of the single omni-directional antenna and the SSB system.

The third measure selected is called the *amount of fading* (AoF), which is defined in [8] as

$$\text{AoF} = \frac{\text{Var}\{P_{\text{r}}\}}{\mathcal{E}^2\{P_{\text{r}}\}} = \frac{\mathcal{E}\{P_{\text{r}}^2\}}{\mathcal{E}^2\{P_{\text{r}}\}} - 1. \tag{5.11}$$

AoF can be used to quantify the severity of fading experienced by the receiver. In some literature P_{r} in Eq. (5.11) is replaced by SNR (signal to noise power ratio), whereas the final result is the same provided that the noise power is constant. The square root of AoF is applied in [80] to assess the effectiveness of their H-S/MRC (hybrid selection/maximal ratio combining) scheme, where it is called the normalized standard deviation of the output SNR. It is derived as:

$$\sigma_{L/N,\text{GSC}} = \sqrt{\text{AoF}} = \frac{\sqrt{1+\sum_{n=L+1}^{N}\frac{1}{n^2}}}{\sqrt{L}(1+\sum_{n=L+1}^{N}\frac{1}{n})},\ N \geqslant L,\ L \geqslant 2. \tag{5.12}$$

Here we use GSC (generalized diversity selection combining) instead of H-S/MRC for simplicity (please refer to Subsection 2.3.2 for details regarding GSC and H-S/MRC). Eq. (5.12) gives the theoretical bound for AoF, which will be compared with our measurement results (see Tab. 5.11) since SSB can be regarded as a special case of GSC. It is necessary to note that the original RSSI values recorded use the logarithmic unit, they must be first converted to the absolute values to calculate the arithmetic mean.

5.4.3 Experiment configurations

The basic experiment scenario and performance measures have been described above. They are default conditions except specially pointed. **Eight** types of experiments have been designed, as illustrated in Tab. 5.6, in which type 1 to 4 have been repeated for **eight** times, respectively. Experiment 1 and 2 are performed on the carrier frequency of 2401 MHz, which is an interference free channel. Those two experiments are expected to give a performance comparison between the single antenna and SSB receivers without interference.

Table 5.6: Experiment configurations

Type	Carrier frequency	TX station	RX station (fixed)	Scatter (person)
1	2401 MHz	mobile	single antenna	mobile
2	2401 MHz	mobile	SSB	mobile
3	2433 MHz	mobile	single antenna	mobile
4	2433 MHz	mobile	SSB	mobile
5	2401 MHz	fixed	single antenna	fixed
6	2401 MHz	fixed	SSB	fixed
7	2401 MHz	fixed	single antenna	mobile
8	2401 MHz	fixed	SSB	mobile

When the experiments were performed on 2433 MHz, we observed that the SSB test-bed without the interference suppression (IS) function couldn't function well and resulted in even worse performances than the single antenna receiver with respect to BER. The reason is that on this frequency channel ORSS was always performed on the interference appearing in the relatively long interval (incorrect t_0 is marked in Fig. 5.15), but not on the beginning of the 28 Bytes preamble of the user signal (correct t_0 is also marked in Fig. 5.15). Therefore, the signal is received in the determined ORS for interference that has a lower SINR (signal to interference plus noise power ratio). As described in Subsection 5.3.2.6, a suboptimal interference suppression measure has been applied when implementing the SSB receiver so that this undesired condition is avoided as much as possible. Experiment 3 and 4 are designed to show how well the SSB receiver functions in an interference environment.

In the experiments from 5 to 8, both TX and RX stations are fixed. Under this condition, the channel fading is only caused by the movements of scatters. There are diverse objects in the office, all of which are static except the tester (1 person). The tester plays the role of the moving scatter in this case. In the course of experiment 5 and 6, the tester tried to keep static as much as possible. During experiment 7 and 8, the tester made some usual actions like slow movements. Only fast fading is supposed to result from such movements of the scatter since there are no obstacles between the static TX and RX stations. We expect to see how much the fast fading affects the RX stations equipped with a single antenna and the SSB module, respectively.

5.4.4 Measurement results and analysis

5.4.4.1 Exemplary figures measured in experiment type 1 to 4

Since experiment 1 to 4 have been repeated for eight times, Fig. 5.17 to 5.20 are selected results corresponding to the experiment type 1 to 4, respectively. For the measurements of the single antenna receiver, 1000 RSSI values (one for each data packet) are plotted versus time. For the SSB receiver, three RSSI values of three sectors for each data packet are recorded and illustrated, and the RSSI of the ORS (that is the maximum RSSI) is also marked with the thick line. Furthermore, the corresponding switching command (SWCMD, 0 / 1 / 2) for each packet reception is also indicated on the same time axis. In each figure, three measures (P_{ave}, AoF and BER) are given.

Fig. 5.17 and Fig. 5.18 are selected results measured on the interference free 2401 MHz frequency channel. By observing them we can intuitively feel that the received signal power of the single antenna receiver fluctuates more strongly than that of the SSB receiver (for the SSB receiver only the RSSI of its ORS is considered). This observation is borne out by the reduction of AoF from 1.03 to 0.3. This coincidence also confirms that the measure AoF can be used to quantify the degree of channel fading. By comparing the other two measures, we can see that the SSB receiver's average power is higher and BER is lower than those of the single antenna receiver, all imply that the SSB receiver exhibits a better performance.

Fig. 5.19 and Fig. 5.20 are selected results measured on the 2433 MHz frequency channel that has interference. By comparing them the same conclusion as on 2401 MHz can be drawn. A new phenomenon is that for the single antenna receiver, the measured BER on 2433 MHz is apparently higher than that measured on 2401 MHz (0.2692% vs. 0.0087%), which is caused by the higher interference power on the 2433 MHz frequency channel. However, even in this frequency channel with strong interference, the SSB receiver still gives the perfect BER (0.000%). This implies that the sub-optimal interference suppression measure (as described in Subsection 5.3.2.6) used by the test-bed functions well. It should be noted that in each experiment run only a limited amount of data (1.8 Mbits) are used for the BER measurement, therefore, the precision of the measured BER is limited. That is, 0% only represents that the BER is very small, not means exactly zero.

5.4.4.2 Measured results for all 8 runs of type 1 to 4 experiment and their overall averages

Three measures obtained in all eight measurement runs of experiment type 1 to 4 are listed in Tab. 5.7 to 5.10, respectively. The overall average values of P_{ave}, AoF

and BER of eight measurements are given in each table, and are further listed in Tab. 5.11. They can be used to make an overall performance comparison between the single antenna receiver and the SSB receiver.

Form Tab. 5.11 we can find that for both 2401 MHz and 2433 MHz frequency channels, the SSB receiver outperforms the single antenna receiver in terms of higher receivd power, smaller amount of fading and smaller BER, all of which are overall average values. This conclusion even holds for each measurement run without any exceptional case. By observing Tab. 5.7 to 5.10 we can find that for all experiment runs, all three measures of the SSB receiver are better than those of the single antenna receiver. The obtained measure of smaller amount of fading for the SSB receiver implies that **the SSB scheme can help to suppress the channel fading**.

Comparing the measurements made on 2401 MHz and 2433 MHz listed on Tab. 5.11, we can observe that the average BER of the single antenna receiver is significantly increased from 0.016% to 0.245%, while the average BER of the SSB receiver always keeps on the perfect value of 0.000%. This result implies that **the SSB scheme can help to suppress the interference** and thus increase the SIR (signal to interference power ratio).

For the average received power listed on Tab. 5.11, we can see that the SSB receiver always obtains higher values than the single antenna receiver, a 1.72 dB increase at 2401 MHz and a 1.93 dB increase at 2433 MHz. Theoretically, the SSB scheme has a 3 dB array gain (broadside case pattern) under the ideal free space condition. However, as indicated in Section 5.2, all RF components of the SSB system are connected by several RF coaxial cables and connectors, which cause an additional loss. Furthermore, the use of RF switches and RF combiner & divider introduces an insertion loss, too. By measuring the S-parameters of the RF cables (refer to Subsection 5.2.4) and using the parameter of insertion loss listed on the data sheet of each corresponding RF component, the additional loss caused by them can be estimated as 2.3 dB in total. Therefore, the actual SNR gain that SSB has achieved reaches 4.23 dB. This indicates that the higher received power of the SSB receiver cannot be explained by the (beamforming) array gain, but should be attributed to **the space diversity gain**. This conclusion is coincident with the analysis made in Subsection 5.4.1 that in a rich-fading environment like an office, the main effect of SSB is not the array gain due to beamforming, but the space diversity gain. Fig. 2.7 illustrates the diversity gains of different schemes, all of which are theoretical values except the gain of SSB. From it we can see that the SSB test-bed exhibits a 1.68 dB degradation compared to its theoretical upper bound (the gain of the 2 out of 6 case GSC scheme), but its diversity gain exceeds the theoretical gain of the 1 out of 6 case selection diversity (SD) scheme. This implies a significant improvement over an actual 1 out of 6 SD system.

The last column of Tab. 5.11 lists the theoretical predictions of AoF, which are given by [8] for the single antenna case and by [80] for the 2 out of 6 GSC case (also see Eq. 5.12). It is clearly shown that in each case the AoF measured on the test-bed closely approaches the corresponding theoretical prediction.

5.4.4.3 Measured results for experiment type 5 to 8

Fig. 5.21 to 5.24 illustrate the measurements of experiment type 5 to 8, respectively, each of which is only performed once. Those experiments are designed to show the fading effect to the single antenna receiver and the SSB receiver due to the movement of a scatter. Measurement type 5 and 6 are used for reference, since all objects in the test environment are static. The graphs in Fig. 5.21 and 5.22 meet our expectation, which exhibit very stable RSSI values. Both of the resulting AoF are small, 0.0173 for the single antenna receiver and 0.0258 for the SSB receiver. Fig. 5.22 also gives a clear separation among three sectors, and we can see that the line for sector 2 doesn't appear. This is because the line for sector 2 overlaps with the line for ORS, or in this measurement sector 2 is always the ORS, which is also indicated by its SWCMD graph.

In Fig. 5.23 we can observe a somewhat strong variance on the RSSI values, and the calculated AoF of 0.064 confirms this observation. And the RSSI line (for ORS) in Fig. 5.24 exhibits a smaller variance, and the resulting AoF of 0.0459 is smaller than 0.064 in Fig. 5.23 as expected. This result indicates that **the SSB receiver suffers less from the fast fading** caused by the movement of a scatter in the environment. In Fig. 5.24 we can also see that the RSSI variance of other two non-optimal sectors is very strong, which implies that this benefit should be attributed to the ORSS diversity gain, but not the beamforming gain of the two-element antenna array.

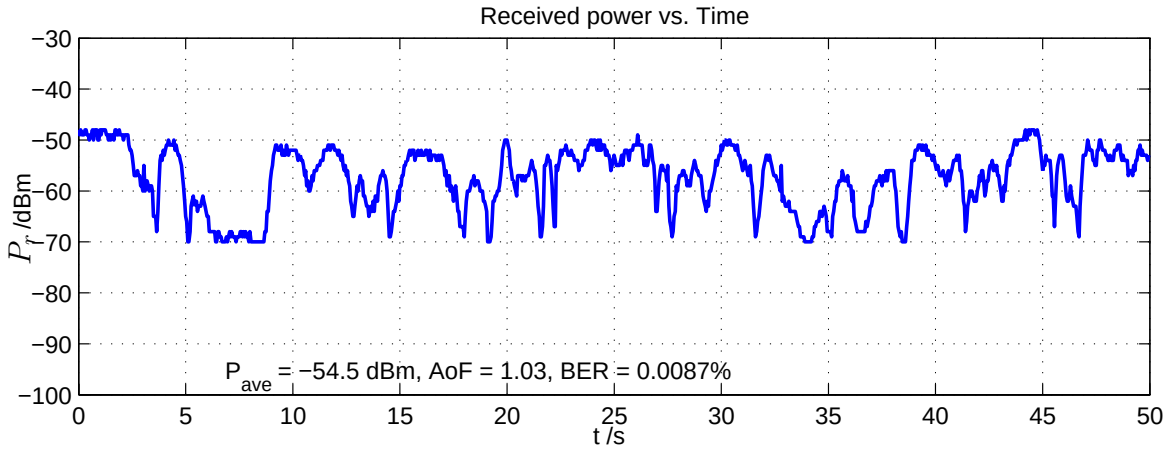

Figure 5.17: Single antenna RX with moving TX station @ 2401 MHz (type 1, run 2).

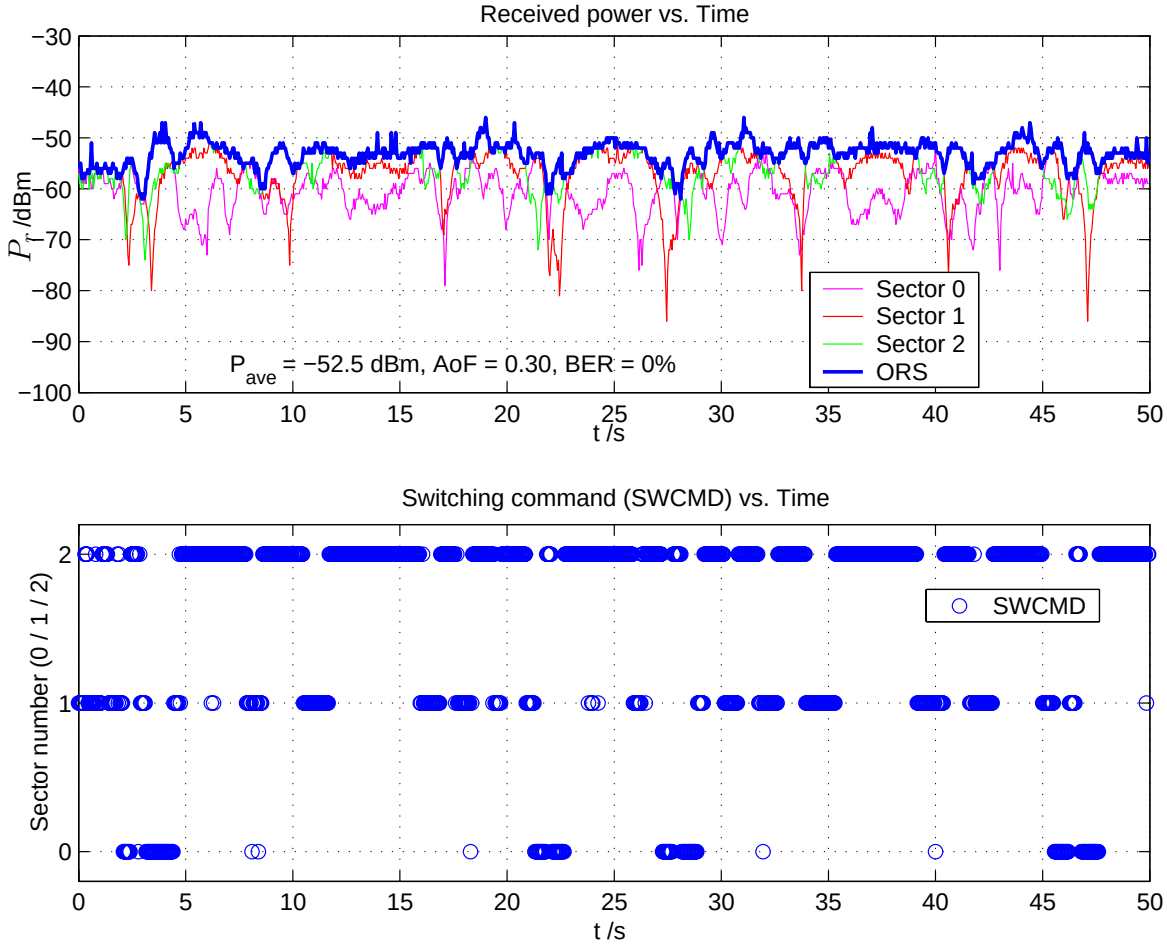

Figure 5.18: SSB RX with moving TX station @ 2401 MHz (type 2, run 4).

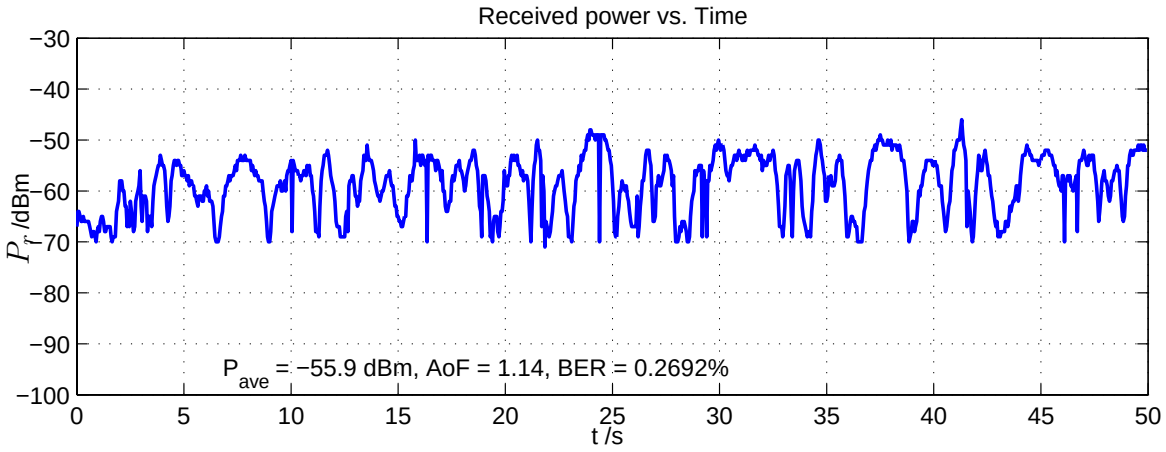

Figure 5.19: Single antenna RX with moving TX station @ 2433 MHz (type 3, run 4).

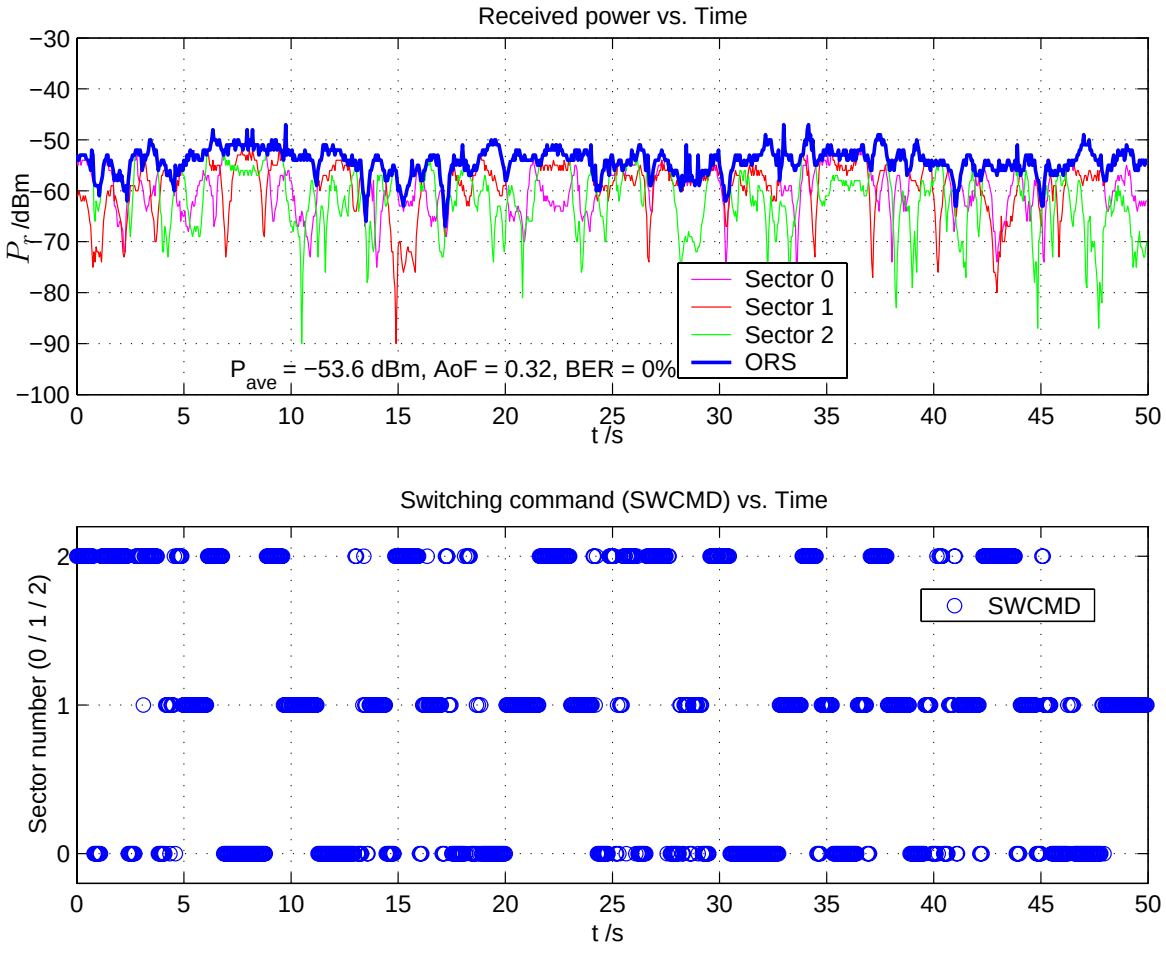

Figure 5.20: SSB RX with moving TX station @ 2433 MHz (type 4, run 8).

Table 5.7: Single antenna RX with moving TX station @ 2401 MHz (type 1).

run	1	**2**	3	4	5	6	7	8	**Average**
P_{ave}/dBm	-55.1	-54.5	-56.2	-55.0	-52.9	-53.2	-54.8	-53.3	**-54.2**
AoF	0.702	1.031	0.909	0.862	0.999	0.905	1.010	0.999	**0.927**
BER/%	0.015	0.009	0.014	0.053	0.001	0.001	0.009	0.024	**0.016**

Table 5.8: SSB RX with moving TX station @ 2401 MHz (type 2).

run	1	2	3	**4**	5	6	7	8	**Average**
P_{ave}/dBm	-52.0	-52.0	-52.7	-52.5	-52.8	-52.8	-52.7	-52.7	**-52.5**
AoF	0.465	0.423	0.394	0.300	0.531	0.262	0.378	0.335	**0.386**
BER/%	0.000	0.000	0.000	0.000	0.000	0.000	0.000	0.000	**0.000**

Table 5.9: Single antenna RX with moving TX station @ 2433 MHz (type 3).

run	1	2	3	**4**	5	6	7	8	**Average**
P_{ave}/dBm	-55.4	-56.4	-56.8	-55.9	-55.5	-56.5	-55.6	-54.9	**-55.8**
AoF	0.835	0.637	1.590	1.144	0.848	0.865	0.931	0.899	**0.969**
BER/%	0.182	0.329	0.413	0.269	0.175	0.150	0.085	0.357	**0.245**

Table 5.10: SSB RX with moving TX station @ 2433 MHz (type 4).

run	1	2	3	4	5	6	7	**8**	**Average**
P_{ave}/dBm	-53.3	-53.5	-54.7	-55.5	-53.2	-54.7	-53.3	-53.6	**-53.9**
AoF	0.379	0.615	0.369	0.369	0.579	0.583	0.614	0.318	**0.478**
BER/%	0.000	0.000	0.000	0.000	0.000	0.000	0.000	0.000	**0.000**

Table 5.11: Overall average measures of eight-run experiments (refer to Tab. 5.6 for the type number).

Type	$\mathcal{E}\{\text{BER}\}$/%	$\mathcal{E}\{P_{\text{ave}}\}$/dBm	$\mathcal{E}\{\text{AoF}\}$	AoF bound
1	0.016	-54.234	0.927	1.0
2	0.000	-52.511	0.386	0.2025
3	0.245	-55.826	0.969	1.0
4	0.000	-53.897	0.478	0.2025

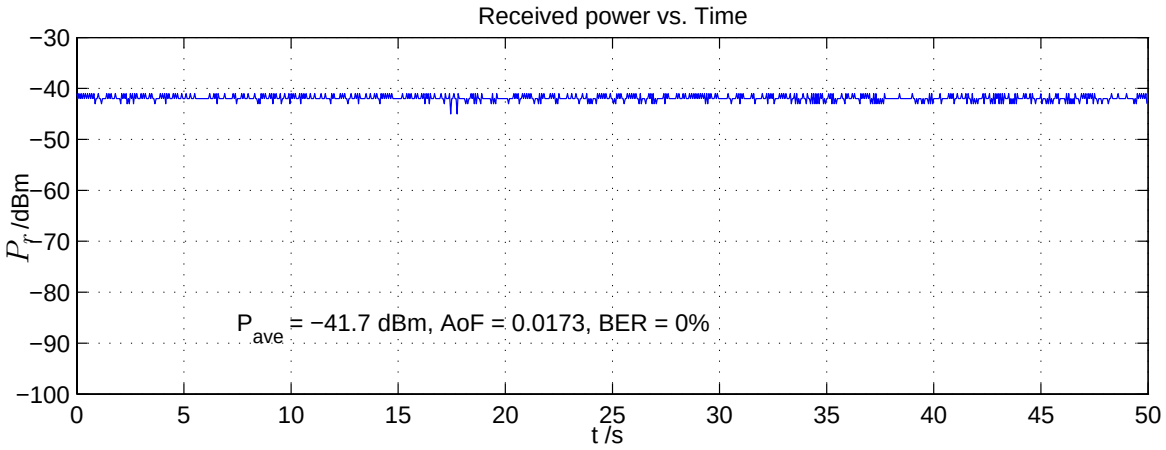

Figure 5.21: Single antenna RX with fixed scatters @ 2401 MHz (type 5).

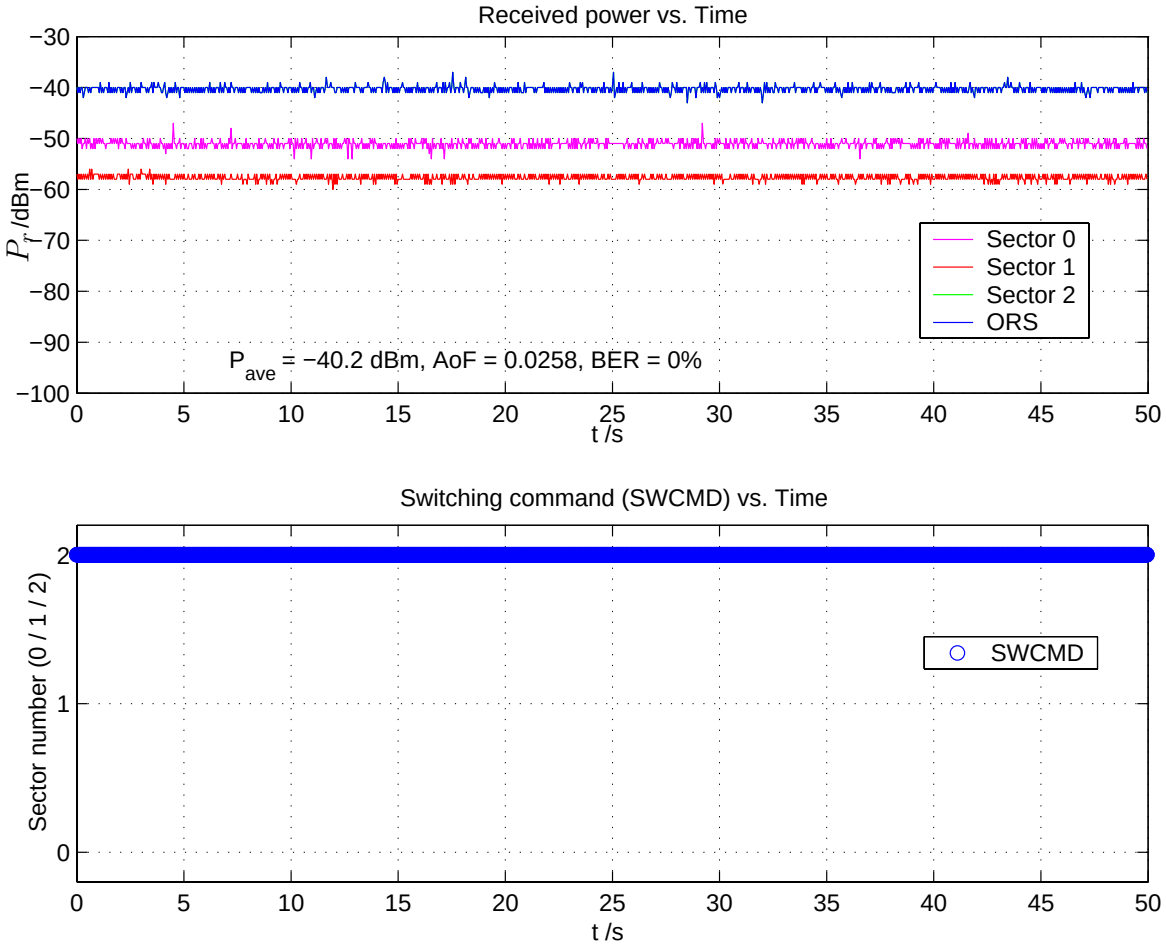

Figure 5.22: SSB RX with fixed scatters @ 2401 MHz (type 6).

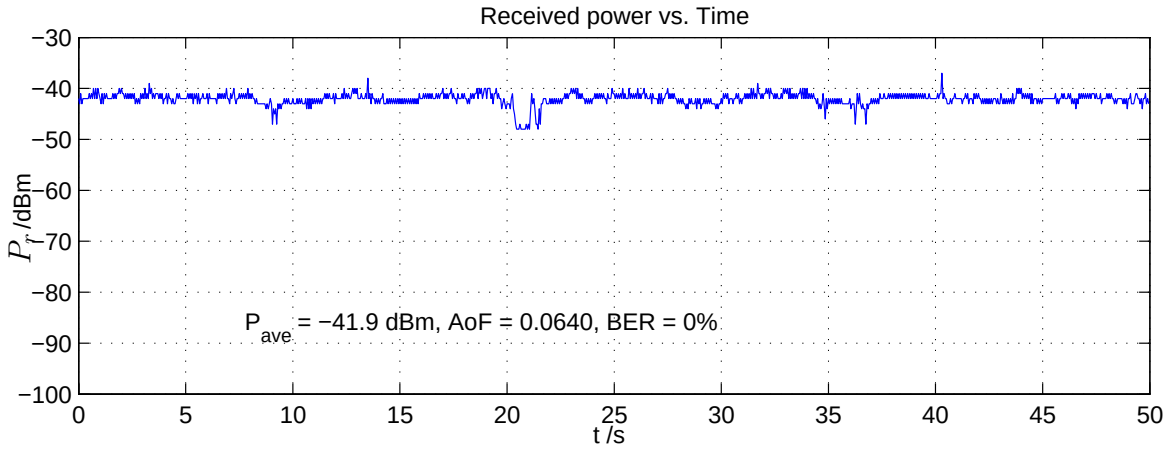

Figure 5.23: Single antenna RX with moving scatters @ 2401 MHz (type 7).

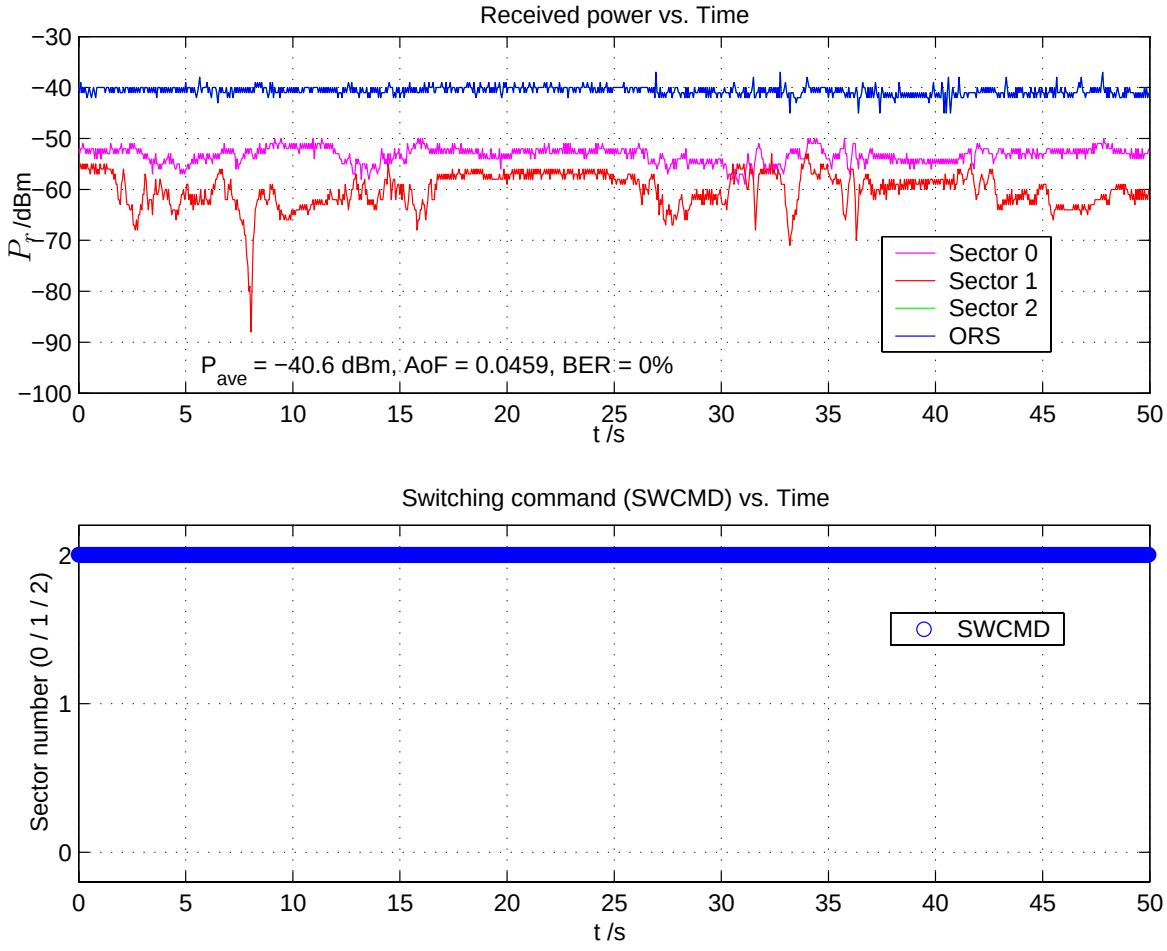

Figure 5.24: SSB RX with moving scatters @ 2401 MHz (type 8).

Chapter 6

Conclusions and Outlook

6.1 Conclusions

This thesis is devoted to resource-efficient designs for mobile ad hoc networks, focusing on the physical layer, the MAC layer and the cross-layer optimization. The designs that are suitable for mobile portable applications are emphasized. The feasibility and advantages of a low complexity six-antenna communication scheme called simplified switched beam (SSB) have been verified by the measurements on its test-bed.

First, the spectrum-efficiency and the energy-efficiency are explicitly defined from the entire network perspective, which are different from the previous definitions based on the point-to-point link. In addition, hardware complexity, cost, and size are taken into account as practical aspects. Those aspects should also be treated as resources, because mobile portable devices are strictly constrained by them.

The new designs are initiated from the physical layer multi-antenna techniques. A variety of multi-antenna techniques have been reviewed and analyzed, mainly from the system principle and hardware implementation perspective. After a careful survey on the existing test-bed trials, we conclude that for mobile portable devices the present focus should be laid on the switched beam and space diversity techniques with a small number of antenna elements. More complex beamforming and MIMO techniques can achieve significant performance improvements only at the cost of extremely high hardware complexity and power consumption, which are not sustainable for mobile portable devices with state-of-the-art technologies.

When new designs on the physical layer are applied, the MAC protocol must be adapted accordingly to match the new features and thus to achieve the best possible network performance. Two types of MAC designs are presented, one based on the beamforming (BF) gain called BF-MAC, the other based on the space diversity (SD) gain called SD-MAC. The novelties and limitations of the previous investigations found in literature are addressed. Based on them, the multi-directional-antenna (MDA) scheme together with its adapted MAC designs MDA-MAC, radiation power control (PC) and transceiver power management (PM) are proposed. The performance evaluation through network simulations shows that higher spectrum- and energy-efficiencies

can be achieved by MDA-MAC together with PM, compared to the traditional single antenna designs. The simulations also reveal that the PC scheme doesn't have an apparent impact on performance and energy saving. However, the MDA-based designs also exhibit a disadvantage of extremely high hardware complexity.

The six-antenna scheme SSB is motivated by the above studies. Comparing with the single antenna system, SSB only requires up to 10% more power consumption and very few additional components, in particular only one RF front-end is required. Therefore, SSB is suitable for mobile portable applications. It can be used on both TX and RX sides. A complete solution for SSB on the physical and MAC layers (SSB + SSB-MAC) is presented, and the concern on the cross-layer optimization is emphasized. Especially, an interference suppression technique is designed, which can effectively distinguish the user signal from the interference signal to avoid its disturbance on correct antenna switchings. SSB functions well in both weak-fading and rich-fading environments. In the former its beamforming array gain plays the main role, while in the latter its space diversity gain plays the main role. The performance evaluation through network simulations shows that higher spectrum- and energy-efficiencies can be achieved by SSB compared to the traditional single antenna designs, although they are lower than the efficiencies of the MDA-based designs. However, a significant saving on the hardware complexity is realized. Therefore, a proper balance between performance and hardware complexity has been achieved by SSB.

To evaluate the real system performance of SSB, its test-bed has been implemented. We have used the off-the-shelf RF components to construct the antenna array and the FPGA rapid prototyping system RAPTOR2000 to carry out its array signal processing. Experimental measurements in the indoor short range scenario have been made with various configurations, in which the SSB system only acts as a receiver. The analysis on the results shows that SSB can help to suppress fading and interference, and increase the received signal power. It gives a better performance than the single antenna receiver in terms of the reduced BER. The measured SNR gain and AoF (amount of fading) closely approach the theoretical predictions.

6.2 Outlook

Three aspects of improvements are left for this test-bed. First, we need to build the compact PCB to alleviate the additional insertion loss; second, we need to investigate the benefits attained by SSB when it is used on both sides of RX and TX; finally, we can realize both SSB and SSB-MAC on the hardware of a real mobile device. With multiple devices of this kind, a real MANET can be organized and tested.

Recently, the new multi-channel techniques (e.g., OFDMA) and spatial multiplexing techniques (refer to section 2.4) have come into use in many applications. Although their employment on mobile portable devices still needs time for a significant progress on the silicon technology, the required adaption on their MAC protocols to achieve the best possible network performance can commence.

Appendix A

SSB Processing Unit (SPU) Implementation Details

A.1 Operating specification of CC2400 SPI

At first, it is necessary to introduce the SPI specification of CC2400 briefly, mainly from [9]. CC2400 is configured via a simple 4-wire SPI-compatible interface (SI, SO, SCLK and CSn) and it acts as a slave device. That is, the CSn and SCLK signals are generated by its communication partner, a master SPI device. In the following, we always use one SPI cycle to refer to the duration when CSn keeps active (low). The control of CC2400 is executed by the upper-layer software (ULS) running on the host computer by writing the command via the SPI to the corresponding register of CC2400. The SPI is also used as the data interface in the buffered mode, since the FIFO in CC2400 is also regarded as a register block.

CC2400 has three types of registers, configuration registers (CR), command strobe registers (CSR) and FIFO. CR and FIFO can be read and written, while CSR can only be addressed. CR has a 2-byte content, and FIFO has a capacity of 32 Bytes. The way of accessing those registers are summarized as follows:

- **Accessing CR** The 2-byte content of a configuration register can be written or read, and each CR corresponds to a 7-bite address (note, some CRs are only readable). To access a CR, the first byte on the SI line after CSn becomes active (low) must be the R/W bit and its 7-bit address, in which the R/W bit is the MSB (most significant bit, or the highest bit). The R/W bit indicates the intention of this access, write (0) or read (1). If write, the next two bytes on SI will be written to the register; if read, then the following signals on SI don't make sense and the 2-byte content of the register will be output by CC2400 on the SO line, see Fig. A.1. In one SPI cycle, half of the register (means 8MSB, or the high byte), the whole register, or multiple registers can be accessed. In the first case, CSn becomes inactive after accessing the 8MSB of the register to save time. However, if the 8LSB (the low byte) of the register needs to be accessed,

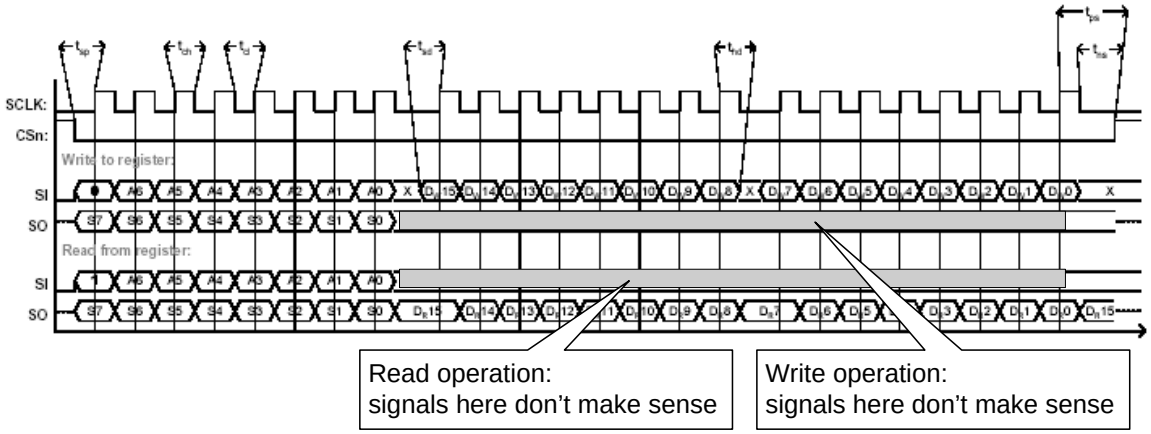

Figure A.1: SPI timing diagram [9].

the whole register must be accessed. In the last case multiple registers can be accessed sequentially (only if their addresses are sequential), and the first byte on the SI line gives the R/W bit and the address of the first register. The last one of those registers can be half accessed in the same manner as the first case to save time.

- **Accessing FIFO** can be treated in the same manner as accessing multiple CRs, as described above. The difference is that FIFO has its own 7-bit address.
- **Accessing CSR** The command strobe register is accessed in the same way as a read/write operation, but no data is transferred. That is, only the R/W bit and the seven address bits are transferred on SI before CSn being set high. The R/W bit doesn't make sense since accessing CSR is not to read or write it, and therefore its SPI cycle only covers one byte. By addressing a CSR the internal sequences of CC2400 will be started. These commands can be used to quickly change it from RX mode to TX mode, for example.

During the transfer of the address, the CC2400 returns a status byte on the SO line containing some important flags, e.g., bit 3 CRC_OK indicates whether the next two bytes in the FIFO are correct CRC values of the current packet, see [9] for details. In the SPU, CRC_OK is applied to determine the success of a packet reception.

The maximum operating speed of the SPI on CC2400 is 20 MHz. However, only 8.33 MHz (50/6 MHz) is used for the SPU, which results in the 8.33 Mbps data rate. Anyhow, it is much faster than the over-the-air speed of CC2400 (1 Mbps). Other timing specifications marked in Fig. A.1 can be found in [9].

A.2 Top-level schematic diagram of the SPU

Fig. 5.9 in Subsection 5.3.2 illustrates the block diagram of the SPU, which is composed of three components: SPI Master, SSB Controller and LocalBus_Slave_Simple.

- **SPI Master** is responsible for generating the CSn and SCLK signals, receiving data from the ULS and transferring them into its SO line, and the reverse operation, receiving data from its SI line and transferring them to the ULS. It should be noticed that the SO pin of the SPU is connected to the SI pin of CC2400, and the SI pin of the SPU is connected to the SO pin of CC2400. Therefore, when mentioning the SI and SO lines, they must be clearly indicated whose lines.
- **SSB Controller** is further composed of three sub-components, the component for PCS (physical carrier sense), ORSS (optimal reception sector selection), and IS (interference suppression).
- **LocalBus_Slave_Simple** is a bus converting logic between the internal bus and the local bus. The RAPTOR2000 mother board applies a PCI bridge chip PLX 9054, which functions as an interface between the local bus and the PCI bus on the host computer.

Fig. A.2 illustrates the top-level schematic diagram of the SPU. The descriptions on each component will be given in Section A.3. Tab. A.1 roughly corresponds the components in Fig. 5.9 and Fig. A.2.

Table A.1: Components correspondence.

Components in Fig. 5.9	Components in Fig. A.2
SPI Master	FIFO_SE, FIFO_S_CTRL, SERIAL_SENDER, FIFO_RE, FIFO_R_CTRL, SERIAL_RECEIVER, SPI_RF_CTRL, SP3T_MUX, ADR_DECODER, DREG_AR_EN_FIFO, MUX, STATE_REG
SSB Controller	PCS_NS, MUX_1, PCS_ORSS
LocalBus_Slave_Simple	LocalBus_Slave_Simple (Note: The local bus side is not illustrated in the figure.)

Tab. A.2 lists the signals of the SPU except the local bus side. Descriptions on the local bus can be found in the documents of RAPTOR2000.

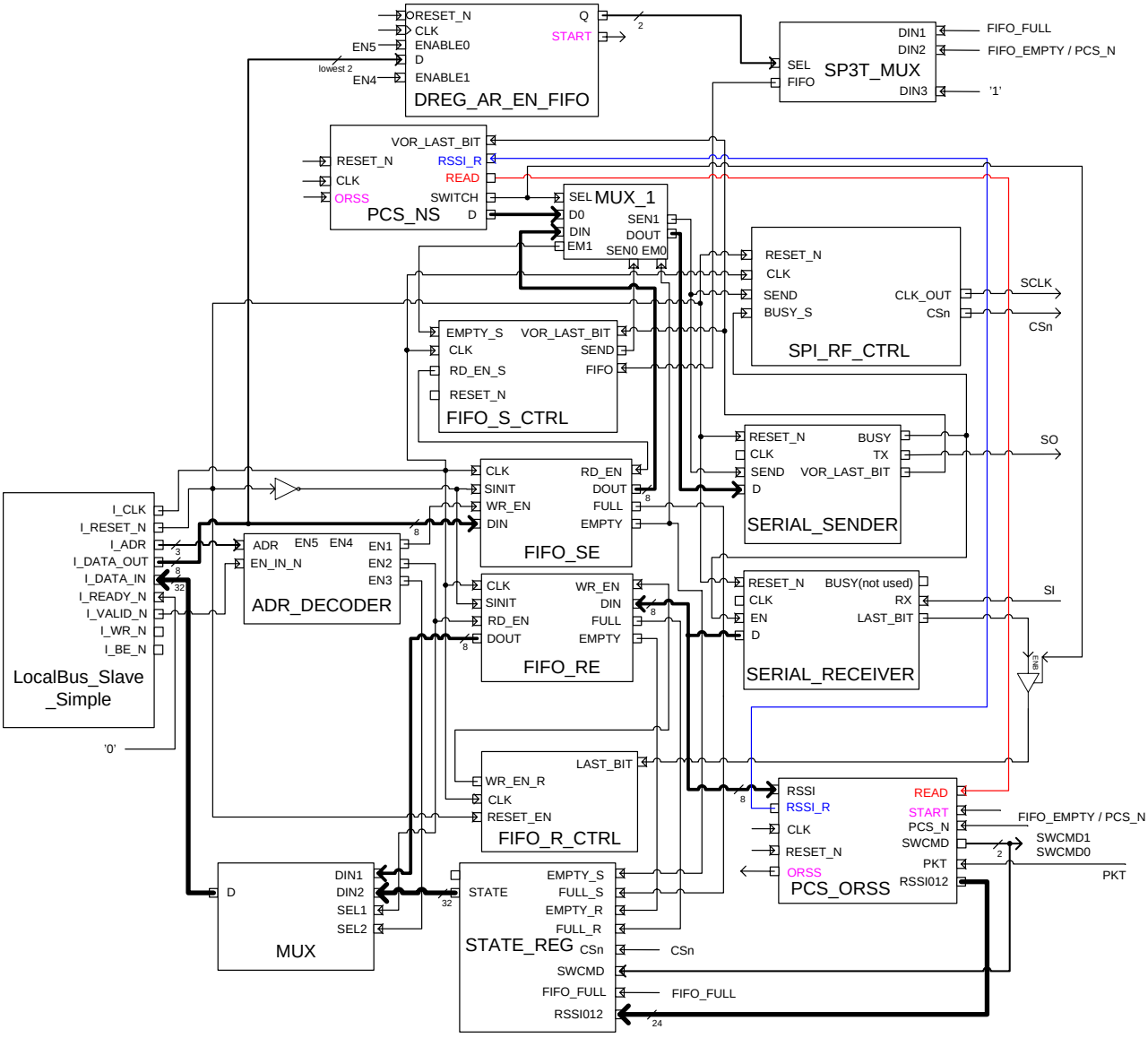

Figure A.2: Top-level schematic diagram of the SSB processing unit (SPU).

Table A.2: The SPU signal description (local-bus side is not included).

Signal name	Direction	Description
SCLK	Output	serial data clock generated by the SPU, 8.33 MHz is used in the SSB test-bed
CSn	Output	chip selection signal generated by the SPU
SO	Output	serial data output, connected to the SI pin of CC2400
SI	Input	serial data input, connected to the SO pin of CC2400
PCS_N / FIFO_EMPTY	Input	A general-purpose pin. It can be switched by configuring CC2400. PCS_N becomes active when CC2400 detects a carrier in the air; FIFO_EMPTY is a FIFO accessing control signal, which becomes active when FIFO is nearly empty, see [9].
PKT	Input	Synchronization word indicator signal generated by CC2400. It becomes active when CC2400 detects the complete Sync word.
FIFO_FULL	Input	CC2400 FIFO accessing control signal, becomes active if FIFO is nearly full (see [9] for detail)
SWCMD[1:0]	Output	switching command generated by the SPU to control the antenna array

A.3 State machine descriptions for each component of the SPU

A.3.1 Sub-modules of SPI master

A.3.1.1 FIFO_SE

FIFO_SE is an IP (Intellectual Property) core designed by using the Xilinx CORE Generator. It is a synchronous FIFO with 8-bit width and 256-Byte depth (capacity). The Synchronous FIFO is a First-In-First-Out memory queue with control logics that manage the read and write pointers (RD_EN and WR_EN) and generate the status flags (FULL and EMPTY). Details on synchronization FIFO can be found in Xilinx's website. In this design, FIFO_SE is used to buffer the data to be transferred to CC2400 via the SPI.

Table A.3: FIFO_S_CTRL signal description.

Signal name	Direction	Description
CLK	Input	synchronous clock
RESER_N	Input	reset signal, low active
EMPTY_S	Input	connects to the EMPTY pin of FIFO_SE to monitor its status
RD_EN_S	Output	connects to the RD_EN pin of FIFO_SE to control whether it is readable
SEND	Output	command to SERIAL_SENDER to enable the transmission of the next byte
FIFO	Input	module activation signal
VOR_LAST_BIT	Input	to be informed that the bit before the last bit of one byte is being sent on the SO line

A.3.1.2 FIFO_S_CTRL

FIFO_S_CTRL is the controlling module for FIFO_SE. Its basic function is to generate RD_EN for FIFO_SE, and generate SEND for SERIAL_SENDER and SPI_RF_CTRL to initiate the transmission process, once it detects FIFO_SE to be nonempty. In addition, it has the following two features:

- Feature 1: It supports the large packet transmission for CC2400. This will be further explained in Subsection A.3.2.
- Feature 2: Its activation can be controlled by the FIFO signal. From Fig. A.3 we can see that if FIFO keeps low, then this module always stays on the IDLE state. This feature is especially important for the large packet transmission support of the SPU, as will be described in Subsection A.3.2.

A.3.1.3 SERIAL_SENDER

The basic function of SERIAL_SENDER is to send the data from its D port (8-bit wide) to its TX port serially when the data is ready (obtaining the active SEND signal from FIFO_S_CTRL), and output BUSY and VOR_LAST_BIT during sending. Fig. A.4 and Fig. A.5 are the schematic diagram and state transition graph of SERIAL_SENDER, respectively. It can be found that this module is further made up of CONTROLLER, SHIFT_REG and COUNT_BITS. CONTROLLER controls SHIFT_REG to serially shift one bit of the data byte to the TX port, and controls COUNT_BITS to count the number of bits transmitted and generate the VOR_LAST_BIT and LAST_BIT signals accordingly.

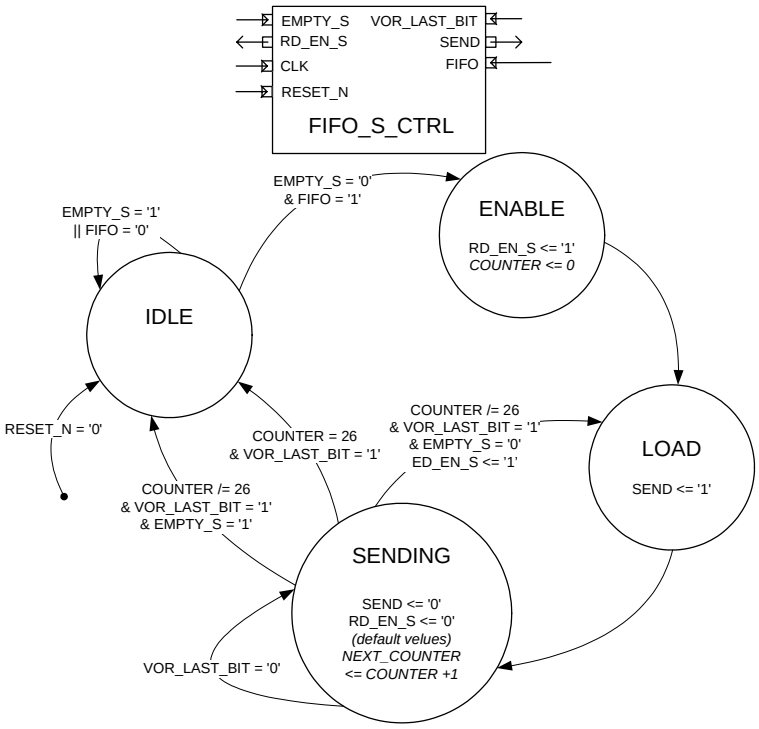

Figure A.3: State transition graph of FIFO_S_CTRL.

A.3.1.4 FIFO_RE

The same as FIFO_SE, FIFO_RE is an IP core designed by using the Xilinx CORE Generator. It is a synchronous FIFO with 8-bit width and 256-Byte depth (capacity). The difference is, FIFO_RE is used to buffer the data received by CC2400 via SPI.

A.3.1.5 FIFO_R_CTRL

FIFO_R_CTRL is the controlling module for FIFO_RE. Its function is much simpler than FIFO_S_CTRL. It is only used to detect the last bit of the received data byte. When this bit has arrived, then it generates the writing enable signal WR_EN for FIFO_RE, since the whole byte is ready on its input port DIN.

A.3.1.6 SERIAL_RECEIVER

The basic function of SERIAL_RECEIVER is to receive the data bit on its RX port serially and output them with the unit of byte. The first coming bit is the MSB. Fig. A.7 and Fig. A.8 are the schematic diagram and state transition graph of SERIAL_RECEIVER, respectively. It can be found that this module is further made up of CONTROLLER, SHIFT_REG and COUNT_BITS. CONTROLLER controls

Table A.4: SERIAL_SENDER signal description.

Signal name	Direction	Description
CLK	Input	synchronous clock
RESER_N	Input	reset signal, low active
SEND	Input	the next byte is ready on its D port, start to send
D[7:0]	Input	the data byte to be sent
TX	Output	serial output
BUSY	Output	to indicate that it is busy on sending
VOR_LAST_BIT	Output	to indicate that the bit before the last bit of one byte is being sent on its TX pin

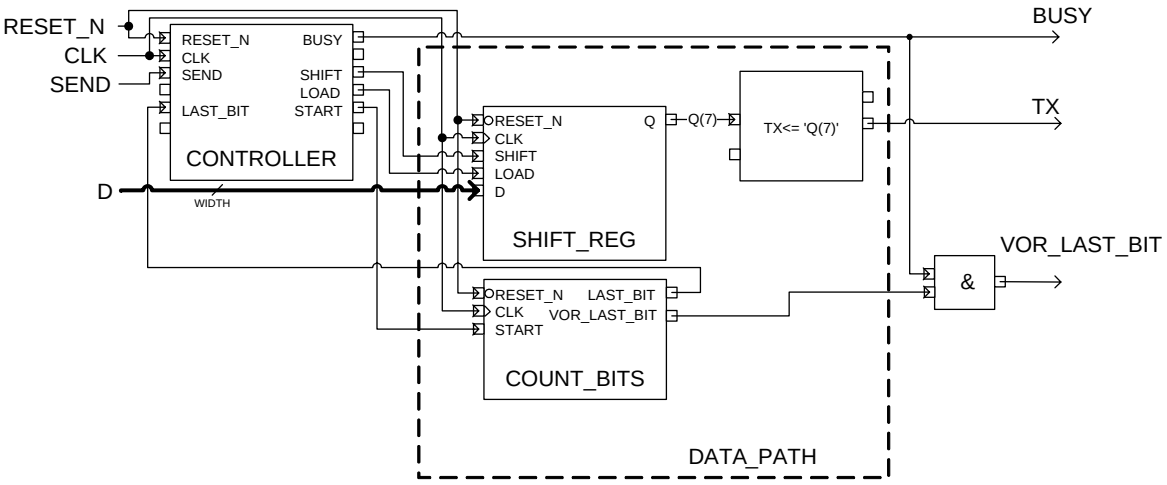

Figure A.4: Schematic diagram of SERIAL_SENDER.

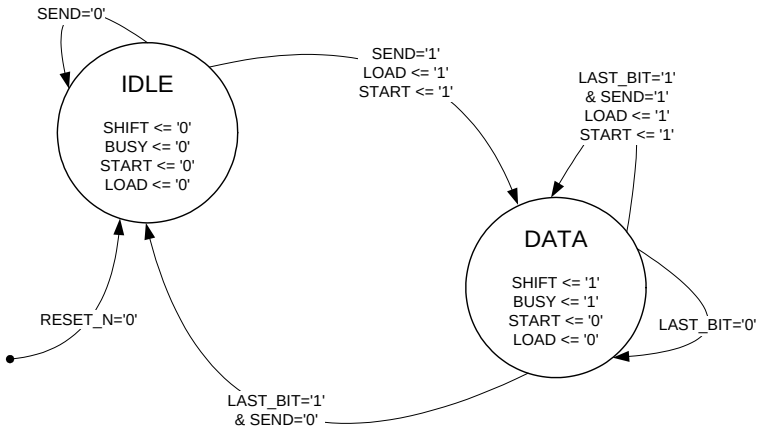

Figure A.5: State transition graph of SERIAL_SENDER.

Table A.5: FIFO_R_CTRL signal description.

Signal name	Direction	Description
CLK	Input	synchronous clock
RESER_N	Input	reset signal, low active
WR_EN_R	Output	write enable signal for FIFO_SE
LAST_BIT	Input	The last bit of the received data byte is arriving, which implies that one clock cycle later the received data byte will be ready on the input port DIN of FIFO_RE

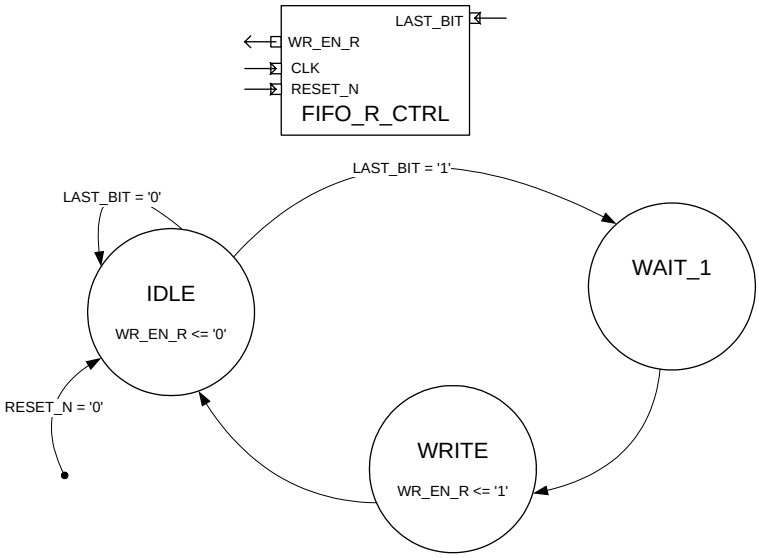

Figure A.6: State transition graph of FIFO_R_CTRL.

SHIFT_REG to serially shift one bit on the RX port to its internal 8-bit register, and controls COUNT_BITS to count the number of bits received and generate LAST_BIT accordingly. The LAST_BIT signal to FIFO_R_CTRL indicates that one received data byte is ready on the output port D[7:0] of SERIAL_RECEIVER, and this data byte will be kept until the next data byte comes.

A.3.1.7 SPI_RF_CTRL

SPI_RF_CTRL is responsible for generating the signals SCLK and CSn that comply with the SPI specification of CC2400. As described in section A.1, one accessing process via SPI is called one SPI cycle, which means the time when CSn is low. The designing principle of this module is very simple, as indicated by its state transition graph Fig. A.9. The CSn signal is kept high during IDLE, and SPI_RF_CTRL begins to output the low state CSn when it detects the active SEND signal from

Table A.6: SERIAL_RECEIVER signal description.

Signal name	Direction	Description
CLK	Input	synchronous clock
RESER_N	Input	reset signal, low active
EN	Input	Reception enable signal
D[7:0]	Output	the received data byte
RX	Input	serial input
BUSY	Output	to indicate that it is busy on receiving
LAST_BIT	Output	to indicate that the last bit of one byte is being received on its RX pin

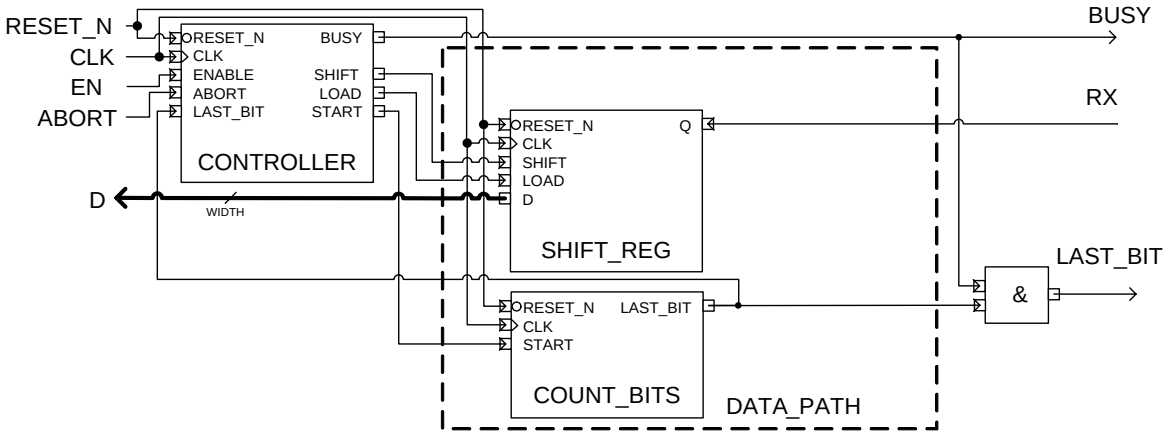

Figure A.7: Schematic diagram of SERIAL_RECEIVER.

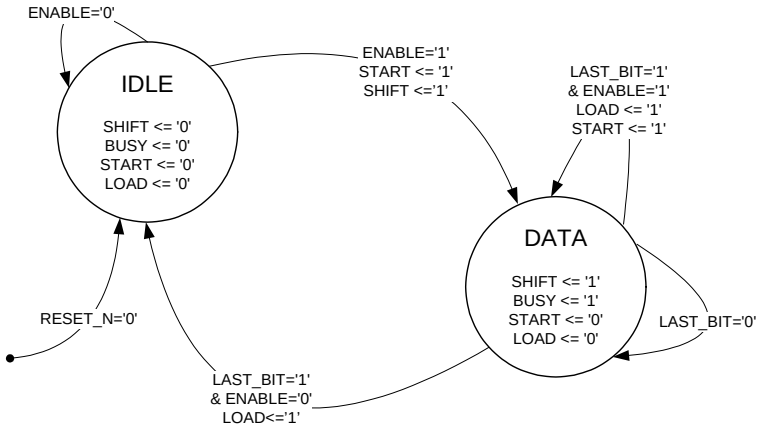

Figure A.8: State transition graph of SERIAL_RECEIVER.

FIFO_S_CTRL. The low state CSn is kept while the input signal BUSY_S is active, which implies that SERIAL_SENDER is sending bits serially. One SPI cycle finishes three clock cycles after the disappearance of the active BUSY_S signal. As for SCLK, it is a gated CLK signal, and the gate signal is exactly BUSY_S.

The idea behind the above simple design is **sending one bit, receiving one bit**. SCLK never stops during one SPI cycle, which lasts for the same duration of the working state (non-IDLE state) of SERIAL_SENDER. From Fig. A.1 and A.2 it can be found that:

- In case that the ULS needs to write the registers of CC2400 via the SPU, the data to be transmitted are first written to FIFO_SE and then transmitted serially on the SI line of CC2400. On the SO line of CC2400, after the first status byte CC2400 doesn't output any valid data. However, those invalid data are still received by SERIAL_RECEIVER and then saved in FIFO_RE due to the sending one bit, receiving one bit design principle. Therefore, those data must be discarded by the ULS. This additional task can be avoided by improving the SERIAL_SENDER module so that it is able to judge the purpose of the SPI cycle by detecting the first bit transmitted, 0 for writing and 1 for reading. If writing, then SERIAL_SENDER generates a dedicated EN signal for SERIAL_RECEIVER so that it only receives the first status byte. However, this improvement would increase the complexity of the SPU. That is, either the SPU or the ULS must perform this additional processing. In the test-bed this task is assigned to the ULS to make the FPGA design as simple as possible.

- In case that the ULS needs to read registers of CC2400 via the SPU, the R/W bit and the 7-bit address of the (first) register need to be first transmitted on the SI line of CC2400. From Fig. A.1 we can see that in this SPI cycle only the first data byte on the SI line of CC2400 makes sense. CC2400 would simply omit the data after the first byte. According to the sending one bit, receiving one bit design principle, the number of data bytes that written to FIFO_SE after the first data byte (R/W bit + 7-bit address) should be equal to the number of data bytes to be read out from CC2400 registers, say N, to let SPI_RF_CTRL generate the appropriate SCLK and CSn signals. Therefore, for each SPI reading cycle, the ULS must write $N + 1$ bytes of data to FIFO_SE, in which the last N bytes data are arbitrary. We can see that this design makes the complexity of the SPU low, while only a simple additional operation is added on the ULS.

- In case that the ULS needs to address the command strobe registers (CSR) of CC2400, only one data byte (arbitrary R/W bit + 7-bit address) needs to be transmitted. Therefore, this SPI cycle is very short, only covers one byte.

Table A.7: SPI_RF_CTRL signal description.

Signal name	Direction	Description
CLK	Input	synchronous clock
RESER_N	Input	reset signal, low active
SEND	Input	the SEND signal generated by FIFO_S_CTRL
BUSY_S	Input	SERIAL_SENDER is busy on sending data
CLK_OUT	Output	the clock signal that complies with the SPI specification of CC2400
CSn	Output	the chip selection signal that complies with the SPI specification of CC2400

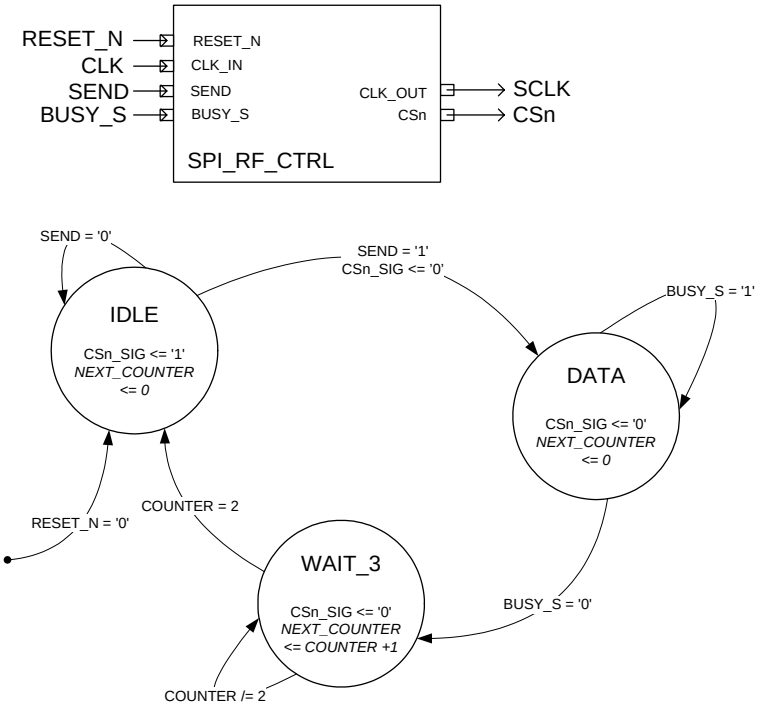

Figure A.9: State transition graph of SPI_RF_CTRL.

A.3.2 Large packet transfer support of SPI master

As mentioned in Section A.1, the FIFO of CC2400 has a limited capacity of 32 Bytes. If the packet to be transmitted exceeds this limitation, then the SPU must be able to control the data stream so that data are written to the FIFO of CC2400 while CC2400 is transmitting data. Similarly, if the packet to be received exceeds this limitation, then the SPU must be able to control the data stream so that data are read from the FIFO of CC2400 while CC2400 is receiving data. The basic principle is

to roughly make the average speeds of SPI transmission and over-the-air transmission equal. However, the former is much faster than the latter (8.33 Mb/s vs. 1 Mb/s). Therefore, the design idea is to temporarily halt the SPI transmission if the FIFO of CC2400 is nearly full/empty (the stop condition), and restart it if the FIFO of CC2400 is nearly empty/full (the restart condition). Two auxiliary general-purpose I/O ports of CC2400, FIFO_FULL and FIFO_EMPTY, make the above operation possible. They are affected by FIFO_THRESHOLD, which can be set by writing the INT register of CC2400. In both RX and TX modes of CC2400, FIFO_FULL becomes active (high) if the number of bytes in the FIFO is equal to or greater than FIFO_THRESHOLD, otherwise keeps low. In TX mode of CC2400, FIFO_EMPTY becomes active (high) if the number of bytes in the FIFO is equal to or less than 32 - FIFO_THRESHOLD, otherwise keeps low. In RX mode, the actual threshold becomes 1 for FIFO_EMPTY, but not 32 - FIFO_THRESHOLD.

According to the SPI timing specification of CC2400, see Fig. A.1, there are two possible solutions to support the large packet transmission/reception :

- Solution 1: Treat the large packet as a whole unit, and transfer this packet over SPI in one SPI cycle. CSn always keeps low within one SPI cycle as usual, however, the transfer can be halted if the stop condition is met by stopping SCLK, and be continued if the restart condition is met by restarting SCLK.

- Solution 2: Select a proper value for FIFO_THRESHOLD, e.g., 25 in this test-bed design, and use this value as the unit capacity. Split the large packet to be transferred according to this basic unit, and transfer each unit with one SPI cycle (during which SCLK doesn't stop). The next unit transfer is executed only if the restart condition is met, e.g., FIFO_EMPTY becomes active in TX mode or FIFO_FULL becomes active in RX mode.

Solution 1 has the advantage that the length of the packet can be arbitrary, while solution 2 requires that the length of the packet is the multiple of the preset threshold FIFO_THRESHOLD. However, solution 2 is more advantageous with respect to the design complexity since solution 1 requires a complex gating control logic for the SCLK signal. For example, in TX mode SPI_RF_CTRL must stop SCLK when FIFO_FULL appears active and restart SCLK when FIFO_EMPTY appears active; however, in RX mode SPI_RF_CTRL must stop SCLK when FIFO_EMPTY becomes active and restart SCLK when FIFO_FULL becomes active. Furthermore, SPI_RF_CTRL should be able to judge the purpose of the current SPI cycle by detecting the first bit (R/W bit) transmitted on the SI line of CC2400. What makes solution 1 more difficult is, SERIAL_SENDER and SERIAL_RECEIVER, two sub-modules of the SPU, must use the gated clock SCLK because they must be synchronous with

the SPI bus. Other than the high complexity, such a design is undesired and should be avoided as much as possible for the FPGA application, because it makes different parts of the FPGA use different sources of clock, and the clock is self-gated, which causes delays.

Taking the above consideration into account, I made up my mind to apply solution 2. In comparison with the the SPU design without the large packet support, solution 2 only slightly increases the complexity of the module FIFO_S_CTRL to enable the large packet support of the SPU, no modifications on other sub-modules are required. From Fig. A.3 we can see that after letting SERIAL_SENDER send 25 Bytes of data, FIFO_S_CTRL transits back to the IDLE sate in despite of the EMPTY signal of FIFO_SE. FIFO_S_CTRL transits again into the ENABLE state only if FIFO_SE is not empty and its FIFO pin becomes active. From the top-level schematic diagram Fig. A.2 we can see that the FIFO signal can be switched among FIFO_FULL, FIFO_EMPTY and '1', which is controlled by the ULS. In TX mode it is switched to FIFO_EMPTY, in RX mode switched to FIFO_FULL. When the ULS needs to access the configuration registers (CS) or address the command strobe registers (CSR) of CC2400, then FIFO can be switched to '1'. The disadvantage of solution 2, restricting the length of the packet to be the multiple of FIFO_THRESHOLD, is not a problem for modern digital communication protocols. In the test-bed the threshold is set to 25, which is the reason why a data packet has the 225 Bytes length in the experiments described in Section 5.4.

It should be noticed that except sending a command to control the FIFO pin of FIFO_S_CTRL, the ULS doesn't make any other additional operation for the large packet transfer support through the SPI. All the relevant operations are automatically made by the SPU. The ULS only needs to write the whole packet to the address of FIFO_SE in TX mode, and read the whole packet from the address of FIFO_RE when it detects the end of the reception (see Subsection A.3.4 for this function) in RX mode.

A.3.3 Sub-modules of SSB controller

In Tab. A.1 we can see that SSB Controller consists of PCS_NS, MUX_1 and PCS_ORSS, in which the first two modules supply some auxiliary supports for the interference suppression (IS) function. They can be combined as IS_AUX. PCS_ORSS realizes directional PCS (physical carrier sense), ORSS (optimal reception sector selection) and IS functions.

A.3.3.1 IS_AUS

IS_AUS supplies some auxiliary supports for the IS function of PCS_ORSS. To explain its function more clearly, we must retrospect the basic principle of sending one bit, receiving one bit described in Subsection A.3.1.7. To read data from CC2400 via the SPU, the ULS needs to send the same number of bytes to FIFO_SE. In RX mode, for each data packet reception the ULS requires to first read three RSSI values of three sectors and then read the whole packet. Since the number of bytes to be read is known for the ULS in advance, this reading process can be carried out without any problem. However, the above RX operation can only occur in the interference free environment, because in the environment with interference the ORSS process will be incorrectly initiated by interference. As will be described in Subsection A.3.3.2, due to the IS function of the PCS_ORSS module, PCS and ORSS will be repeated until it is determined that ORSS has been performed on the intended user signal. In this case, the ULS is not aware of how many times it requires to read the RSSI register of CC2400. IS_AUX is able to solve this problem.

From the top-level schematic diagram of the SPU (Fig. A.2), we can see that IS_AUS seems like a relay station between FIFO_S_CTRL, FIFO_SE, SPI_RF_CTRL and SERIAL_SENDER. It relays SEND from FIFO_S_CTRL to SERIAL_SENDER and SPI_RF_CTRL, the signal EMPTY from FIFO_SE to FIFO_S_CTRL and the data bus D[7:0] from FIFO_SE to SERIAL_SENDER. From its state transition graph Fig. A.10 we can see that its state can be clearly separated into two phases:

- **IDLE** When its input pin ORSS is low, then IS_AUX always stays on the IDLE state. In this duration it acts as an actual relay for the signals of SEND, EMPTY and D[7:0] so that the whole system operates like in the case that IS_AUX doesn't exist. In this duration the ULS can access all kinds of registers of CC2400 as usual, and all the received data can be written to FIFO_RE due to the enable signal SWITCH (high active).

- **ACTIVE** A high ORSS signal implies that PCS_ORSS is operating the PCS or ORSS process, and IS_AUS transits into the active phase correspondingly to provide its auxiliary supports. It first enters into the IDLE_1 state, during which it outputs the low SWITCH signal and switches the signals SEND, EMPTY and D[7:0] to their internally-set values. Those signals keep constant until IS_AUX transits back to the IDLE state. They are set as follows: the EMPTY signal (from FIFO_SE) is set to high to disable FIFO_S_CTRL, D[7:0] are set to be the RSSI register address of CC2400 (plus '1' as MSB for the reading purpose) and the SEND signal is generated by IS_AUX in such a way that it emulates the function of FIFO_S_CTRL. A low SWITCH signal is to disable the output LAST_BIT of SERIAL_RECEIVER so that FIFO_R_CTRL

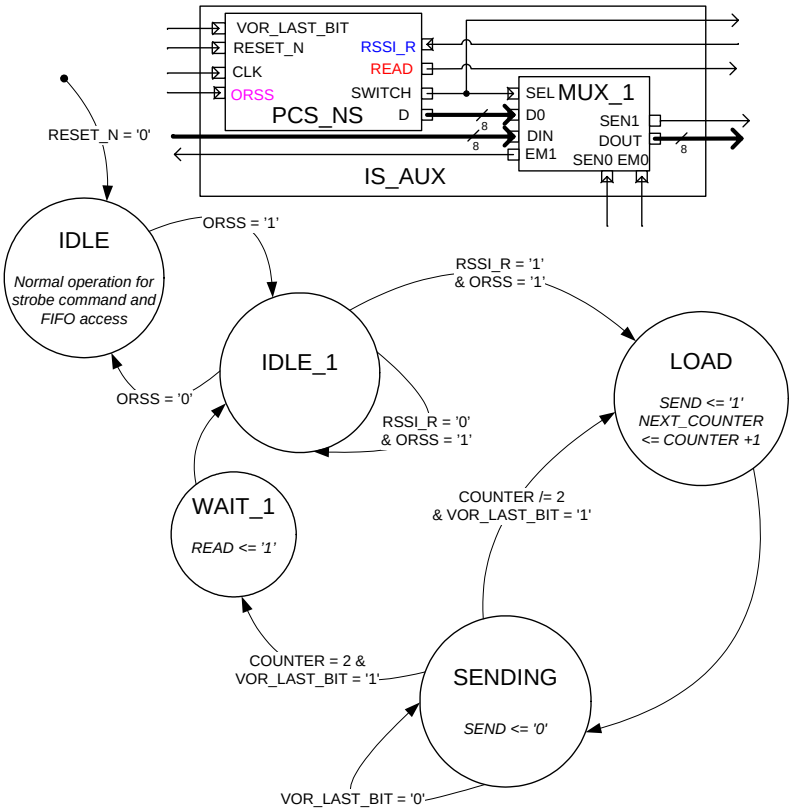

Figure A.10: Block diagram and state transition graph of IS_AUX.

will not allow FIFO_RE to read values on its DIN port (since they are RSSI values to be recorded by PCS_ORSS). After that, if IS_AUX gets the active RSSI_R signal, which implies that PCS_ORSS requires to read the RSSI register of CC2400, then it begins to emulate the function of FIFO_S_CTRL to let SERIAL_SENDER to send the internally-set D[7:0] continuously for two times. After the transmission is finished, IS_AUX outputs an active READ signal to inform PCS_ORSS that a RSSI value is ready on its RSSI port. IS_AUX repeats the above operation until it detects a low ORSS signal during the IDLE_1 state, which implies that PCS_ORSS has finished the ORSS operation and the SPU enters into the RX state, see Fig. 5.10 in Subsection 5.3.2.

The idea of IS_AUX is to replace the functions of FIFO_SE and FIFO_S_CTRL and disable FIFO_RE in the active duration (non-IDLE states, see Fig. A.11) of PCS_ORSS, so that the SPU is able to read the RSSI register of CC2400 with an uncertain number of times. This number is not necessary for the ULS to be aware in advance. Due to this auxiliary but crucial function, the PCS_ORSS module can repeat the PCS and ORSS operations with unlimited times when it determines that the last ORSS process is performed on an interference signal.

Table A.8: IS_AUX signal description.

Signal name	Direction	Description
CLK	Input	synchronous clock
RESER_N	Input	reset signal, low active
DIN[7:0]	Input	connect to DOUT of FIFO_SE
DOUT[7:0]	Output	connect to D of SERIAL_SENDER
SEN0	Input	connect to SEND of FIFO_S_CTRL
SEN1	Output	connect to SEND of SERIAL_SENDER and SPI_RF_CTRL
EM0	Input	connect to EMPTY of FIFO_SE
EM1	Output	connect to EMPTY_S of FIFO_S_CTRL
ORSS	Input	if active, implies that PCS_ORSS is not on the IDLE state
READ	Output	inform PCS_ORSS that an 8-bit RSSI value is ready on its RSSI port
SWITCH	Output	enable signal for the LAST_BIT entering into FIFO_R_CTRL

A.3.3.2 PCS_ORSS

Three functions have been realized by the PCS_ORSS module: PCS (physical carrier sense), ORSS (optimal reception sector selection) and IS (interference suppression), which correspond to the functions of the **PCS** and **ORSS** states illustrated in Figs. 5.10 and 5.11 of Subsection 5.3.2. However, Figs. 5.10 and 5.11 only give the basic operation principle, which is significantly different from the implementation details illustrated in Fig. A.11, because the module is designed with a more resource-efficient way. Fig. A.11 illustrates the state transition graph of PCS_ORSS, which seems somewhat complex. However, its operation route will be very clear with the following explanation. It mainly consists of four phases:

- **Initiation** The operation of PCS_ORSS is initiated by an impulse of START, which is a command sent by the upper level software (ULS) through the SSB processing unit (SPU), see Fig. A.2. The SPU allocates a dedicated address for generating the START signal (see Tab. A.10). After PCS_ORSS is initiated, it automatically operates PCS, ORSS and IS until an ORSS process on the intended user signal is finished, and then it transits back to the IDLE state. PCS_ORSS outputs a low ORSS signal during the IDLE state, otherwise it outputs a high ORSS signal.

- **PCS circle**: WAIT_30us —>SWCMD_1 —>WAIT_30us. After the initiation, PCS_ORSS first transits to the WAIT_30us state to wait for 30 μs and monitor PCS_N in the meanwhile. If PCS FLAG (this will be further explained

later) and an inactive PCS_N is detected at the end of the WAIT_30us state, it transits to SWCMD_1. In SWCMD_1 the switching command SWCMD[1:0] is updated and then it transits back to WAIT_30us. Above is the PCS circle, which will be repeated again and again until one of the following two conditions occurs.

Condition 1: if PCS FLAG and an active PCS_N is detected **during** the WAIT_30us state. This condition implies that a carrier is detected by CC2400, then PCS_ORSS transits to CHECK_30us immediately; condition 2: if ORSS FLAG, then PCS_ORSS transits to RSSI_READ at the end of WAIT_30us regardless of PCS_N. A FLAG is used to distinguish between the PCS circle and the ORSS circle. In the PCS circle PCS_N is used to decide its transition destination (SWCMD_1 or CHECK_30us), and in the ORSS circle there is only one transition destination (RSSI_READ).

- **ORSS circle**: WAIT_30us —>CHECK_30us —>RSSI_READ —>WAIT_3 —>WRITE_REG —>SWCMD_1 —>WAIT_30us —> RSSI_READ. In the PCS circle, if an active PCS_N is detected during WAIT_30us, then PCS_ORSS begins its ORSS circle by transiting to CHECK_30us, during which PCS_N is continuously monitored for 30 μs. Once PCS_N is detected to be inactive, then it immediately goes back to the PCS circle by transiting from CHECK_30us to SWCMD_1. Two conditions cause this refluence: an active PCS_N caused by an interference is shorter than 30 μs for the current antenna pair or a glitch on the PCS_N pin. The refluence due to the former reason is a part of the IS operation.

  If PCS_N keeps low until the end of CHECK_30us, then PCS_ORSS transits to the state RSSI_READ, which implies that it formally enters into the ORSS circle, and PCS FLAG will be updated to ORSS FLAG in this case. During the ORSS circle, the RSSI register of CC2400 will be read for three times (corresponding to three sectors) with a 30 μs interval. Unlike the PCS circle, the duration of the ORSS circle is fixed (only going through for three rounds). The first round begins on the transition from CHECK_30us to RSSI_READ. In the state of RSSI_READ, PCS_ORSS outputs an active RSSI_R signal to IS_AUX and waits for an active READ signal from IS_AUX (see Subsection A.3.3.1 the ACTIVE phase of IS_AUX). The active READ signal makes it transit to the WAIT_3 state to wait for 3 clock cycles and then it transits to WRITE_REG, during which the data on RSSI[7:0] are recorded into a register relevant to the current switching command SWCMD[1:0]. And then PCS_ORSS updates its SMCMD[1:0] in SWCMD_1 and transits back to WAIT_30us. After 30 μs it directly transits to RSSI_READ for the second round due to ORSS FLAG, regardless of PCS_N. This is because the carrier may not be sensed for the present

antenna pair (corresponding to the updated SWCMD[1:0]). After reading the third RSSI value, PCS_ORSS transits from WRITE_REG to DEC_SWC to determine the optimal reception sector (ORS) and output the corresponding SWCMD[1:0]. Until now, ORSS_PCS finishes its ORSS circle and jumps into its IS (interference suppression) phase.

- **IS phase** As mentioned in Subsections 4.3.5 and 5.3.2.6, interferences may cause a serious disturbance on the correct determination of ORS. If the ORSS process is performed on the interference signal but not the intended user signal, then the determined ORS is incorrect (not for the user signal), which would result in even worse performances than the single antenna system. PCS_ORSS applies the PKT signal generated by CC2400, which is a synchronization indicator signal appearing after the correct detection of the whole synchronization word, to realize its IS function. PKT is usually used as an interrupt to read the received data, and here it is additionally used to distinguish between the interference and the intended user signals, because the synchronization word cannot be detected for interference, and therefore an active PKT would not appear.

  After the DEC_SWC state, PCS_ORSS transits to the NS state, during which PCS_N is continuously monitored and an active PKT is waited. Only in the condition that PCS_N keeps low and an active PKT appears within 192 μs can PCS_ORSS transit back to the IDLE state (and the SPU transits to the RX state in Fig. 5.10). Otherwise, PCS_ORSS determines that the last ORSS process is performed on an interference signal and the resulting ORS is incorrect, and it goes back to the PCS circle by entering into WAIT_30us from NS and resetting ORSS FLAG to PCS FLAG. The above operation is based on either an inactive PCS_N or the no-show of an active PKT within 192 μs. If the detected carrier is the intended user signal, then the former case would not occur at that moment. And the latter case must occur for an interference signal because a complete synchronization world cannot be detected by CC2400 due to interference.

  One weakness of this IS design is that it must use relatively long time (at most 192 μs) to wait for the active PKT signal after the ORSS process, during which the selected antenna pair is fixed. Considering the length, 192 μs account for the majority of the preamble of the packet signal (please refer to Fig. 5.15 in Subsection 5.3.2.6). In case that the last ORSS process was initiated by an interference signal and the user signal appears at the early phase of the 192 μs waiting duration, then the majority of the preamble has passed at the time when PCS_ORSS judges that the last ORSS was performed on interference. Furthermore, if the determined ORS for interference is not suitable for the intended user signal (marked as condition 1), then the packet may be incorrectly received or completely lost by CC2400, because a correct reception requires the correct

detection on the usual preamble and the synchronization word even for a single antenna receiver (refer to [9]). In opposite to condition 1, another condition is that the determined ORS for interference is also suitable for the user signal, then the usual preamble and the synchronization word will be correctly detected by CC2400 and an active PKT will appear but outside the 192 μs waiting duration. In this condition (marked as condition 2), PCS_ORSS would transit from NS to WAIT_30us to repeat PCS and ORSS since it judges that the last ORSS is on interference. However, CC2400 is receiving the packet in this case and the SPU doesn't transit into the RX state synchronously, which would result in a failing reception. Condition 2 can be relieved by the following counter-measure (which is not illustrated in Fig. A.11): during each state of the PCS or ORSS circle, the PKT signal is also checked. If an active PKT is detected, then PCS_ORSS keeps the present switching command and immediately transits to the IDLE state to let the SPU transit to the RX state, refer to Fig. 5.10 of Subsection 5.3.2. The above condition 1 is the worst case that can only be solved by using the optimal LQI-based scheme described in Subsection 4.3.5. There are some other less serious conditions (in comparison with condition 1) that may cause problems. Fortunately, they and condition 1 occur very occasionally and therefore don't degrade the the performance of the test-bed obviously.

In an interference-free environment, PCS_ORSS functions perfectly without any error. In an environment with interference, PCS_ORSS functions correctly in most cases. This has been verified by the real system measurements described in Section 5.4. However, as we have mentioned in Subsections 4.3.5 and 5.3.2.6, the used IS technique is a suboptimal solution. The optimal LQI-based scheme is not feasible for CC2400. During the measurements in the environment with interference, the following abnormal case occurs occasionally: at the end of one measurement run the upper-layer software (ULS) reports errors on some packets, however the final bit error rate (BER) is reported as 0%. Packet error is determined by checking the CRC, and BER is calculated by counting the number of wrong bits and dividing it to the number of bits of the entire user data. This contradiction can be explained as follows: the 225 bytes **Data** field of each packet (see Fig. 5.12) consists of two parts, the physical header and the user data. Both of them will be used to generate the CRC code, however, only the user data are used to calculate the BER. By checking the wrong packets reported, I found that all errors occurred in their physical headers. The physical head consists of a 2-Byte packet sequence and a 1-Byte length indicator, which are generated by the associated SmartRF software of the CC2400 development kit. The reception errors on the physical header can probably be attributed to the counter-measure against the condition 2 described above. Those errors can be ignored because an additional 3-Byte physical header can be reserved as a margin.

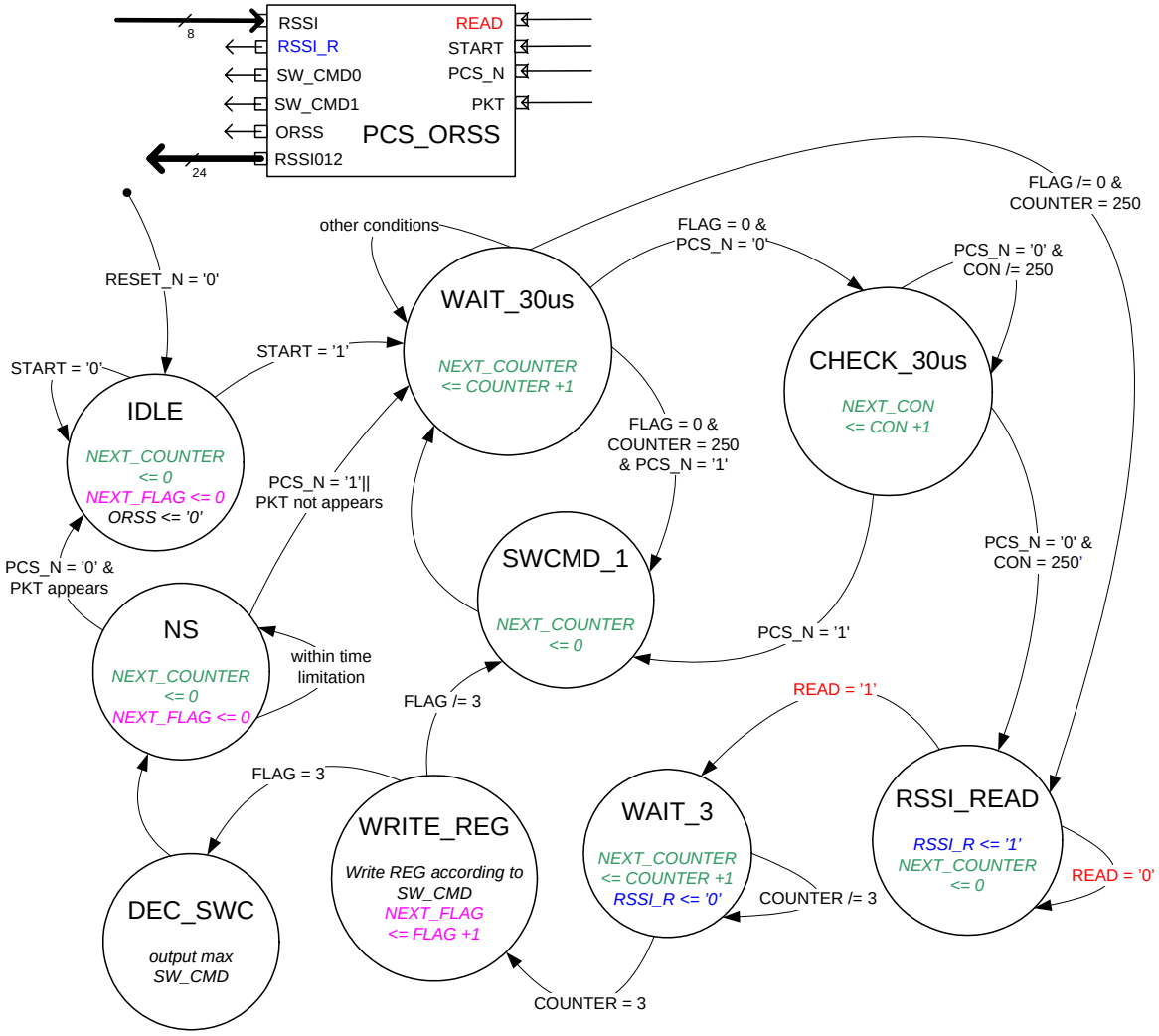

Figure A.11: Block diagram and state transition graph of PCS_ORSS.

A.3.4 Other auxiliary modules of the SPU

In Tab. A.1, the modules MUX, STATE_REG, ADR_DECODER, SP3T_MUX and DREG_AR_EN_FIFO are listed as the sub-modules of SPI Master. However, their functions are not limited to SPI Master, actually they act as auxiliary modules for the whole SPU module.

- Tab. A.10 describes the address allocation of the SPU, which is realized by the module ADR_DECODER. The addresses are not continuous because the least significant two bits of I_ADR of LocalBus_Slave_Simple (see Fig. A.2) are not used.
- DREG_AR_EN_FIFO provides two functions: to generate an impulse on its START pin, and to transfer data to SP3T_MUX to control its output pin FIFO.

Table A.9: PCS_ORSS signal description.

Signal name	Direction	Description
CLK	Input	synchronous clock
RESET_N	Input	reset signal, low active
START	Input	this signal is generated by the ULS, the whole process is initiated by this signal
PCS_N	Input	PCS_N signal generated by CC2400
SWCMD[1:0]	Output	switching command to control the antenna array
PKT	Input	PKT signal generated by CC2400, indicates that a Synchronization word is detected
RSSI012[23:0]	Output	three 8-bit RSSI values for three sectors of the antenna array, to be recorded by the register of STATE_REG
RSSI[7:0]	Input	an 8-bit RSSI value to be read
ORSS	Output	informs IS_AUX that it is not in the IDLE state
RSSI_R	Output	inform IS_AUX to read the RSSI register of CC2400
READ	Input	be informed by IS_AUX that an 8-bit RSSI value is ready on its RSSI port

The START signal to PCS_NS should usually keep low. Only in case that the ULS requires to initiate the PCS process (after sending the RX command to CC2400), it first writes to the address 0x0C with '1' and then with '0' to generate an impulse on START (refer to the initiation phase described in Subsection A.3.3.2 and Fig. A.11). The duration of this impulse can be variable, depending on the executing condition of the ULS, and a wide range from one to a couple of clock cycles is acceptable for PCS_ORSS.

If the address 0x10 is used by the ULS to write data, then the least significant two bits of data will be sent to the SEL[1:0] port of SP3T_MUX to select its output FIFO. As for how the ULS controls the pin FIFO, please refer to Subsection A.3.2 and Fig. A.2.

- MUX is a multiplexer between the output DOUT[7:0] of FIFO_RE and the output STATE[31:0] of STATE_REG. The most significant 24 bits (D[31:8] of MUX) are always connected to STATE[31:8], see Fig. A.2. The data on the least significant 8 bits are distinguished by different addresses, see Tab. A.10.

- STATE_REG is used to record the important states of the SPU. Its signal description is given in Tab. A.11. Some status values recorded by this module are very important to the test-bed, e.g., EMPTY_S is used by the ULS to judge whether CC2400 has been configured, received the command, or finished

Table A.10: Address allocation of the SPU.

Address	Function	Description
0x00	write to FIFO	this address is used to write data to FIFO_SE
0x04	reading from FIFO	this address is used to read data from FIFO_RE
0x08	reading STATE_REG	this address is used to read data from STATE_REG
0x0C	setting START	an impulse on START pin of PCS_ORSS can be generated by writing proper values to this address for two times
0x10	setting FIFO of FIFO_S_CTRL	the FIFO pin of FIFO_S_CTRL can be set by writing a proper data to this address to control SP3T_MUX

its RX operation (because of the sending one bit, receiving one bit principle, see Subsection A.3.1.7), and SWCMD[1:0] of the ORS and RSSI012[23:0] are used for the post-processing in the ULS.

A.4 Experiences learned from the implementation

The author of [54] has spent a majority of effort to implement each individual block of a wireless communication system, including the RF front-end and the baseband processing unit, to demonstrate their switched beam antenna system. Thanks to the high integration of CC2400 and the powerful functionality of its development kit, it is not necessary for me to build those individual blocks. Therefore, a lot of effort and time have been saved and I am able to concentrate on designing and implementing the antenna array and the array signal processing unit of the test-bed. Furthermore, thanks to the RAPTOR2000 system, a FPGA rapid prototyping system designed and implemented by the research group that I am working, the time-critical tasks of the array signal processing can be successfully realized.

Although owning the above two advantages, I still have encountered many problems during the practice of implementation. Here I only give some typical experiences learned in this course.

Table A.11: STATE_REG signal description.

Signal name	Direction	Description
EMPTY_S	Input	to record the status of FIFO_SE, whether it is empty
FULL_S	Input	to record the status of FIFO_SE, whether it is full
EMPTY_R	Input	to record the status of FIFO_RE, whether it is empty
FULL_R	Input	to record the status of FIFO_RE, whether it is full
CSn	Input	to record the current status of CSn (the output of the SPU)
SWCMD[1:0]	Input	to record the current switching command (the output of the SPU)
FIFO_FULL	Input	to record the status of the CC2400 FIFO, whether it is nearly full
RSSI012[23:0]	Input	to record the three RSSI values recorded in PCS_ORSS. They will be read by the ULS once for each RX process.
STATE[31:0]	Output	the most significant 24 bits are allocated to RSSI012[23:0], and the remaining 8 bits are allocated to the other input signals listed above.

A.4.1 The array signal processing must be performed using the hardware-based solution

As described in Subsection 5.3.2.3, the array signal processing, mainly consisting of PCS, ORSS and IS, is a time-critical task. That is the reason why all of them have been implemented on the FPGA. At the beginning of implementation, I have tried to implement the PCS and ORSS functions on the host computer using the software-based solution. This attempt failed because the host computer is not able to instantly respond to the changing of PCS_N. The trial system is designed as follows.

We first assume that there is no interference in the air. The output PCS_N of CC2400 is connected to one pin of STATE_REG (refer to Fig. A.2), and the ULS detects the state of PCS_N by reading on the address of STATE_REG. The algorithm can be itemized as the following steps:

1. The ULS sends the RX command, and then outputs SWCMD0;

2. The ULS sends 32 Bytes arbitrary data (e.g., to read registers of CC2400 continuously) to generate a 30 μs interval, since the SPU applies the principle of sending one bit, receiving one bit (see Subsection A.3.1.7). By monitoring the

status of FIFO_SE of the SPU (EMPTY_S), an accurate interval can be generated. The possible inaccuracy may be caused by the non-instant detection on EMPTY_S by the ULS.

3. The ULS read STATE_REG to check PCS_N, if inactive then updates SWCMD and jumps back to step 2; otherwise it jumps to step 4.
4. The ULS generates a 30 μs interval (with the same principle of step 2), then reads the RSSI register of CC2400;
5. The ULS repeats the operation of step 4 for two times;
6. The ULS determines the ORS and sends the corresponding SWCMD;
7. The ULS writes data to FIFO_SE to let the SPU read data from the FIFO of CC2400 (because of the principle sending one bit, receiving one bit);
8. The ULS monitors the status of FIFO_SE of the SPU. If it is empty, this implies that the whole packet has been read from CC2400 and written to FIFO_RE of the SPU, then the ULS jumps to step 9; if this status doesn't appear in the expected time, this implies that something is abnormal (the packet is lost). Then the ULS will halt here and keep on waiting. A time-out function should be associated to avoid the halt of the whole system and let the SPU anyway jump to step 10.
9. The ULS reads data from FIFO_RE of the SPU;
10. CC2400 transits to the FSON state, no matter whether the packet has been successfully received or not. The ULS is aware of his condition due to its operation in step 8.
11. IF the ULS needs to perform the next RX process, it jumps to step 1; otherwise, the ULS sends the SRFOFF command to let CC2400 be idle.

Experiments showed that even in the interference-free environment a lot of packet losses occurred, and the time-out function in step 8 has been called very frequently. By an intensive analysis, I found that the above problem may be attributed to the executing style of the ULS on the host computer, which is a Linux-based PC. The operating system's multi-course property makes it inappropriate for the time-critical tasks like PCS and ORSS. For example, the host computer can be interrupted to execute other operations after finishing step 3 of the ULS, which makes the interval between step 3 and step 4 too long so that the actual duration of ORSS exceeds the length of the reserved 28 Bytes preamble.

Due to the above reason, the entire array signal processing, including the PCS, ORSS and IS operations, must be realized by the SPU.

A.4.2 Two VHDL design tips

If I knew the following two VHDL design tips in advance, lots of effort and time can be saved. Later, I also found the similar descriptions in some FPGA or ASIC design books, like [28].

1. Avoid gating the clock and using the different clock sources on the same FPGA chip. The solution 1 described in Subsection A.3.2 requires to use multiple clock sources, and one of them is the self-gated clock. The use of multiple clock sources complicates the synthesis and makes the system metastable, and the clock gating causes an additional delay and possibly makes the synchronous components to be asynchronous. Therefore, this kind of design should be avoided. In case that such a design is definitely required due to the reason like realizing some special system functionality or the resource-efficient purpose, special cares must be taken for the signals crossing the clock boundaries. The guidelines to solve this problem have been given in [28], which are beyond the scope of this thesis.

2. Avoid triggering different modules with different clock edges. Similarly, this kind of design complicates the synthesis and makes the system metastable. The designer should try best to uniform the triggering edge for the whole design. If different triggering edges are really necessary, they can be only used on the boundary Flip-Flops that act as the interface to the external circuits.

A.5 Measured timing diagrams on I/Os between CC2400 and SPU

In this section some measured timing diagrams on CC2400's I/O pins will be illustrated. The 4-channel high speed (2 GSa/s) oscilloscope HP 54542C is used for the measurements. Its function to directly transfer the figure to computer ensures high resolution and creditability on the measured diagrams.

First it is necessary to make a brief introduction on the CC2400DK (development kit), which consists of two CC2400EB (mother evaluation boards), two CC2400EM (daughter evaluation modules) and an associated SmartRF studio software. The CC2400 chip is mounted on CC2400EM, which should be plugged on CC2400EB. There are two test ports on each CC2400EB. In the operating mode 2, each time after CC2400DK loads the firmware, the test port 1 can completely emulate the I/O ports of the chip CC2400 and is used to communicate with the SSB processing unit (SPU) in the test-bed, and the test port 2 is able to duplicate the signals on the test port 1 (via FPGA) for the

measuring purpose. For details refer to Subsection 5.2.5 and [9]. All signals illustrated in this section are measured on the test port 2.

Fig. A.12 illustrates the overall communication behavior between CC2400 and the SPU, including the waveforms of the physical carrier sense signal PCS_N, the synchronization word indicator signal PKT, the chip selection signal CSn and the CC2400 FIFO status signal FIFO_FULL. As shown in the figure, all four signals must become active for each RX process, which occurs with an approximate period of 50 ms. This is coincident with the packet transmission rate 20 packets/second of the TX station (refer to Subsection 5.3.2.3).

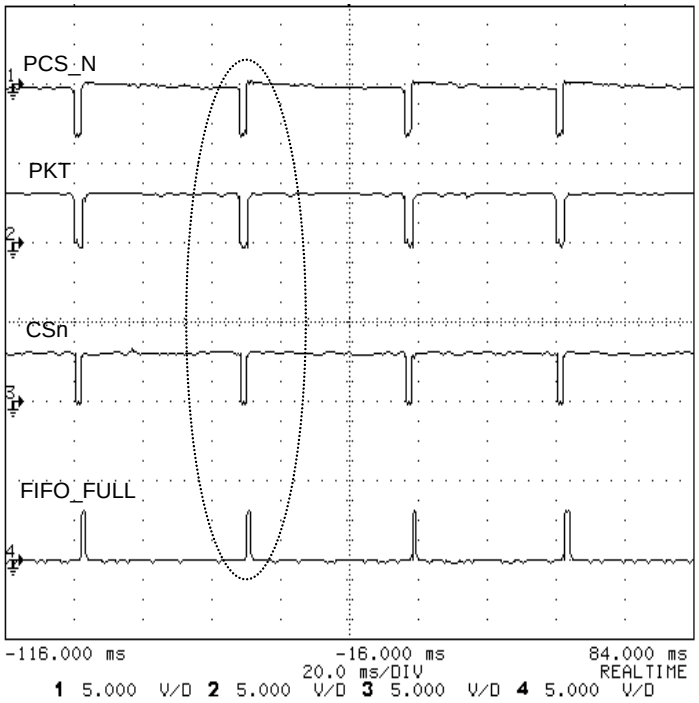

Figure A.12: The overall communication behavior between CC2400 and the SPU.

Fig. A.13 is obtained by zooming in the part enclosed in the dashed ellipse of Fig. A.12. From it we can observe that for each RX process the PCS_N signal becomes active for around 2.1 ms, which is very near to the value 2.088 ms illustrated in Fig. 5.15 of Subsection 5.3.2.6. The PKT signal becomes active with a delay of around 300 μs, and its active duration is nearly the same with PCS_N. The delay is very near to the time 288 μs indicated by Fig. 5.15, however, the length of PKT is disobedient to the description in [9] (on P31) that the PKT pin will stay low for the period of time CC2400 would take to receive 32 Bytes, no matter how long the received packet is. Since the real system measurement is more believable, I think this description is an error of the data sheet. The first three short inverse impulses on CSn are for the ORSS process, after which the ORS is determined for data reception. Then CSn has

nine relatively long inverse impulses, which implies that the SPU reads the FIFO of CC2400 for nine times. It is mentioned in Subsection A.3.2 that in each SPI cycle 25 Bytes can be maximally read by the SPU since FIFO_THRESHOLD of CC2400 is set to 25. Each data packet (including 3 Bytes physical header) consists of 225 Bytes, which exactly requires nine reading processes. Each impulse of FIFO_FULL corresponds to a CSn inverse pulse. As a matter of fact, each read process is initiated by an active FIFO_FULL impulse.

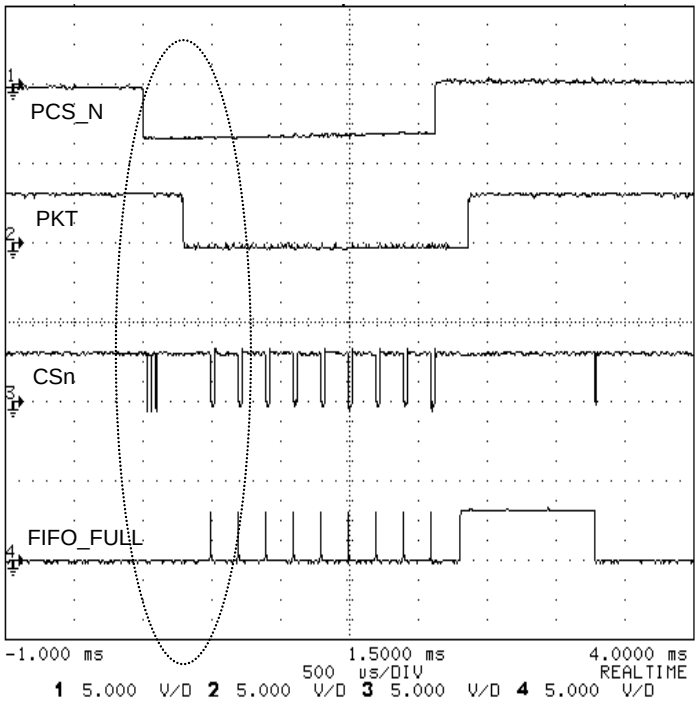

Figure A.13: The communication details for one RX process.

Fig. A.14 illustrates the communication details on the head of each RX process. It shows that the first RSSI value reading process occurs around 30 μs later than the appearance of the active PCS_N, and the following two occur with an approximate interval of 30 μs, all of which comply with the design intention described in Subsection A.3.3.2. The dashed ellipse part will be further zoomed in.

Fig. A.15 shows the relation between CSn and FIFO_FULL. It mainly indicates the following two facts: an active FIFO_FULL appears a bit earlier than an active CSn, and each reading process consumes around 25.5 μs. Both of them conform to the design intention described in Subsection A.3.2. Its dashed ellipse enclosed part is further zoomed in and illustrated in Fig. A.16, which indicates that an active CSn appears around 360 ns later than the appearance of an active FIFO_FULL, which is exactly 3 clock cycles (each with 120 ns period). A glitch is recorded at the beginning of the active CSn, which however doesn't impact on the reading process.

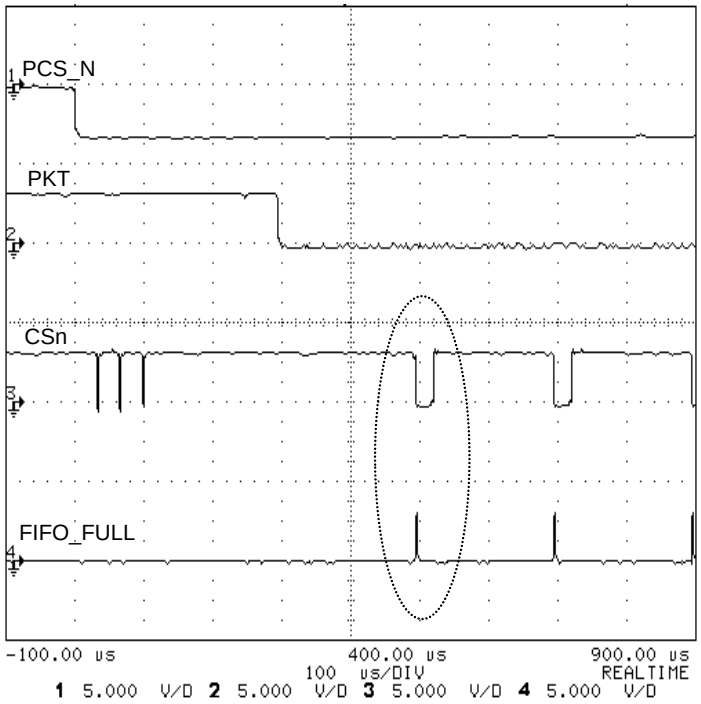

Figure A.14: The communication details on the head of one RX process.

Fig. A.17 illustrates the timing diagram on the SPI bus for one SPI cycle, which means the duration while CSn stays low. We can see that the timing diagram strictly obeys the SPI specification of CC2400 described in Section A.1 and [9]. Because there are 16 clock cycles for SCLK, two bytes of data have been sent to CC2400 via the SI line. The process for the first byte is enclosed by the dashed ellipse and zoomed in in Fig. A.18.

It can be clearly observed from Fig. A.18 that SCLK holds the period of 120 ns, which exactly corresponds to the clock frequency used by the test-bed (50 MHz/6). The byte transferred on the SI line is 0x86, which indicates that it is a reading process (R/W bit = '1') for the RSSI register (with 0x06 address) of CC2400. In the meanwhile a status byte 0x44 is transferred back via the SO line. A glitch is detected on the SI line, which nevertheless doesn't impact on the correct transfer of data while it doesn't occur at the rising edge of SCLK.

Fig. A.19 to Fig. A.21 reveal the relations among CSn, FIFO_FULL and FIFO pins of CC2400. In the the SPU design the active CSn signal is initiated by the active FIFO_FULL signal. Here FIFO is an output pin of CC2400 that gives the similar function as FIFO_FULL in the RX process and as FIFO_EMPTY in the TX process [9]. Fig. A.19 illustrates that the activities of FIFO and FIFO_FULL are nearly synchronous, and Fig. A.21 indicates that FIFO only has one clock cycle (120 ns) delay compared to FIFO_FULL. Therefore, this measurement certifies that at least

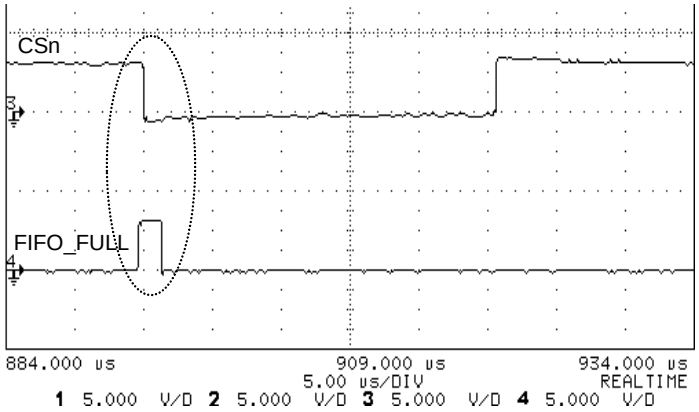

Figure A.15: The relation between CSn and FIFO_FULL.

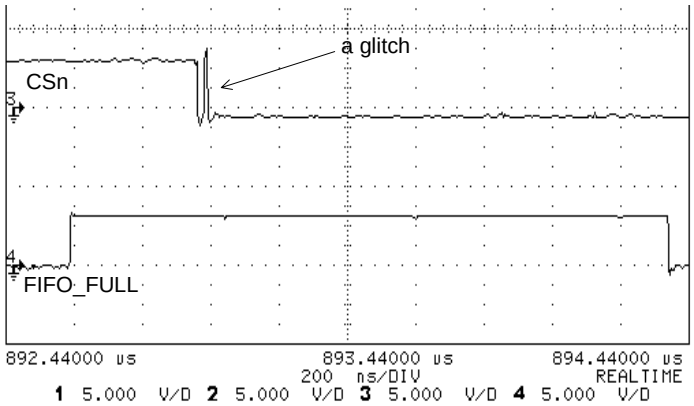

Figure A.16: The relation detail between CSn and FIFO_FULL.

in the RX process FIFO_FULL can be replaced by FIFO to save one I/O pin, because the pin for FIFO_FULL is a multi-function I/O that can be programmed for other functions [9].

As mentioned in Subsection A.3.3.2, an interference suppression function is realized on the SPU so that it is able to distinguish between intended user signal and the interference signal to avoid the case that ORSS is performed on the latter. Fig. A.22 shows two ORSS processes performed on the interference signal on 2433 MHz since no user signal is transmitted then. As described in Subsection A.3.3.2, only the interference signal that generates an active PCS_N longer than 30 μs can initiate an ORSS process. The signal is recognized as an interference very quickly in Fig. A.22 since an inactive PCS_N is immediately detected after each ORSS process.

Fig. A.23 shows how the SPU makes the RX process successfully in the environment with interference. Before the user signal appears, the ORSS process has been initiated by the interference signal for nine times. For the first six times and the 9th time, the signal is recognized as an interference very quickly since an inactive PCS_N is

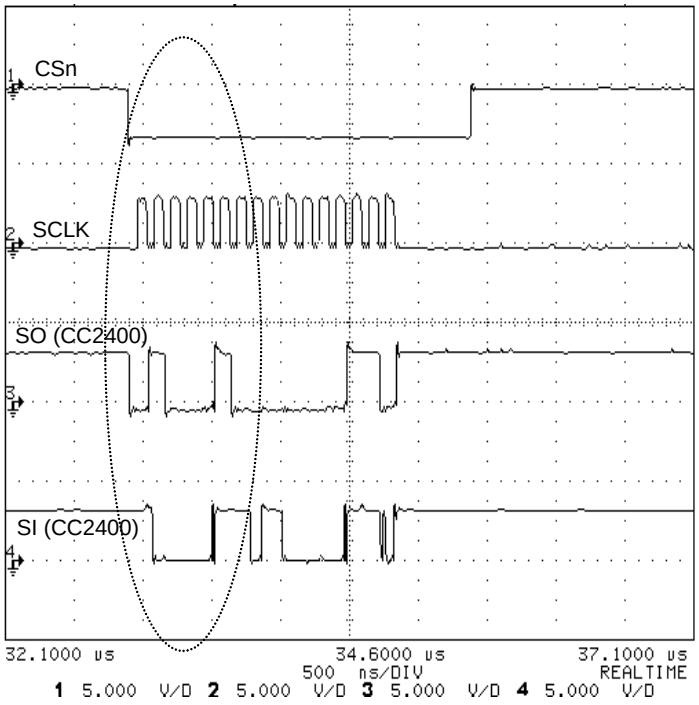

Figure A.17: One SPI cycle.

immediately detected after each ORSS process; however, the determining condition for the 7th and 8th time is different. The interference initiating the last three ORSS processes lasts very long, therefore the SPU recognizes it as an interference for the 7th and 8th ORSS process by the fact that no active PKT signal appears within 192 μs after ORSS. This also explains why the interval between them is relatively long (should be at least 192 μs + 30 μs). Fig. A.24 further shows that the 10th ORSS process is performed on the user signal since the active PKT signal appears in time, and the RX process is performed successfully afterwards. The interval between the active PCS_N (for the user signal) and the active PKT is around 288 μs, which is exactly the time the designer expects (refer to Fig. 5.15).

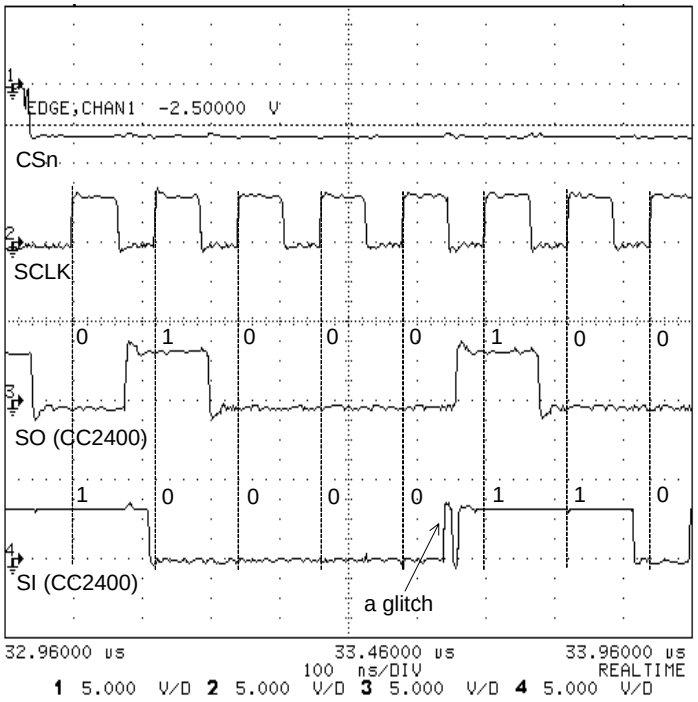

Figure A.18: The detail for the first half process of one SPI cycle.

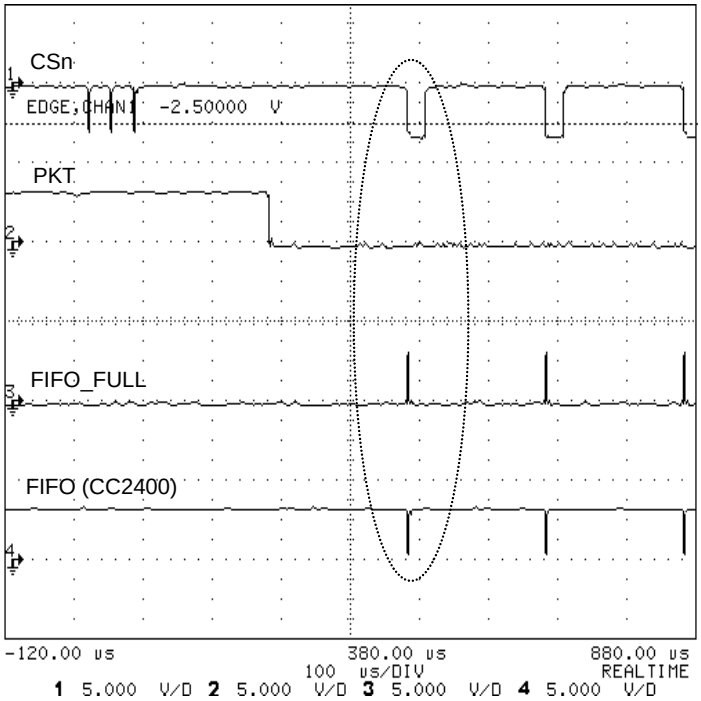

Figure A.19: The relations among the CSn, FIFO_FULL and FIFO pins of CC2400.

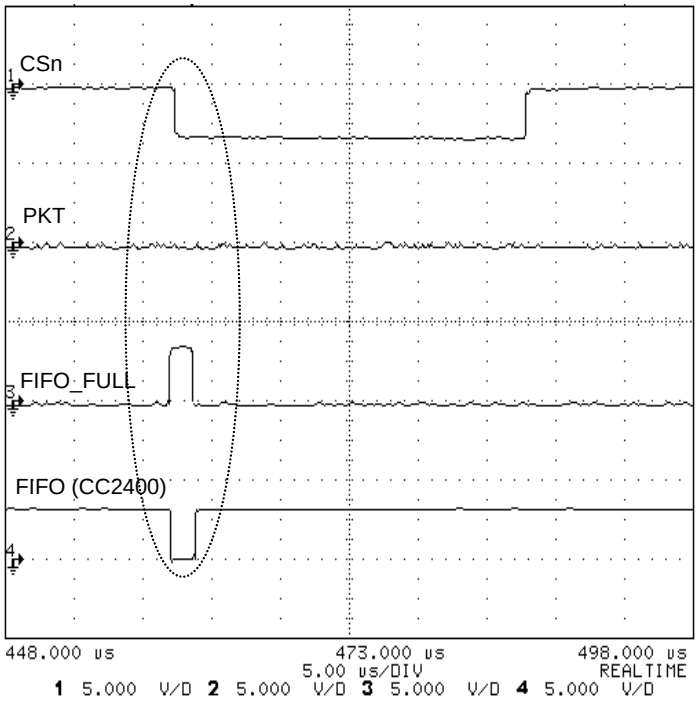

Figure A.20: The relations among the CSn, FIFO_FULL and FIFO pins of CC2400.

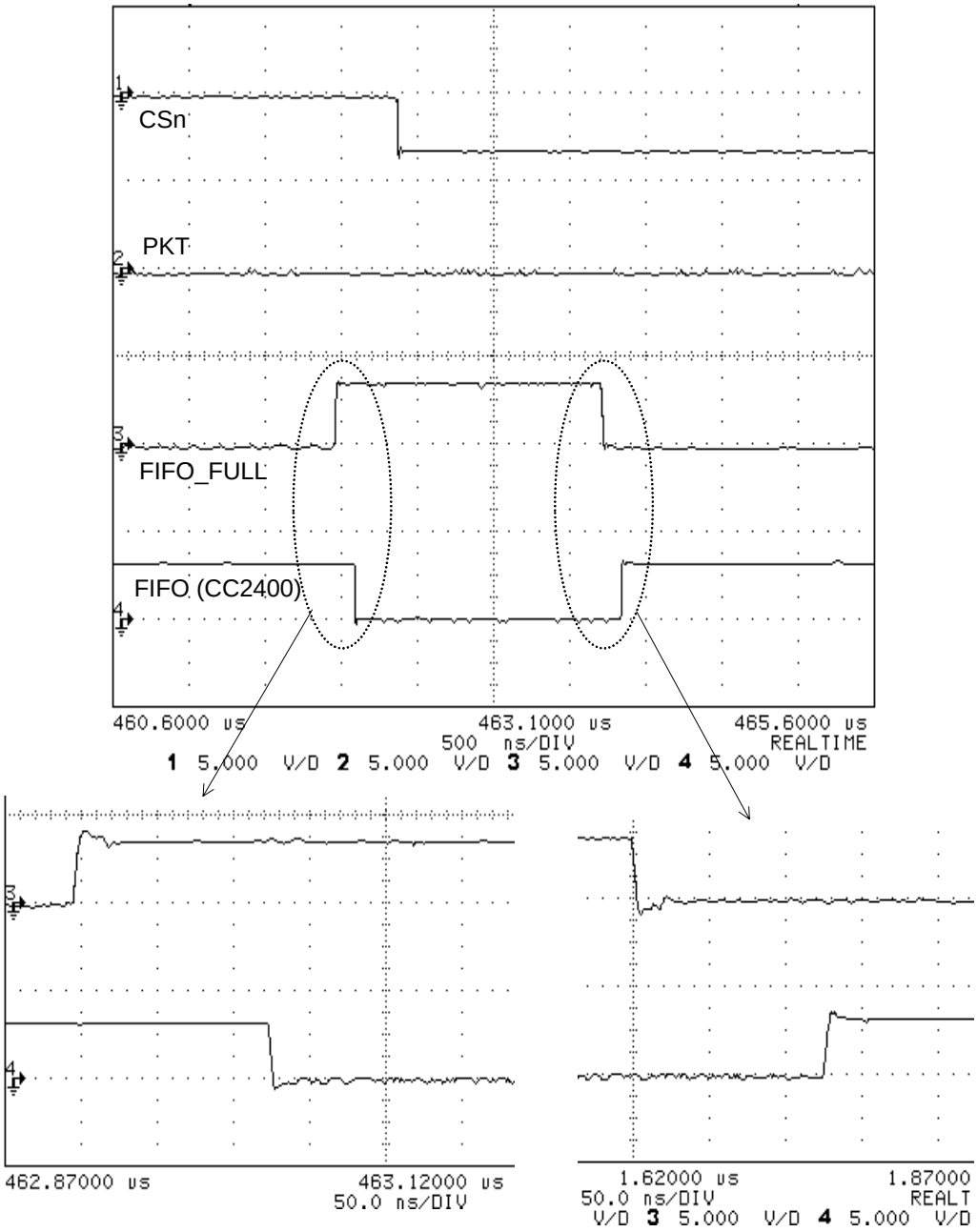

Figure A.21: The relations among the CSn, FIFO_FULL and FIFO pins of CC2400.

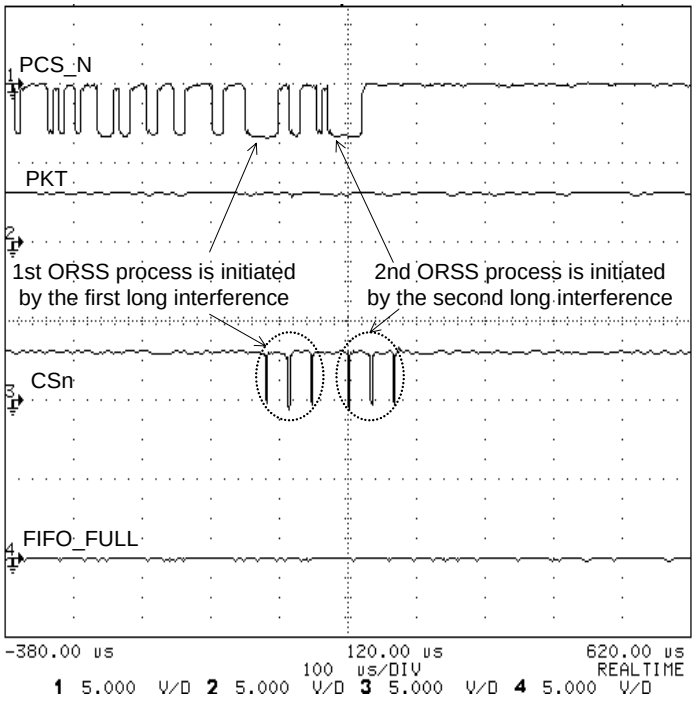

Figure A.22: Two ORSS processes are initiated by interference.

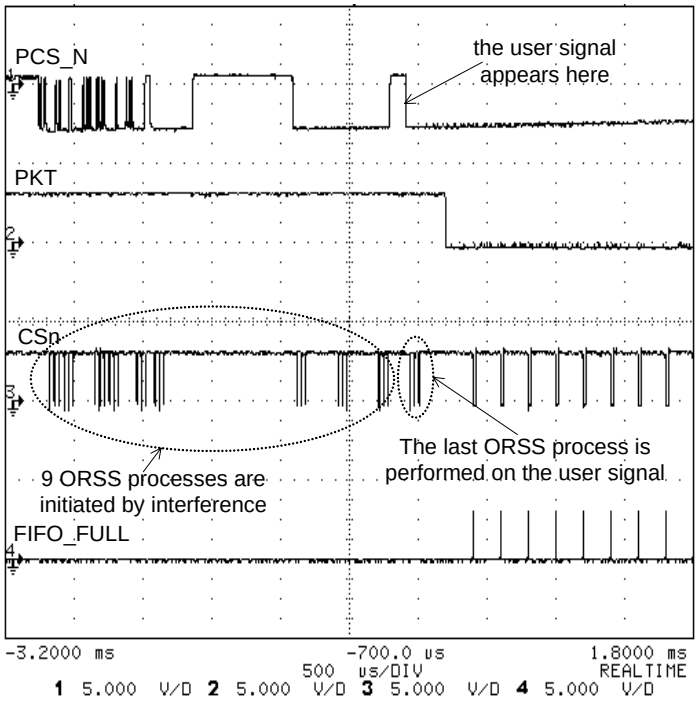

Figure A.23: An exemplary RX process in the environment with interference.

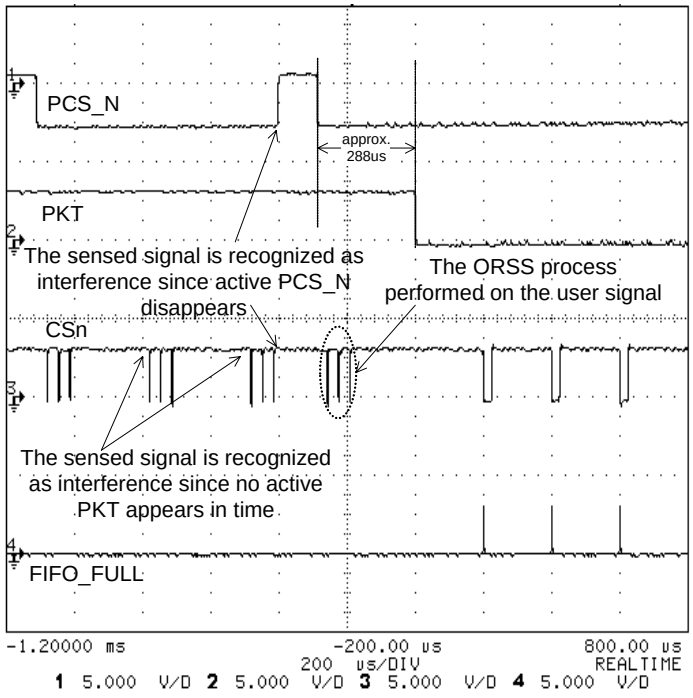

Figure A.24: More details on the exemplary RX process in the environment with interference.

Appendix B

Derivation of IF and Baseband Signals with Phase Shift

As described in Subsection 2.1.2, the RF signal can be expressed as

$$x_{\mathrm{RF}}(t) = x_{\mathrm{i}}(t)\cos(2\pi f_{\mathrm{RF}}t) - x_{\mathrm{q}}(t)\sin(2\pi f_{\mathrm{RF}}t), \tag{B.1}$$

where $x_{\mathrm{i}}(t)$ and $x_{\mathrm{q}}(t)$ are in-phase (I) and quadrature (Q) baseband signals, respectively, and f_{RF} denotes the radio carrier frequency. Applying the Fourier transform, we can obtain its frequency domain representation

$$X_{\mathrm{RF}}(f) = \frac{1}{2}[X_{\mathrm{i}}(f - f_{\mathrm{RF}}) + X_{\mathrm{i}}(f + f_{\mathrm{RF}})] - \frac{1}{2\mathrm{j}}[X_{\mathrm{q}}(f - f_{\mathrm{RF}}) - X_{\mathrm{q}}(f + f_{\mathrm{RF}})]. \tag{B.2}$$

In the following, we will first derive its intermediate frequency (IF) signal with the phase shift on the I- and Q-channel, respectively. As described in Subsection 2.1.2, the I-channel IF signal $x_{\mathrm{IF,I}}(t)$ and the Q-channel IF signal $x_{\mathrm{IF,Q}}(t)$ are redundant as they carry the same baseband signals. Then we will apply the analytic signal processing to verify the above two derivations. Finally, we will simply describe the derivation from IF or directly from RF to baseband. The up-conversion is just a reverse process of the corresponding down-conversion, hence they share the basic properties described below.

B.1 Derivation on the I-channel

The Fourier transform of the delayed RF signal $x_{\mathrm{RF}}(t-\tau)$ is $X_{\mathrm{RF}}(f)\cdot e^{-\mathrm{j}2\pi f_{\mathrm{RF}}\tau}$, it is then down-converted by being multiplied by $2\cos[2\pi(f_{\mathrm{RF}} - f_{\mathrm{IF}})t]$ (in the time domain) and then being bandpass filtered. That is, the frequency domain representation of the delayed IF signal is

$$\begin{aligned} X_{\mathrm{IF,I}}(f)\cdot e^{-\mathrm{j}2\pi f\tau} &= [\tfrac{1}{2}X_{\mathrm{i}}(f + f_{\mathrm{IF}}) + \tfrac{1}{2\mathrm{j}}X_{\mathrm{q}}(f + f_{\mathrm{IF}})]\cdot e^{-\mathrm{j}2\pi f\tau}\cdot e^{\mathrm{j}2\pi(f_{\mathrm{RF}} - f_{\mathrm{IF}})\tau} \\ &+ [\tfrac{1}{2}X_{\mathrm{i}}(f - f_{\mathrm{IF}}) - \tfrac{1}{2\mathrm{j}}X_{\mathrm{q}}(f - f_{\mathrm{IF}})]\cdot e^{-\mathrm{j}2\pi f\tau}\cdot e^{-\mathrm{j}2\pi(f_{\mathrm{RF}} - f_{\mathrm{IF}})\tau}. \end{aligned} \tag{B.3}$$

After applying the reverse Fourier transform, the delayed IF signal is derived as

$$x_{\mathrm{IF,I}}(t-\tau) = x_{\mathrm{i}}(t-\tau)\cdot\cos[2\pi(f_{\mathrm{IF}}t - f_{\mathrm{RF}}\tau)] - x_{\mathrm{q}}(t-\tau)\cdot\sin[2\pi(f_{\mathrm{IF}}t - f_{\mathrm{RF}}\tau)]. \quad \text{(B.4)}$$

B.2 Derivation on the Q-channel

The Fourier transform of the delayed RF signal $x_{\mathrm{RF}}(t-\tau)$ is $X_{\mathrm{RF}}(f)\cdot e^{-\mathrm{j}2\pi f_{\mathrm{RF}}\tau}$, it is then down-converted by being multiplied by $-2\sin[2\pi(f_{\mathrm{RF}} - f_{\mathrm{IF}})t]$ (in the time domain) and then being bandpass filtered. That is, the frequency domain representation of the delayed IF signal is

$$\begin{aligned} X_{\mathrm{IF,Q}}(f)\cdot e^{-\mathrm{j}2\pi f\tau} &= \mathrm{j}[\tfrac{1}{2}X_{\mathrm{i}}(f-f_{\mathrm{IF}}) - \tfrac{1}{2\mathrm{j}}X_{\mathrm{q}}(f-f_{\mathrm{IF}})]\cdot e^{-\mathrm{j}2\pi f\tau}\cdot e^{-\mathrm{j}2\pi(f_{\mathrm{RF}}-f_{\mathrm{IF}})\tau} \\ &- \mathrm{j}[\tfrac{1}{2}X_{\mathrm{i}}(f+f_{\mathrm{IF}}) + \tfrac{1}{2\mathrm{j}}X_{\mathrm{q}}(f-f_{\mathrm{IF}})]\cdot e^{\mathrm{j}2\pi f\tau}\cdot e^{-\mathrm{j}2\pi(f_{\mathrm{RF}}+f_{\mathrm{IF}})\tau}. \end{aligned} \quad \text{(B.5)}$$

After applying the reverse Fourier transform, the delayed IF signal is derived as

$$x_{\mathrm{IF,Q}}(t-\tau) = -x_{\mathrm{i}}(t-\tau)\cdot\sin[2\pi(f_{\mathrm{IF}}t - f_{\mathrm{RF}}\tau)] - x_{\mathrm{q}}(t-\tau)\cdot\cos[2\pi(f_{\mathrm{IF}}t - f_{\mathrm{RF}}\tau)]. \quad \text{(B.6)}$$

B.3 Derivation applying the analytic signal representation

The analytic RF signal can be expressed as

$$x_{\mathrm{RF,analy}}(t) = x_{\mathrm{RF}}(t) + \mathrm{j}\hat{x}_{\mathrm{RF}}(t), \quad \text{(B.7)}$$

in which $\hat{x}_{\mathrm{RF}}(t)$ is the Hilbert transform of $x_{\mathrm{RF}}(t)$. Its frequency domain representation is

$$X_{\mathrm{RF,analy}}(f) = 2\mathrm{U}(f)\cdot X_{\mathrm{RF}}(f), \quad \text{(B.8)}$$

in which $\mathrm{U}(f)$ denotes the step function. Substitute Eq. (B.2) into Eq. (B.8), we can obtain

$$X_{\mathrm{RF,analy}}(f) = X_{\mathrm{i}}(f-f_{\mathrm{RF}}) + \mathrm{j}X_{\mathrm{q}}(f-f_{\mathrm{RF}}). \quad \text{(B.9)}$$

After performing the inverse Fourier transform, we can obtain another expression of the analytic RF signal

$$x_{\mathrm{RF,analy}}(t) = [x_{\mathrm{i}}(t) + \mathrm{j}x_{\mathrm{q}}(t)]\cdot e^{\mathrm{j}2\pi f_{\mathrm{RF}}t}. \quad \text{(B.10)}$$

The complex envelop $x_{\mathrm{i}}(t)+\mathrm{j}x_{\mathrm{q}}(t)$ is the low pass equivalent of the analytic RF signal, which is exactly the analytic baseband signal. The frequency domain representation of

the RF analytic signal with the time delay τ is $X_{\mathrm{RF,analy}}(f)\cdot e^{-\mathrm{j}2\pi f\tau}$. For the frequency domain analytic representation, the down-conversion is simply the spectrum shift from RF to IF (that is, the spectrum shifts $f_{\mathrm{RF}}-f_{\mathrm{IF}}$ in the direction to 0), which is equivalent to the process that $X_{\mathrm{RF,analy}}(f)\cdot e^{-\mathrm{j}2\pi f\tau}$ convolves with an impulse function $\delta[f+(f_{\mathrm{RF}}-f_{\mathrm{IF}})]$. Considering the corresponding process in the time domain, it is just a multiplication of $x_{\mathrm{RF,analy}}(t-\tau)$ and $e^{-\mathrm{j}2\pi(f_{\mathrm{RF}}-f_{\mathrm{IF}})t}$, that is

$$\begin{aligned} x_{\mathrm{IF,analy}}(t-\tau) &= x_{\mathrm{RF,analy}}(t-\tau)\cdot e^{-\mathrm{j}2\pi(f_{\mathrm{RF}}-f_{\mathrm{IF}})t} \\ &= [x_{\mathrm{i}}(t-\tau)+\mathrm{j}x_{\mathrm{q}}(t-\tau)]\cdot e^{\mathrm{j}2\pi(f_{\mathrm{IF}}t-f_{\mathrm{RF}}\tau)}. \end{aligned} \tag{B.11}$$

It should be noted that unlike the usual signal analysis in the I- and Q-channel, the bandpass filtering is not necessary for the down-conversion of the analytic signal. The delayed I-channel IF signal is exactly the real part of Eq. (B.11), that is

$$x_{\mathrm{IF,I}}(t-\tau)=x_{\mathrm{i}}(t-\tau)\cdot\cos[2\pi(f_{\mathrm{IF}}t-f_{\mathrm{RF}}\tau)]-x_{\mathrm{q}}(t-\tau)\cdot\sin[2\pi(f_{\mathrm{IF}}t-f_{\mathrm{RF}}\tau)], \tag{B.12}$$

and the delayed Q-channel IF signal is exactly the imaginary part of Eq. (B.11), that is

$$x_{\mathrm{IF,Q}}(t-\tau)=x_{\mathrm{i}}(t-\tau)\cdot\sin[2\pi(f_{\mathrm{IF}}t-f_{\mathrm{RF}}\tau)]+x_{\mathrm{q}}(t-\tau)\cdot\cos[2\pi(f_{\mathrm{IF}}t-f_{\mathrm{RF}}\tau)]. \tag{B.13}$$

It can be observed that Eq. (B.12) is the same as Eq. (B.4), and Eq. (B.13) is the negative of Eq. (B.6). This is due to the fact that in the derivation of Eq. (B.6) the signal $-2\sin[2\pi(f_{\mathrm{RF}}-f_{\mathrm{IF}})t]$ (which is a 90^{o} phase shifted signal of the LO signal $2\cos[2\pi(f_{\mathrm{RF}}-f_{\mathrm{IF}})t]$) instead of $2\sin[2\pi(f_{\mathrm{RF}}-f_{\mathrm{IF}})t]$ is utilized.

B.4 Derivation of baseband signals with phase shift

The down-conversion from IF to baseband is similar to the process from RF to IF. The sole difference is, the down-conversion on both I and Q channels is indispensable. That is, the IF to baseband down-conversion is accompanied with the I/Q separation (or called demodulation). Usually, the I-channel IF signal $x_{\mathrm{IF,I}}(t)$ is used as an intermediate between the RF and baseband signals, as we can see that the RF signal of Eq. (B.1) and the I-channel IF signal of Eq. (B.4) (if not delayed) have the same structure. Therefore, the down-conversion from the I-channel IF signal $x_{\mathrm{IF,I}}(t)$ to the I-channel baseband signal $x_{\mathrm{i}}(t)$ is like the down-conversion from the RF signal to the I-channel IF signal described in Section B.1, just treat both f_{IF} and τ in Eq. (B.4) as 0; and the down-conversion from the I-channel IF signal $x_{\mathrm{IF,I}}(t)$ to the Q-channel baseband signal $-x_{\mathrm{q}}(t)$ is like the down-conversion from the RF signal to the Q-channel IF signal described in Section B.2, just treat both f_{IF} and τ in Eq. (B.6) as 0. As for the

analytic signal case, we just need to treat both f_{IF} and τ in Eq. (B.11) as 0 to obtain the analytic baseband signal $[x_{\mathrm{i}}(t) + \mathrm{j}x_j(t)]$. Furthermore, consider that if the time delay τ is not 0 for the above processing, then the I- and Q-channel baseband signals cannot be completely separated since the impact of the phase shift $-2\pi f_{\mathrm{RF}}\tau$ is still kept on the baseband signals. Therefore, the analytic baseband signal with phase shift is

$$x_{\mathrm{BB}}(t-\tau) = [x_{\mathrm{i}}(t-\tau) + \mathrm{j}x_{\mathrm{q}}(t-\tau)]e^{-\mathrm{j}2\pi f_{\mathrm{RF}}\tau}. \tag{B.14}$$

As for the direct conversion from RF to baseband, just consider the above down-conversions from the I-channel IF signal to the I/Q baseband signals and substitute the RF signal $x_{\mathrm{RF}}(t)$ for the I-channel IF signal $x_{\mathrm{IF,I}}(t)$.

B.5 Concluding remarks

Based on the above derivations, mainly on Eqs. (B.4), (B.6) and (B.11), we can see that in the course of the down-conversion from RF to IF, the time delay τ experienced by the RF signal $x_{\mathrm{RF}}(t)$ is kept on the baseband components $x_{\mathrm{i}}(t)$ and $x_{\mathrm{q}}(t)$, but is increased to $\frac{f_{\mathrm{RF}}}{f_{\mathrm{IF}}}\tau$ for the IF carrier signal; and the phase shift $-2\pi f_{\mathrm{RF}}\tau$ is kept on the IF carrier signal.

As for the down-conversion from IF to baseband, or directly from RF to baseband, applying Eq. (B.11) and treating its f_{IF} as 0 to obtain $[x_{\mathrm{i}}(t-\tau)+\mathrm{j}x_{\mathrm{q}}(t-\tau)]\cdot e^{-\mathrm{j}2\pi f_{\mathrm{RF}}\tau}$, we can find that the time delay τ is kept on the baseband analytic signal, and the phase shift $-2\pi f_{\mathrm{RF}}\tau$ still causes an impact with the factor $e^{-\mathrm{j}2\pi f_{\mathrm{RF}}\tau}$.

Appendix C

List of Abbreviations

AF	Array Factor
AoF	Amount of Fading
AGC	Automatic Gain Control
AMHA	Axial Mode Helical Antenna
ANL	Awake Neighbors List
AP	Access Point
AS	Angle Spread
ASIC	Application Specific Integrated Circuit
BER	Bit Error Rate
BF	Beamforming
BF-MAC	Beamforming MAC
BLAST	Bell Laboratories Layered Space-time
BPF	Bandpass Filter
BS	Base Station
CDMA	Code Division Multiple Access
CCI	Co-channel Interference
CRC	Cyclic Redundancy Check
CSI	Channel State Information
CSMA/CA	Carrier Sense Multiple Access with Collision Avoidance
CSn	Chip Selection negative valid
CTS	Clear-To-Send
CW	Contention Window
DCF	Distributed Coordination Function
DIFS	DCF Interframe Space
Dir-MAC	Directional MAC
DOA	Direction of Arrival
EGC	Equal Gain Combining
ESPRIT	Estimation of Signal Parameters via Rotational Invariance Techniques
FDD	Frequency Division Duplex
FDMA	Frequency Division Multiple Access
FHSS	Frequency Hopping Spread Spectrum
FIFO	First-In First-Out
FPGA	Filed Programmable Gate Array

GMACs	Giga Multiply-Accumulates per second
GSC	Generalized Diversity Selection Combining
HPBW	Half Power Beam Width
H-S/MRC	Hybrid Selection/Maximal Ratio Combining
IF	Intermediate Frequency
IP	Intellectual Property
IS	Interference Sprression
LAN	Local Area Network
LMS	Least Mean Square
LOS	Line-of-Sight
LPF	Low-pass Filter
LSB	Least Significant Bit
MAC	Medium Access Control
MANETs	Mobile Ad Hoc Networks
MDA-MAC	Multi-directional-antenna MAC
MIMO	Multi-Input Multi-Output
MISO	Multi-Input Single-Output
MMACs	Million Multiply-Accumulates per second
MRC	Maximal Ratio Combining
MS	Mobile Station
MSB	Most Significant Bit
MUSIC	Multiple Signal Classification
MVDR	Minimum Variance Distortionless Response
NAV	Network Allocation Vector
NMHA	Normal Mode Helical Antenna
OFDM	Orthogonal Frequency Division Multiplexing
OFDMA	Orthogonal Frequency Division Multiple Access
ORS	Optimal Reception Sector
ORSS	Optimal Reception Sector Selection
OTS	Optimal Transmission Sector
PC	Radiation Power Control
PDR	Packet Delivery Ratio
PCF	Point Coordination Function
PCI	Personal Computer Interface
PCS	Physical Carrier Sense
PDA	Personal Digital Assistant
PM	Transceiver Power Management
RF	Radio Frequency
RMS	Root Mean Square
RSSI	Received Signal Strength Indicator
RTS	Request-To-Send
RX	Receive
SA	Smart Antennas

SAHNE	Simulation of an Ad Hoc Networking Environment
SCLK	Synchronized Clock
SD	Space Diversity
SD-MAC	Space Diversity MAC
SDMA	Space Division Multiple Access
SI	Serial Input
SIFS	Short Interframe Space
SIMO	Single-Input Multiple-Output
SIR	Signal to Interference Power Ratio
SM	Spatial Multiplexing
SMA	SubMiniature version A
SNIR	Signal to Noise Plus Interference Power Ratio
SNOI	Signal-Not-of-Interest
SNR	Signal to Noise Power Ratio
SO	Serial Output
SOI	Signal-of-Interest
SPI	Serial Peripheral Interface
SPU	SSB Processing Unit
SS	Spatial Signature
SSB	Simplified Switched Beam
STC	Space Time Coding
STBC	Space Time Block Coding
STTC	Space Time Trellis Coding
SVD	Singular Value Decomposition
SWCMD	Switching Command
TDMA	Time Division Multiple Access
TX	Transmit
ULA	Uniform Linear Array
ULS	Upper-layer Software
VCS	Virtual Carrier Sense
VGA	Variable Gain Amplifier
UMTS	Universal Mobile Telecommunications System
VHDL	Very High Speed Integrated Circuit Hradware Description Language
W-CDMA	Wideband Code Division Multiple Access
WLAN	Wireless Local Area Network
WSS	Wide Sense Stationary

Appendix D

List of Symbols

η_{B}	spectrum-efficiency from the entire network perspective
η_{E}	energy-efficiency from the entire network perspective
λ	carrier wavelength
θ	elevation angle of the spherical coordinates
ϕ	azimuth angle of the spherical coordinates
$U(\theta,\phi)$	radiation intensity of the direction (θ,ϕ)
U_0	average radiation intensity over the entire solid angles
$U_{\max}$	maximum radiation intensity
D	directivity of an antenna or an antenna array
G	gain of an antenna or an antenna array, or the number of traffic generators
G_{t}	transmitting antenna gain
G_{r}	receiving antenna gain
η	radiation efficiency of an antenna element
$x_{\mathrm{RF}}(t)$	radio frequency (RF) signal
$x_{\mathrm{IF}}(t)$	intermediate frequency (IF) signal
$x_{\mathrm{IF,I}}(t)$	in-phase channel IF signal
$x_{\mathrm{IF,Q}}(t)$	quadrature channel IF signal
$x_{\mathrm{i}}(t)$	in-phase channel baseband signal
$x_{\mathrm{q}}(t)$	quadrature channel baseband signal
f_{RF}	radio frequency
f_{IF}	intermediate frequency
$\mathbf{a}(\phi_0)$	array response vector of the signal impinging from the direction ϕ_0
$\mathbf{w}$	weighting coefficients vector
$\mathrm{AF}(\phi,\phi_0)$	array factor of the horizontal plane with the peak direction ϕ_0
$\mathbf{a}_1$	spatial signature associated with the signal $s_1(t)$
$\mathbf{R}_{\mathrm{xx}}$	spatial correlation matrix of the array signal vector $\mathbf{x}$
$\mathbf{R}_{\mathrm{x}}$	sample covariance matrix of the data matrix $\mathbf{X}$
γ_n	local mean signal to noise power ratio (SNR) on the n-th branch
Γ	global mean SNR
γ_{SD}	output SNR of the selection diversity (SD) scheme
γ_{MRC}	output SNR of the maximum ratio combining (MRC) diversity scheme
γ_{EGC}	output SNR of the equal gain combining (EGC)diversity scheme
γ_{GSC}	output SNR of the generalized diversity selection combining (GSC) scheme

P_{t}	transmission (radiation) power of the signal
P_{r}	received signal power
$P_{\mathrm{t,in}}$	transmission power of the last received packet (extracted from its header)
$P_{\mathrm{r,in}}$	measured reception power of the last received packet
sec_{in}	sector that transmitted the last packet
$P_{\mathrm{t,out}}$	transmission power of the current packet
sec_{out}	sector that transmits the current packet
L_P	path loss
$L_{\mathrm{nom,in}}$	nominal path loss of the incoming signal at the receiver
$L_{\mathrm{nom,out}}$	nominal path loss of the outgoing signal from the sender
$P_{\mathrm{t,opt}}$	optimal transmission power
E_{RX}	accumulated energy for receiving all packet
E_{TX}	accumulated energy for transmitting all packet
E_{SX}	accumulated energy for sensing the medium
E_{DX}	accumulated energy for unsuccessful receptions (discarding packets)
E_{RF}	accumulated radiation energy for sending packets of any type
S	network throughput
D_{E2E}	accumulated time the data packet have been in delivery
PDR	packet delivery ratio
P_{SX}	power consumption for sensing
P_{RX}	power consumption for reception
P_{TX}	static power consumption for transmission (excluding the power amplifier)
$P_{\mathrm{PA}}(P_{\mathrm{t}})$	power consumption of the power amplifier in dependent of P_{t}
K	number of sectors of a node
t_{slot}	time slot duration
p_{data}	data packet size
T_{ND}	neighborhood discovery period
T_{n}	neighbor delete time-out
Δt_{ND}	neighborhood discovery jitter
p_{RTS}	RTS/CTS threshold
T_{a}	awake time
T_{d}	sleep time
$\#awake$	awake period
P_{s}	sensing threshold
P_{r}	receiving threshold
t_{IFS}	interframe spacing
T_{TR}	training period
T_{sw}	response time of the RF switch
T_{RSSI}	RSSI rise time
T_{ad}	A/D conversion and data acquisition time
T_{comp}	comparison time of the judging unit
Δt	margin time
τ_{c}	channel coherence time
f_{d}	maximum Doppler frequency
$\sigma_{L/N,\mathrm{GSC}}$	normalized standard deviation of the output SNR of the L out of N GSC scheme

List of Figures

List of Tables

Bibliography

[1] S. M. Alamouti. A Simple Transmit Diversity Technique for Wireless Communications. *IEEE Journal on Selected Areas in Communications*, 16(8), October 1998.

[2] P. Alriksson, B. Bernhardsson, and B. Lindoff. Automatic Gain Control in WCDMA Terminals. In *Proceedings of Reglermöte*, Göteborg, Sweden, 2004.

[3] C. A. Balanis. *Antenna Theory - Analysis and Design*. John Wiley & Sons, 1997.

[4] C. A. Balanis et al. Smart Antennas for Future Reconfigurable Wireless Communication Networks. Technical report, Arizona State University, April 2000.

[5] F. Bektas. *Investigation of Antenna Diversity Techniques for Bluetooth Communication*. PhD Thesis, Technical University of Wien, 2003.

[6] S. Bellofiore, J. Foutz, C. A. Balanis, and A. S. Spanias. Smart-Antenna Systems for Mobile Communication Networks, Part 2: Beamforming and Network Throughput. *IEEE Antenna's Propagation Magazine*, 44(4), August 2002.

[7] S. Bellofiore et al. Smart Antenna System Analysis, Integration and Performance for Mobile Ad-Hoc Networks (MANETs). *IEEE Transactions on Antennas and Propagation*, 50(5), May 2002.

[8] U. Charash. Reception Through Nakagami Fading Multipath Channels with Random Delays. *IEEE Transaction on Communications*, 27(4), April 1979.

[9] CHIPCON. *Datasheet of CC2400 (rev. 1.3), and relevant documents on its development kit (CC2400DK)*, 2004.

[10] R. R. Choudhury, X. Yang, R. Ramanathan, and N. H. Vaidya. Using Directional Antennas for Medium Access Control in Ad Hoc Networks. In *Proceedings of MobiCom*, Atlanta, Georgia, USA, September 23-28 2002.

[11] K. R. Dandekar, Hao Ling, and G. H. Xu. Experimental Study of Mutual Coupling Compensation in Smart Antenna Applications. *IEEE Transactions on Wireless Communications*, 1(3), July 2002.

[12] C. Descleves. Introduction to ADMS RF (Digital AGC Loop). Technical report, Mentor Graphics Corporation, www.mentor.com/dsm, August 2003.

[13] C. B. Dietrich Jr., K. Dietze, J. R. Nealy, and W. L. Stutzman. Spatial, Polarization, and Pattern Diversity for Wireless Handheld Terminals. *IEEE Transactions on Antennas and Propagation*, 49(9), September 2001.

[14] L. M. Feeney and M. Nilsson. Investigating the energy consumption of a wireless network interface in an ad hoc networking environment. In *Proceedings of IEEE INFOCOM*, Anchorage, Alaska, April 22-26 2001.

[15] M. Feng, S.-C. Shen, D. Caruth, and J.-J. Huang. Device Technologies for RF Front-End Circuits in Next-Generation Wireless Communications. *Proceedings of the IEEE*, 92(2):354–375, February 2004.

[16] G. J. Foschini. Layered Space-Time Architecture for Wireless Communication in a Fading Environment When Using Multi-Element Antennas. *Bell Labs Technical Journal*, Autumn 1996.

[17] G. J. Foschini Jr. and M. J. Gans. On Limits of Wireless Communication in a Fading Environment when Using Multiple Antennas. *Wireless Personal Communications*, 6(3), March 1998.

[18] J. D. Fredrick, Y. Wang, and T. Itoh. A Smart Antenna receiver Array using a Single RF Channel and Digital Beamforming. *IEEE Transactions on Microwave Theory and Techniques*, 50(12), Dec. 2002.

[19] L. C. Godara. Application of Antenna Arrays to Mobile Communications, Part II: Beam-Forming and Direction-of-Arrival Considerations. *Proceedings of the IEEE*, 85(8), August 1997.

[20] M. Grünewald, J.-C. Niemann, M. Porrmann, and U. Rückert. A framework for design space exploration of resource efficient network processing on multiprocessor socs. In *Proceedings of the 3rd Workshop on Network Processors & Applications*, pages 87–101, Madrid, Spain, 14 - 15 February 2004.

[21] M. Grünewald, F. Xu, and U. Rückert. Power Control in Directional Mobile Ad Hoc Networks. In *ITG Fachtagung 'Ambient Intelligence'*, Berlin, Germany, October 18-20 2004.

[22] M. Grünewald, F. Xu, and U. Rückert. Increasing the resource-efficiency of the csma/ca protocol in directional ad hoc networks. In *Proceedings of the 4th International Conference on AD-HOCNetworks & Wireless*, pages 71–84, Cancun, Mexico, 6-8. Oct. 2005.

[23] R. C. Hansen. *Phased Array Antennas.* JOHN WILEY & SONS, INC., 1997.

[24] N. Haridas, A. T. Erdogan, T. Arslan, and M. Begbie. Adaptive Micro-Antenna on Silicon Substrate. In *Proceedings of 1st NASA/ESA Conference on Adaptive Hardware and Systems (AHS'06)*, 2006.

[25] R. W. Heath Jr. and A. J. Paulraj. Switching Between Diversity and Multiplexing in MIMO Systems. *IEEE Transactions on Communications*, 53(6), June 2005.

[26] W. R. Heinzelman, A. Chandrakasan, and H. Balakrishnan. Energy-efficient communication protocol for wireless microsensor networks. In *Proceedings of the Hawaii International Conference on System Science*, January 2000.

[27] I. Hen. MIMO Architecture for Wireless Communication. *Intel Technology Journal*, 10(2), 2006.

[28] N. Horspool and P. Gorman. *The ASIC Handbook.* Pretice Hall PTR, 2001.

[29] M. Hu. *A Cross-Layer Design Framework for Resource Allocation in Wireless Data Networks.* PhD Thesis, Arizona State University, 2004.

[30] Intersil Americas Inc. *Intersil PRISM 2.5 chip set: baseband processor ISL3873B, I/Q modulator/demodulator HFA3783, RF/IF converter ISL3685*, 2000-2002.

[31] W. C. Jakes. *Microwave Mobile Communications.* New York: Wiley, 1974.

[32] S.-S. Jeng, G. T. Okamoto, G. Xu, H.-P. Lin, and W. J. Volgel. Experimental Evaluation of Smart Antenna System Performance for Wireless Communications. *IEEE Transaction on Antennas and Propagations*, 46(6), June 1998.

[33] S.-S. Jeng, G. Xu, H.-P. Lin, and W. J. Volgel. Experimental Studies of Spatial Signature variation at 900 MHz for Smart Antenna Systems. *IEEE Transaction on Antennas and Propagations*, 46(7), July 1998.

[34] S.-S. Jeon, Y. Wang, Y. Qian, and T. Itoh. A Novel Smart Antenna System Implementation for Broad-Band Wireless Communications. *IEEE Transactions on Antennas and Propagation*, 50(5), May 2002.

[35] H. Kalte, M. Porrmann, and U. Rückert. A Prototyping Platform for Dynamically Reconfigurable System on Chip Designs . In *Proceedings of the IEEE Workshop Heterogeneous Reconfigurable Systems on Chip (SoC)*, Hamburg, Germany, 2002.

[36] A. Khaleghi, A. Azoulay, J.C. Bolomey, and Supélec. Diversity techniques with dipole antennas in indoor multipath propagation. In *Proceedings of the 16th IEEE International Symposium on Personal Indoor and Mobile Radio Communications (PIMRC05)*, Berlin, Germany, 11-14 Sep. 2005.

[37] T. Kluwer. *Development of a Test-bed for Smart Antennas, using digital Beamforming*. M. Sc. Thesis, University of Twente, the Netherlands, 2001.

[38] Y.-B. Ko, V. Shankarkumar, and N. H. Vaidya. Medium Access Control Protocols Using Directional Antennas in Ad Hoc Networks. In *Proc. of IEEE INFOCOM*, March 2000.

[39] N. Kong and L. B. Milstein. Average SNR of a Generalized Diversity Selection Combining Scheme. *IEEE Communication Letter*, 3(3), March 1999.

[40] T. Korakis, G. Jakllari, and L. Tassiulas. A MAC protocol for full exploitation of Directional Antennas in Ad-hoc Wireless Networks. In *Proc. of MobiHoc*, Annapolis, USA, June 2003.

[41] R. Kraemer. Siliziumbasierte Mikroelektronik für die drahtlose Hochleistungskommunikation. In *Proceedings of VDE Kongress - ITG Fachtagung 'Mobility'*, Aachen, Germany, 23-25 Oct. 2006.

[42] J. D. Kraus and R. J. Marhefka. *Antennas for All Applications*. McGraw-Hill, 2002.

[43] W. Kuropatwinski-Kaiser. *MIMO-Demonstrator basierend auf GSM-Komponenten*. PhD Thesis, Universität Fridericiana Karlsruhe, 2005.

[44] Lal, D. and Gupta, R. and Agrawal, D. P. Throughput Enhancement in Wireless Ad Hoc Networks with Spatial Channels- A MAC Layer Perspective. In *Proceedings of the Seventh IEEE Symposium on Computers and Communications (ISCC)*, Taormina, Italy, July 2002.

[45] Lal, D. and Toshniwal, R. and Radhakrishnan, R. and Agrawal, D. P. and Caffery, J. A Novel MAC Layer Protocol for Space Division Multiple Access in Wireless Ad Hoc Networks. In *Proc. of the IEEE ICCCN*, Miami, October 2002.

[46] LAN/MAN Standards Committee of the IEEE Computer Society. *ANSI/IEEE Std 802.11 – Wireless LAN Medium Access Control (MAC) and Physical Layer (PHY) Specifications*, 1999.

[47] P. H. Lehne and M. Pettersen. An Overview of Smart Antenna Technology for Mobile Communications Systems. *IEEE Communications Surveys*, 2(4):2–13, 1999.

[48] Z. D. Lei and T. J. Lim. Estimation of Directions of Arrival of Multipath Signals in CDMA Systems. *IEEE Transactions on Communications*, 48(6), June 2000.

[49] J. Liberti and T. S. Rappaport. *Smart Antennas for Wireless Communications: IS-95 and Third Generation CDMA Applications*. Prentice Hall, 1999.

[50] R. Ludwig and P. Bretchko. *RF Circuit Design Theory and Applications*. Prentice Hall, 2002.

[51] J. Mietzner and P. A. Hoeher. Boosting the Performance of Wireless Communication Systems: Theory and Practice of Multiple-Antenna Techniques. *IEEE Communications Magazine*, 42(10), October 2004.

[52] J.C. Mundarath, P. Ramanathan, and B.D. Van Veen. NULLHOC: A MAC Protocol for Adaptive Antenna Array Based Wireless Ad Hoc NEtworks in Multipath Enviroments. In *Proceedings of IEEE GLOBECOM*, 2004.

[53] A. Nasipuri, S. Ye, and R. E. Hiromoto. A MAC Protocol for Mobile Ad Hoc Networks Using Directional Antennas. In *Proc. of IEEE WCNC*, Chicago, IL, September 26-29 2000.

[54] H. Novak. *Switched-Beam Adaptive Antenna System*. PhD Thesis, Technical University of Wien, 1999.

[55] B. O'Hara and A. Petrick. *The IEEE 802.11 Handbook, a Designer's Companion*. IEEE Press, 1999.

[56] J.-S. Park and M. Gerla. MIMOMAN: A MIMO MAC Protocol for Ad Hoc Networks. In *Proceedings of the 4th International Conference on AD-HOCNetworks & Wireless*, 6-8. Oct. 2005.

[57] J.-S. Park, A. Nandan, M. Gerla, and H. Lee. SPACE-MAC: Enabling Spatial Reuse using MIMO channel-aware MAC. In *Proceedings of IEEE ICC*, 2005.

[58] A. J. Paulraj, D. Gesbert, and C. Papadias. *Smart Antennas for Mobile Communications (In: Encyclopedia for Electrical Engineering)*. John Wiley, 2000.

[59] A. J. Paulraj and C. B. Papadias. Space-Time Processing for Wireless Communications. *IEEE Signal Processing Magazine*, November 1997.

[60] P. L. Perini and C. L. Holloway. Angle and Space Diversity Comparisons in Different Mobile Radio Environments. *IEEE Transactions on Antennas and Propagation*, 46(6), June 1998.

[61] Philips Semiconductors. *SA2411: +20dBm single chip linear amplifier for WLAN*, 2003.

[62] R. Ramanathan. On the Performance of Ad Hoc Networks with Beamforming Antennas. In *Proceedings of MobiHOC*, Long Beach, CA, USA, October 4-5 2001.

[63] T. S. Rappaport. *Wireless Communications*. Prentice Hall, 2002.

[64] B. Razavi. *RF Microelectronics*. Pearson Education, Inc., 1998.

[65] J. Razavilar, F. Rashid-Farrokhi, and K. J. Liu. Software Radio Architecture with Smart Antennas: A Tutorial on Algorithms and Complexity. *IEEE Transaction on Selected Areas in Communications*, 17(4), April 1999.

[66] V. Rodoplu and T. H. Meng. Minimum energy mobile wireless networks. *IEEE Journal on Selected Areas in Communication*, 17(8):1333–1344, 1999.

[67] S. Rührup, C. Schindelhauer, K. Volbert, and M. Grünewald. Performance of distributed algorithms for topology control in wireless networks. In *Proceedings of the International Parallel and Distributed Processing Symposium*, Nice, France, 22 - 26 2003.

[68] S. Sanayei and A. Nosratinia. Antenna Selection in MIMO Systems. *IEEE Communications Maganize*, 42(10), October 2004.

[69] S. Sharma. Analysis of 802.11b MAC: A QoS, Fairness, and Performance Perspective. Technical report, Department of Computer Science, Stony Brook University, Jan. 2003.

[70] J. D. Solomon. *Mobile IP, the Internet Unplugged*. Prentice Hill PTR, 1998.

[71] C. Sun, A. Hirata, T. Ohira, and N. C. Karmakar. Fast Beamforming of Electronically Steerable Parasitic Array Radiator Antennas: Theory and Experiment. *IEEE Transactions on Antennas and Propagation*, 52(7), July 2004.

[72] C. Sun and N. C. Karmakar. Direction of Arrival Estimation Based on a Single Port Smart Antenna Using MUSIC Algorithm with Periodic Signals. *International Journal of Signal Processing*, 1(2), 2004.

[73] M. Takai, J. Martin, R. Bagrodia, and A. Ren. Directional Virtual Carrier Sensing for Directional Antennas in Mobile Ad Hoc Networks. In *Proceedings of ACM MobiHoc*, June 2002.

[74] M. X. Tao. *Space-Time Coding Schemes for Wireless Communications over Flat Fading Channels*. PhD Thesis, Hong Kong University of Science and Technology, 2003.

[75] V. Tarokh, H. Jafarkhani, and A. R. Calderbank. Space-Time Block Codes from Orthogonal Designs. *IEEE Transactions on Information Theory*, 45(5), July 1999.

[76] V. Tarokh, H. Jafarkhani, and A. R. Calderbank. Space-Time Block Coding for Wireless Communications: Performance Results. *IEEE Journal on Selected Aeras in Communications,*, 17(3), March 1999.

[77] V. Tarokh, N. Seshadri, and A. R. Calderbank. Space-Time Codes for High Data Rate Wireless Communication: Performance Criterion and Code Construction. *IEEE Transactions on Information Theory*, 44(2), March 1998.

[78] E. Telatar. Capacity of Multi-antenna Gaussian Channels. Technical report, AT&T-Bell Lab, June 1995.

[79] B. D. Van Veen and K. M. Buckley. Beamforming: A Versatile Approach for Spatial Filtering. *IEEE ASSP Magazine*, April 1988.

[80] M. Z. Win and J. H. Winters. Analysis of Hybrid Selection/Maximal-Ratio Combining in Raylei Fading. *IEEE Transaction on Communications*, 47(12), December 1999.

[81] P. Wolniansky, G. J. Foschini, G. D. Golden, and R. A. Valenzuela. V-BLAST: An Architecture for Realizing Very High Data Rates Over the Rich-Scattering Wireless Channel. In *ISSSE*, 1998.

[82] A. M. Wyglinski and S. D. Blostein. On Uplink CDMA Cell Capacity: Mutual Coupling and Scattering Effects on Beamforming. *IEEE Transactions on Vehicular Technology*, 52(2), March 2003.

[83] F. Xu and U. Rückert. Neighborhood discovery and mac protocol for manets using the multiple-directional-antennas scheme. In *Proceedings of VDE Kongress - ITG Fachtagung 'Mobility'*, Aachen, Germany, 23-25 Oct. 2006.

[84] F. Xu and U. Rückert. Neighborhood discovery and mac protocol for manets using using a low complexity directional scheme. In *Proceedings of World Mobile Congress (WMC'06)*, Beijing, China, 11-13. Sep. 2006.

[85] L. H. Zheng and David N. C. Tse. Diversity and Multiplexing: A Fundamental Tradeoff in Multiple-Antenna Channels. *IEEE Transactions on Information Theory*, 49(5), May 2003.

Publication List

- Xu, Feng; Rückert, Ulrich: SSB: *A New Diversity Selection Combining Scheme and Its test-bed Implementation.* In: Proceedings of the 14th IEEE International Conference on Telecommunications (ICT 2007), Penang, Malaysia. 14 - 17, May, 2007

- Xu, Feng; Rückert, Ulrich: *Interference Suppression Technique for Diversity selection Combining in an Indoor Environment.* In: Proceedings of the 2nd International ITG Conference on Antennas (INICA 2007), Munich, Germany. 28 - 30, March, 2007

- Xu, Feng; Rückert, Ulrich: *Neighborhood Discovery and MAC Protocol for MANETs using the Multiple-Directional-Antennas Scheme.* In: Proceedings of VDE Kongress - ITG Fachtagung 'Mobility', Aachen, Germany, 23 - 25, Oct., 2006

- Xu, Feng; Rückert, Ulrich: *Neighborhood Discovery and MAC Protocol for MANETs using a Low Complexity Directional Scheme.* In: Proceedings of World Mobile Congress (WMC'06), Beijing, China. 9 - 11, Oct., 2006

- Grünewald, Matthias; Xu, Feng; Rückert, Ulrich: *Increasing the Resource-Efficiency of the CSMA/CA Protocol in Directional Ad Hoc Networks.* In: Proceedings of the 4th International Conference on AD-HOCNetworks & Wireless (adhocNOW '05), Cancun, Mexico. 6 - 8, Oct., 2005

- Xu, Feng; Grünewald, Matthias; Rückert, Ulrich: *A Low Complexity Directional Scheme for Mobile Ad Hoc Networks.* In: Proceedings of the 16th IEEE International Symposium on Personal Indoor and Mobile Radio Communications (PIMRC'05), Berlin, Germany 11 - 14, Sep., 2005

- Grünewald, Matthias; Xu, Feng; Rückert, Ulrich: *Power Control in Directional Mobile Ad Hoc Networks.* In: Proceedings of VDE Kongress - ITG Fachtagung 'Ambient Intelligence', P. 169-174, Berlin, Germany. 18 - 20, Oct., 2004